Universität Duisburg-Essen
Fakultät für Mathematik

Inauguraldissertation zur Erlangung des Grades Dr. rer. nat.

Hyperbolic Maxwell Variational Inequalities in Type-II Superconductivity

Doctoral Dissertation of:
Malte Winckler

Advisor:
Prof. Dr. Irwin Yousept

Reviewer:
Prof. Dr. Michael Hintermüller

Reviewer:
Prof. Dr. Fredi Tröltzsch

Day of the oral exam: 2 Dezember 2020

DOI: 10.17185/duepublico/73610
URN: urn:nbn:de:hbz:464-20210112-115117-8

Preface

The present doctoral thesis has been written during the past three years at the University of Duisburg–Essen and is the product of my research on mixed hyperbolic Maxwell variational inequalities of the second kind. This time has been extremely educational for me and filled with great memories, not least thanks to the people around me. Therefore, let me spend a few words expressing my gratitude.

I thank my *family and friends* without whom I would not be who I am today. First and foremost this includes my *Mom and Dad*; thank you for your love, affection and patience over almost three decades. You will always mean the world to me!

I am also grateful to all the people who have supported me in my professional life; starting with my *teachers* and *professors*, from whom I was able to learn the basics and the beauty of mathematical sciences, through my *fellow students* with whom I could study (and sometimes despair) in endless hours in our beloved *LuDi*, to all the *scientists* who showed interest in my research and supported it with advice and action.

The greatest direct influence on this dissertation is without question *Irwin Yousept*. I very much appreciate your guidance and continuing support in so many ways. Throughout the entire period of our collaboration, you provided a great supervision that I could not have imagined better. Whenever I had a question or I was stuck with a proof, your door was always wide open and we spent hour after hour discussing our papers and teaching. Furthermore, it was only through your support that I was able to attend the numerous international conferences and present our results to the community. This level of commitment is by no means a matter of course; thank you.

Malte Winckler
Essen, December 2020

Abstract

This thesis aims at getting better insights in the theory and numerics of hyperbolic Maxwell variational inequalities of the second kind. Motivated by Bean's critical state model for type-II (high-temperature) superconductivity replacing the classical Ohm's law in Maxwell's equations, we establish a novel well-posedness result for the concerned problem by means of a fully discrete scheme and a rigorous convergence analysis thereof. One major advantage of this approach is the natural derivation of a numerical algorithm to compute the corresponding solution based on the semismooth Newton method and a Moreau–Yosida penalization. Moreover, from a physical point of view, the problem features unknown interfaces between the superconducting and normal regions of the domain. Therefore, we propose an adaptive mesh refinement algorithm based on a posteriori error estimators in careful combination with the mentioned penalization. This results not only in an increased numerical accuracy, but it also provides a way to identify these unknown interfaces without any additional a priori assumption. The main results consist of the equivalence of the estimators to the actual error between the analytical solution and its penalized finite element approximation, as well as rigorous verification of the convergence of our novel algorithm. The final chapter is dedicated to a shape optimization problem subject to the variational inequality of the second kind. We compute the shape derivative of a penalized problem to cope with the low regularity of the dual variable mapping due to the underlying variational inequality structure. Thereafter, a limiting analysis with respect to the penalization parameter yields the existence of a minimizer to the original shape optimization problem. Finally, we establish an efficient level set method where the shape derivative provides a descent direction. All our analytical results in this thesis are complemented by various numerical experiments.

Zusammenfassung

Ziel dieser Arbeit ist es, bessere Einblicke in die Theorie und Numerik hyperbolischer Maxwell-Variationsungleichungen der zweiten Art zu erhalten. Motiviert durch das Beansche kritische Zustandsmodell für Typ-II Supraleitung, das das klassische Ohmsche Gesetz in den Maxwell-Gleichungen ersetzt, stellen wir mit Hilfe eines volldiskreten Ansatzes und einer rigorosen Konvergenzanalyse ein neuartiges Wohlgestelltheitsresultat für das betreffende Problem auf. Ein großer Vorteil dieses Ansatzes ist die natürliche Herleitung eines numerischen Algorithmus zur Berechnung der entsprechenden Lösung auf der Grundlage der semiglatten Newton-Methode und einer Moreau-Yosida-Penalisierung. Darüber hinaus weist unser Problem aus physikalischer Sicht unbekannte Grenzflächen zwischen den supraleitenden und den normalen Bereichen auf. Daher entwickeln wir einen Algorithmus zur adaptiven Gitterverfeinerung, der auf a-posteriori-Fehlerschätzern in Kombination mit der erwähnten Penalisierung basiert. Dies führt nicht nur zu einer verbesserten numerischen Präzision, sondern bietet auch die Möglichkeit, diese unbekannten Grenzflächen ohne zusätzliche Annahmen zu identifizieren. Die Hauptergebnisse bestehen in der Äquivalenz unserer Schätzer zum tatsächlichen Fehler zwischen der analytischen Lösung und ihrer penalisierten Finite-Elemente-Approximation sowie in der Überprüfung der Konvergenz unseres Algorithmus. Das letzte Kapitel ist einem Formoptimierungsproblem gewidmet, das unserer Variationsungleichung der zweiten Art als Nebenbedingung unterliegt. Wir berechnen die Formableitung eines penalisierten Problems, um mit der geringen Regularität der dualen Variablen umgehen zu können, welche aus der Struktur der Variationsungleichung resultiert. Danach ergibt eine Grenzwertanalyse in Bezug auf den Penalisierungsparameter die Existenz eines Minimierers für das ursprüngliche Formoptimierungsproblem. Schließlich etablieren wir eine effiziente Level-Set-Methode, bei der unsere Formableitung eine Abstiegsrichtung liefert. All unsere analytischen Ergebnisse werden durch verschiedene numerische Experimente ergänzt.

Contents

Chapter 1
Introduction

"One of the beautiful things about mathematical physics is that equations contain stories."
— Brian Cox, *Human Universe* [54]

Ever since their first appearance in the mathematical literature, variational inequalities have been application driven problems that demand a careful analysis and bring tough challenges to the numerical implementation. Historically, Signorini [153] was the first to formulate a problem with an inequality structure. In most simple terms, the *Signorini problem* is to determine the displacements in a heavy, linearly elastic body resting on a rigid, frictionless horizontal plane (see [6]). The great, until then completely novel, difficulty was that the regions of contact between the body and the plane are not known priorily. Therefore, the Signorini problem is often called a *free boundary problem*.

After Fichera [72] had made the initial contribution to find a solution to the Signorini problem, Stampacchia [156] established a more general well-posedness result in the spirit of the famous Lax–Milgram lemma. He also coined the name *variational inequality*. In the 1960s, the analysis of variational inequalities developed at an enormous pace by the work of many authors including Brezis [29], Browder [30], Lions [119], and Stampacchia [156]. The former melted the theory of variational inequalities with (pseudo-)monotone operators. At that time, if not before, the physical formulations were fully embedded into an abstract analytical framework that opened the way for more profound mathematical studies. One of the most important results from this time is surely the well-posedness theorem by Lions and Stampacchia [120] from 1967.

Besides these rapid developments, Fichera's initial solution to the Signorini problem had been the major concrete application of abstract analysis to actual physics for a long time. However, the significance of the vast theory became evident when numerous applications of free boundary problems were found in diverse fields, such as plasticity and fluid dynamics. We refer the reader to the monographs by Duvaut and Lions [64], Kinderlehrer and Stampacchia [105], Hlaváček et al. [94], as well as Barbu [12] with the extensive bibliography therein.

All of the mentioned developments are more or less motivated by *classical physics*.[1] In this thesis we are interested in variational inequalities that occur in modern electromagnetism – stemming from the *type-II (or high-temperature) superconductivity*. We include a description of this physical phenomenon below. Our modeling is based on *Bean's critical state law* and *Maxwell's equations*. The first contribution that linked these with a variational inequality structure using an *eddy current approximation* goes back to Prigozhin [141, 142]. We will give a more comprehensive list of literature concerning this topic in section 3.3.

The remainder of this chapter is structured as follows. First, we introduce the reader to the physical

[1] By classical physics we refer to pre-1900 physical phenomena not involving quantum mechanics or relativity.

phenomenon of type-II superconductivity. Thereafter, we set up Maxwell's equations and modify them according to Bean's critical state law. This results in a nonsmooth[2] hyperbolic system of equations. We end this chapter by summarizing the research contribution of this thesis and specify some basic mathematical notations.

1.1 ▪ Type-II Superconductivity

The most characteristic property of superconductors is that their electrical resistance drops to zero if they are cooled down below a certain critical temperature θ_c. However, these temperatures may be very low sometimes – depending on the material down to 4.15K (roughly -269°C). As a comparison we note that the temperature of liquid nitrogen lies around 77K (or -196°C). Over one century ago, in 1911, Heike Kamerlingh Onnes [103] discovered this effect during his low-temperature studies with mercury and coined the term *superconductivity*. An important observation was the sharp transition between the superconducting and the normal state, meaning that the superconducting effects disappear abruptly once the critical temperature is exceeded. Materials with this characteristic are classified as *type-I superconductors*. The research group around Onnes attached a considerable hope to superconductors in the generation of extremely strong magnetic fields. Be that as it may, they soon found out that there is an upper bound for the current that flows through a superconductor at zero resistance. This is called the *critical current density* j_c (cf. [73]).

In 1933, the German researchers Walther Meissner and Robert Ochsenfeld [125] uncovered that superconductors expell weak magnetic fields entirely from their inside. This phenomenon is also observed for different non-superconducting materials and is called *perfect diamagnetism*. However, the Meissner–Ochsenfeld effect in superconductivity goes further. When the superconductivity first forms, there is an exclusion of magnetic fields which have already penetrated the object. What actually happens is that shielding currents occur on the surface of the material and generate a magnetic field themselves. Inside the material the induced and the applied field cancel exactly to zero, whereas they add up on the outside. In the course of this thesis, we will verify the Meissner–Ochsenfeld effect by numerical experiments and build solid mathematical foundations. Figure 1.1 presents a schematic drawing to visualize the Meissner–Ochsenfeld effect.

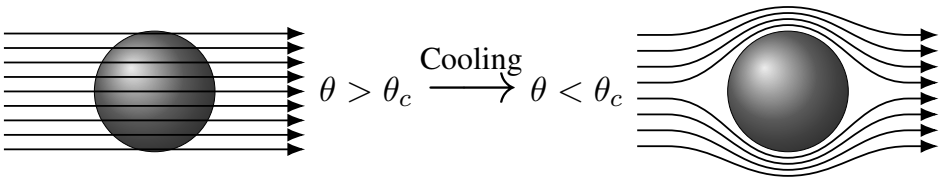

Figure 1.1. *Normal state (left): Magnetic field penetrates the material. Superconducting state (right): Magnetic field lines are expelled from the superconductor.*

As the critical temperatures in type-I superconductors are extremely low, their practical use is very limited. After decades of research, Georg Bednorz and Karl Alexander Müller [21] achieved a breakthrough in 1986 discovering *high-temperature superconductors* (HTS). Those are usually compositions manufactured from different ceramic materials and obtain remarkably higher critical temperatures. For instance, the ceramic compound $YBa_2Cu_3O_7$ obtains a critical temperature of 93K (or -180.15°C) – easily reached with liquid nitrogen (cf. [174]).

These materials are classified as *type-II superconductors* as they do not feature a sharp transition between the phases. Now, there are two critical field strengths $H_{C1} < H_{C2}$: As long as the magnetic field strength H remains below H_{C1}, the Meissner–Ochsenfeld effect is completely present. In the case of $H_{C1} < H < H_{C2}$, there is a partial penetration of the magnetic field but the material is still a

[2] In our context, the term *nonsmooth* indicates the absence of (classical) differentiability properties in the problem.

perfect electric conductor.[3] This is the so-called *mixed state* or *Shubnikov-phase*. If $H > H_{C2}$, then the superconducting state is broken down entirely.

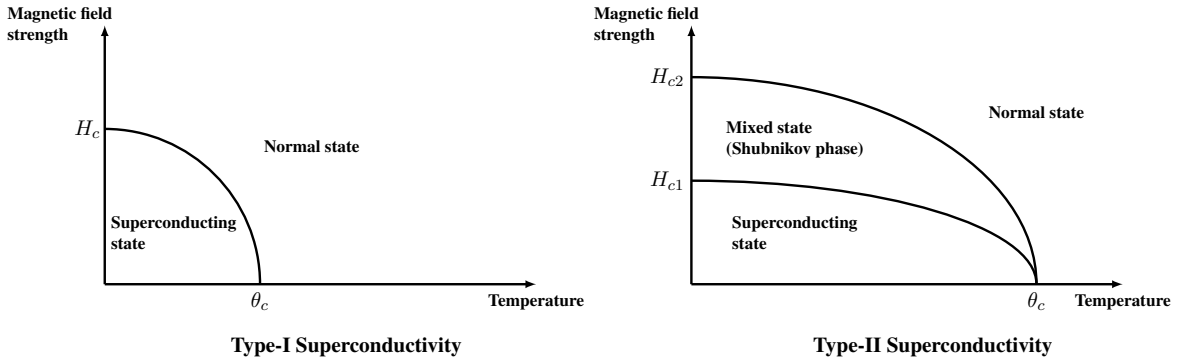

Figure 1.2. *Schematic comparison of type-I and type-II superconductivity.*

In the Shubnikov-phase, the magnetic field lines penetrate through the material in the form of magnetic vortices of quantized circulation called *flux tubes*.[4] Every tube is surrounded by a supercurrent vortex. The density of such flux tubes increases with rising applied magnetic field strength. This dynamic magnetization process is not reversible and exhibits hysteresis. Theoretical models that describe the phenomena in superconductivity include the London equations [123] and the Ginzburg–Landau theory [79]. In this work, we focus on the modeling proposed by Charles P. Bean [18, 19] known as *Bean's critical state law*. It postulates a nonsmooth constitutive relation between the electrical field and the current density. In Maxwell's equations, it replaces Ohm's law. In section 1.2 we present a more detailed description of Maxwell's equations and the combination with Bean's law.

Nowadays, the application of superconductors has become an inherent part of modern technologies; magnetic resonance imaging (MRI), high-energy particle accelerators, and magnetic levitation trains (MAGLEV) cannot be imagined without them. Moreover, their property of perfect electric conductivity motivates the use of HTS cables for power transmission and distribution in urban areas. With this aim, the companies around the power supplier RWE and the cable manufacturer Nexans installed an HTS cable through the inner city of Essen, Germany, in 2014 which carries electrical power for the equivalent of 10,000 households [87, 157]. These high-technological cables work with several HTS wire layers which are screened by copper and kept under the critical temperature by liquid nitrogen (see Figure 1.3).

1.2 ▪ Setting the Problem

Let us dedicate this section to the motivation and description of the mathematical modeling of the macroscopic effects occurring in type-II superconductors, which will be the fundamental problem throughout this thesis. Firstly, in order to introduce all the physical quantities, we briefly outline the full (time-dependent) Maxwell's equations named after the Scottish physicist James Clerk Maxwell describing the propagation and diffusion of electromagnetic fields.

The initial attempts to propose a rigorous mathematical formulation of physical effects in electromagnetism were made by André-Marie Ampère and Michael Faraday. Based on experimental results in a medium $\Omega \subset \mathbb{R}^3$ and some time interval $[0, T]$, Ampère stated his equation that relates the current $\boldsymbol{J} \colon \Omega \times [0, T] \to \mathbb{R}^3$ through a surface S to the total amount of magnetic field $\boldsymbol{H} \colon \Omega \times [0, T] \to \mathbb{R}^3$

[3] A perfect electric conductor has no electrical resistance, and thus a current can move without energy dissipation.

[4] Often they are also called *vortex lines* and in many cases one may interchange these terms. However, there is a conceptual difference for which we refer the reader to [73, Section 1.6].

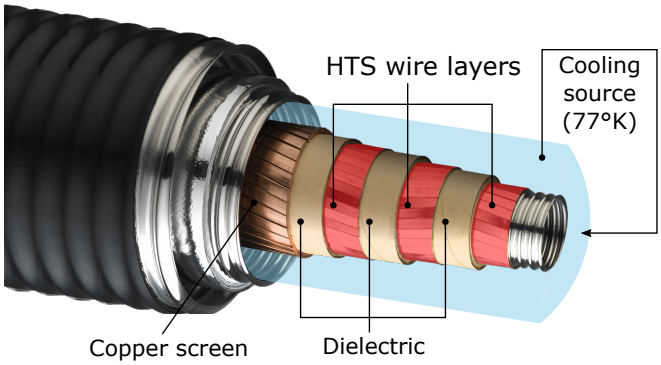

Figure 1.3. *Superconducting wire with three HTS layers and a cooling unit with liquid nitrogen (cf. [158, Figure 2]).*

around its boundary:

$$I = \int_S \boldsymbol{J} \cdot \boldsymbol{n} = \int_{\partial S} \boldsymbol{H} \cdot \boldsymbol{\tau}, \tag{1.1}$$

where $\boldsymbol{n}$ is the outer unit normal vector on S and $\boldsymbol{\tau}$ is the unit tangent vector on ∂S oriented counterclockwise to $\boldsymbol{n}$. By the infamous Stokes' Theorem, the *integral form* (1.1) of Ampère's law is equivalent to

$$\mathbf{curl}\, \boldsymbol{H} = \boldsymbol{J}, \tag{1.2}$$

which is called the *differential form*. All physical laws that we discuss in this section possess different integral and differential representations which, however, are usually equivalent due to Stokes' or Gauss' theorem. For this reason, we will solely use the differential representation in the remainder.

In his studies of electromagnetism, Maxwell discovered that Ampère's law in the present form (1.2) is not entirely adequate. One important issue concers the *charge conservation law*. It states that the divergence of the current density $\boldsymbol{J}$ equals the negative rate of change of the charge density $\rho\colon \Omega \times [0,T] \to \mathbb{R}$ with respect to time, i.e.,

$$\operatorname{div} \boldsymbol{J} = -\frac{\partial \rho}{\partial t}. \tag{1.3}$$

However, by classical vector calculus, it is known that the divergence of a $\mathbf{curl}$ is 0. Thus,

$$\operatorname{div} \boldsymbol{J} \overset{(1.2)}{=} \operatorname{div}(\mathbf{curl}\, \boldsymbol{H}) = 0 \quad \Rightarrow \quad \frac{\partial \rho}{\partial t} = 0,$$

which is in general not true for a time-varying charge density ρ. By considering *Gauss' law* for the electrical flux $\boldsymbol{D}\colon \Omega \times [0,T] \to \mathbb{R}^3$, i.e., $\rho = \operatorname{div} \boldsymbol{D}$ in combination with (1.3), it follows that

$$\operatorname{div}\left(\frac{\partial \boldsymbol{D}}{\partial t} + \boldsymbol{J}\right) = 0.$$

This divergence-free condition yields that $\frac{\partial \boldsymbol{D}}{\partial t} + \boldsymbol{J}$ has to be equal to the $\mathbf{curl}$ of some vector field. This vector field is precisely the magnetic field $\boldsymbol{H}$ since Ampère's law holds true in the stationary (time independent) case. Therefore, Maxwell established the following generalization of the classical Ampère law which is the first part of the full Maxwell's equations:

$$\frac{\partial \boldsymbol{D}}{\partial t} - \mathbf{curl}\, \boldsymbol{H} + \boldsymbol{J} = 0. \tag{1.4}$$

The additional term $\frac{\partial \boldsymbol{D}}{\partial t}$ is known as the *displacement current*. The second important law in Maxwell's equations goes back to Faraday and reads (in its differential form) as follows:

$$\frac{\partial \boldsymbol{B}}{\partial t} + \mathbf{curl}\, \boldsymbol{E} = 0 \tag{1.5}$$

with the magnetic induction $\boldsymbol{B}\colon \Omega \times [0,T] \to \mathbb{R}^3$ and the electric field $\boldsymbol{E}\colon \Omega \times [0,T] \to \mathbb{R}^3$. Moreover, for many materials, the electric field $\boldsymbol{E}$ and the magnetic field $\boldsymbol{H}$ are linearly dependent on the electric current $\boldsymbol{D}$ and the magnetic induction $\boldsymbol{B}$ satisfying the constitutive relations $\boldsymbol{D} = \epsilon \boldsymbol{E}$ and $\boldsymbol{B} = \mu \boldsymbol{H}$. The quantities ϵ and μ are called *electric permittivity* and *magnetic permeability*. In the simplest case of an *isotropic* material they are simply scalar-valued. For *anisotropic* materials they are in general matrix-valued.[5] In order to finally state the full Maxwell system we have to take another material law into account – the classical Ohm's law. Again, based on experimental measurements in electrical circuits, it holds that $\boldsymbol{J} = \sigma \boldsymbol{E} + \boldsymbol{f}$ with σ denoting the electric conductivity and some external current density $\boldsymbol{f}$. Finally, bringing everything together, the full Maxwell system in a domain Ω and a time interval $[0,T]$ is given by

$$\begin{cases} \epsilon \dfrac{\partial \boldsymbol{E}}{\partial t} - \mathbf{curl}\, \boldsymbol{H} + \sigma \boldsymbol{E} = \boldsymbol{f} & \text{in } \Omega \times (0,T) \\ \mu \dfrac{\partial \boldsymbol{H}}{\partial t} + \mathbf{curl}\, \boldsymbol{E} = 0 & \text{in } \Omega \times (0,T) \end{cases} \tag{1.6}$$

which should be accompanied by some (mathematical) boundary condition

$$\boldsymbol{E} \times \boldsymbol{n} = 0 \quad \text{ on } \partial\Omega \times (0,T)$$

and suitable initial conditions $\boldsymbol{E}(x,0) = \boldsymbol{E}_0(x)$ and $\boldsymbol{H}(x,0) = \boldsymbol{H}_0(x)$.

However, the classical Maxwell system (1.6) only holds for materials where Ohm's law is valid. In the case of a *superconducting material* we have to consider a more sophisticated (nonlinear) model – Bean's critical state law. In contrast to Ohm's law, it postulates a nonsmooth constitutive relation between the electrical field and the current density as follows:

(B1) the current density strength $|\boldsymbol{J}|$ cannot exceed some critical value $j_c \in \mathbb{R}^+$;
(B2) the electric field $\boldsymbol{E}$ vanishes if the current density strength is strictly less than j_c;
(B3) the electric field $\boldsymbol{E}$ is parallel to the current density $\boldsymbol{J}$.

We note that the original work by Bean [18, 19] proposes that the critical current density is simply a positive constant. This neglects the temperature dependence of type-II superconductors which is, however, a crucial characteristic (cf. Figure 1.1). Throughout the mathematical analysis of this thesis, we allow a more general class of nonnegative functions $j_c\colon \Omega \times \mathbb{R} \to \mathbb{R}$. Therefore, consider the following nonlinear nonsmooth function $g\colon \Omega \times (0,T) \to \mathbb{R}$ given by

$$g(x,t) := j_c\big(x, \theta(x,t)\big)\chi_{\Omega_{\mathrm{sc}}}(x), \tag{1.7}$$

where $\theta\colon \Omega \times (0,T) \to \mathbb{R}$ stands for the temperature distribution in Ω and $\chi_{\Omega_{\mathrm{sc}}}$ denotes the characteristic function of the superconducting domain $\Omega_{\mathrm{sc}} \subset \Omega$. Based on physical experiments, Aponte et al. [7] propose that the temperature dependence in j_c for a $YBa_2Cu_3O_7$ superconductor exhibits a monotonically decreasing and Lipschitz continuous character (cf. Figure 1.4). More precisely, it features a linear behaviour if the temperature θ is sufficiently small compared to θ_c. If θ is close to θ_c, then a nonlinear relation of the type $(1 - \frac{\theta}{\theta_c})^{3/2}$ is measured. Of course, $j_c(\theta) = 0$ if $\theta \geq \theta_c$. Similar observations were reported by Pashitskii et al. [139]. For high-temperature superconducting crystals and epitaxial films they propose a behaviour of the type $(1 - \frac{\theta}{\theta_c})^{\nu}$ with $\nu \in \{3/2, 2\}$ in the case of $\theta \approx \theta_c$. These properties will be incorporated in our analysis by Assumption 3.10.

[5] Isotropic materials exhibit the same behaviour in all space directions. On the other hand, anisotropy means that the material reacts differently to stresses or electromagnetic fields applied in different directions.

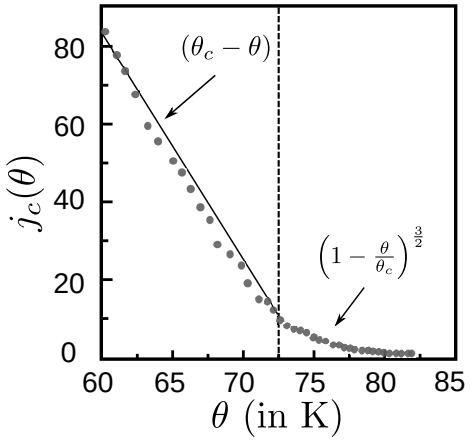

Figure 1.4. *Temperature dependence of the critical current density j_c in a $YBa_2Cu_3O_7$ superconductor according to Aponte et al. [7, Figure 2].*

By means of g we may reformulate (B1) to (B3) equivalently as

$$\begin{cases} \boldsymbol{J}(x,t) \cdot \boldsymbol{E}(x,t) = g(x,t)|\boldsymbol{E}(x,t)| & \text{a.e. in } \Omega \times (0,T), \\ |\boldsymbol{J}(x,t)| \leq g(x,t) & \text{a.e. in } \Omega \times (0,T). \end{cases} \tag{1.8}$$

Hence, by replacing the classical (linear) Ohm's law in (1.6) by the nonlinear Bean's law (1.8), we obtain a system of nonsmooth hyperbolic Maxwell equations:

$$\begin{cases} \epsilon \partial_t \boldsymbol{E} - \mathbf{curl}\, \boldsymbol{H} + \boldsymbol{J} = \boldsymbol{f} & \text{in } \Omega \times (0,T), \\ \mu \partial_t \boldsymbol{H} + \mathbf{curl}\, \boldsymbol{E} = 0 & \text{in } \Omega \times (0,T), \\ \boldsymbol{E} \times \boldsymbol{n} = 0 & \text{in } \Omega \times (0,T), \\ (\boldsymbol{E}, \boldsymbol{H})(\,\cdot\,, 0) = (\boldsymbol{E}_0, \boldsymbol{H}_0) & \text{in } \Omega, \\ \boldsymbol{J}(x,t) \cdot \boldsymbol{E}(x,t) = g(x,t)|\boldsymbol{E}(x,t)| & \text{a.e. in } \Omega \times (0,T), \\ |\boldsymbol{J}(x,t)| \leq g(x,t) & \text{a.e. in } \Omega \times (0,T). \end{cases} \tag{1.9}$$

System (1.9) is at the center of interest throughout this thesis.

1.3 ▪ Contribution

We aim at getting a better understanding of the nonsmooth hyperbolic Maxwell system (1.9). In order to prove its well-posedness, we carry out a careful numerical analysis demanding a variational formulation of (1.9). It comes in the form of a nonsmooth mixed hyperbolic variational inequality of the second kind, where $\boldsymbol{J}$ may be interpreted as the corresponding Lagrange multiplier (Proposition 3.12). Our methodology, novel contributions, and main results regarding (1.9) can be summarized as follows:

(a.) Based on a fully discrete scheme consisting of an implicit Euler in time and a mixed finite element method in space, we are able to extend the well-posedness result by Yousept [180] (cf. [102]) to our case of a time-dependent critical current density j_c. Our approach relies on a decoupling of the discrete mixed problems into an elliptic variational inequality with a $\mathbf{curl}$-$\mathbf{curl}$ structure for the electrical field $\boldsymbol{E}$ and a discrete version of Faraday's law to compute the magnetic field $\boldsymbol{H}$ (Theorem 4.4). A rigorous convergence analysis of the sequence of discrete solutions in the spirit of

$$\text{Stability estimates} \quad \rightarrow \quad \text{Weak convergence} \quad \rightarrow \quad \text{Strong convergence}$$

yields the well-posedness of (1.9) in particular (Theorems 4.8 and 4.10). We also present an efficient numerical algorithm along with numerical experiments. Thanks to the decoupling, the most challenging part in the numerical implementation is the computation of a **curl-curl** variational inequality in each time step. This is accomplished by means of a semismooth Newton method and the Moreau–Yosida regularization strategy (cf. section 3.2).

(b.) It is well-known that solutions to Maxwell's equations may feature various singularities (cf. [52, 53]). Moreover, the solution of (1.9) involves interfaces between the superconducting and the normal areas of the material which are priorily unknown. All in all, this calls for an adaptive mesh refinement algorithm based on a posteriori error estimators for a stationary **curl-curl** variational inequality stemming from the decoupling method mentioned in (a.). By a special combination of the Moreau–Yosida regularization (cf. Definition 3.3) and Nédélec's first family of edge elements (2.14), we prove the efficiency and reliability of the proposed estimators (Theorems 5.6 and 5.7). Thereafter, the strong convergence of our adaptive finite element algorithm (Algorithm 5.1) is verified by the use of limiting spaces (Theorem 5.17). Finally, we apply our algorithm to similar experiments as tested in (a.).

(c.) Motivated by our numerical results and physical experiments (cf. [110]), we will finally investigate the following question: how shall we design superconducting shields in order to save material and still keep the electromagnetic field penetration of a certain area at a minimum? We approach this question by the sensitivity analysis and numerical investigation for a shape optimization problem governed by a **curl-curl** variational inequality. Due to the variational inequality structure, we cannot guarantee the differentiability of the dual variable mapping which is, however, indispensable for our shape sensitivity analysis. Therefore, we employ a penalization to the dual formulation of the governing variational inequality (6.7). Now, after the verification of its assumptions (Lemmas 6.11 and 6.12), the averaged adjoint method (Theorem 6.10; cf. [114]) enables us to compute the corresponding shape derivative (Theorem 6.13). A rigorous convergence analysis of the penalized problem along with stability estimates for the shape derivative conclude our theoretical studies. Finally, numerical results are computed by means of an adapted level set method (Algorithm 6.1), where the shape derivative yields a descent direction for the minimization problem.

The remainder is structured as follows: In Chapters 2 and 3 we introduce some basic concepts and theories that are necessary throughout this work. The derivation of a weak formulation of (1.9) is the subject of section 3.3. The results from contribution (a.) are presented in Chapter 4. Chapter 5 is dedicated to the a posteriori error estimation and the AFEM algorithm for our **curl-curl** variational inequality and its convergence analysis, i.e., contribution (b.). Finally, we approach the shape optimization problem from (c.) in Chapter 6. Some parts of this thesis, mostly section 3.3 and Chapters 4 to 6, roughly coincide – small changes notwithstanding – with one of the publications [115, 171–173]. Thus, we will not indicate similarities with or quotations from these papers separately.

Publications

[115] A. Laurain, M. Winckler, and I. Yousept. Shape optimization for superconductors governed by H(curl)-elliptic variational inequalities. *SIAM J. Control Optim.*, submitted, 2019

[170] M. Winckler and I. Yousept. Fully discrete solution for Bean's critical-state model in type-II superconductivity. *PAMM*, 18(1):e201800173, 2018

[171] M. Winckler and I. Yousept. Fully discrete scheme for Bean's critical-state model with temperature effects in superconductivity. *SIAM J. Numer. Anal.*, 57(6):2685–2706, 2019

[172] M. Winckler and I. Yousept. Hyperbolic Maxwell variational inequalities in type-II superconductivity. In M. Hintermüller et. al., *SPP1962 Special Issue*. Birkhäuser, 2019. (accepted)

[173] M. Winckler, I. Yousept, and J. Zou. Adaptive edge element approximation for H(curl) elliptic variational inequalities of second kind. *SIAM J. Numer. Anal.*, 58(3):1941–1964, 2020

1.4 ▪ Notation

Let us introduce some basic notations that are necessary in this thesis. For a given Banach space X, we denote its norm by $\|\cdot\|_X$ and the duality pairing with the corresponding dual space X^* by $\langle\cdot,\cdot\rangle_{X^*,X}$. Except for possible confusion with the involved spaces, we drop the subscript and use the shorter notation $\langle\cdot,\cdot\rangle$. If X is a Hilbert space, then $(\cdot,\cdot)_X$ stands for its scalar product and $\|\cdot\|_X$ for the induced norm. In the case of $X = \mathbb{R}^n$, we renounce the subscript in the (Euclidean) norm and write $|\cdot|$. The Euclidean scalar product is denoted by a dot, and $\otimes$ is the standard outer product for vectors in $\mathbb{R}^3$, meaning

$$x \otimes y = x \cdot y^{\mathsf{T}} \quad \forall x, y \in \mathbb{R}^3.$$

Unless stated otherwise, we identify the dual space H^* of a Hilbert space H by itself. A continuous embedding between two Banach spaces X, Y is denoted by $X \hookrightarrow Y$ and if the embedding is compact, we write $X \hookrightarrow^c Y$.

Also note that we use bold letters for vector-valued (in our $\mathbb{R}^3$-valued) functions and the respective spaces. Moreover, we denote by $C > 0$ a generic constant that can change during an estimation without further comments.

Let us now introduce some standard Banach spaces. The space $\boldsymbol{\mathcal{C}}(\Omega)$ consists of the vector-valued continuous functions on Ω. For $k \in \mathbb{N}$, the space $\boldsymbol{\mathcal{C}}^k(\Omega) \coloneqq \mathcal{C}^k(\Omega, \mathbb{R}^3)$ stands for the space of k-times continuously differentiable vector-valued functions. They are equipped with the standard supremum norms. Moreover, $\boldsymbol{\mathcal{C}}^{0,1}(\Omega)$ is the space of Lipschitz continuous functions endowed with the norm given by

$$\|\boldsymbol{\theta}\|_{\boldsymbol{\mathcal{C}}^{0,1}(\Omega)} = \sup_{x\in\Omega} |\boldsymbol{\theta}(x)| + \sup_{\substack{x,y\in\Omega \\ x\neq y}} \frac{|\boldsymbol{\theta}(x) - \boldsymbol{\theta}(y)|}{|x-y|} \quad \forall \boldsymbol{\theta} \in \boldsymbol{\mathcal{C}}^{0,1}(\Omega).$$

As usual, we set $\boldsymbol{\mathcal{C}}^\infty(\Omega)$ as the space of all vector-valued infinitely differentiable functions. The subscript 0 at one of these classical spaces indicates functions with a compact support in Ω. Moreover, by $\boldsymbol{L}^2(\Omega)$ we denote the Hilbert space of all vector-valued, square-integrable functions with the standard scalar product $(\cdot,\cdot)_{\boldsymbol{L}^2(\Omega)}$ inducing the standard norm $\|\cdot\|_{\boldsymbol{L}^2(\Omega)}$. Due to the material parameters ϵ, μ occurring in the problem statement, we introduce $\boldsymbol{L}^2_\alpha(\Omega)$ as the weighted $\boldsymbol{L}^2(\Omega)$-space with the weighted scalar product $(\alpha\cdot,\cdot)_{\boldsymbol{L}^2(\Omega)}$ for a given positive function $\alpha \in L^\infty(\Omega)$ or a uniformly positive definite symmetric matrix-valued function $\alpha \in L^\infty(\Omega, \mathbb{R}^{3\times3})$. Note that $\epsilon, \mu \in L^\infty(\Omega, \mathbb{R}^{3\times3})$ are assumed to be uniformly positive definite and symmetric throughout this thesis (cf. Assumption 3.10).

Part I

Background

Chapter 2

Background Knowledge for Maxwell's Equations

This chapter is concerned with the basic concepts that are necessary for the (numerical) analysis of Maxwell's equations. After a brief introduction of the natural Hilbert spaces and the notation, we summarize well-known results such as compact embeddings and Poincaré–Friedrichs-type inequalities (Theorem 2.2 and Corollary 2.3). Thereafter, we give a more detailed overview of the finite element discretization of $\boldsymbol{H}(\mathbf{curl})$ which is the most basic requirement for all numerical experiments in this thesis. Finally, we propose an operator that possesses a *best approximation property* for $\boldsymbol{H}(\mathbf{curl})$-functions, and, by the use of recent results by Ern and Guermond [69, 70], we obtain error estimates for low regularity fields (Corollary 2.9).

2.1 ▪ Properties of the Curl-Spaces

Due to the nature of Maxwell's equations, the usage of the *standard* Sobolev spaces $W^{1,p}(\Omega)$, where weak gradients exist, is not sufficient. Therefore, we have to define the function spaces with less regularity that incorporate the $\mathbf{curl}$- and the div-operator. We define

$$\boldsymbol{H}(\mathbf{curl}) \coloneqq \{\boldsymbol{v} \in \boldsymbol{L}^2(\Omega) : \mathbf{curl}\, \boldsymbol{v} \in \boldsymbol{L}^2(\Omega)\} \quad \text{and} \quad \boldsymbol{H}(\mathrm{div}) \coloneqq \{\boldsymbol{v} \in \boldsymbol{L}^2(\Omega) : \mathrm{div}\, \boldsymbol{v} \in L^2(\Omega)\},$$

where $\mathbf{curl}$ and div are understood in the distributional sense. They are endowed with their respective graphs norms, i.e.,

$$\|\boldsymbol{v}\|_{\boldsymbol{H}(\mathbf{curl})} \coloneqq \left(\|\boldsymbol{v}\|^2_{\boldsymbol{L}^2(\Omega)} + \|\mathbf{curl}\, \boldsymbol{v}\|^2_{\boldsymbol{L}^2(\Omega)}\right)^{\frac{1}{2}},$$
$$\|\boldsymbol{v}\|_{\boldsymbol{H}(\mathrm{div})} \coloneqq \left(\|\boldsymbol{v}\|^2_{\boldsymbol{L}^2(\Omega)} + \|\mathrm{div}\, \boldsymbol{v}\|^2_{L^2(\Omega)}\right)^{\frac{1}{2}}$$

and the corresponding scalar products. The spaces $\boldsymbol{H}_0(\mathbf{curl})$ and $\boldsymbol{H}_0(\mathrm{div})$ stand for the closure of $\boldsymbol{C}_0^\infty(\Omega)$ with respect to the $\boldsymbol{H}(\mathbf{curl})$-norm and the $\boldsymbol{H}(\mathrm{div})$-norm, respectively. We may now characterize the space $\boldsymbol{H}_0(\mathbf{curl})$ via an integration by parts formula. The following result is well-known (see [182, Appendix A]).

Lemma 2.1. *For any open set $\Omega \subset \mathbb{R}^3$ it holds that*

$$\boldsymbol{H}_0(\mathbf{curl}) = \{\boldsymbol{q} \in \boldsymbol{H}(\mathbf{curl}) \,:\, (\boldsymbol{q}, \mathbf{curl}\, \boldsymbol{v})_{\boldsymbol{L}^2(\Omega)} = (\mathbf{curl}\, \boldsymbol{q}, \boldsymbol{v})_{\boldsymbol{L}^2(\Omega)} \quad \forall \boldsymbol{v} \in \boldsymbol{H}(\mathbf{curl})\}. \tag{2.1}$$

Furthermore, the spaces of divergence-free vector functions are

$$\boldsymbol{H}(\mathrm{div}{=}0) \coloneqq \{\boldsymbol{v} \in \boldsymbol{L}^2(\Omega) \,:\, (\boldsymbol{v}, \nabla\phi)_{\boldsymbol{L}^2(\Omega)} = 0 \quad \forall \phi \in H^1_0(\Omega)\},$$
$$\boldsymbol{H}_0(\mathrm{div}{=}0) \coloneqq \{\boldsymbol{v} \in \boldsymbol{L}^2(\Omega) \,:\, (\boldsymbol{v}, \nabla\phi)_{\boldsymbol{L}^2(\Omega)} = 0 \quad \forall \phi \in H^1(\Omega)\},$$

which are endowed with the $\boldsymbol{L}^2(\Omega)$-norm.

The theory of Maxwell's equations is mainly complicated by the fact that the continuous embeddings $\boldsymbol{H}_0(\mathbf{curl}) \hookrightarrow \boldsymbol{L}^2(\Omega)$ and $\boldsymbol{H}_0(\mathrm{div}) \hookrightarrow \boldsymbol{L}^2(\Omega)$ are *not* compact. Therefore, we *cannot* expect to obtain Poincaré–Friedrichs-type inequalities of the form

$$\begin{aligned} \|\boldsymbol{v}\|_{\boldsymbol{L}^2(\Omega)} &\leq C\|\,\mathbf{curl}\,\boldsymbol{v}\|_{\boldsymbol{L}^2(\Omega)} \quad \forall \boldsymbol{v} \in \boldsymbol{H}_0(\mathbf{curl}), \\ \|\boldsymbol{v}\|_{\boldsymbol{L}^2(\Omega)} &\leq C\|\,\mathrm{div}\,\boldsymbol{v}\|_{L^2(\Omega)} \quad \forall \boldsymbol{v} \in \boldsymbol{H}_0(\mathrm{div}). \end{aligned}$$

Firstly, note that even the space $\boldsymbol{X}(\Omega) \coloneqq \boldsymbol{H}(\mathbf{curl}) \cap \boldsymbol{H}(\mathrm{div})$ is not compactly embedded into $\boldsymbol{L}^2(\Omega)$ (cf. [5, Proposition 2.7]). However, if we include a boundary condition to one of the respective spaces, the compactness of the embedding follows (see [168, 169]):

Theorem 2.2. *Let $\Omega \subset \mathbb{R}^3$ be a bounded Lipschitz domain. Then,*

$$\boldsymbol{X}_N(\Omega) \coloneqq \boldsymbol{H}_0(\mathbf{curl}) \cap \epsilon^{-1}\boldsymbol{H}(\mathrm{div}) \hookrightarrow^c \boldsymbol{L}^2(\Omega), \tag{2.2}$$

where $\epsilon \in L^\infty(\Omega) \cup L^\infty(\Omega, \mathbb{R}^{3\times 3})$ is uniformly positive definite.

Additionally, we can give a characterization of the kernel $\boldsymbol{K}_N(\Omega) \coloneqq \{\boldsymbol{v} \in \boldsymbol{X}_N(\Omega) : \mathbf{curl}\,\boldsymbol{v} = 0,\ \mathrm{div}\,\boldsymbol{v} = 0\}$. For instance, if Ω has a connected Lipschitz boundary, [5, Proposition 3.18.] yields

$$\boldsymbol{K}_N(\Omega) = \{0\}. \tag{2.3}$$

With (2.2) and (2.3) at hand, we obtain a Poincaré–Friedrichs-type inequality for $\boldsymbol{X}_N(\Omega)$ of the following form:

Corollary 2.3. *Let $\Omega \subset \mathbb{R}^3$ be a bounded Lipschitz domain with a connected boundary $\partial\Omega$. Then, there exists a constant $C_F > 0$ such that*

$$\|\boldsymbol{v}\|_{\boldsymbol{L}^2(\Omega)} \leq C_F(\|\,\mathbf{curl}\,\boldsymbol{v}\|_{\boldsymbol{L}^2(\Omega)} + \|\,\mathrm{div}(\epsilon\boldsymbol{v})\|_{\boldsymbol{L}^2(\Omega)}) \quad \forall \boldsymbol{v} \in \boldsymbol{X}_N(\Omega). \tag{2.4}$$

Proof. The proof follows a simple contradiction argument: Assume that (2.4) does not hold. Then, there exists a sequence $\{\boldsymbol{v}_n\}_{n\in\mathbb{N}} \subset \boldsymbol{X}_N(\Omega)$ with $\|\boldsymbol{v}_n\|_{\boldsymbol{L}^2(\Omega)} = 1$ and

$$\|\,\mathbf{curl}\,\boldsymbol{v}_n\|_{\boldsymbol{L}^2(\Omega)} + \|\,\mathrm{div}(\epsilon\boldsymbol{v}_n)\|_{\boldsymbol{L}^2(\Omega)} \leq \frac{1}{n} \quad \forall n \in \mathbb{N}.$$

Thanks to (2.2), there exists an element $\boldsymbol{v} \in \boldsymbol{X}_N(\Omega)$ such that

$$\boldsymbol{v}_n \to \boldsymbol{v} \quad \text{and} \quad \mathbf{curl}\,\boldsymbol{v}_n \rightharpoonup \mathbf{curl}\,\boldsymbol{v} \quad \text{and} \quad \mathrm{div}(\epsilon\boldsymbol{v}_n) \rightharpoonup \mathrm{div}(\epsilon\boldsymbol{v}) \quad \text{in } \boldsymbol{L}^2(\Omega).$$

Now, due to (2.3), we have $\boldsymbol{K}_N(\Omega) = \{0\}$ which implies that $\mathbf{curl}\,\boldsymbol{v} = 0$ and $\mathrm{div}(\epsilon\boldsymbol{v}) = 0$ contradicts $\|\boldsymbol{v}\|_{\boldsymbol{L}^2(\Omega)} = 1$ right away. ∎

2.2 ▪ Nédélec's Edge Elements

Originating in the 1940s, the *finite element method* was created as a technique to solve (infinite-dimensional) boundary value problems stemming from physical applications approximately. It was initially applied to the Sobolev space $H^1(\Omega)$. We will construct the finite element space to discretize $\boldsymbol{H}(\mathbf{curl})$ which go back to Nédélec [131]. As we will restrict ourselves to the case of piecewise linear (first-order) finite elements, we refer the reader to the monographs by Monk [127], Boffi et al. [22], and Girault and Raviart [80] for a more comprehensive introduction into the theory of finite element methods for Maxwell's equations.

In the following, let $\Omega \subset \mathbb{R}^3$ be a Lipschitz polyhedral domain. A decomposition $\mathcal{T}_h$ of Ω with the property

$$\overline{\Omega} = \bigcup_{T \in \mathcal{T}_h} T$$

is called a *triangulation* if the following conditions hold

- each $T \in \mathcal{T}_h$ is a closed polyhedron with positive volume;
- $\operatorname{int}(T_1) \cap \operatorname{int}(T_2) = \emptyset$ if $T_1 \neq T_2$;
- if $F = T_1 \cap T_2 \neq \emptyset$ and $T_1 \neq T_2$, then F is a common face, edge, or vertex of T_1 and T_2.

Here, $\operatorname{int}(T)$ denotes the interior of the set T. Moreover, h_T stands for the diameter of T and ρ_T for the diameter of the largest ball contained in T. The subscript h denotes the maximum of h_T for $T \in \mathcal{T}_h$. A family of triangulations $\{\mathcal{T}_h\}_{h>0}$ is called *quasi-uniform* if there exist constants $\rho > 0$ and $\nu > 0$ such that

$$\frac{h_T}{\rho_T} \leq \rho \quad \text{and} \quad \frac{h}{h_T} \leq \nu \quad \forall T \in \mathcal{T}_h, \quad \forall h > 0. \tag{2.5}$$

If only the first property of (2.5) is satisfied, then $\{\mathcal{T}_h\}_{h>0}$ it is called *shape-regular*. We note that every element T of $\mathcal{T}_h$ can be obtained by suitable affine transformation $\boldsymbol{F}_T$ of a reference element $\hat{T}$, i.e., $T = \boldsymbol{F}_T(\hat{T})$, where

$$\boldsymbol{F}_T(\hat{x}) = B_T(\hat{x}) + b_T, \quad b_T \in \mathbb{R}^3,\ B_T \in \mathbb{R}^{3\times 3},\ \det(B_T) \neq 0. \tag{2.6}$$

For our case, the reference element $\hat{T}$ is the tetrahedron of vertices $(0,0,0)$, $(1,0,0)$, $(0,1,0)$, and $(0,0,1)$. Note that there are various possibilities on how to construct a triangulation. We only refer to [22, 145] and the references therein.

In many cases, finite element spaces are constructed by polynomials on each $T \in \mathcal{T}_h$ that are *put together* on the faces of neighbouring elements in a conforming way. That is, the resulting piecewise polynomial functions still belong to the respective function space. For $\boldsymbol{H}(\mathbf{curl})$, we have the following property (see [127, Lemma 5.3]): If T_1, T_2 are two neighbouring elements of $\mathcal{T}_h$ with a common face $f = T_1 \cap T_2$, the function $\boldsymbol{z} \in \boldsymbol{L}^2(T_1 \cup T_2)$ defined by

$$\boldsymbol{z} = \begin{cases} \boldsymbol{z}_1 \text{ in } T_1, \\ \boldsymbol{z}_2 \text{ in } T_2, \end{cases} \tag{2.7}$$

with $\boldsymbol{z}_i \in \boldsymbol{H}(\mathbf{curl}; T_i)$, $i \in \{1,2\}$, satisfies $\boldsymbol{z} \in \boldsymbol{H}(\mathbf{curl}; T_1 \cup T_2)$ if $\boldsymbol{z}_1 \times \boldsymbol{\nu} = \boldsymbol{z}_2 \times \boldsymbol{\nu}$ on f. Here, $\boldsymbol{\nu}$ denotes a unit normal vector on f. Therefore, the piecewise polynomial functions are required to have a *continuous* transition with respect to the tangential trace on the faces to be $\boldsymbol{H}(\mathbf{curl})$-conforming. The construction of a finite element space with polynomials of arbitrary degree for $\boldsymbol{H}(\mathbf{curl})$ goes back to Nédélec [131]. We follow his approach and introduce piecewise linear polynomials on some subset $\omega \subset \Omega$ of the form:

$$\boldsymbol{R}(\omega) = \{\boldsymbol{p} \colon \omega \to \mathbb{R}^3 \,:\, \boldsymbol{p}(x) = a + b \times x \text{ with } a, b \in \mathbb{R}^3\}.$$

Now, we make use of the reference tetrahedron $\hat{T}$ and define a set of *degrees of freedom* for $\hat{\boldsymbol{z}} \in \boldsymbol{R}(\hat{T})$

$$m_e(\hat{\boldsymbol{z}}) \coloneqq \left\{ \hat{\phi}_{\hat{e}}(\hat{\boldsymbol{z}}) = \int_{\hat{e}} \hat{\boldsymbol{z}} \cdot \hat{\boldsymbol{\tau}}\, ds, \quad \text{for all edges } \hat{e} \text{ of } \hat{T} \right\}, \tag{2.8}$$

where $\hat{\boldsymbol{\tau}}$ denotes a unit vector in the direction of the respective edge $\hat{e}$ of $\hat{T}$. A triple $(T, \boldsymbol{R}(T), m_e)$ is called a *finite element*. For a general element $T \in \mathcal{T}_h$ we use a transformation based on the affine map $\boldsymbol{F}_T$ to construct a function $\boldsymbol{z} \colon T \to \mathbb{R}^3$ from a reference function $\hat{\boldsymbol{z}} \in \boldsymbol{R}(\hat{T})$ by

$$\boldsymbol{z} = B_T^{-\mathsf{T}} \hat{\boldsymbol{z}} \circ \boldsymbol{F}_T^{-1}. \tag{2.9}$$

This formula has the advantage that $\mathbf{curl}\, \boldsymbol{z}$ exists and it is linked to $\mathbf{curl}\, \hat{\boldsymbol{z}}$ in a simple way. For convenience of the reader, we provide a short proof of this classical result.

Lemma 2.4. *Let $T \in \mathcal{T}_h$ and $\boldsymbol{F}_T$ be an affine transformation with* (2.6) *and $\boldsymbol{F}_T(\hat{T}) = T$. Then, $\boldsymbol{z}$ given by* (2.9) *for some $\hat{\boldsymbol{z}} \in \boldsymbol{H}(\mathbf{curl}, \hat{T})$ satisfies $\boldsymbol{z} \in \boldsymbol{H}(\mathbf{curl}, T)$ with*

$$\mathbf{curl}\, \boldsymbol{z} = \frac{1}{\det(B_T)} B_T\, \mathbf{curl}\, \hat{\boldsymbol{z}} \circ \boldsymbol{F}_T^{-1}. \tag{2.10}$$

Proof. At first, we verify (2.10) for a smooth function $\hat{\boldsymbol{z}} \in \boldsymbol{\mathcal{C}}^\infty(\hat{T})$. Then, by the chain rule, we deduce that $\boldsymbol{z}$ itself is also smooth and we may compute the Jacobian matrix

$$D\boldsymbol{z} = B_T^{-\mathsf{T}} \big(D\hat{\boldsymbol{z}} \circ \boldsymbol{F}_T^{-1} \big) B_T^{-1}. \tag{2.11}$$

Moreover, the following vector calculus rule holds:

$$(\mathbf{curl}\, \boldsymbol{z}) \times w = \big(D\boldsymbol{z}^{\mathsf{T}} - D\boldsymbol{z} \big) w \quad \forall w \in \mathbb{R}^3. \tag{2.12}$$

Hence, by combining (2.11) and (2.12) we obtain

$$\begin{aligned} (\mathbf{curl}\, \boldsymbol{z}) \times w &= B_T^{-\mathsf{T}} \big(\big(D\hat{\boldsymbol{z}} \circ \boldsymbol{F}_T^{-1} \big)^{\mathsf{T}} - D\hat{\boldsymbol{z}} \circ \boldsymbol{F}_T^{-1} \big) B_T^{-1} w \\ &= B_T^{-\mathsf{T}} \big(\mathbf{curl}\, \hat{\boldsymbol{z}} \circ \boldsymbol{F}_T^{-1} \big) \times B_T^{-1} w. \end{aligned} \tag{2.13}$$

Now, let us denote $(\tilde{b}_1\ \tilde{b}_2\ \tilde{b}_3) \coloneqq B_T^{-1}$ with $\tilde{b}_i \in \mathbb{R}^3$, $i \in \{1, 2, 3\}$. By means of this, inserting $\boldsymbol{w} = e_1 = (1\ 0\ 0)^{\mathsf{T}}$ and $\boldsymbol{w} = e_2$ into (2.13) yields by straightforward calculations that

$$\begin{bmatrix} 0 \\ (\mathbf{curl}\, \boldsymbol{z})_3 \\ -(\mathbf{curl}\, \boldsymbol{z})_2 \end{bmatrix} = \mathbf{curl}\, \boldsymbol{z} \times e_1 = B_T^{-\mathsf{T}} \big(\mathbf{curl}\, \hat{\boldsymbol{z}} \circ \boldsymbol{F}_T^{-1} \big) \times \tilde{b}_1 = \begin{bmatrix} \tilde{b}_1 \cdot \big(\mathbf{curl}\, \hat{\boldsymbol{z}} \circ \boldsymbol{F}_T^{-1} \big) \times \tilde{b}_1 \\ \tilde{b}_2 \cdot \big(\mathbf{curl}\, \hat{\boldsymbol{z}} \circ \boldsymbol{F}_T^{-1} \big) \times \tilde{b}_1 \\ \tilde{b}_3 \cdot \big(\mathbf{curl}\, \hat{\boldsymbol{z}} \circ \boldsymbol{F}_T^{-1} \big) \times \tilde{b}_1 \end{bmatrix}$$

and analogously

$$\begin{bmatrix} -(\mathbf{curl}\, \boldsymbol{z})_3 \\ 0 \\ (\mathbf{curl}\, \boldsymbol{z})_1 \end{bmatrix} = \mathbf{curl}\, \boldsymbol{z} \times e_2 = \begin{bmatrix} \tilde{b}_1 \cdot \big(\mathbf{curl}\, \hat{\boldsymbol{z}} \circ \boldsymbol{F}_T^{-1} \big) \times \tilde{b}_2 \\ \tilde{b}_2 \cdot \big(\mathbf{curl}\, \hat{\boldsymbol{z}} \circ \boldsymbol{F}_T^{-1} \big) \times \tilde{b}_2 \\ \tilde{b}_3 \cdot \big(\mathbf{curl}\, \hat{\boldsymbol{z}} \circ \boldsymbol{F}_T^{-1} \big) \times \tilde{b}_2 \end{bmatrix}.$$

Now, with these identities at hand and by using the well-known identity from the classical vector calculus $a \cdot b \times c = c \times a \cdot b$ for every $a, b, c \in \mathbb{R}^3$, we may compute

$$\mathbf{curl}\, \boldsymbol{z} = \begin{bmatrix} \tilde{b}_2 \times \tilde{b}_3 \cdot \big(\mathbf{curl}\, \hat{\boldsymbol{z}} \circ \boldsymbol{F}_T^{-1} \big) \\ \tilde{b}_3 \times \tilde{b}_1 \cdot \big(\mathbf{curl}\, \hat{\boldsymbol{z}} \circ \boldsymbol{F}_T^{-1} \big) \\ \tilde{b}_1 \times \tilde{b}_2 \cdot \big(\mathbf{curl}\, \hat{\boldsymbol{z}} \circ \boldsymbol{F}_T^{-1} \big) \end{bmatrix} = \operatorname{cof} \big(B_T^{-1} \big)\, \mathbf{curl}\, \hat{\boldsymbol{z}} \circ \boldsymbol{F}_T^{-1},$$

where $\operatorname{cof} \big(B_T^{-1} \big)$ denotes the cofactor matrix of B_T^{-1}. Note that the latter identity follows again by straightforward computations. Finally, we make use of the fact (see [159, page 232; 4C]) that $\operatorname{cof}(B_T^{-1}) = \det(B_T)^{-1} B_T$ which implies the assertion for $\hat{\boldsymbol{z}} \in \boldsymbol{\mathcal{C}}^\infty(\hat{T})$.

Let us now consider $\hat{\boldsymbol{z}} \in \boldsymbol{H}(\mathbf{curl}, \hat{T})$. Thus, fix $\boldsymbol{\rho} \in \boldsymbol{\mathcal{C}}_0^\infty(T)$ and compute $\mathbf{curl}\, \boldsymbol{z}$ in the sense of distributions using the change of variables $x \mapsto \hat{x} = \boldsymbol{F}_T(x)$ along with (2.9) and (2.10)

$$\begin{aligned} &\int_T \boldsymbol{z} \cdot \mathbf{curl}\, \boldsymbol{\rho}\, dx = \int_{\hat{T}} \boldsymbol{z} \circ \boldsymbol{F}_T \cdot \mathbf{curl}\, \boldsymbol{\rho} \circ \boldsymbol{F}_T |\det(B_T)|\, dx \\ &= \operatorname{sign} \big(\det(B_T) \big) \int_{\hat{T}} B_T^{-\mathsf{T}} \hat{\boldsymbol{z}} \cdot B_T\, \mathbf{curl}\, \hat{\boldsymbol{\rho}}\, d\hat{x} = \frac{1}{\det(B_T)} \int_{\hat{T}} \hat{\boldsymbol{z}} \cdot \mathbf{curl}\, \hat{\boldsymbol{\rho}} |\det(B_T)|\, d\hat{x} \\ &= \frac{1}{\det(B_T)} \int_{\hat{T}} \mathbf{curl}\, \hat{\boldsymbol{z}} \cdot \hat{\boldsymbol{\rho}} |\det(B_T)|\, d\hat{x} = \int_T \underbrace{\frac{1}{\det(B_T)} B_T\, \mathbf{curl}\, \hat{\boldsymbol{z}} \circ \boldsymbol{F}_T^{-1}}_{= \mathbf{curl}\, \boldsymbol{z}} \cdot \boldsymbol{\rho}\, dx. \end{aligned}$$

Hence, $\boldsymbol{z} \in \boldsymbol{H}(\mathbf{curl}, T)$ holds with (2.10) and the proof is finished. ∎

Remark 2.5. In fact, Lemma 2.4 remains valid if we replace the affine mapping $\boldsymbol{F}_T$ with a more general bi-Lipschitz transformation $\boldsymbol{G}_T\colon \hat{T} \to T$. We refer to [101, Lemma 11], where similar arguments with an additional mollification strategy are used.

Additionally, under (2.9), we readily see that $\hat{\boldsymbol{z}} \in \boldsymbol{R}(\hat{T})$ implies $\boldsymbol{z} \in \boldsymbol{R}(T)$, meaning that $\boldsymbol{R}(\hat{T})$ is *invariant* under (2.9). Moreover, the degrees of freedom (2.8) defined for $T \in \mathcal{T}_h$ are invariant in a similar sense (see [127, Lemma 5.34]): The degrees of freedom for $\boldsymbol{z}$ on T given by (2.9) are identical to those defined for $\hat{\boldsymbol{z}}$ on $\hat{T}$, i.e.,

$$\hat{\phi}_{\hat{e}}(\hat{\boldsymbol{z}}) = \phi_e(\boldsymbol{z}) = \int_e \boldsymbol{z} \cdot \boldsymbol{\tau}\, ds, \qquad \text{for every edge } \hat{e} \text{ of } \hat{T},$$

where $e = \boldsymbol{F}_T(\hat{e})$ provided that $\det(B_T) > 0$ and the tangential vectors $\boldsymbol{\tau}$ on the edges of T are related to those on $\hat{T}$ by

$$\boldsymbol{\tau} = \frac{B_T \hat{\boldsymbol{\tau}}}{|B_T \hat{\boldsymbol{\tau}}|}.$$

In fact, this definition of τ yields a unit tangential vector to the corresponding edge e of T which is the image under $\boldsymbol{F}_T$ of $\hat{e}$.

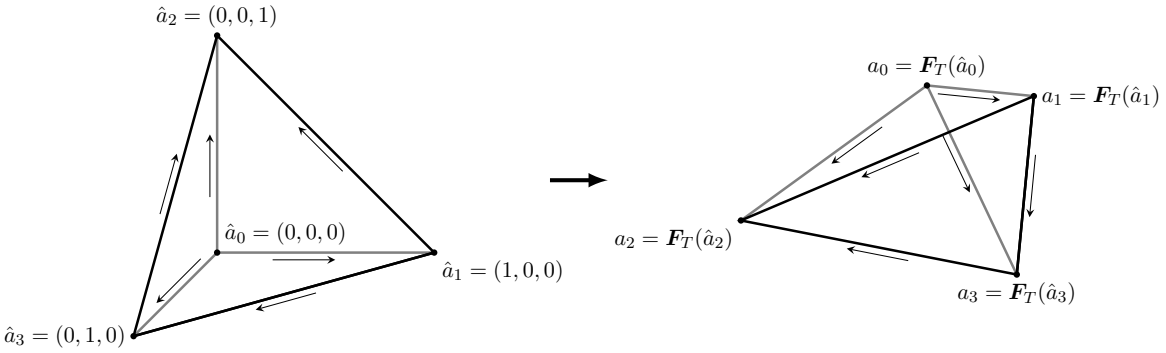

Figure 2.1. *Schematic transformation from reference tetrahedron to a general element with transformed degrees of freedom.*

The following lemma summarizes two important features of the degrees of freedom and yields the *conformity*[1] and the *unisolvence*[2] of the finite element (see [127, Lemmas 5.35 and 5.36]).

Lemma 2.6. *Let $\boldsymbol{z} \in \boldsymbol{R}(T)$ for some $T \in \mathcal{T}_h$. If $\boldsymbol{z}$ is such that $\phi_e(\boldsymbol{z}) = 0$*
(i) for all edges e of a face f in T, then $\boldsymbol{z} \times \boldsymbol{\nu} = 0$ on f;
(ii) for all edges e of T, then $\boldsymbol{z} = 0$.

With Lemma 2.6 at hand, we define the space of $\boldsymbol{H}(\mathbf{curl})$-conforming piecewise $\boldsymbol{R}$-functions by

$$\boldsymbol{V}_h^{\mathrm{Ned}} := \{\boldsymbol{v}_h \in \boldsymbol{H}(\mathbf{curl}) \,:\, \boldsymbol{v}_h|_T \in \boldsymbol{R}(T) \quad \forall T \in \mathcal{T}_h\}.$$

It is referred to as *the first family of Nédélec's edge elements*. For our application we are mostly interested in discretizing $\boldsymbol{H}_0(\mathbf{curl})$. This however can be achieved by considering only functions in $\boldsymbol{V}_h^{\mathrm{Ned}}$ where the degrees of freedom associated with edges on the boundary of Ω vanish (see (i) of Lemma 2.6). For the sake of a short notation, we denote

$$\boldsymbol{V}_h := \boldsymbol{V}_h^{\mathrm{Ned}} \cap \boldsymbol{H}_0(\mathbf{curl}). \tag{2.14}$$

[1] A finite element is called conforming if the global finite element space is a subspace of the respective function space.
[2] A finite element is called unisolvent if specifying a value for each degree of freedom uniquely determines a function in the respective polynomial space.

For every $\boldsymbol{v}_h \in \boldsymbol{V}_h$, we readily see by definition that $\mathbf{curl}\, \boldsymbol{v}_h$ is a piecewise constant function. Therefore, let us introduce the finite element space of piecewise constant functions by

$$\boldsymbol{W}_h \coloneqq \{\boldsymbol{w}_h \in \boldsymbol{L}^2(\Omega) \,:\, \boldsymbol{w}_h|_T = a_T \text{ with } a_T \in \mathbb{R}^3,\ \forall T \in \mathcal{T}_h\}, \tag{2.15}$$

which satisfy $\mathbf{curl}\, \boldsymbol{V}_h \subset \boldsymbol{W}_h$. Finally, in addition to the finite element spaces of Nédélec, the space of continuous piecewise linear elements with vanishing traces is defined by

$$\Theta_h \coloneqq \{\xi_h \in H_0^1(\Omega) \,:\, \xi_h|_T = a_T \cdot x + b_T \text{ with } a_T \in \mathbb{R}^3, b_T \in \mathbb{R} \quad \forall T \in \mathcal{T}_h\}. \tag{2.16}$$

The construction of Θ_h is similar to the one of $\boldsymbol{V}_h^{\mathrm{Ned}}$: We use the property that two $H_0^1(\Omega)$-functions with a continuous transition over a face f yield another $H_0^1(\Omega)$-function by the same procedure as (2.7). The degrees of freedom are thus given by the values on the vertices of $T \in \mathcal{T}_h$, i.e.,

$$m_v(\xi) \coloneqq \{\xi(a), \quad \text{for all vertices } a \text{ of } T\}.$$

This classical finite element space was originally introduced by Ciarlet [47]. Furthermore, the spaces of all discrete edge element functions with a discrete divergence are defined by

$$\begin{aligned} \boldsymbol{Z}_h &\coloneqq \{\boldsymbol{v}_h \in \boldsymbol{V}_h \,:\, (\boldsymbol{v}_h, \nabla\psi_h)_{\boldsymbol{L}^2(\Omega)} = 0 \quad \forall \psi_h \in \Theta_h\}, \\ \boldsymbol{Z}_h(\boldsymbol{w}) &\coloneqq \{\boldsymbol{v}_h \in \boldsymbol{V}_h \,:\, (\boldsymbol{v}_h, \nabla\psi_h)_{\boldsymbol{L}^2(\Omega)} = (\boldsymbol{w}, \nabla\psi_h)_{\boldsymbol{L}^2(\Omega)} \quad \forall \psi_h \in \Theta_h\} \end{aligned}$$

for some $\boldsymbol{w} \in \boldsymbol{L}^2(\Omega)$. It is well-known that $\boldsymbol{Z}_h$ satisfies a discrete Poincaré–Friedrichs-type inequality analogous to (2.4) (see [93, Theorem 4.7.]): If Ω additionally has a connected Lipschitz boundary $\partial\Omega$, then there exists a constant $C_F > 0$ independent of $h > 0$ such that

$$\|\boldsymbol{v}_h\|_{\boldsymbol{L}^2(\Omega)} \le C_F \|\mathbf{curl}\, \boldsymbol{v}_h\|_{\boldsymbol{L}^2(\Omega)} \quad \forall \boldsymbol{v}_h \in \boldsymbol{Z}_h. \tag{2.17}$$

Let us now construct a natural interpolation operator $\boldsymbol{r}_h \colon \boldsymbol{H}(\mathbf{curl}) \to \boldsymbol{V}_h^{\mathrm{Ned}}$ based on our (edge) degrees of freedom (2.8). For $\boldsymbol{y} \in \boldsymbol{H}(\mathbf{curl})$, we define $\boldsymbol{r}_h\boldsymbol{y}$ as the unique function that has the same degrees of freedom as $\boldsymbol{y}$, i.e.,

$$\phi_e(\boldsymbol{r}_h\boldsymbol{y} - \boldsymbol{y}) = 0 \quad \text{for every edge } e \text{ of } \mathcal{T}_h.$$

According to Boffi and Gastaldi [23], the degrees of freedom (and therefore $\boldsymbol{r}_h$) are well-defined for functions $\boldsymbol{y} \in \boldsymbol{H}^s(\Omega)$ for some $s > \frac{1}{2}$ with $\mathbf{curl}\, \boldsymbol{y} \in \boldsymbol{L}^p(\Omega)$ for some $p > 2$, where the techniques of Amrouche et al. [5] are used. It is well-known (see [3, Proposition 5.6]) that there exists a constant $C > 0$ independent of h such that

$$\|\boldsymbol{y} - \boldsymbol{r}_h\boldsymbol{y}\|_{\boldsymbol{H}(\mathbf{curl})} \le Ch^s \|\boldsymbol{y}\|_{\boldsymbol{H}^s(\mathbf{curl})} \quad \forall \boldsymbol{y} \in \boldsymbol{H}^s(\mathbf{curl}) \tag{2.18}$$

for $1/2 < s \le 1$, where

$$\boldsymbol{H}^s(\mathbf{curl}) \coloneqq \{\boldsymbol{y} \in \boldsymbol{H}^s(\Omega) \,:\, \mathbf{curl}\, \boldsymbol{y} \in \boldsymbol{H}^s(\Omega)\}. \tag{2.19}$$

Here, $\boldsymbol{H}^s(\Omega)$ denotes the fractional Sobolev-Slobodeckiĭ space defined for arbitrary exponents $s \ge 0$ (see [148, p. 18]). An interpolation operator $\Pi_h \colon H_0^1(\Omega) \to \Theta_h$ is defined analogously by $m_v(\Pi_h\xi - \xi) = 0$ for $\xi \in H_0^1(\Omega)$. A more detailed construction of the piecewise linear continuous elements can be found in [22, 47, 145].

Of course, the degrees of freedom (2.8) are not well-defined for a general function in $\boldsymbol{H}(\mathbf{curl})$. However, combining the density of $\boldsymbol{C}_0^\infty(\Omega)$ in $\boldsymbol{H}_0(\mathbf{curl})$ with (2.18) implies a strong approximation property of $\boldsymbol{V}_h$ in $\boldsymbol{H}_0(\mathbf{curl})$ in the sense that

$$\forall \boldsymbol{v} \in \boldsymbol{H}_0(\mathbf{curl})\ \forall \delta > 0\ \exists \tilde{h} > 0\ \forall h \in (0, \tilde{h})\ \exists \boldsymbol{v}_h \in \boldsymbol{V}_h \colon \ \|\boldsymbol{v} - \boldsymbol{v}_h\|_{\boldsymbol{H}(\mathbf{curl})} \le \delta, \tag{2.20}$$

A similar density property holds for $\boldsymbol{W}_h$ in $\boldsymbol{L}^2(\Omega)$:

$$\forall \boldsymbol{w} \in \boldsymbol{L}^2(\Omega)\ \forall \delta > 0\ \exists \tilde{h} > 0\ \forall h \in (0, \tilde{h})\ \exists \boldsymbol{w}_h \in \boldsymbol{W}_h : \quad \|\boldsymbol{w} - \boldsymbol{w}_h\|_{\boldsymbol{L}^2(\Omega)} \leq \delta. \tag{2.21}$$

Thus, we may also write (2.20) and (2.21) equivalently as

$$\boldsymbol{H}_0(\mathbf{curl}) = \overline{\bigcup_{h>0} \boldsymbol{V}_h}^{\|\cdot\|_{\boldsymbol{H}(\mathbf{curl})}} \quad \text{and} \quad \boldsymbol{L}^2(\Omega) = \overline{\bigcup_{h>0} \boldsymbol{W}_h}^{\|\cdot\|_{\boldsymbol{L}^2(\Omega)}}.$$

More technical details on interpolation estimates can be found, for instance, in Ciarlet Jr. and Zou [46] and Alonso and Valli [3].

We emphasize that by construction the error estimate (2.18) can only be applied for functions in $\boldsymbol{H}^s(\mathbf{curl})$ for $s > 1/2$. In general, $s \leq 1/2$ is *not* possible for $\boldsymbol{r}_h$. For this reason – amongst other things – the usage of $\boldsymbol{r}_h$ is not optimal. We will spend the remainder of this section on the development of an operator that is well-defined for $\boldsymbol{H}_0(\mathbf{curl})$-functions and satisfies a best approximation property. Therefore, let us now discuss a discrete mixed variational problem the well-posedness of which is the foundation for our desired operator.

Proposition 2.7. *Let $\Omega \subset \mathbb{R}^3$ be a bounded polyhedral Lipschitz domain with a connected boundary $\partial\Omega$. Moreover, $\nu \in L^\infty(\Omega) \cup L^\infty(\Omega, \mathbb{R}^{3\times 3})$ is supposed to be uniformly positive definite and symmetric. For every $h > 0$ and $\boldsymbol{y} \in \boldsymbol{H}_0(\mathbf{curl})$, the discrete variational mixed problem*

$$\begin{cases} (\mathbf{curl}\, \boldsymbol{y}_h, \mathbf{curl}\, \boldsymbol{v}_h)_{\boldsymbol{L}^2_\nu(\Omega)} = (\mathbf{curl}\, \boldsymbol{y}, \mathbf{curl}\, \boldsymbol{v}_h)_{\boldsymbol{L}^2_\nu(\Omega)} & \forall \boldsymbol{v}_h \in \boldsymbol{V}_h, \\ (\boldsymbol{y}_h, \nabla \psi_h)_{\boldsymbol{L}^2(\Omega)} = (\boldsymbol{y}, \nabla \psi_h)_{\boldsymbol{L}^2(\Omega)} & \forall \psi_h \in \Theta_h \end{cases} \tag{2.22}$$

obtains a unique solution $\boldsymbol{y}_h \in \boldsymbol{V}_h$ satisfying the best-approximation property

$$\|\boldsymbol{y}_h - \boldsymbol{y}\|_{\boldsymbol{H}(\mathbf{curl})} \leq C \left(\inf_{\boldsymbol{\chi}_h \in \boldsymbol{V}_h} \|\boldsymbol{y} - \boldsymbol{\chi}_h\|_{\boldsymbol{H}(\mathbf{curl})} \right) \tag{2.23}$$

with a constant $C > 0$ independent of h and $\boldsymbol{y}$.

Proof. According to the discrete Poincaré–Friedrichs-type inequality (2.17), we readily have the $\boldsymbol{Z}_h$-coercivity[3] of the bilinear form in the first equation of (2.22). Moreover, by the discrete de Rham diagram (see [127, p. 150]), it holds that $\nabla\Theta_h \subset \boldsymbol{V}_h$ with $\mathbf{curl}\, \nabla\psi_h = 0$ for every $\psi_h \in \Theta_h$. Thus, the discrete LBB condition is also satisfied since

$$\sup_{0 \neq \boldsymbol{v}_h \in \boldsymbol{V}_h} \frac{\left|(\boldsymbol{v}_h, \nabla\psi_h)_{\boldsymbol{L}^2(\Omega)}\right|}{\|\boldsymbol{v}_h\|_{\boldsymbol{H}(\mathbf{curl})}} \geq \frac{\left|(\nabla\psi_h, \nabla\psi_h)_{\boldsymbol{L}^2(\Omega)}\right|}{\|\nabla\psi_h\|_{\boldsymbol{L}^2(\Omega)}} = \|\nabla\psi_h\|_{\boldsymbol{L}^2(\Omega)} \quad \forall \psi_h \in \Theta_h. \tag{2.24}$$

Now, by the theory of mixed problems (cf. [127, Theorem 2.45]), there exists a unique solution $(\boldsymbol{y}_h, p_h) \in \boldsymbol{V}_\mathcal{T} \times \Theta_h$ to

$$\begin{cases} (\mathbf{curl}\, \boldsymbol{y}_h, \mathbf{curl}\, \boldsymbol{v}_h)_{\boldsymbol{L}^2_\nu(\Omega)} + (\boldsymbol{v}_h, \nabla p_h)_{\boldsymbol{L}^2(\Omega)} = (\mathbf{curl}\, \boldsymbol{y}, \mathbf{curl}\, \boldsymbol{v}_h)_{\boldsymbol{L}^2_\nu(\Omega)} & \forall \boldsymbol{v}_h \in \boldsymbol{V}_h, \\ (\boldsymbol{y}_h, \nabla \psi_h)_{\boldsymbol{L}^2(\Omega)} = (\boldsymbol{y}, \nabla \psi_h)_{\boldsymbol{L}^2(\Omega)} & \forall \psi_h \in \Theta_h. \end{cases}$$

However, if we insert $\boldsymbol{v}_h = \nabla p_h$, we readily obtain that $\nabla p_h = 0$ since $\mathbf{curl}\, \nabla p_h = 0$. Hence, the classical Poincaré–Friedrichs inequality for $H^1_0(\Omega)$ implies $p_h = 0$ and $\boldsymbol{y}_h \in \boldsymbol{V}_h$ solves (2.22). Uniqueness follows by energy estimates and (2.17).

Let us finish this proof by establishing the best-approximation property (2.23). At first, fix an arbitrary $\boldsymbol{w}_h \in \boldsymbol{Z}_h(\boldsymbol{y})$. Then, we have for $\boldsymbol{v}_h \coloneqq \boldsymbol{y}_h - \boldsymbol{w}_h \in \boldsymbol{Z}_h$ that

$$\|\boldsymbol{v}_h\|^2_{\boldsymbol{H}(\mathbf{curl})} \overset{(2.17)}{\leq} (1 + C_F^2) \|\mathbf{curl}\, \boldsymbol{v}_h\|^2_{\boldsymbol{L}^2(\Omega)} \overset{(2.22)}{=} (1 + C_F^2)(\mathbf{curl}(\boldsymbol{y} - \boldsymbol{w}_h), \mathbf{curl}\, \boldsymbol{v}_h)_{\boldsymbol{L}^2(\Omega)}$$

[3] This means that the bilinear form is coercive on the space $\boldsymbol{Z}_h$.

which yields by the triangle inequality

$$\|\boldsymbol{y}-\boldsymbol{y}_h\|_{\boldsymbol{H}(\mathbf{curl})} \leq (2+C_F^2)\|\boldsymbol{y}-\boldsymbol{w}_h\|_{\boldsymbol{H}(\mathbf{curl})} \quad \forall \boldsymbol{w}_h \in \boldsymbol{Z}_h(\boldsymbol{y}). \tag{2.25}$$

Now, it remains to verify that we can replace $\boldsymbol{w}_h \in \boldsymbol{Z}_h(\boldsymbol{y})$ on the right-hand side of (2.25) by an arbitrary $\boldsymbol{v}_h \in \boldsymbol{V}_h$. According to [127, Lemma 2.41], the discrete LBB condition (2.24) implies that for any $\boldsymbol{v}_h \in \boldsymbol{V}_h$ there exists a solution $\boldsymbol{z}_h \in \boldsymbol{Z}_h$ of

$$(\boldsymbol{z}_h, \nabla\psi_h)_{\boldsymbol{L}^2(\Omega)} = (\boldsymbol{y}-\boldsymbol{v}_h, \nabla\psi_h)_{\boldsymbol{L}^2(\Omega)} \quad \forall \psi_h \in \Theta_h \tag{2.26}$$

satisfying

$$\|\boldsymbol{z}_h\|_{\boldsymbol{H}(\mathbf{curl})} \leq C\|\boldsymbol{y}-\boldsymbol{v}_h\|_{\boldsymbol{H}(\mathbf{curl})} \tag{2.27}$$

with a constant $C > 0$ independent of h and $\boldsymbol{y}$. Thanks to (2.26), we may insert $\boldsymbol{w}_h = \boldsymbol{z}_h + \boldsymbol{v}_h \in \boldsymbol{Z}_h(\boldsymbol{y})$ into (2.25) to obtain

$$\|\boldsymbol{y}-\boldsymbol{y}_h\|_{\boldsymbol{H}(\mathbf{curl})} \overbrace{\leq}^{(2.25)} C\big(\|\boldsymbol{y}-\boldsymbol{v}_h\|_{\boldsymbol{H}(\mathbf{curl})} + \|\boldsymbol{z}_h\|_{\boldsymbol{H}(\mathbf{curl})}\big) \overbrace{\leq}^{(2.27)} C\|\boldsymbol{y}-\boldsymbol{v}_h\|_{\boldsymbol{H}(\mathbf{curl})}$$

for a constant $C > 0$ independent of h and $\boldsymbol{y}$. Since $\boldsymbol{v}_h \in \boldsymbol{V}_h$ was chosen arbitrarily, the proof is finished. ■

Definition 2.8. Let $h > 0$. Under the assumption of Proposition 2.7 we define the solution operator to (2.22) by

$$\boldsymbol{\Phi}_h \colon \boldsymbol{H}_0(\mathbf{curl}) \to \boldsymbol{V}_h, \quad \boldsymbol{y} \mapsto \boldsymbol{y}_h,$$

where $\boldsymbol{y}_h \in \boldsymbol{V}_h$ is the unique solution of (2.22). As a direct consequence of (2.23) it is readily seen that $\boldsymbol{\Phi}_h$ satisfies

$$\|\boldsymbol{\Phi}_h\boldsymbol{y}\|_{\boldsymbol{H}(\mathbf{curl})} \leq (C+1)\|\boldsymbol{y}\|_{\boldsymbol{H}(\mathbf{curl})} \quad \forall h > 0, \quad \forall \boldsymbol{y} \in \boldsymbol{H}_0(\mathbf{curl}). \tag{2.28}$$

Moreover, (2.23) along with the density property (2.20) of $\boldsymbol{V}_h$ implies that

$$\lim_{h\to 0} \|\boldsymbol{\Phi}_h\boldsymbol{y}-\boldsymbol{y}\|_{\boldsymbol{H}(\mathbf{curl})} = 0 \quad \forall \boldsymbol{y} \in \boldsymbol{H}_0(\mathbf{curl}). \tag{2.29}$$

As another immediate consequence of (2.23) and the error estimate for the canonical interpolation operator (2.18), we obtain an analogous estimate for functions in $\boldsymbol{H}^s(\mathbf{curl})$ with $s \in (1/2, 1]$ for the operator $\boldsymbol{\Phi}_h$. However, the best-approximation property opens the way to establish error estimates for fields with lower regularity as we will briefly discuss below. These estimates go back to the recent studies of Ern and Guermond [69, 70], where stable commuting quasi-interpolation operators are constructed and applied to $\boldsymbol{H}(\mathbf{curl})$.

In the classical literature quasi-interpolation operators for H^1-conforming finite element spaces are well-studied. Here, the classical *Scott–Zhang interpolation operator* allows optimal decay estimates (cf. [43, 151]). Seminal work on the construction of quasi-interpolation operators in the framework of Maxwell's equations goes back to Schöberl [149, 150] and Christiansen [41]. Their results rely on a composition of the canonical interpolation operators and mollification techniques. Additional results regarding this topic can be found in Christiansen and Winther [42] and Arnold et al. [8].

The stable commuting quasi-interpolation operators developed in [70, Theorem 6.4] revisit [42] by invoking mollification operators. They satisfy a sharp approximation result [69, Corollary 6.5] for low regularity functions in $\boldsymbol{H}^s(\Omega)$ for $s \in (0, 1]$ which may be arbitrarily close to zero. Their idea is based on a projection onto a broken finite element space and the averaging of the degrees of freedom in the broken space resulting in a smoothing operator.

Coming back to our operator ϕ_h, we obtain an error estimate result with low regularity fields by applying the quasi-interpolation operator with the sharp approximation result in combination with (2.23). The proof is completely analogous to [71, Theorem 3.3].

Corollary 2.9. *Let $s \in (0,1]$. There exists a constant $C > 0$ independent of h and $\boldsymbol{y}$ such that*

$$\|\boldsymbol{y} - \boldsymbol{\Phi}_h \boldsymbol{y}\|_{\boldsymbol{H}(\mathbf{curl})} \leq C h^s \|\boldsymbol{y}\|_{\boldsymbol{H}^s(\mathbf{curl})} \quad \forall \boldsymbol{y} \in \boldsymbol{H}_0^s(\mathbf{curl})$$

for all $h > 0$. Here, $\boldsymbol{H}_0^s(\mathbf{curl}) \coloneqq \{\boldsymbol{y} \in \boldsymbol{H}^s(\Omega) \cap \boldsymbol{H}_0(\mathbf{curl}) \,:\, \mathbf{curl}\, \boldsymbol{y} \in \boldsymbol{H}^s(\Omega)\}$.

A similar result with an alternative proof based on a Helmholtz-type decomposition can be found in the paper by Ciarlet Jr. [44, Proposition 4].

Chapter 3

Variational inequalities

Our analysis of the nonsmooth Maxwell system (1.9) relies on a discretization based on the finite element method from the previous section in combination with an implicit Euler in time. Hence, it is necessary that we propose a suitable *variational formulation* which comes – in our case of (1.9) – as a mixed hyperbolic variational inequality of the second kind (Proposition 3.12).

In the forthcoming section we will present the most basic well-posedness result for a general class of variational inequalities and introduce the Moreau–Yosida regularization which is crucial for the numerical computation of a solution. Thereafter, we revise the semismooth Newton method for variational inequalities involving the $\mathbf{curl}$-operator (cf. [99]).

3.1 ▪ Elliptic Variational Inequalities of the Second Kind

Before we dedicate ourselves to the studies of (1.9), we will recall some basic properties of elliptic variational inequalities in a real Hilbert space H. Therefore, let $a\colon H \times H \to \mathbb{R}$ be a continuous and coercive bilinear form, i.e., there exist $0 < \underline{\kappa} < \overline{\kappa}$ such that a satisfies

$$\begin{aligned} |a(u,v)| &\leq \overline{\kappa}\|u\|_H\|v\|_H \quad \forall u, v \in H, \\ a(v,v) &\geq \underline{\kappa}\|v\|_H^2 \quad \forall v \in H. \end{aligned} \tag{3.1}$$

Moreover, let $f \in H^*$ and $\psi\colon H \to \overline{\mathbb{R}} \coloneqq \mathbb{R} \cup \{+\infty\}$ be a proper, convex and sequentially lower semicontinuous (l.s.c.) functional. Then, we consider the problem of finding $v \in H$ such that

$$a(v, u - v) + \psi(u) - \psi(v) \geq \langle f, u - v\rangle \quad \forall u \in H. \tag{3.2}$$

Usually, if ψ is the indicator function of a convex, closed set $K \subset H$, (3.2) is called a *variational inequality of the first kind* or – depending on the structure of K – an *obstacle problem*. Otherwise (3.2) is said to be of the *second kind*. In any case, the well-posedness of (3.2) is guaranteed by a classical result from the theory of variational inequalities (cf. [120, Theorem 2.2]):

Theorem 3.1 (Well-posedness of elliptic variational inequalities of the second kind). *Let H be a real Hilbert space. Moreover, suppose that $a\colon H \times H \to \mathbb{R}$ is a continuous and coercive bilinear form, $\psi\colon H \to \overline{\mathbb{R}}$ is a convex, l.s.c. function and $f \in H^*$. Then,* (3.2) *admits a unique solution $u \in H$.*

One major difficulty when dealing with variational inequalities is the low regularity of the nonlinearity. In fact, in the case that ψ is Gâteaux-differentiable, (3.2) is equivalent to a variational equality. For convenience, we provide a short proof for this result.

Proposition 3.2. *Let H be a real Hilbert space and $\psi\colon H \to \mathbb{R}$ be Gâteaux-differentiable with derivative $\psi'\colon H \to H^*$. Then, $u \in H$ solves* (3.2) *if and only if there holds*

$$a(u,v) + \langle \psi'(u), v\rangle = \langle f, v\rangle \quad \forall v \in H. \tag{3.3}$$

Proof. If $u \in H$ solves (3.2), we may insert $v \coloneqq u + tw$ for $t > 0$ and $w \in H$ to obtain after division by t that

$$a(u,w) + \frac{\psi(u+tw)-\psi(u)}{t} \geq \langle f, w\rangle \quad \overbrace{\Rightarrow}^{t\to 0} \quad a(u,w) + \langle \psi'(u), w\rangle \geq \langle f, w\rangle.$$

Since $w \in H$ was chosen arbitrarily, we conclude that (3.3) holds. To derive (3.2) from (3.3), note that ψ satisfies

$$\psi(v) - \psi(u) - \langle \psi'(u), v-u\rangle \geq 0 \quad \forall v \in H \tag{3.4}$$

due to its convexity (see [17, Proposition 17.6]). Hence, the following estimate holds:

$$a(u,v-u) + \psi(v) - \psi(u) \overbrace{=}^{(3.3)} \langle f, v-u\rangle + \psi(v) - \psi(u) - \langle \psi'(u), v-u\rangle \overbrace{\geq}^{(3.4)} \langle f, v-u\rangle.$$

This corresponds to (3.2) and the proof is finished. ■

In the context of Proposition 3.2, the functionals occurring in variational inequalities are *not* Gâteaux-differentiable. This does not only bring additional challenges for the analysis and the optimization but also makes the usage of efficient Newton-type methods to compute numerical solutions rather intricate. Therefore, we will now introduce a popular regularization strategy for proper, convex, and sequentially lower semicontinuous functionals; the *Moreau–Yosida approximation*.

Definition 3.3. Let H be a Hilbert space and $\gamma > 0$. Then, the Moreau–Yosida approximation $\psi_\gamma\colon H \to \overline{\mathbb{R}}$ for a proper, convex, and sequentially lower semicontinuous function $\psi\colon H \to \mathbb{R}$ is defined by

$$\psi_\gamma(x) \coloneqq \inf_{v\in H} \rho_\gamma(v,x) \coloneqq \frac{\gamma}{2}\|v-x\|_H^2 + \psi(v). \tag{3.5}$$

Note that (3.5) is well-defined since ψ, being proper, has an affine minorant (see [17, Theorem 9.20]) and therefore, $\rho_\gamma(\cdot, x)$ is coercive for every $x \in H$. Additionally, $\rho_\gamma(\cdot, x)$ is sequentially lower semicontinuous, such that the direct method of calculus[1] (cf. [163]) implies the existence of a minimizer to (3.5) (cf. [13, Proposition 2.4]). The next lemma states some helpful and well-known properties of (3.5) (see [148, Lemma 5.17]).

Lemma 3.4. *Let $\{v_\gamma\}_{\gamma>0} \subset H$ and $v \in H$. For every $\gamma > 0$ it holds that $\psi_\gamma(v) \leq \psi(v)$ and the following convergence properties are satisfied:*

$$\begin{aligned} v_\gamma \rightharpoonup v \text{ weakly in } H \text{ for } \gamma \to \infty \quad &\Rightarrow \quad \liminf_{\gamma\to\infty} \psi_\gamma(v_\gamma) \geq \psi(v) \\ v_\gamma \to v \text{ strongly in } H \text{ for } \gamma \to \infty \quad &\Rightarrow \quad \limsup_{\gamma\to\infty} \psi_\gamma(v_\gamma) \leq \psi(v). \end{aligned}$$

Moreover, $\psi_\gamma\colon H \to \mathbb{R}$ is Lipschitz continuous with constant γ^{-1} and Gâteaux-differentiable for every $\gamma > 0$.

[1] The direct method of calculus is a mathematical tool to prove the existence of minimizers. It is based on the convergence analysis of minimizing sequences when the given functional is sequentially lower semicontinuous (with respect to some topology).

For our studies we are interested in functionals where the nonlinear character of the inequality is induced by the Euclidean norm. Therefore, let us compute $\eta_\gamma\colon \mathbb{R}^3 \to \mathbb{R}$ for $\eta = |\cdot|\colon \mathbb{R}^3 \to \mathbb{R}$ in the sense of Definition 3.3.

Proposition 3.5 (The Moreau–Yosida Approximation of $|\cdot|$). *Let $\gamma > 0$ be fixed. According to Definition* 3.3*, it holds that*

$$\eta_\gamma(x) = \begin{cases} |x| - \dfrac{1}{2\gamma} & \text{, for } |x| \geq \dfrac{1}{\gamma} \\ \dfrac{\gamma}{2}|x|^2 & \text{, for } |x| \leq \dfrac{1}{\gamma}. \end{cases} \tag{3.6}$$

Proof. Fix $x \neq 0$. We may split the minimization problem in (3.5) as follows:

$$\begin{aligned} \eta_\gamma(x) &\underbrace{=}_{(3.5)} \min_{v\in\mathbb{R}^3} \frac{\gamma}{2}|v|^2 - \gamma v \cdot x + \frac{\gamma}{2}|x|^2 + |v| \\ &= \min_{r\geq 0} \min_{v\in\mathbb{R}^3, |v|=r} \frac{\gamma}{2} r^2 - \gamma v \cdot x + \frac{\gamma}{2}|x|^2 + r \end{aligned} \tag{3.7}$$

For every fixed $r \geq 0$, the Cauchy–Schwarz inequality yields that the inner minimization problem in (3.7) obtains the minimizer

$$v_{\min}(r) = r\frac{x}{|x|}.$$

Hence,

$$\eta_\gamma(x) = \min_{r\geq 0} \frac{\gamma}{2}(r - |x|)^2 + r. \tag{3.8}$$

Now, since (3.8) is a one-dimensional minimization problem, we may compute its minimizer by standard calculus arguments. It is given by

$$r_{\min} = \max\left(0, |x| - \frac{1}{\gamma}\right). \tag{3.9}$$

Finally, inserting $r_{\min}$ into (3.8) implies that (3.6) holds for every $x \neq 0$. The case $x = 0$ is trivial. ■

$\boldsymbol{H}(\mathbf{curl})$ elliptic VIs with L^1-type Functionals

As already mentioned, we are interested in variational inequalities where ψ is an L^1-type functional and the corresponding Hilbert space consists of vector-valued functions with $\boldsymbol{H}_0(\mathbf{curl})$-regularity. Therefore, let $\Omega \subset \mathbb{R}^3$ be bounded and $\boldsymbol{V} \subset \boldsymbol{H}_0(\mathbf{curl})$ be a Hilbert space. We either choose $\boldsymbol{V} = \boldsymbol{H}_0(\mathbf{curl})$ or a suitable finite element discretization thereof. Let us also specify the bilinear form $a\colon \boldsymbol{V} \times \boldsymbol{V} \to \mathbb{R}$ by

$$a(\boldsymbol{u}, \boldsymbol{v}) \coloneqq \int_\Omega \epsilon \boldsymbol{u} \cdot \boldsymbol{v}\, dx + \int_\Omega \nu\, \mathbf{curl}\, \boldsymbol{u} \cdot \mathbf{curl}\, \boldsymbol{v}\, dx \quad \forall \boldsymbol{u}, \boldsymbol{v} \in \boldsymbol{V}, \tag{3.10}$$

where $\epsilon, \nu \in L^\infty(\Omega)$ or $\epsilon, \nu \in L^\infty(\Omega, \mathbb{R}^{3\times 3})$ are chosen such that (3.1) is satisfied. Now, consider the problem of finding $\boldsymbol{E} \in \boldsymbol{V}$ such that

$$a(\boldsymbol{E}, \boldsymbol{v} - \boldsymbol{E}) + \int_\Omega g|\boldsymbol{v}|\, dx - \int_\Omega g|\boldsymbol{E}|\, dx \geq \langle \boldsymbol{f}, \boldsymbol{v} - \boldsymbol{E}\rangle \quad \forall \boldsymbol{v} \in \boldsymbol{V} \tag{3.11}$$

with a nonnegative function $g \in L^\infty(\Omega)$ and $\boldsymbol{f} \in \boldsymbol{V}^*$. Therefore, $\psi\colon \boldsymbol{V} \to \mathbb{R}$ is defined by

$$\psi(\boldsymbol{v}) \coloneqq \int_\Omega g|\boldsymbol{v}|\,dx \quad \forall \boldsymbol{v} \in \boldsymbol{V}.$$

One very important equivalent representation of (3.11) is one with *Lagrange multipliers*. In [82, Chapter 1.3] it is shown that $\boldsymbol{E} \in \boldsymbol{V}$ is the unique solution to (3.11) if and only if there exists $\boldsymbol{\lambda} \in \boldsymbol{L}^\infty(\Omega)$ such that

$$\begin{cases} a(\boldsymbol{E}, \boldsymbol{v}) + \displaystyle\int_\Omega \boldsymbol{\lambda} \cdot \boldsymbol{v}\,dx = \langle \boldsymbol{f}, \boldsymbol{v}\rangle \quad \forall \boldsymbol{v} \in \boldsymbol{V} \\ |\boldsymbol{\lambda}(x)| \le g(x), \quad \boldsymbol{\lambda}(x) \cdot \boldsymbol{E}(x) = g(x)|\boldsymbol{E}(x)| \ \text{ for a.e. } x \in \Omega. \end{cases} \tag{3.12}$$

For (3.12), we introduce the active and inactive sets by

$$\mathcal{A} \coloneqq \{x \in \Omega : \ |\boldsymbol{E}(x)| > 0\} \quad \text{and} \quad \mathcal{I} \coloneqq \Omega \setminus \mathcal{A}. \tag{3.13}$$

However, the multiplier $\boldsymbol{\lambda}$ cannot be given explicitly and no additional regularity can be shown which makes numerical computations of (3.12) challenging. Besides standard fixed-point techniques, some direct approaches are the *relaxation method* [81, 176], *multigrid methods* [95] or the *inexact Uzawa algorithm* [40]. All of them converge at most with a linear rate and are only applicable in finite-dimensional function spaces if no further approximation is employed. In our case, we will rely on a generalization of the Newton method which guarantees superlinear convergence (cf. [99, Chapter 8]). Unfortunately, it is not directly applicable to (3.11) so that we consider the Moreau–Yosida regularized version of (3.11): Find $\boldsymbol{E}^\gamma \in \boldsymbol{V}$ such that

$$a(\boldsymbol{E}^\gamma, \boldsymbol{v} - \boldsymbol{E}^\gamma) + \psi_\gamma(\boldsymbol{v}) - \psi_\gamma(\boldsymbol{E}^\gamma) \ge \langle \boldsymbol{f}, \boldsymbol{v} - \boldsymbol{E}^\gamma\rangle \quad \forall \boldsymbol{v} \in \boldsymbol{V}, \tag{3.14}$$

where $\psi_\gamma\colon \boldsymbol{V} \to \mathbb{R}$ is defined by (see Proposition 3.5)

$$\psi_\gamma(\boldsymbol{v}) \coloneqq \int_\Omega g\eta_\gamma(\boldsymbol{v})\,dx \quad \forall \boldsymbol{v} \in \boldsymbol{V}.$$

Thanks to Lemma 3.4, η_γ is Lipschitz continuous and Gâteaux-differentiable. Thus, Lebesgue's dominated convergence theorem yields that ψ_γ is Gâteaux-differentiable and straightforward calculations show that the derivative $\psi_\gamma'\colon \boldsymbol{L}^2(\Omega) \to \boldsymbol{L}^2(\Omega)$ is given by

$$\psi_\gamma'(\boldsymbol{v}) = g\frac{\gamma \boldsymbol{v}}{\max\{1, \gamma|\boldsymbol{v}|\}} \quad \forall \boldsymbol{v} \in \boldsymbol{L}^2(\Omega). \tag{3.15}$$

Now, we may apply Proposition 3.2 to obtain that (3.14) is equivalent to

$$\begin{cases} a(\boldsymbol{E}^\gamma, \boldsymbol{v}) + \displaystyle\int_\Omega \boldsymbol{\lambda}^\gamma \cdot \boldsymbol{v}\,dx = \langle \boldsymbol{f}, \boldsymbol{v}\rangle \quad \forall \boldsymbol{v} \in \boldsymbol{V} \\ \boldsymbol{\lambda}^\gamma(x) = \psi_\gamma'(\boldsymbol{E}^\gamma)(x) = g(x)\dfrac{\gamma \boldsymbol{E}^\gamma(x)}{\max\{1, \gamma|\boldsymbol{E}^\gamma(x)|\}} \quad \text{for a.e. } x \in \Omega. \end{cases} \tag{3.16}$$

Compared to the dual formulation of (3.11) (see (3.12)), the dual variable $\boldsymbol{\lambda}^\gamma$ in (3.16) is now explicitly given by ψ_γ'. In this context, we denote the active and inactive sets by

$$\mathcal{A}_\gamma \coloneqq \{x \in \Omega : \ \gamma|\boldsymbol{E}^\gamma(x)| > 1\} \quad \text{and} \quad \mathcal{I}_\gamma \coloneqq \Omega \backslash \mathcal{A}_\gamma. \tag{3.17}$$

Before we discuss the numerical computation of (3.16), we use straightforward calculations on the active and inactive sets to prove that the error induced by the Moreau–Yosida regularization is of order $\sqrt{\gamma}^{-1}$.

Lemma 3.6. *Let $\gamma > 0$ and $\boldsymbol{E}, \boldsymbol{E}^\gamma \in \boldsymbol{V}$ be the solutions to* (3.11) *and* (3.14)*. Then, the following error estimate holds*

$$\|\boldsymbol{E} - \boldsymbol{E}^\gamma\|^2_{\boldsymbol{H}(\mathbf{curl})} \leq \frac{C}{\gamma} \tag{3.18}$$

with the constant $C = \underline{\kappa}^{-1}\|g\|_{L^1(\Omega)}$.

Proof. We begin by subtracting (3.12) from (3.16) to obtain

$$a(\boldsymbol{E}^\gamma - \boldsymbol{E}, \boldsymbol{v}) = \int_\Omega (\boldsymbol{\lambda} - \boldsymbol{\lambda}^\gamma) \cdot \boldsymbol{v}\, dx \quad \forall \boldsymbol{v} \in \boldsymbol{V}. \tag{3.19}$$

Next, we exploit the properties of $\boldsymbol{\lambda}$ and $\boldsymbol{\lambda}^\gamma$ in (3.12) and (3.16) and prove

$$\int_\Omega (\boldsymbol{\lambda} - \boldsymbol{\lambda}^\gamma) \cdot (\boldsymbol{E}^\gamma - \boldsymbol{E})\, dx \leq \frac{1}{\gamma}\|g\|_{L^1(\Omega)}. \tag{3.20}$$

To this aim, we divide Ω using the active and inactive sets introduced in (3.13) and (3.17) into $\mathcal{A} \cap \mathcal{A}_\gamma$, $\mathcal{A} \cap \mathcal{I}_\gamma$, $\mathcal{I} \cap \mathcal{A}_\gamma$, as well as $\mathcal{I} \cap \mathcal{I}_\gamma$. With this, we prove pointwise estimates of the integrand in (3.20). For $x \in \mathcal{A} \cap \mathcal{A}_\gamma$, (3.12) and (3.16) imply

$$\begin{aligned}
&\big(\boldsymbol{\lambda}(x) - \boldsymbol{\lambda}^\gamma(x)\big) \cdot \big(\boldsymbol{E}^\gamma(x) - \boldsymbol{E}(x)\big) \\
&= \boldsymbol{\lambda}(x) \cdot \boldsymbol{E}^\gamma(x) - \boldsymbol{\lambda}(x) \cdot \boldsymbol{E}(x) + \boldsymbol{\lambda}^\gamma(x) \cdot \boldsymbol{E}(x) - \boldsymbol{\lambda}^\gamma(x) \cdot \boldsymbol{E}^\gamma(x) \\
&\leq g(x)|\boldsymbol{E}^\gamma(x)| - g(x)|\boldsymbol{E}(x)| + g(x)|\boldsymbol{E}(x)| - g(x)|\boldsymbol{E}^\gamma(x)| = 0.
\end{aligned}$$

For $x \in \mathcal{A} \cap \mathcal{I}_\gamma$, (3.12) and (3.16) yield $g(x)\boldsymbol{E}^\gamma(x) = \gamma^{-1}\boldsymbol{\lambda}^\gamma(x)$, $|\boldsymbol{\lambda}^\gamma(x)| \leq g(x)$ as well as $|\boldsymbol{E}^\gamma(x)| \leq \gamma^{-1}$ and $|\boldsymbol{\lambda}(x)| = g(x)$. Hence, we can derive

$$\begin{aligned}
&\big(\boldsymbol{\lambda}(x) - \boldsymbol{\lambda}^\gamma(x)\big) \cdot \big(\boldsymbol{E}^\gamma(x) - \boldsymbol{E}(x)\big) \\
&= \boldsymbol{\lambda}(x) \cdot \boldsymbol{E}^\gamma(x) - g(x)|\boldsymbol{E}(x)| - \gamma g(x)|\boldsymbol{E}^\gamma(x)|^2 + \boldsymbol{\lambda}^\gamma(x) \cdot \boldsymbol{E}(x) \\
&\leq \frac{1}{\gamma}g(x) - g(x)|\boldsymbol{E}(x)| + g(x)|\boldsymbol{E}(x)| - \gamma g(x)|\boldsymbol{E}^\gamma|^2 \leq \frac{1}{\gamma}g(x).
\end{aligned}$$

For $x \in \mathcal{I} \cap \mathcal{A}_\gamma$, we have $\boldsymbol{E}(x) = 0$ and thus

$$\big(\boldsymbol{\lambda}(x) - \boldsymbol{\lambda}^\gamma(x)\big) \cdot \big(\boldsymbol{E}^\gamma(x) - \boldsymbol{E}(x)\big) = \big(\boldsymbol{\lambda}(x) - \boldsymbol{\lambda}^\gamma(x)\big) \cdot \boldsymbol{E}^\gamma(x) \leq 0.$$

Finally, for $x \in \mathcal{I} \cap \mathcal{I}_\gamma$ we have $\boldsymbol{E}(x) = 0, g(x)\boldsymbol{E}^\gamma(x) = \gamma^{-1}\boldsymbol{\lambda}^\gamma(x)$ as well as $|\boldsymbol{E}^\gamma(x)| \leq \gamma^{-1}$. This implies

$$\big(\boldsymbol{\lambda}(x) - \boldsymbol{\lambda}^\gamma(x)\big) \cdot \big(\boldsymbol{E}^\gamma(x) - \boldsymbol{E}(x)\big) \leq \frac{1}{\gamma}g(x) - \gamma g(x)|\boldsymbol{E}^\gamma|^2 \leq \frac{1}{\gamma}g(x).$$

After taking all the pointwise estimates above together, (3.20) follows by integration over Ω. Ultimately, we insert $\boldsymbol{v} = \boldsymbol{E}^\gamma - \boldsymbol{E}$ into (3.19) and obtain

$$\underline{\kappa}\|\boldsymbol{E}^\gamma - \boldsymbol{E}\|^2_{\boldsymbol{H}(\mathbf{curl})} \overbrace{\leq}^{(3.1)} a(\boldsymbol{E}^\gamma - \boldsymbol{E}, \boldsymbol{E}^\gamma - \boldsymbol{E}) \overbrace{\leq}^{(3.19)\&(3.20)} \frac{1}{\gamma}\|g\|_{L^1(\Omega)}.$$

Hence, the proof is finished. ∎

We emphasize that the constant in Lemma 3.6 is explicitly given and independent of $\boldsymbol{V}$. That is, the choice of $\boldsymbol{V}$ as a finite element space leaves the constant independent of the discretization parameter. Thus, (3.16) is a well-controlled regularization of (3.11) and we may now dedicate ourselves to the actual computation thereof.

3.2 ▪ The Semismooth Newton Method

With the Moreau–Yosida regularization in (3.11), we face the problem of computing a solution to a nonlinear equation (3.16) involving a composition of the Euclidean norm $|\cdot|$ and the $\max$-operator. Note that for this section, the regularization parameter $\gamma \gg 1$ is fixed. Therefore, we will mostly renounce it in the notation.

Thus, rewrite (3.16) as the nonlinear problem of finding the root of a function $\boldsymbol{\mathcal{W}}\colon \boldsymbol{V} \to \boldsymbol{V}^*$ defined by

$$\boldsymbol{\mathcal{W}}(\boldsymbol{v}) \coloneqq \boldsymbol{A}\boldsymbol{v} + \boldsymbol{Q}(\boldsymbol{v}) - \boldsymbol{F}(\boldsymbol{v}), \tag{3.21}$$

where $\boldsymbol{A}$ is the operator associated with the bilinear form a and $\boldsymbol{Q}$ and $\boldsymbol{F}$ are given by

$$\boldsymbol{Q}(\boldsymbol{v}) \coloneqq (\psi_\gamma'(\boldsymbol{v}), \cdot)_{\boldsymbol{L}^2(\Omega)} \quad \text{and} \quad \boldsymbol{F}(\boldsymbol{v}) \coloneqq \langle \boldsymbol{f}, \cdot \rangle \quad \forall \boldsymbol{v} \in \boldsymbol{V}. \tag{3.22}$$

In general, the standard approach to compute the solution $u^* \in X$ of $K(u^*) = 0$ for a function $K\colon X \to Y$ between two Banach spaces X and Y is the classical Newton method which is described as follows (cf. [50, Chapter 9]): Set $u^0 \in X$ and compute u^{k+1} iteratively by

$$u^{k+1} = u^k - K'(u^k)^{-1} K(u^k). \tag{3.23}$$

From this definition, it becomes apparent that we need strong differentiability properties of K for the method to be well defined. Moreover, in order to guarantee a (local) superlinear convergence, i.e.,

$$\lim_{k\to\infty} \frac{\|u^{k+1} - u^*\|_X}{\|u^k - u^*\|_X} = 0, \tag{3.24}$$

we would have to employ even more assumptions on the operator K and its derivative. Let us specify those and denote $e^k = u^k - u^*$. A simple computation yields

$$\begin{aligned} \|u^{k+1} - u^*\|_X &= \|u^k - K'(u^k)^{-1}K(u^k) - u^*\|_X \\ &= \|K'(u^k)^{-1}\big[K(u^k) - K(u^*) - K'(u^k)(u^k - u^*)\big]\|_X \\ &= \|K'(u^* + e^k)^{-1}\big[K(u^* + e^k) - K(u^*) - K'(u^* + e^k)e^k\big]\|_X \\ &\le \|K'(u^* + e^k)^{-1}\|_{\mathcal{L}(Y,X)} \|K(u^* + e^k) - K(u^*) - K'(u^* + e^k)e^k\|_Y. \end{aligned} \tag{3.25}$$

Hence, (3.24) requires K to be, for instance, Fréchet-differentiable since the weaker property of Gâteaux-differentiability does not suffice (cf. [50]). More general, (3.24) holds if there exists a constant $C > 0$ independent of $k \in \mathbb{N}$ such that

$$\|K'(u^* + e^k)^{-1}\|_{\mathcal{L}(X,Y)} \le C \quad \forall k \in \mathbb{N} \tag{3.26}$$

and

$$\lim_{k\to\infty} \frac{\|K(u^* + e^k) - K(u^*) - K'(u^* + e^k)e^k\|_Y}{\|e^k\|_X} = 0. \tag{3.27}$$

Coming back to our problem, we readily see that the $\max$-operator occurring in (3.16) does not possess a Fréchet-derivative[2] that satisfies (3.26) and (3.27) such that the classical Newton method cannot be applied. Based on this consideration the concept of *Newton (or slant) differentiability* was coined. Let us recall the definition from [37, 88].

[2] Not even close: One may prove that a directional derivative of the nonlinear function in (3.16) exists if and only if the biactive set $\{x \in \Omega : \gamma|\boldsymbol{E}^\gamma(x)| = 1\}$ has zero Lebesgue measure.

Definition 3.7 (Newton-Differentiability). Let X, Y be Banach spaces. A function $F\colon X \to Y$ is called *Newton differentiable* at $x \in X$ if there exists a family of mappings $D_N F\colon X \to \mathcal{L}(X,Y)$ such that

$$\lim_{\|h\|_X \to 0} \frac{\|F(x+h) - F(x) - D_N F(x+h)h\|_Y}{\|h\|_X} = 0.$$

The function $D_N F$ is referred to as a *Newton derivative*.

Note that F does not need to be Fréchet-differentiable to satisfy Definition 3.7. In general, a Newton-derivative is not necessarily unique, meaning there exists a set of Newton-derivatives becoming a singleton if F is Fréchet-differentiable.

This concept goes back to the term of *semismoothness* introduced by Mufflin [126] for real-valued functions and later for vector-valued functions by Qi and Sun [144]. In their definition, they rely on Rademacher's theorem[3] and the generalized Jacobian $\partial F(x)$ in the sense of Clark [49, Chapter 2.6]. For their Newton method an element $V_k \in \partial F(u_k)$ is used as a substitute of the classical derivative in (3.23). In our case, a Newton-derivative according to Definition 3.7 does the job. However, the term *semismooth Newton method* was established regardless of which (non-classical) derivative is used.

Let us quickly note that Definition 3.7 is in fact a generalization of the concept of semismoothness (cf. [126, 144]): If a locally Lipschitz function $K\colon \mathbb{R}^n \to \mathbb{R}^m$ is semismooth at $x \in X$, then any single valued selection of $\partial K(x)$ is a Newton-derivative of K at x (see [37, p. 1204]). Additionally, Rademacher's theorem does not hold true in general Banach spaces which makes the definition from [126, 144] only valid in finite dimensions. The local superlinear convergence of (3.23) with $D_N K$ in place of K' follows from the construction and our preliminary thoughts. We will provide a proof of this result (see [99, Theorem 8.16]).

Theorem 3.8. *Let X, Y be Banach spaces and $K\colon X \to Y$ be Newton-differentiable in $u^* \in X$ with $F(u^*) = 0$ and a Newton-derivative $D_N K(u^*)$. Furthermore, we assume that there exists an open neighbourhood $N(u^*) \subset X$ of u^* and $C > 0$ such that*

$$\|D_N K(u)^{-1}\|_{\mathcal{L}(Y,X)} \leq C \quad \forall u \in N(u^*). \tag{3.28}$$

Then, the semismooth Newton method converges superlinearly in the sense (3.24) *if $\|u^0 - u^*\|_X$ is sufficiently small.*

Proof. The same computation from (3.25) for $K'(u_k)$ replaced with $D_N K(u_k)$ implies that the Newton iterates satisfy

$$\|u^{k+1} - u^*\|_X \leq \|D_N K(u^k)^{-1}\|_{\mathcal{L}(Y,X)} \|K(u^k) - K(u^*) - D_N K(u^k)(u^k - u^*)\|_Y. \tag{3.29}$$

Let $\eta \in (0,1)$ be arbitrary. By applying Definition 3.7 with $x = u^*$ we deduce that there exists $\rho > 0$ such that $B_\rho(x^*) \subset N(u^*)$ and

$$\|K(u^* + h) - K(u^*) - D_N K(x^* + h)h\|_Y \leq \frac{\eta}{C}\|h\|_X \quad \forall h \in X,\ \|h\|_X \leq \rho. \tag{3.30}$$

Consequently, if we choose u^0 such that $\|u^0 - u^*\|_X < \rho$, we deduce by (3.29) and (3.30) for $h = u^0 - u^*$ that

$$\|u^1 - u^*\|_X \leq \eta\|u^0 - u^*\|_X \leq \rho \quad \overset{\text{Induction}}{\Rightarrow} \quad \|u^{k+1} - u^*\|_X \leq \eta\|u^k - u^*\|_X \quad \forall k \in \mathbb{N}.$$

In particular, this yields that the iterates are well defined since $u^k \in B_\rho(u^*) \subset N(u^*)$. Moreover, η was chosen arbitrarily which allows us to take in each step a different $\eta^k \to 0$ as $k \to \infty$. Hence, the convergence is in fact superlinear. ■

[3] Rademacher's theorem states that locally Lipschitz continuous functions in finite dimensional spaces are almost everywhere differentiable.

While our definition provides just enough properties to guarantee superlinear convergence of the semismooth Newton method, the construction of an actual Newton-derivative can be quite involved. In fact, a Newton-derivative is not necessarily linked to the generalized Jacobian $\partial F(x)$ or the directional derivative $F'(x,\cdot)$, meaning a function is Newton-differentiable with a choice rather than a computation of a Newton-derivative (cf. [50]). Regarding an extensive analysis of semismooth Newton methods in the function space for various kinds of constrained optimization problems and variational inequalities we refer to the papers by Hintermüller, Ito, and Kunisch [88–90, 98].

In our case of the (Moreau–Yosida regularized) variational inequality of the second kind (3.16), the nonsmoothness is given by a composition of $|\cdot|$ and the $\max$-operator. It is known that $\max\colon L^r(\Omega) \to L^s(\Omega)$ is Newton-differentiable with Newton-derivative

$$D_N(\max)(w)(x) = \begin{cases} 1 & \text{if } w(x) > 1, \\ 0 & \text{if } w(x) \leq 1 \end{cases} \tag{3.31}$$

if and only if $1 \leq s < r \leq \infty$ (see [88, Proposition 4.1]). An analogous result (see [99, Example 8.1 and Theorem 8.1] for the one-dimensional case) holds for the Euclidean-norm functional $|\cdot|\colon \boldsymbol{L}^r(\Omega) \to L^s(\Omega)$, where a Newton-derivative is given by

$$D_N(|\cdot|)(\boldsymbol{w})(x) = \begin{cases} \dfrac{\boldsymbol{w}(x)}{|\boldsymbol{w}(x)|} & \text{if } |\boldsymbol{w}(x)| > 0, \\ 0 & \text{if } |\boldsymbol{w}(x)| = 0. \end{cases} \tag{3.32}$$

Hence, a chain rule[4] similar to the one for Fréchet-derivatives implies that

$$\boldsymbol{q}\colon \boldsymbol{L}^r(\Omega) \to \boldsymbol{L}^2(\Omega), \quad \boldsymbol{w} \mapsto g\frac{\gamma \boldsymbol{w}}{\max\{1, \gamma|\boldsymbol{w}|\}}$$

is Newton-differentiable for $r > 2$ with a Newton-derivative

$$D_N\boldsymbol{q}(\boldsymbol{w})(x) = \begin{cases} \gamma g(x) I_3 & \text{if } |\boldsymbol{w}(x)| \leq \dfrac{1}{\gamma}, \\ \dfrac{g(x)}{|\boldsymbol{w}(x)|}\left(I_3 - \dfrac{\boldsymbol{w}(x)\boldsymbol{w}^{\mathsf{T}}(x)}{|\boldsymbol{w}(x)|^2}\right) & \text{if } |\boldsymbol{w}(x)| > \dfrac{1}{\gamma}. \end{cases} \tag{3.33}$$

Here, I_3 denotes the 3×3 identity matrix.

Unfortunately, in our case, we cannot expect that the solution $\boldsymbol{E}^\gamma \in \boldsymbol{H}_0(\mathbf{curl})$ of (3.16) satisfies any additional regularity and, in general, there is no embedding

$$\boldsymbol{H}_0(\mathbf{curl}) \hookrightarrow \boldsymbol{L}^r(\Omega)$$

for some $r > 2$. Therefore, we cannot apply the semismooth Newton method in the function space. Under mentioned regularity assumptions on the solution to the regularized problem, De Los Reyes and Hintermüller [58] have developed a unifying framework to solving variational inequalities of the second kind. However, apart from the extensive analysis in the function space, De Los Reyes and González Andrade [56, 57] have studied semismooth Newton method for $H^1(\Omega)$-variational inequalities of the second kind in the finite element space stemming from Bingham fluids. They introduce the finite dimensional analogue of (3.16) based on the assembled forms in $\mathbb{R}^n$. We will proceed slightly different by staying in the elegant structure of the function space setting for the space $\boldsymbol{V}_h$ consisting of Nédélec's first family of edge elements for $h > 0$ (see (2.14)). All of our previous results in this section remain valid for the choice $\boldsymbol{V} = \boldsymbol{V}_h$.

[4] We follow [50, Theorem 9.2] which assumes that the Newton derivatives of the composed function are uniformly bounded in neighborhoods of the respective points. This property is clearly satisfied for (3.31) and (3.32).

Due to the specific structure of its functions and Ω being bounded, it holds that $\boldsymbol{V}_h \subset \boldsymbol{L}^\infty(\Omega)$. For this reason and since all norms on finite-dimensional spaces are equivalent, we have the continuous embedding

$$\boldsymbol{V}_h \hookrightarrow \boldsymbol{L}^p(\Omega) \quad \forall 1 \leq p \leq \infty. \tag{3.34}$$

Now, let us state the semismooth Newton method for (3.16) or equivalently the problem of finding $\boldsymbol{v}_h \in \boldsymbol{V}_h$ such that

$$\boldsymbol{\mathcal{W}}(\boldsymbol{v}_h) = 0, \tag{3.35}$$

where $\boldsymbol{\mathcal{W}}$ is defined in (3.21) for $\boldsymbol{V} = \boldsymbol{V}_h$. As the linear operator $\boldsymbol{A}\colon \boldsymbol{V}_h \to \boldsymbol{V}_h^*$ is Fréchet-differentiable, (3.33) and (3.34) yield that $\boldsymbol{\mathcal{W}}$ is Newton-differentiable and a Newton-derivative is given by

$$D_N\boldsymbol{\mathcal{W}}(\boldsymbol{v}_h) = \boldsymbol{A} + D_N\boldsymbol{q}(\boldsymbol{v}_h) \in \mathcal{L}(\boldsymbol{V}_h, \boldsymbol{V}_h^*). \tag{3.36}$$

for every $\boldsymbol{v}_h \in \boldsymbol{V}_h$. Therefore, in order to perform the Newton-steps at the $(k+1)$th iteration, we have to compute (cf. (3.23))

$$\boldsymbol{\delta}_h^{k+1} = -D_N\boldsymbol{\mathcal{W}}(\boldsymbol{v}_h^k)^{-1}\boldsymbol{\mathcal{W}}(\boldsymbol{v}_h^k) \in \boldsymbol{V}_h \quad \Leftrightarrow \quad D_N\boldsymbol{\mathcal{W}}(\boldsymbol{v}_h^k)\boldsymbol{\delta}_h^{k+1} = -\boldsymbol{\mathcal{W}}(\boldsymbol{v}_h^k),$$

where $\boldsymbol{v}_h^k$ was computed in the kth step. Note that this is equivalent to the problem of finding $\boldsymbol{\delta}_h^{k+1} \in \boldsymbol{V}_h$ such that

$$\begin{aligned} a(\boldsymbol{\delta}_h^{k+1}, \boldsymbol{w}_h) + (D_N\boldsymbol{q}(\boldsymbol{v}_h^k)\boldsymbol{\delta}_h^{k+1}, \boldsymbol{w}_h)_{\boldsymbol{L}^2(\Omega)} \\ = \langle \boldsymbol{f}, \boldsymbol{w}_h\rangle - a(\boldsymbol{v}_h^k, \boldsymbol{w}_h) - \left(g\frac{\gamma \boldsymbol{v}_h^k}{\max\{1, \gamma|\boldsymbol{v}_h^k|}, \boldsymbol{w}_h\right)_{\boldsymbol{L}^2(\Omega)} \quad \forall \boldsymbol{w}_h \in \boldsymbol{V}_h. \end{aligned} \tag{3.37}$$

Before we dedicate ourselves to the well-posedness of (3.37) and the convergence of the semismooth Newton method for (3.16), let us state the actual algorithm:

Algorithm 3.1 Semismooth Newton Method

1: Fix $\gamma \gg 1$, choose $\boldsymbol{v}_h^0 \in \boldsymbol{V}_h$ and set $k = 0$
2: Compute $\boldsymbol{\delta}_h^k$ as the solution to (3.37)
3: Set $\boldsymbol{v}_h^{k+1} = \boldsymbol{v}_h^k + \boldsymbol{\delta}_h^k$
4: Stop, or set $k = k + 1$ and go to step 2.

Theorem 3.9. *The semismooth Newton method for* (3.16) *is well defined, meaning that the map* $D_N\boldsymbol{\mathcal{W}}(\boldsymbol{w}_h) \in \mathcal{L}(\boldsymbol{V}_h, \boldsymbol{V}_h^*)$ *is invertible for every* $\boldsymbol{w}_h \in \boldsymbol{V}_h$. *If* $\boldsymbol{v}_h^0 \in \boldsymbol{V}_h$ *is sufficiently close to the solution* $\boldsymbol{v}_h$ *of* (3.16)*, then Algorithm* 3.1 *converges superlinearly in the sense of* (3.24).

Proof. Fix $\boldsymbol{w}_h \in \boldsymbol{V}_h$. We begin by proving that $\boldsymbol{\mathcal{W}}(\boldsymbol{v})$ is coercive. To this aim, we use (3.33) and obtain that

$$(D_N\boldsymbol{q}(\boldsymbol{w}_h)\boldsymbol{v}_h, \boldsymbol{v}_h)_{\boldsymbol{L}^2(\Omega)} = \int_{\mathcal{I}_\gamma} \gamma g|\boldsymbol{v}_h|^2\,dx + \int_{\mathcal{A}_\gamma} \frac{g}{|\boldsymbol{w}_h|}\left(I_3 - \frac{\boldsymbol{w}_h\boldsymbol{w}_h^\mathsf{T}}{|\boldsymbol{w}_h|^2}\right)\boldsymbol{v}_h \cdot \boldsymbol{v}_h\,dx \geq 0$$

since the matrix valued function $I_3 - \frac{\boldsymbol{w}_h\boldsymbol{w}_h^\mathsf{T}}{|\boldsymbol{w}_h|^2}$ is positive definite almost everywhere in Ω. Therefore, we deduce

$$\langle D_N\boldsymbol{\mathcal{W}}(\boldsymbol{w}_h)\boldsymbol{v}_h, \boldsymbol{v}_h\rangle \geq \langle \boldsymbol{A}\boldsymbol{v}_h, \boldsymbol{v}_h\rangle \overbrace{\geq}^{(3.1)} \underline{\kappa}\|\boldsymbol{v}_h\|^2_{\boldsymbol{H}(\mathbf{curl})} \quad \forall \boldsymbol{v}_h \in \boldsymbol{V}_h.$$

Note that the constant $\underline{\kappa}$ depends only on the parameters ϵ, ν from (3.10). By means of this, we obtain the uniform boundedness of $\|D_N \boldsymbol{\mathcal{W}}(\boldsymbol{w}_h)^{-1}\|_{\mathcal{L}(\boldsymbol{V}_h, \boldsymbol{V}_h^*)}$. In fact, for an arbitrary element $\boldsymbol{\xi} \in \boldsymbol{V}_h^*$, we set $\tilde{\boldsymbol{v}}_h = D_N \boldsymbol{\mathcal{W}}(\boldsymbol{w}_h)^{-1}(\boldsymbol{\xi})$ and deduce

$$\underline{\kappa}\|\tilde{\boldsymbol{v}}_h\|^2_{\boldsymbol{H}(\mathbf{curl})} \leq \langle D_N \boldsymbol{\mathcal{W}}(\boldsymbol{w}_h)\tilde{\boldsymbol{v}}_h, \tilde{\boldsymbol{v}}_h\rangle \leq \|\boldsymbol{\xi}\|_{\boldsymbol{V}_h^*}\|\tilde{\boldsymbol{v}}_h\|_{\boldsymbol{H}(\mathbf{curl})}$$
$$\Rightarrow \quad \|D_N \boldsymbol{\mathcal{W}}(\boldsymbol{w}_h)^{-1}\|_{\mathcal{L}(\boldsymbol{V}_h, \boldsymbol{V}_h^*)} \leq \underline{\kappa}^{-1}.$$

Thus, we have fulfilled all requirements to apply Theorem 3.8 which yields the local superlinear convergence of Algorithm 3.1 and finishes the proof. ∎

3.3 ▪ Hyperbolic Maxwell Variational Inequalities

For our analysis of (1.9), we require a set of assumptions on the material parameters $\Omega, \epsilon, \mu, j_c$ and the given data $\boldsymbol{f}, \theta$. They are stated in their *minimal* form below. Throughout this thesis, they may be adjusted depending on the specific application.

Assumption 3.10 (regularity assumptions on the material parameters and the given data).

(A3.1) The holdall-domain $\Omega \subset \mathbb{R}^3$ is a bounded polyhedral domain with a connected Lipschitz-boundary $\partial\Omega$. The domain of the superconductor $\Omega_{\text{sc}} \subset \Omega$ is a Lipschitz domain.

(A3.2) The material parameters $\epsilon, \mu \in L^\infty(\Omega) \cup L^\infty(\Omega, \mathbb{R}^{3\times 3})$ are assumed to be symmetric and uniformly positive definite, i.e., there exist positive constants $\underline{\epsilon}, \underline{\mu} \in \mathbb{R}_{>0}$ such that

$$\xi^T \epsilon(x)\xi \geq \underline{\epsilon}|\xi|^2 \quad \text{and} \quad \xi^T \mu(x)\xi \geq \underline{\mu}|\xi|^2 \quad \text{for a.e. } x \in \Omega \text{ and all } \xi \in \mathbb{R}^3.$$

Thus, for $\nu := \mu^{-1} \in L^\infty(\Omega) \cup L^\infty(\Omega, \mathbb{R}^{3\times 3})$ there exists $\underline{\nu} > 0$ such that

$$\xi^{\mathsf{T}} \nu(x)\xi \geq \underline{\nu}|\xi|^2 \quad \text{for a.e. } x \in \Omega \text{ and all } \xi \in \mathbb{R}^3.$$

(A3.3) For every $y \in \mathbb{R}$, $j_c(\cdot, y)\colon \Omega \to \mathbb{R}$ is Lebesgue-measurable and nonnegative.

(A3.4) For every $M > 0$, there exists a constant $C(M) > 0$ such that

$$0 \leq j_c(x, y) \leq C(M)$$

for a.e. $x \in \Omega$ and every $y \in [-M, M]$.

(A3.5) For every $M > 0$, there exists a constant $L(M) > 0$ such that

$$|j_c(x, y) - j_c(x, z)| \leq L(M)|y - z|$$

for a.e. $x \in \Omega$ and every $y, z \in [-M, M]$.

(A3.6) Suppose that

$$\boldsymbol{f} \in \mathcal{C}^{0,1}([0, T], \boldsymbol{L}^2(\Omega)) \quad \text{and} \quad \theta \in \mathcal{C}^{0,1}([0, T], L^2(\Omega)) \cap \mathcal{C}([0, T], L^\infty(\Omega)).$$

From (2.3) we recall that the assumption of the connected boundary of Ω (A3.1) guarantees that

$$K_N(\Omega) = \{\boldsymbol{v} \in \boldsymbol{X}_N(\Omega) \,:\, \mathbf{curl}\, \boldsymbol{v} = 0, \operatorname{div} \boldsymbol{v} = 0\} = \{0\}.$$

This is necessary for the application of a (discrete) Poincaré–Friedrichs-type inequality (see (2.4) and (2.17)). As for this section, it is not mandatory that Ω is polyhedral. However, in Chapter 4, this assumption is indispensable. Moreover, let us remark that the local Lipschitz property (A3.5) and the local boundedness property (A3.4) for the temperature dependence in the critical current are justified by experimental measurements reported in [7, 62]. However, in contrast to (A3.1) and (A3.3)

to (A3.5), from a physical point of view, Bean's law (B1) to (B3) is not suitable for matrix-valued material parameters ϵ, μ. Due to (B3), the conductivity σ occurring in Ohm's law $\boldsymbol{J} = \sigma \boldsymbol{E} + \boldsymbol{f}$ has to be scalar-valued. This cannot be guaranteed if we consider matrix-valued material parameters ϵ, μ. However, our mathematical theory is not affected by this issue. Therefore, we retain the more general assumption (A3.2) but keep this fact in mind for the numerical experiments.

Now, let us derive a *variational formulation* of (1.9). Therefore, we show that the Maxwell system (1.9) is equivalent to a hyperbolic mixed Maxwell variational inequality of the second kind. This formulation will later be the foundation for our numerical analysis. The variational inequality in question comes in the form of finding

$$(\boldsymbol{E}, \boldsymbol{H}) \in W^{1,\infty}\big((0,T), \boldsymbol{L}^2_\epsilon(\Omega) \times \boldsymbol{L}^2_\mu(\Omega)\big) \times L^\infty\big((0,T), \boldsymbol{H}_0(\mathbf{curl}) \times \boldsymbol{L}^2_\mu(\Omega)\big)$$

such that

$$\text{(VI)} \qquad \begin{cases} \displaystyle\int_\Omega \epsilon \partial_t \boldsymbol{E}(t) \cdot (\boldsymbol{v} - \boldsymbol{E}(t)) + \mu \partial_t \boldsymbol{H}(t) \cdot (\boldsymbol{w} - \boldsymbol{H}(t))\, dx \\ \qquad + \displaystyle\int_\Omega \mathbf{curl}\, \boldsymbol{E}(t) \cdot \boldsymbol{w} - \boldsymbol{H}(t) \cdot \mathbf{curl}\, \boldsymbol{v}\, dx \\ \qquad + \varphi(t, \boldsymbol{v}) - \varphi(t, \boldsymbol{E}(t)) \geq \displaystyle\int_\Omega \boldsymbol{f}(t) \cdot (\boldsymbol{v} - \boldsymbol{E}(t))\, dx \\ \quad \text{for a.e. } t \in (0,T) \text{ and every } (\boldsymbol{v}, \boldsymbol{w}) \in \boldsymbol{H}_0(\mathbf{curl}) \times \boldsymbol{L}^2(\Omega), \\ \quad (\boldsymbol{E}(0), \boldsymbol{H}(0)) = (\boldsymbol{E}_0, \boldsymbol{H}_0), \end{cases}$$

where the nonsmooth L^1-type functional $\varphi\colon [0,T] \times \boldsymbol{L}^1(\Omega) \to \mathbb{R}$ is given by

$$\varphi(t, \boldsymbol{v}) \coloneqq \int_\Omega g(x,t) |\boldsymbol{v}(x)|\, dx \overset{(1.7)}{=} \int_{\Omega_{\mathrm{sc}}} j_c(x, \theta(t)) |\boldsymbol{v}(x)|\, dx.$$

In fact, this idea goes back to Yousept who established a similar result [180, Theorem 3.1] in the case of a constant critical current density $j_c \in \mathbb{R}^+$. He takes up a well-posedness result for (1.9) by Jochmann [102] and shows that the corresponding solution is also the unique solution of (VI). Jochmann has used the maximal monotone structure imposed by (1.8) along with the Yosida regularization technique and classical results from the semigroup theory to prove existence of a strong solution to (1.9). For convenience of the reader, we specify the meaning of *strong solution to* (1.9) (cf. [102, Section 3]).

Definition 3.11. A strong solution to (1.9) is a tuple $(\boldsymbol{E}, \boldsymbol{H}, \boldsymbol{J})$ with

$$(\boldsymbol{E}, \boldsymbol{H}) \in W^{1,\infty}((0,T), \boldsymbol{L}^2_\epsilon(\Omega) \times \boldsymbol{L}^2_\mu(\Omega)) \times L^\infty((0,T), \boldsymbol{H}_0(\mathbf{curl}) \times \boldsymbol{H}(\mathbf{curl}))$$

and $\boldsymbol{J} \in L^\infty((0,T), L^\infty(\Omega))$ satisfying (1.8) and

$$(3.38) \qquad \begin{cases} \epsilon \partial_t \boldsymbol{E}(t) - \mathbf{curl}\, \boldsymbol{H}(t) + \boldsymbol{J}(t) = \boldsymbol{f}(t) & \text{for a.e. } t \in (0,T) \\ \mu \partial_t \boldsymbol{H}(t) + \mathbf{curl}\, \boldsymbol{E}(t) = 0 & \text{for a.e. } t \in (0,T) \\ (\boldsymbol{E}(0), \boldsymbol{H}(0)) = (\boldsymbol{E}_0, \boldsymbol{H}_0). \end{cases}$$

As a generalization of Jochmann's results, we mention the recent studies by Yousept [182] which prove the well-posedness of (VI) with a general time-independent nonlinearity – meaning that $\varphi(t, \boldsymbol{v})$ in (VI) is replaced by some proper, convex and lower semicontinuous function

$$\psi\colon \boldsymbol{X} \coloneqq \boldsymbol{L}^2_\epsilon(\Omega) \times \boldsymbol{L}^2_\mu(\Omega) \to \overline{\mathbb{R}} \coloneqq \mathbb{R} \cup \{+\infty\}.$$

In contrast to [102], Yousept employs a local boundedness assumption for the subdifferential of ψ (cf. [182, Assumption 3.1]) replacing the specific L^1-structure. Moreover, a weaker well-posedness

result is established for functionals that do not satisfy the local boundedness assumption. Thereby he includes indicator functionals.

However, in our case of a time-dependent critical current density j_c all the previously mentioned results from [102, 182] are no longer applicable. Thus, we choose a different approach where the analysis relies on discretization instead of regularization. We use a fully discrete approximation to establish the well-posedness of (VI) in Chapter 4. Now, let us prove the equivalence of (1.9) and (VI) under $\boldsymbol{H}(\mathbf{curl})$ regularity of the magnetic field $\boldsymbol{H}$ in the following proposition.

Proposition 3.12. *Let Assumption* 3.10 *hold. If a tuple* $(\boldsymbol{E}, \boldsymbol{H}, \boldsymbol{J})$ *is a strong solution to* (1.9)*, then* $(\boldsymbol{E}, \boldsymbol{H})$ *solves* (VI)*. On the other hand, if* $(\boldsymbol{E}, \boldsymbol{H})$ *solves* (VI) *with the additional regularity property*

$$\boldsymbol{H} \in L^\infty\big((0,T), \boldsymbol{H}(\mathbf{curl})\big), \tag{3.39}$$

then there exists $\boldsymbol{J} \in L^\infty((0,T), L^\infty(\Omega))$ *such that* $(\boldsymbol{E}, \boldsymbol{H}, \boldsymbol{J})$ *is a strong solution of* (1.9)*.*

Proof. Let $(\boldsymbol{E}, \boldsymbol{H}, \boldsymbol{J})$ be a strong solution to (1.9) according to Definition 3.11. After multiplication of the first equation in (1.9) with $\boldsymbol{v} - \boldsymbol{E}(t)$ and the second equation with $\boldsymbol{w} - \boldsymbol{H}(t)$ for some $(\boldsymbol{v}, \boldsymbol{w}) \in \boldsymbol{H}_0(\mathbf{curl}) \times \boldsymbol{L}^2(\Omega)$, integration over Ω and summing of the resulting equations yields

$$\begin{aligned} &\int_\Omega \epsilon \partial_t \boldsymbol{E}(t) \cdot (\boldsymbol{v} - \boldsymbol{E}(t)) + \mu \boldsymbol{H}(t) \cdot (\boldsymbol{w} - \boldsymbol{H}(t))\, dx \\ &\quad + \int_\Omega \mathbf{curl}\, \boldsymbol{E}(t) \cdot (\boldsymbol{w} - \boldsymbol{H}(t)) - \mathbf{curl}\, \boldsymbol{H}(t) \cdot (\boldsymbol{v} - \boldsymbol{E}(t))\, dx \\ &\quad + \int_\Omega \boldsymbol{J}(t) \cdot (\boldsymbol{v} - \boldsymbol{E}(t))\, dx = \int_\Omega \boldsymbol{f}(t) \cdot (\boldsymbol{v} - \boldsymbol{E}(t))\, dx \end{aligned} \tag{3.40}$$

for almost every $t \in (0,T)$. Now, the integration by parts formula for $\boldsymbol{H}_0(\mathbf{curl})$ functions (see (2.1)) implies that (3.40) is equivalent to

$$\begin{aligned} &\int_\Omega \epsilon \partial_t \boldsymbol{E}(t) \cdot (\boldsymbol{v} - \boldsymbol{E}(t)) + \mu \boldsymbol{H}(t) \cdot (\boldsymbol{w} - \boldsymbol{H}(t))\, dx \\ &\quad + \int_\Omega \mathbf{curl}\, \boldsymbol{E}(t) \cdot \boldsymbol{w} - \boldsymbol{H}(t) \cdot \mathbf{curl}\, \boldsymbol{v}\, dx \\ &\quad + \int_\Omega \boldsymbol{J}(t) \cdot (\boldsymbol{v} - \boldsymbol{E}(t))\, dx = \int_\Omega \boldsymbol{f}(t) \cdot (\boldsymbol{v} - \boldsymbol{E}(t))\, dx. \end{aligned} \tag{3.41}$$

If we take into account that $\boldsymbol{J}$ fulfills (1.8), we deduce that

$$\begin{aligned} \int_\Omega \boldsymbol{J}(t) \cdot (\boldsymbol{v} - \boldsymbol{E}(t))\, dx &= \int_\Omega \boldsymbol{J}(t) \cdot \boldsymbol{v}\, dx - \int_\Omega \boldsymbol{J}(t) \cdot \boldsymbol{E}(t)\, dx \\ &\leq \int_\Omega g(t)|\boldsymbol{v}|\, dx - \int_\Omega g(t)|\boldsymbol{E}(t)|\, dx = \varphi(t, \boldsymbol{v}) - \varphi(t, \boldsymbol{E}(t)). \end{aligned} \tag{3.42}$$

Hence, inserting (3.42) into (3.41), implies that $(\boldsymbol{E}, \boldsymbol{H})$ is a solution to (VI).

It remains to prove that we can construct a strong solution to (1.9) from a solution to (VI). For the sake of a short notation and by means of (3.39), we denote the solution to (VI) again by

$$(\boldsymbol{E}, \boldsymbol{H}) \in W^{1,\infty}((0,T), \boldsymbol{L}^2_\epsilon(\Omega) \times \boldsymbol{L}^2_\mu(\Omega)) \times L^\infty((0,T), \boldsymbol{H}_0(\mathbf{curl}) \times \boldsymbol{H}(\mathbf{curl}))$$

First, we observe that we can recover Faraday's law

$$\mu \partial_t \boldsymbol{H}(t) + \mathbf{curl}\, \boldsymbol{E}(t) = 0 \tag{3.43}$$

for almost every $t \in (0,T)$ directly from (VI). In fact, by inserting $\boldsymbol{v} = \boldsymbol{E}(t)$ into (VI) we obtain by (2.1) that

$$\int_\Omega (\mu \partial_t \boldsymbol{H}(t) + \mathbf{curl}\, \boldsymbol{E}(t)) \cdot (\boldsymbol{w} - \boldsymbol{H}(t))\, dx \geq 0 \quad \forall \boldsymbol{w} \in \boldsymbol{L}^2(\Omega)$$

which implies (3.43). On the other hand, keeping (3.39) in mind, inserting (3.43) back into (VI) yields after some simple rearrangements involving (2.1) that

$$\int_\Omega (\underbrace{\boldsymbol{f}(t) - \epsilon \partial_t \boldsymbol{E}(t) + \mathbf{curl}\, \boldsymbol{H}(t)}_{=:\boldsymbol{J}(t)}) \cdot (\boldsymbol{v} - \boldsymbol{E}(t))\, dx \leq \varphi(t,\boldsymbol{v}) - \varphi(t,\boldsymbol{E}(t)) \quad \forall \boldsymbol{v} \in \boldsymbol{H}_0(\mathbf{curl}). \tag{3.44}$$

Indeed, (3.44) holds for all $\boldsymbol{v} \in \boldsymbol{L}^2(\Omega)$ due to the density of $\boldsymbol{H}_0(\mathbf{curl}) \subset \boldsymbol{L}^2(\Omega)$. Thus, by the definition of $\boldsymbol{J}$ and (3.43), we deduce that $(\boldsymbol{E}, \boldsymbol{H}, \boldsymbol{J})$ satisfies

$$\begin{aligned} \epsilon \partial_t \boldsymbol{E}(t) - \mathbf{curl}\, \boldsymbol{H}(t) + \boldsymbol{J}(t) &= \boldsymbol{f}(t) \quad \text{for a.e. } t \in (0,T), \\ \mu \partial_t \boldsymbol{H}(t) + \mathbf{curl}\, \boldsymbol{E}(t) &= 0 \qquad\quad \text{for a.e. } t \in (0,T). \end{aligned}$$

Together with the boundary and initial conditions, it only remains to verify that $\boldsymbol{J}$ satisfies (1.8). Thus, we may insert $\boldsymbol{v} = 0$ and $\boldsymbol{v} = 2\boldsymbol{E}(t)$ into (3.44). This yields

$$\int_\Omega \boldsymbol{J}(t) \cdot \boldsymbol{E}(t)\, dx = \varphi(t, \boldsymbol{E}(t)). \tag{3.45}$$

Moreover, by adding (3.44) and (3.45) it follows that

$$\int_\Omega \boldsymbol{J}(t) \cdot \boldsymbol{v}\, dx \leq \varphi(t,\boldsymbol{v}) = \int_\Omega g(t) |\boldsymbol{v}|\, dx \quad \forall \boldsymbol{v} \in \boldsymbol{L}^2(\Omega). \tag{3.46}$$

If we assume that there exists $\omega \subset \Omega$ with $|\omega| \neq 0$ such that $|\boldsymbol{J}(t)| > g(t) \geq 0$ for almost every $x \in \omega$, then we may insert $\boldsymbol{v} = \chi_\omega \frac{\boldsymbol{J}(t)}{|\boldsymbol{J}(t)|} \in \boldsymbol{L}^2(\Omega)$ in (3.46) and obtain a contradiction right away. Hence,

$$|\boldsymbol{J}(t)| \leq g(t) \quad \text{for a.e. } t \in (0,T).$$

By means of this we obtain from (3.45) that

$$0 = \int_\Omega g(t)|\boldsymbol{E}(t)| - \boldsymbol{J}(t) \cdot \boldsymbol{E}(t)\, dx \quad \Rightarrow \quad \boldsymbol{J}(t) \cdot \boldsymbol{E}(t) = g(t)|\boldsymbol{E}(t)|. \tag{3.47}$$

Therefore, $(\boldsymbol{E}, \boldsymbol{H}, \boldsymbol{J})$ is a strong solution of (1.9) in the sense of Definition 3.11. ■

Up to this point, we have only considered the electric field $\boldsymbol{E}$ and the magnetic field $\boldsymbol{H}$ as unknown variables in our system (VI). However, as we are interested in studying a fully discretization thereof, it is more convenient to use the so called $\boldsymbol{E}$-$\boldsymbol{B}$ formulation, where $\boldsymbol{B}$ stands for the magnetic induction and is given by the constitutive relation (see section 1.2)

$$\boldsymbol{B} = \mu \boldsymbol{H}. \tag{3.48}$$

We also refer to Makridakis and Monk [124] who introduced the $\boldsymbol{E}$-$\boldsymbol{B}$ formulation for their fully discrete approximation of the classical Maxwell's equations. The benefit becomes visible when rewriting Faraday's law by means of (3.48) using the fact that μ is independent of t (see (A3.2)). For almost every $t \in (0,T)$, it holds that

$$\mu \partial_t \boldsymbol{H}(t) + \mathbf{curl}\, \boldsymbol{E}(t) = 0 \quad \Leftrightarrow \quad \partial_t \boldsymbol{B}(t) + \mathbf{curl}\, \boldsymbol{E}(t) = 0.$$

Thus, the computation of $\partial_t \boldsymbol{B}$ does no longer involve μ. The same remains true for discretizations thereof. Therefore, this formulation is more convenient for the spatial discretization in the case of μ being *not* constant with respect to x in our fully discrete approximation.

Finally, using (3.48) in (VI) and replacing μ^{-1} by ν, we arrive at the variational problem of finding

$$(\boldsymbol{E}, \boldsymbol{B}) \in W^{1,\infty}\big((0,T), \boldsymbol{L}^2_\epsilon(\Omega) \times \boldsymbol{L}^2_\nu(\Omega)\big) \cap L^\infty\big((0,T), \boldsymbol{H}_0(\mathbf{curl}) \times \boldsymbol{L}^2_\nu(\Omega)\big)$$

such that

$$\text{(VI)} \qquad \begin{cases} \displaystyle\int_\Omega \epsilon \partial_t \boldsymbol{E}(t) \cdot (\boldsymbol{v} - \boldsymbol{E}(t)) + \nu \partial_t \boldsymbol{B}(t) \cdot (\boldsymbol{w} - \boldsymbol{H}(t))\, dx \\ \quad + \displaystyle\int_\Omega \nu\, \mathbf{curl}\, \boldsymbol{E}(t) \cdot \boldsymbol{w} - \nu \boldsymbol{B}(t) \cdot \mathbf{curl}\, \boldsymbol{v}\, dx \\ \quad + \varphi(t, \boldsymbol{v}) - \varphi(t, \boldsymbol{E}(t)) \geq \displaystyle\int_\Omega \boldsymbol{f}(t) \cdot (\boldsymbol{v} - \boldsymbol{E}(t))\, dx \\ \quad \text{for a.e. } t \in (0,T) \text{ and every } (\boldsymbol{v}, \boldsymbol{w}) \in \boldsymbol{H}_0(\mathbf{curl}) \times \boldsymbol{L}^2(\Omega), \\ \quad (\boldsymbol{E}(0), \boldsymbol{B}(0)) = (\boldsymbol{E}_0, \boldsymbol{B}_0). \end{cases}$$

For the remainder of this thesis, we will focus on this weak formulation of (1.9).

Part II

Numerical Analysis

Chapter 4

Numerical Analysis of Hyperbolic Maxwell Variational Inequalities

We have already noted in section 3.3 that all contributions proving the well-posedness of hyperbolic Maxwell's variational inequalities of the form (VI) use regularization strategies and potent arguments from the semigroup theory. Unfortunately, their results are not applicable in our case since all of them neglect the temperature dependence in the superconductor. These effects however have to be considered in a physically reasonable model due to the nature of superconductivity itself (cf. Figure 1.4). We recall that superconducting effects occur solely when the operating temperature is below a critical value. Otherwise, the critical current density j_c drops to zero and the system (1.9) reduces to the classical Maxwell's equations (1.6).

Our approach to study (VI) differs from the previously mentioned methods as we rely on *discretization* instead of *regularization*. Thus, this chapter is focused on a fully discrete scheme of (VI) consisting of space and time discretizations and the analysis thereof. Regarding the numerical analysis of Bean's critical state model in combination with the Maxwell's equations, the existing literature is mainly focused on the *eddy current approximation*. That is, if the displacement current $\epsilon\partial_t \boldsymbol{E}$ is small compared to $-\mathbf{curl}\,\boldsymbol{H} + \boldsymbol{J}$, then $\epsilon\partial_t \boldsymbol{E}$ is neglected. In the case of magnetic field dependence in the critical current $j_c = j_c(\boldsymbol{H})$ one obtains a parabolic quasi-variational inequality (QVI) of the first (or obstacle) kind. Prigozhin [141, 142] was the first, who introduced and analyzed this formulation. Barrett and Prigozhin [15] analyzed it in a scalar two-dimensional (2D) setting and its dual formulation. The finite element analysis for the associated parabolic variational inequality in a 2D setting was investigated in [66] (see also [67] for a similar 2D model using an $\boldsymbol{E}$-$\boldsymbol{J}$-formulation). Furthermore, the numerical analysis for the three-dimensional (3D) setting was studied by Elliot and Kashima in [65]. Recent results on the numerical analysis for the parabolic QVI in a 2D setting were obtained in [16].

From a physical point of view, the eddy current approximation excludes many modern physical phenomena – for instance all applications of high-frequency physics. The first work that studied Bean's critical state model with the *full* Maxwell's equations by means of a semi-discrete Ritz-Galerkin approximation was [180]. This chapter roughly coincides – small changes and additional explanations notwithstanding – with the publication [171]. Henceforth, quotes from this work will be dispensed. To the best of the author's knowledge, [171] is the only present study of (VI) where the temperature dependence is considered.

In upcoming chapters, we will very much rely on a structure that is induced by a time discretization of (VI). Therefore, let us now apply the implicit Euler method to (VI). To this aim, fix $N \in \mathbb{N}$ and define an equidistant partition of $[0, T]$ in the following way:

$$\tau := \frac{T}{N}, \quad 0 = t_0 < t_1 < \cdots < t_N = T \quad \text{with} \quad t_n := n\tau$$

for all $n \in \{0, \dots, N\}$. Furthermore, we define

$$\boldsymbol{f}^n := \boldsymbol{f}(t_n) \in \boldsymbol{L}^2(\Omega), \quad \varphi^n(\boldsymbol{v}) := \int_\Omega j_c(x, \theta(x, t_n))|\boldsymbol{v}(x)|\, dx \quad \forall n \in \{0, \dots, N\}.$$

Thus, we introduce a time-discrete approximation of (VI) as follows:

$$(\mathrm{VI}_N) \qquad \begin{cases} \displaystyle\int_\Omega \epsilon \delta \boldsymbol{E}^n \cdot (\boldsymbol{v} - \boldsymbol{E}^n) + \nu \delta \boldsymbol{B}^n \cdot (\boldsymbol{w} - \boldsymbol{B}^n)\, dx \\ \quad \displaystyle + \int_\Omega \nu\, \mathbf{curl}\, \boldsymbol{E}^n \cdot \boldsymbol{w} - \nu \boldsymbol{B}^n \cdot \mathbf{curl}\, \boldsymbol{v}\, dx \\ \quad + \varphi^n(\boldsymbol{v}) - \varphi^n(\boldsymbol{E}^n) \geq \displaystyle\int_\Omega \boldsymbol{f}^n \cdot (\boldsymbol{v} - \boldsymbol{E}^n)\, dx \\ \quad \text{for every } (\boldsymbol{v}, \boldsymbol{w}) \in \boldsymbol{H}_0(\mathbf{curl}) \times \boldsymbol{L}^2(\Omega) \text{ and } n \in \{1, \dots, N\} \\ \quad (\boldsymbol{E}^0, \boldsymbol{B}^0) = (\boldsymbol{E}_0, \boldsymbol{B}_0), \end{cases}$$

where

$$\delta \boldsymbol{E}^n := \frac{\boldsymbol{E}^n - \boldsymbol{E}^{n-1}}{\tau} \quad \text{and} \quad \delta \boldsymbol{B}^n := \frac{\boldsymbol{B}^n - \boldsymbol{B}^{n-1}}{\tau}.$$

The discrete problem (VI_N) – although still infinite-dimensional – has the advantage over (VI) that we are now able to decouple the mixed variational inequality for every $n \in \{1, \dots, N\}$. Therefore, fix $n \in \{1, \dots, N\}$ and assume that $(\boldsymbol{E}^{n-1}, \boldsymbol{B}^{n-1}) \in \boldsymbol{H}_0(\mathbf{curl}) \times \boldsymbol{L}^2_\nu(\Omega)$ is already computed. Inserting $\boldsymbol{v} = \boldsymbol{E}^n \in \boldsymbol{H}_0(\mathbf{curl})$ yields an explicit formula for $\boldsymbol{B}^n$ depending on $\boldsymbol{E}^n$:

$$\delta \boldsymbol{B}^n = -\,\mathbf{curl}\, \boldsymbol{E}^n \quad \Leftrightarrow \quad \boldsymbol{B}^n = \boldsymbol{B}^{n-1} - \tau\, \mathbf{curl}\, \boldsymbol{E}^n. \tag{4.1}$$

Thereafter, we test (VI_N) with $\boldsymbol{w} = \boldsymbol{B}^n$ and employ (4.1) to obtain an elliptic **curl-curl** variational inequality of the form

$$a(\boldsymbol{E}^n, \boldsymbol{v} - \boldsymbol{E}^n) + \varphi^n(\boldsymbol{v}) - \varphi^n(\boldsymbol{E}^n) \geq \langle \tilde{\boldsymbol{f}}^n, \boldsymbol{v} - \boldsymbol{E}^n \rangle \quad \forall \boldsymbol{v} \in \boldsymbol{H}_0(\mathbf{curl}), \tag{4.2}$$

with the continuous and coercive bilinear form $a\colon \boldsymbol{H}_0(\mathbf{curl}) \times \boldsymbol{H}_0(\mathbf{curl}) \to \mathbb{R}$ defined by

$$a(\boldsymbol{u}, \boldsymbol{v}) := \int_\Omega \tau^{-1} \epsilon \boldsymbol{u} \cdot \boldsymbol{v}\, dx + \int_\Omega \tau \nu\, \mathbf{curl}\, \boldsymbol{u} \cdot \mathbf{curl}\, \boldsymbol{v}\, dx \quad \forall \boldsymbol{u}, \boldsymbol{v} \in \boldsymbol{H}_0(\mathbf{curl})$$

and the right-hand side $\tilde{\boldsymbol{f}}^n \in \boldsymbol{H}_0(\mathbf{curl})^*$ by

$$\langle \tilde{\boldsymbol{f}}^n, \boldsymbol{v} \rangle := \int_\Omega (\boldsymbol{f}^n + \tau^{-1} \epsilon \boldsymbol{E}^{n-1}) \cdot \boldsymbol{v}\, dx + \int_\Omega \nu \boldsymbol{B}^{n-1} \cdot \mathbf{curl}\, \boldsymbol{v}\, dx \quad \forall \boldsymbol{v} \in \boldsymbol{H}_0(\mathbf{curl}).$$

We readily see that $\tilde{\boldsymbol{f}}^n$ only depends on quantities that are computed in the $(n-1)$th step or known priorily. Hence, the well-posedness of (4.2) is covered by Theorem 3.1. By inductively applying Theorem 3.1 to (4.2) and using (4.1), we obtain $\{(\boldsymbol{E}^n, \boldsymbol{B}^n)\}_{n=1}^N \subset \boldsymbol{H}_0(\mathbf{curl}) \times \boldsymbol{L}^2_\nu(\Omega)$ that solves (VI_N). The formulas (4.1) and (4.2) will be of crucial significance throughout this thesis.

The remainder of this chapter is devoted to the *fully* discrete analysis of (VI). Therefore, we employ a mixed finite element method consisting of Nédélec's edge elements for $\boldsymbol{E}$ and piecewise constant elements for $\boldsymbol{B}$ (cf. section 2.2) on top of the time-discrete approximation (VI_N). Furthermore, we consider finite element approximations for the initial data $(\boldsymbol{E}_0, \boldsymbol{B}_0)$ by solving an elliptic **curl-curl** variational inequality (4.4). This specific setting enables us to prove the well-posedness of ($\mathrm{VI}_{N,h}$) with a magnetic induction regularity in $\mathbf{curl}\, \boldsymbol{V}_h$ (see Theorem 4.4), where $\boldsymbol{V}_h$ denotes the

Nédélec edge element space. Our main goal is the uniform convergence of ($\mathrm{VI}_{N,h}$) towards (VI) (Theorem 4.10), which in particular yields the global well-posedness for (VI). The proof follows some consecutive steps: First of all, by the compatibility system (4.4) and exploiting the regularity properties of the critical current density and the given data, we derive stability estimates for the zero-order and first-order terms of the fully discrete solution (Lemmas 4.6 and 4.7). These a priori estimates together with the mathematical properties of φ allow us to extract weakly-* converging subsequences whose limits turn out to solve the original variational inequality (Theorem 4.8). In particular, this implies the well-posedness of (VI). Hereafter, we use the properties of the operator $\boldsymbol{\Phi}_h\colon \boldsymbol{H}_0(\mathbf{curl}) \to \boldsymbol{V}_h$ introduced in Definition 2.8 in combination with the magnetic induction regularity in $\mathbf{curl}\, \boldsymbol{V}_h$ and the weak-* convergence result to complete the proof of the uniform convergence. The final part of the paper is devoted to the a priori error analysis for the proposed fully discrete scheme ($\mathrm{VI}_{N,h}$). Under a low Sobolev regularity assumption on the electric field $\boldsymbol{E}$ of (VI), we derive a priori estimates for the error between the fully discrete solution and the continuous one (Theorem 4.13). The proof is based on sharp error estimate Corollary 2.9 for $\boldsymbol{\Phi}_h\colon \boldsymbol{H}_0(\mathbf{curl}) \to \boldsymbol{V}_h$. Last but not least, we refer the reader to some existing works [45, 46, 116, 117, 124] concerning fully discrete approximations for the time-dependent Maxwell's equations.

4.1 ▪ Fully Discrete Scheme

Let $\boldsymbol{V}_h$ and $\boldsymbol{W}_h$ denote the finite element space of Nédélec's first family of edge elements and piecewise constant functions (see (2.14) and (2.15)) which satisfy $\mathbf{curl}\, \boldsymbol{V}_h \subset \boldsymbol{W}_h$.

Thus, we now propose the following fully discrete scheme to (VI) based on (VI_N):

$$
(\mathrm{VI}_{N,h}) \qquad \begin{cases} \displaystyle\int_\Omega \epsilon \delta \boldsymbol{E}_h^n \cdot (\boldsymbol{v}_h - \boldsymbol{E}_h^n) + \nu \delta \boldsymbol{B}_h^n \cdot (\boldsymbol{w}_h - \boldsymbol{B}_h^n)\, dx \\ \qquad + \displaystyle\int_\Omega \nu\, \mathbf{curl}\, \boldsymbol{E}_h^n \cdot \boldsymbol{w}_h - \nu \boldsymbol{B}_h^n \cdot \mathbf{curl}\, \boldsymbol{v}_h\, dx \\ \qquad + \varphi^n(\boldsymbol{v}_h) - \varphi^n(\boldsymbol{E}_h^n) \geq \displaystyle\int_\Omega \boldsymbol{f}^n \cdot (\boldsymbol{v}_h - \boldsymbol{E}_h^n)\, dx \\ \quad \text{for every } (\boldsymbol{v}_h, \boldsymbol{w}_h) \in \boldsymbol{V}_h \times \boldsymbol{W}_h \text{ and } n \in \{1, \dots, N\} \\ \quad (\boldsymbol{E}_h^0, \boldsymbol{B}_h^0) = (\boldsymbol{E}_{0h}, \boldsymbol{B}_{0h}), \end{cases}
$$

where

$$
\delta \boldsymbol{E}_h^n \coloneqq \frac{\boldsymbol{E}_h^n - \boldsymbol{E}_h^{n-1}}{\tau} \quad \text{and} \quad \delta \boldsymbol{B}_h^n \coloneqq \frac{\boldsymbol{B}_h^n - \boldsymbol{B}_h^{n-1}}{\tau} \quad \forall n \in \{1, \dots, N\},
$$

Moreover, $(\boldsymbol{E}_{0h}, \boldsymbol{B}_{0h}) \in \boldsymbol{V}_h \times \boldsymbol{W}_h$ denotes a suitable finite element approximation of the initial data $(\boldsymbol{E}_0, \boldsymbol{B}_0)$. Before we construct $(\boldsymbol{E}_{0h}, \boldsymbol{B}_{0h})$ we have to state the assumption on $(\boldsymbol{E}_0, \boldsymbol{B}_0)$.

Assumption 4.1 (regularity assumption on the initial data).
(A4.7) The initial data $(\boldsymbol{E}_0, \boldsymbol{B}_0) \in \boldsymbol{H}_0(\mathbf{curl}) \times \boldsymbol{H}_0(\mathrm{div}{=}0)$ fulfills the compatibility system

$$
(4.3) \qquad \begin{cases} \displaystyle\int_\Omega \epsilon \boldsymbol{E}_0 \cdot (\boldsymbol{v} - \boldsymbol{E}_0) + \nu \boldsymbol{B}_0 \cdot (\boldsymbol{w} - \boldsymbol{B}_0)\, dx \\ \qquad + \displaystyle\int_\Omega \nu\, \mathbf{curl}\, \boldsymbol{E}_0 \cdot \boldsymbol{w} - \nu \boldsymbol{B}_0 \cdot \mathbf{curl}\, \boldsymbol{v}\, dx \\ \qquad + \varphi(\theta(0), \boldsymbol{v}) - \varphi(\theta(0), \boldsymbol{E}_0) \geq \displaystyle\int_\Omega \boldsymbol{f}(0) \cdot (\boldsymbol{v} - \boldsymbol{E}_0)\, dx \\ \text{for all } (\boldsymbol{v}, \boldsymbol{w}) \in \boldsymbol{H}_0(\mathbf{curl}) \times \boldsymbol{L}^2(\Omega). \end{cases}
$$

Now, we define $(\boldsymbol{E}_{0h}, \boldsymbol{B}_{0h}) \in \boldsymbol{V}_h \times \boldsymbol{W}_h$ as the unique solution to the discrete mixed problem

$$\begin{cases} \displaystyle\int_\Omega \epsilon \boldsymbol{E}_{0h} \cdot (\boldsymbol{v}_h - \boldsymbol{E}_{0h}) + \nu \boldsymbol{B}_{0h} \cdot (\boldsymbol{w}_h - \boldsymbol{B}_{0h})\, dx \\ \quad + \displaystyle\int_\Omega \nu\, \mathbf{curl}\, \boldsymbol{E}_{0h} \cdot \boldsymbol{w}_h - \nu \boldsymbol{B}_{0h} \cdot \mathbf{curl}\, \boldsymbol{v}_h\, dx \\ \quad + \varphi(\theta(0), \boldsymbol{v}_h) - \varphi(\theta(0), \boldsymbol{E}_{0h}) \geq \displaystyle\int_\Omega \boldsymbol{f}(0) \cdot (\boldsymbol{v}_h - \boldsymbol{E}_{0h})\, dx \\ \text{for all } (\boldsymbol{v}_h, \boldsymbol{w}_h) \in \boldsymbol{V}_h \times \boldsymbol{W}_h. \end{cases} \tag{4.4}$$

The well-posedness of (4.3) and (4.4) follow the same argumentation as (VI_N), i.e., the decoupling method in combination with Theorem 3.1 (cf. also the proof of Theorem 4.4).

In view of (4.4), it makes sense to set $(\delta \boldsymbol{E}_h^0, \delta \boldsymbol{B}_h^0) \coloneqq (\boldsymbol{E}_{0h}, \boldsymbol{B}_{0h})$. Indeed, if we set $n = 0$ and replace $(\delta \boldsymbol{E}_h^n, \delta \boldsymbol{B}_h^n)$ by $(\boldsymbol{E}_{0h}, \boldsymbol{B}_{0h})$ in ($\mathrm{VI}_{N,h}$), then we arrive exactly at (4.4). Note that $(\delta \boldsymbol{E}_h^0, \delta \boldsymbol{B}_h^0) = (\boldsymbol{E}_{0h}, \boldsymbol{B}_{0h})$ is important for our stability analysis (see (4.20) in the proof of Lemma 4.7).

Remark 4.2. All mathematical findings in this chapter remain true if we replace $\boldsymbol{W}_h$ by $\boldsymbol{W}_h \cap \boldsymbol{H}_0(\mathrm{div})$. Both $\boldsymbol{W}_h$ and $\boldsymbol{W}_h \cap \boldsymbol{H}_0(\mathrm{div})$ are dense in $\boldsymbol{L}^2(\Omega)$ and contain $\mathbf{curl}\, \boldsymbol{V}_h$. The condition of $\mathbf{curl}\, \boldsymbol{V}_h$ being a subspace is necessary to prove the regularity properties $\boldsymbol{B}_{0h}, \boldsymbol{B}_h^n \in \mathbf{curl}\, \boldsymbol{V}_h$ for the solutions to (4.4) and ($\mathrm{VI}_{N,h}$) (see Lemma 4.3 and Theorem 4.4). Furthermore, the density property is required for the derivation of the weak-* convergence result (Theorem 4.8). We note that the choice $\boldsymbol{W}_h = \mathbf{curl}\, \boldsymbol{V}_h$ is not suitable for our analysis, as $\mathbf{curl}\, \boldsymbol{V}_h$ is not dense in $\boldsymbol{L}^2(\Omega)$.

The operator $\boldsymbol{\Phi}_h \colon \boldsymbol{H}_0(\mathbf{curl}) \to \boldsymbol{V}_h$ which was introduced in Definition 2.8 enables us to verify the strong convergence of the discrete initial values towards $(\boldsymbol{E}_0, \boldsymbol{B}_0)$ in the next lemma. Moreover, it will be of crucial importance in the convergence analysis of ($\mathrm{VI}_{N,h}$).

Lemma 4.3. *Under Assumptions* 3.10 *and* 4.1*, the discrete approximation* $(\boldsymbol{E}_{0h}, \boldsymbol{B}_{0h}) \in \boldsymbol{V}_h \times \boldsymbol{W}_h$ *of the initial value satisfies* $\boldsymbol{B}_{0h} \in \mathbf{curl}\, \boldsymbol{V}_h$ *for all* $h > 0$ *and*

$$\lim_{h \to 0} \|\boldsymbol{E}_{0h} - \boldsymbol{E}_0\|_{\boldsymbol{L}^2_\epsilon(\Omega)} = \lim_{h \to 0} \|\boldsymbol{B}_{0h} - \boldsymbol{B}_0\|_{\boldsymbol{L}^2_\nu(\Omega)} = 0.$$

Proof. Let $h > 0$. Inserting $\boldsymbol{v}_h = \boldsymbol{E}_{0h}$ in (4.4), we obtain that

$$\int_\Omega \nu(\boldsymbol{B}_{0h} + \mathbf{curl}\, \boldsymbol{E}_{0h}) \cdot (\boldsymbol{w}_h - \boldsymbol{B}_{0h}) dx = 0 \quad \forall \boldsymbol{w}_h \in \boldsymbol{W}_h. \tag{4.5}$$

Since $\mathbf{curl}\, \boldsymbol{V}_h \subset \boldsymbol{W}_h$, we may set $\boldsymbol{w}_h \coloneqq 2\boldsymbol{B}_{0h} + \mathbf{curl}\, \boldsymbol{E}_{0h}$ in (4.5) implying

$$\boldsymbol{B}_{0h} = -\mathbf{curl}\, \boldsymbol{E}_{0h}. \tag{4.6}$$

Thus, $\boldsymbol{B}_{0h} \in \mathbf{curl}\, \boldsymbol{V}_h \subset \boldsymbol{H}_0(\mathrm{div}{=}0)$ follows. Moreover, testing (4.4) with $(\boldsymbol{v}_h, \boldsymbol{w}_h) = (0, 0)$ as well as $(\boldsymbol{v}_h, \boldsymbol{w}_h) = (2\boldsymbol{E}_{0h}, 2\boldsymbol{B}_{0h})$ yields

$$\|\boldsymbol{E}_{0h}\|^2_{\boldsymbol{L}^2_\epsilon(\Omega)} + \|\boldsymbol{B}_{0h}\|^2_{\boldsymbol{L}^2_\nu(\Omega)} + \int_\Omega j_c(x, \theta(x,0)) |\boldsymbol{E}_{0h}(x)|\, dx = \int_\Omega \boldsymbol{f}(0) \cdot \boldsymbol{E}_{0h}\, dx \\ \Rightarrow \|\boldsymbol{E}_{0h}\|_{\boldsymbol{L}^2_\epsilon(\Omega)} \leq \|\epsilon^{-1/2} \boldsymbol{f}(0)\|_{\boldsymbol{L}^2(\Omega)}. \tag{4.7}$$

Next, we insert $(\boldsymbol{v}, \boldsymbol{w}) = (\boldsymbol{E}_{0h}, \boldsymbol{B}_{0h})$ into (4.3) and $(\boldsymbol{v}_h, \boldsymbol{w}_h) = (\boldsymbol{\Phi}_h \boldsymbol{E}_0, 0)$ into (4.4) and obtain after

adding the resulting inequalities together that

$$
\begin{aligned}
(4.8)\qquad & \|\boldsymbol{E}_{0h}-\boldsymbol{E}_0\|^2_{\boldsymbol{L}^2_\epsilon(\Omega)}+\|\boldsymbol{B}_{0h}-\boldsymbol{B}_0\|^2_{\boldsymbol{L}^2_\nu(\Omega)}\\
&\le \int_\Omega \boldsymbol{f}(0)\cdot(\boldsymbol{E}_0-\boldsymbol{\Phi}_h\boldsymbol{E}_0)\,dx+\int_\Omega \epsilon\boldsymbol{E}_{0h}\cdot(\boldsymbol{\Phi}_h\boldsymbol{E}_0-\boldsymbol{E}_0)\,dx\\
&\quad-\int_\Omega \nu(\boldsymbol{B}_{0h}+\mathbf{curl}\,\boldsymbol{E}_{0h})\cdot\boldsymbol{B}_0\,dx+\int_\Omega \nu\boldsymbol{B}_{0h}\cdot\mathbf{curl}(\boldsymbol{E}_0-\boldsymbol{\Phi}_h\boldsymbol{E}_0)\,dx\\
&\quad+\int_\Omega j_c(x,\theta(x,0))\big(|\boldsymbol{\Phi}_h\boldsymbol{E}_0|-|\boldsymbol{E}_0|\big)\,dx.
\end{aligned}
$$

Due to (4.6), the third term on the right-hand side of (4.8) vanishes. Moreover,

$$
\int_\Omega \nu\boldsymbol{B}_{0h}\cdot\mathbf{curl}(\boldsymbol{E}_0-\boldsymbol{\Phi}_h\boldsymbol{E}_0)\,dx\underbrace{=}_{(4.6)}\int_\Omega \nu\,\mathbf{curl}\,\boldsymbol{E}_{0h}\cdot\mathbf{curl}(\boldsymbol{E}_0-\boldsymbol{\Phi}_h\boldsymbol{E}_0)\,dx\underbrace{=}_{(2.22)}0.
$$

Thus, applying Hölder's inequality together with (A3.3), (A3.5) and (4.7) to (4.8) yields

$$
(4.9)\qquad \|\boldsymbol{E}_{0h}-\boldsymbol{E}_0\|^2_{\boldsymbol{L}^2_\epsilon(\Omega)}+\|\boldsymbol{B}_{0h}-\boldsymbol{B}_0\|^2_{\boldsymbol{L}^2_\nu(\Omega)}\le C\|\boldsymbol{\Phi}_h\boldsymbol{E}_0-\boldsymbol{E}_0\|_{\boldsymbol{L}^2_\epsilon(\Omega)}
$$

with a constant $C>0$ only depending on ϵ, $\boldsymbol{f}$, j_c and θ. Finally, passing to the limit $h\to 0$ in (4.9), (2.29) yields the assertion. ■

The following theorem proves the well-posedness of ($\mathrm{VI}_{N,h}$) and gives an important regularity property for the discrete magnetic induction. The proof relies on the same decoupling argument that we used to obtain (4.1) and (4.2).

Theorem 4.4. *Let Assumptions* 3.10 *and* 4.1 *hold. Then, for every $h>0$ and $N\in\mathbb{N}$, the system of discrete variational inequalities* ($\mathrm{VI}_{N,h}$) *admits a unique solution $\{(\boldsymbol{E}_h^n,\boldsymbol{B}_h^n)\}_{n=1}^N\subset\boldsymbol{V}_h\times\mathbf{curl}\,\boldsymbol{V}_h$.*

Proof. Let $N\in\mathbb{N}$, $h>0$ and $n\in\{1,\dots,N\}$. Furthermore, assume that $(\boldsymbol{E}_h^{n-1},\boldsymbol{B}_h^{n-1})$ is already known. Now, we may decouple the variational inequality into two parts by testing ($\mathrm{VI}_{N,h}$) with $\boldsymbol{v}_h=\boldsymbol{E}_h^n$ to obtain that

$$
(4.10)\qquad \delta\boldsymbol{B}_h^n=-\,\mathbf{curl}\,\boldsymbol{E}_h^n.
$$

By definition, (4.10) yields the following explicit formula for $\boldsymbol{B}_h^n$:

$$
(4.11)\qquad \boldsymbol{B}_h^n=\boldsymbol{B}_h^{n-1}-\tau\,\mathbf{curl}\,\boldsymbol{E}_h^n.
$$

Next, we insert $\boldsymbol{w}_h=\boldsymbol{B}_h^n$ in ($\mathrm{VI}_{N,h}$) and employ (4.11) to obtain the variational inequality

$$
\begin{aligned}
(4.12)\qquad &\int_\Omega \epsilon\delta\boldsymbol{E}_h^n\cdot(\boldsymbol{v}_h-\boldsymbol{E}_h^n)\,dx+\int_\Omega \tau\nu\,\mathbf{curl}\,\boldsymbol{E}_h^n\cdot\mathbf{curl}(\boldsymbol{v}_h-\boldsymbol{E}_h^n)\,dx+\varphi^n(\boldsymbol{v}_h)\\
&\qquad-\varphi^n(\boldsymbol{E}_h^n)\ge\int_\Omega \boldsymbol{f}^n\cdot(\boldsymbol{v}_h-\boldsymbol{E}_h^n)+\nu\boldsymbol{B}_h^{n-1}\cdot\mathbf{curl}(\boldsymbol{v}_h-\boldsymbol{E}_h^n)\,dx\quad\forall\boldsymbol{v}_h\in\boldsymbol{V}_h.
\end{aligned}
$$

The well-posedness of (4.12) follows again by Theorem 3.1 (cf. (4.1) and (4.2)), because it is equivalent to an elliptic **curl-curl** variational inequality of the form

$$
(4.13)\qquad a(\boldsymbol{E}_h^n,\boldsymbol{v}_h-\boldsymbol{E}_h^n)+\varphi^n(\boldsymbol{v}_h)-\varphi^n(\boldsymbol{E}_h^n)\ge\langle\tilde{\boldsymbol{f}}^n,\boldsymbol{v}_h-\boldsymbol{E}_h^n\rangle\quad\forall\boldsymbol{v}_h\in\boldsymbol{V}_h,
$$

with the continuous and coercive bilinear form $a\colon\boldsymbol{V}_h\times\boldsymbol{V}_h\to\mathbb{R}$ defined by

$$
a(\boldsymbol{u}_h,\boldsymbol{v}_h):=\int_\Omega \tau^{-1}\epsilon\boldsymbol{u}_h\cdot\boldsymbol{v}_h\,dx+\int_\Omega \tau\nu\,\mathbf{curl}\,\boldsymbol{u}_h\cdot\mathbf{curl}\,\boldsymbol{v}_h\,dx\quad\forall\boldsymbol{u}_h,\boldsymbol{v}_h\in\boldsymbol{V}_h
$$

and the right-hand side $\tilde{\boldsymbol{f}}^n \in \boldsymbol{H}_0(\mathbf{curl})^*$ by

$$\langle \tilde{\boldsymbol{f}}^n, \boldsymbol{v} \rangle \coloneqq \int_\Omega (\boldsymbol{f}^n + \tau^{-1}\epsilon \boldsymbol{E}_h^{n-1}) \cdot \boldsymbol{v}\, dx + \int_\Omega \nu \boldsymbol{B}_h^{n-1} \cdot \mathbf{curl}\, \boldsymbol{v}\, dx \quad \forall \boldsymbol{v} \in \boldsymbol{H}_0(\mathbf{curl}).$$

Inserting the solution $\boldsymbol{E}_h^n$ of (4.12) into (4.11), we finally obtain a unique solution

$$\{(\boldsymbol{E}_h^n, \boldsymbol{B}_h^n)\}_{n=1}^N \subset \boldsymbol{V}_h \times \boldsymbol{W}_h$$

of ($\mathrm{VI}_{N,h}$). Finally, (4.11) and Lemma 4.3 give $\boldsymbol{B}_h^n \in \mathbf{curl}\, \boldsymbol{V}_h$ by inductive reasoning. ■

Remark 4.5. We note that the formulas (4.11) and (4.12) are the discrete counterparts of (4.1) and (4.2). They are the foundation for the computation of the numerical solution in section 4.4 by means of the semismooth Newton method Algorithm 3.1.

The following Lemmas prove the zero-order and first-order stability estimates for the fully discrete solution to ($\mathrm{VI}_{N,h}$):

Lemma 4.6. *Let Assumptions* 3.10 *and* 4.1 *be satisfied. Then, there exists a constant $C > 0$, depending only on $\boldsymbol{f}, \boldsymbol{E}_0, \boldsymbol{B}_0$ and T, ϵ, ν, such that for every $N \in \mathbb{N}$ and $h > 0$, the solution $\{(\boldsymbol{E}_h^n, \boldsymbol{B}_h^n)\}_{n=1}^N$ of ($\mathrm{VI}_{N,h}$) fulfills the estimate*

$$\begin{aligned}(4.14)\qquad &\max_{n\in\{1,\dots,N\}} \|\boldsymbol{E}_h^n\|^2_{\boldsymbol{L}^2_\epsilon(\Omega)} + \max_{n\in\{1,\dots,N\}} \|\boldsymbol{B}_h^n\|^2_{\boldsymbol{L}^2_\nu(\Omega)} \\ &\qquad + \sum_{n=1}^N \|\boldsymbol{E}_h^n - \boldsymbol{E}_h^{n-1}\|^2_{\boldsymbol{L}^2_\epsilon(\Omega)} + \sum_{n=1}^N \|\boldsymbol{B}_h^n - \boldsymbol{B}_h^{n-1}\|^2_{\boldsymbol{L}^2_\nu(\Omega)} + 2\tau \sum_{n=1}^N \varphi^n(\boldsymbol{E}_h^n) \le C.\end{aligned}$$

Proof. Let $N \in \mathbb{N}$ and $h > 0$. We start by testing ($\mathrm{VI}_{N,h}$) with $(\boldsymbol{v}_h, \boldsymbol{w}_h) = (2\boldsymbol{E}_h^n, 2\boldsymbol{B}_h^n)$ as well as with $(\boldsymbol{v}_h, \boldsymbol{w}_h) = (0,0)$ to obtain

$$(4.15)\qquad \int_\Omega \epsilon \delta \boldsymbol{E}_h^n \cdot \boldsymbol{E}_h^n\, dx + \int_\Omega \nu \delta \boldsymbol{B}_h^n \cdot \boldsymbol{B}_h^n\, dx + \varphi^n(\boldsymbol{E}_h^n) = \int_\Omega \boldsymbol{f}^n \cdot \boldsymbol{E}_h^n\, dx \quad \forall n \in \{1,\dots,N\}.$$

Now, fix $i_0 \in \{1,\dots,N\}$ and sum (4.15) up over $\{1,\dots,i_0\}$. Then, applying the binomial formulas along with the Hölder and Young inequalities, we deduce that

$$\begin{aligned}(4.16)\qquad &\|\boldsymbol{E}_h^{i_0}\|^2_{\boldsymbol{L}^2_\epsilon(\Omega)} + \|\boldsymbol{B}_h^{i_0}\|^2_{\boldsymbol{L}^2_\nu(\Omega)} + \sum_{n=1}^{i_0} \|\boldsymbol{E}_h^n - \boldsymbol{E}_h^{n-1}\|^2_{\boldsymbol{L}^2_\epsilon(\Omega)} \\ &\quad + \sum_{n=1}^{i_0} \|\boldsymbol{B}_h^n - \boldsymbol{B}_h^{n-1}\|^2_{\boldsymbol{L}^2_\nu(\Omega)} + 2\tau \sum_{n=1}^{i_0} \varphi^n(\boldsymbol{E}_h^n) \\ &\le \|\boldsymbol{E}_{0h}\|^2_{\boldsymbol{L}^2_\epsilon(\Omega)} + \|\boldsymbol{B}_{0h}\|^2_{\boldsymbol{L}^2_\nu(\Omega)} + \frac{2T\tau}{\underline{\epsilon}} \sum_{n=1}^{i_0} \|\boldsymbol{f}^n\|^2_{\boldsymbol{L}^2(\Omega)} + \frac{\tau}{2T} \sum_{n=1}^{i_0} \|\boldsymbol{E}_h^n\|^2_{\boldsymbol{L}^2_\epsilon(\Omega)}.\end{aligned}$$

This, combined with (A3.5), (A3.6), Lemma 4.3, and the fact that $\tau/T = 1/N \le 1$ gives us an estimate of the form

$$\|\boldsymbol{E}_h^{i_0}\|^2_{\boldsymbol{L}^2_\epsilon(\Omega)} \le C + \sum_{n=1}^{i_0-1} \frac{1}{N} \|\boldsymbol{E}_h^n\|^2_{\boldsymbol{L}^2_\epsilon(\Omega)} \quad \Rightarrow \quad \|\boldsymbol{E}_h^{i_0}\|^2_{\boldsymbol{L}^2_\epsilon(\Omega)} \le C \exp\left(\sum_{n=1}^{i_0-1} \frac{1}{N}\right) \le C,$$

where we have used the discrete Gronwall inequality. Hence, since i_0 was chosen arbitrarily, the boundedness $\max_{n\in\{1,\dots,N\}} \|\boldsymbol{E}_h^n\|_{\boldsymbol{L}^2_\epsilon(\Omega)} \le C$ follows. By employing this to (4.16), we see that the proof is finished. ■

Lemma 4.7. *Let Assumptions* 3.10 *and* 4.1 *hold. Then, there exists a constant $C > 0$, depending only on $\boldsymbol{f}, \boldsymbol{E}_0, \boldsymbol{B}_0$ and $T, \epsilon, \nu, \theta, j_c$, such that for every $N \in \mathbb{N}$ and $h > 0$ the solution $\{(\boldsymbol{E}_h^n, \boldsymbol{B}_h^n)\}_{n=1}^N$ of* ($\mathrm{VI}_{N,h}$) *satisfies*

$$\begin{aligned}(4.17)\qquad &\max_{n\in\{1,\dots,N\}} \|\delta \boldsymbol{E}_h^n\|^2_{\boldsymbol{L}^2_\epsilon(\Omega)} + \max_{n\in\{1,\dots,N\}} \|\delta \boldsymbol{B}_h^n\|^2_{\boldsymbol{L}^2_\nu(\Omega)} \\ &\qquad + \sum_{n=1}^N \|\delta \boldsymbol{E}_h^n - \delta \boldsymbol{E}_h^{n-1}\|^2_{\boldsymbol{L}^2_\epsilon(\Omega)} + \sum_{n=1}^N \|\delta \boldsymbol{B}_h^n - \delta \boldsymbol{B}_h^{n-1}\|^2_{\boldsymbol{L}^2_\nu(\Omega)} \le C\end{aligned}$$

and

$$(4.18)\qquad \max_{n\in\{1,\dots,N\}} \|\operatorname{\mathbf{curl}} \boldsymbol{E}_h^n\|^2_{\boldsymbol{L}^2_\nu(\Omega)} \le C.$$

Proof. Let $N \in \mathbb{N}$, $h > 0$ and $n \in \{1, \dots, N\}$. Inserting $(\boldsymbol{v}_h, \boldsymbol{w}_h) = (\boldsymbol{E}_h^{n-1}, \boldsymbol{B}_h^{n-1})$ in the nth inequality of ($\mathrm{VI}_{N,h}$) and then adding it with the $(n-1)$th inequality of ($\mathrm{VI}_{N,h}$) tested with $(\boldsymbol{v}_h, \boldsymbol{w}_h) = (\boldsymbol{E}_h^n, \boldsymbol{B}_h^n)$ lead to

$$\begin{aligned}(4.19)\qquad &\int_\Omega \epsilon(\delta \boldsymbol{E}_h^n - \delta \boldsymbol{E}_h^{n-1}) \cdot (\boldsymbol{E}_h^n - \boldsymbol{E}_h^{n-1}) + \nu(\delta \boldsymbol{B}_h^n - \delta \boldsymbol{B}_h^{n-1}) \cdot (\boldsymbol{B}_h^n - \boldsymbol{B}_h^{n-1})\, dx \\ &\le \int_\Omega (\boldsymbol{f}^n - \boldsymbol{f}^{n-1}) \cdot (\boldsymbol{E}_h^n - \boldsymbol{E}_h^{n-1})\, dx + \int_\Omega j_c(x, \theta(x, t_n))(|\boldsymbol{E}_h^{n-1}| - |\boldsymbol{E}_h^n|)\, dx \\ &\qquad + \int_\Omega j_c(x, \theta(x, t_{n-1}))(|\boldsymbol{E}_h^n| - |\boldsymbol{E}_h^{n-1}|)\, dx.\end{aligned}$$

In this notation, we use compatibility system (4.4) for the 0th inequality of ($\mathrm{VI}_{N,h}$). Now, we sum (4.19) up over $\{1, \dots, i_0\}$ for a fixed $i_0 \in \{1, \dots, N\}$ and divide the resulting inequality by τ to get

$$\begin{aligned}&\sum_{n=1}^{i_0} \bigg[\int_\Omega \epsilon(\delta \boldsymbol{E}_h^n - \delta \boldsymbol{E}_h^{n-1}) \cdot \delta \boldsymbol{E}_h^n\, dx + \int_\Omega \nu(\delta \boldsymbol{B}_h^n - \delta \boldsymbol{B}_h^{n-1}) \cdot \delta \boldsymbol{B}_h^n\, dx \bigg] \\ &\le \sum_{n=1}^{i_0} \bigg[\int_\Omega (\boldsymbol{f}^n - \boldsymbol{f}^{n-1}) \cdot \delta \boldsymbol{E}_h^n\, dx + \int_\Omega \big(j_c(x, \theta(x, t_n)) - j_c(x, \theta(x, t_{n-1})) \big) \\ &\qquad \left(\frac{|\boldsymbol{E}_h^{n-1}| - |\boldsymbol{E}_h^n|}{\tau} \right) dx \bigg].\end{aligned}$$

Then, as in the proof of Lemma 4.6, the binomial formulas along with the Hölder and Young inequalities yield

$$\begin{aligned}(4.20)\qquad &\|\delta \boldsymbol{E}_h^{i_0}\|^2_{\boldsymbol{L}^2_\epsilon(\Omega)} + \|\delta \boldsymbol{B}_h^{i_0}\|^2_{\boldsymbol{L}^2_\nu(\Omega)} + \sum_{n=1}^{i_0} \|\delta \boldsymbol{E}_h^n - \delta \boldsymbol{E}_h^{n-1}\|^2_{\boldsymbol{L}^2_\epsilon(\Omega)} + \|\delta \boldsymbol{B}_h^n - \delta \boldsymbol{B}_h^{n-1}\|^2_{\boldsymbol{L}^2_\nu(\Omega)} \\ &\le \frac{4T\tau}{\underline{\epsilon}} \sum_{n=1}^{i_0} \left\| \frac{\boldsymbol{f}^n - \boldsymbol{f}^{n-1}}{\tau} \right\|^2_{\boldsymbol{L}^2(\Omega)} + \frac{4T\tau}{\underline{\epsilon}} \sum_{n=1}^{i_0} \left\| \frac{j_c(x, \theta(x, t_n)) - j_c(x, \theta(x, t_{n-1}))}{\tau} \right\|^2_{\boldsymbol{L}^2(\Omega)} \\ &\quad + \|\boldsymbol{E}_{0h}\|^2_{\boldsymbol{L}^2_\epsilon(\Omega)} + \|\boldsymbol{B}_{0h}\|^2_{\boldsymbol{L}^2_\nu(\Omega)} + \underbrace{\frac{\tau}{2T}}_{=\frac{1}{2N}} \sum_{n=1}^{i_0} \|\delta \boldsymbol{E}_h^n\|^2_{\boldsymbol{L}^2_\epsilon(\Omega)},\end{aligned}$$

where we have also used $\delta \boldsymbol{E}_{0h} = \boldsymbol{E}_{0h}$ and $\delta \boldsymbol{B}_{0h} = \boldsymbol{B}_{0h}$. Therefore, (A3.4), (A3.5) and Lemma 4.3 applied to (4.20) imply

$$\|\delta \boldsymbol{E}_h^{i_0}\|^2_{\boldsymbol{L}^2_\epsilon(\Omega)} \le C + \sum_{n=1}^{i_0-1} \frac{1}{N} \|\delta \boldsymbol{E}_h^n\|^2_{\boldsymbol{L}^2_\epsilon(\Omega)} \quad \Rightarrow \quad \|\delta \boldsymbol{E}_h^{i_0}\|^2_{\boldsymbol{L}^2_\epsilon(\Omega)} \le C \exp\left(\sum_{n=1}^{i_0-1} \frac{1}{N} \right) \le C,$$

by the discrete Gronwall inequality (see [48]). Since i_0 was chosen arbitrarily, applying the above estimate to (4.20) yields (4.17). Finally, (4.18) follows immediately from (4.10) and (4.17). ■

With these stability estimates at hand, we will establish a weak-* convergence result for ($\mathrm{VI}_{N,h}$), which particularly implies the well-posedness of (VI). First, we denote

$$\text{(4.21)}\qquad \begin{cases} \boldsymbol{E}_{N,h}(0) \coloneqq \boldsymbol{E}_{0h} \\ \boldsymbol{E}_{N,h}(t) \coloneqq \boldsymbol{E}_h^{n-1} + (t-t_{n-1})\delta \boldsymbol{E}_h^n \end{cases} \quad \text{and} \quad \begin{cases} \overline{\boldsymbol{E}}_{N,h}(0) \coloneqq \boldsymbol{E}_{0h} \\ \overline{\boldsymbol{E}}_{N,h}(t) \coloneqq \boldsymbol{E}_h^n \end{cases}$$

for $t \in (t_{n-1}, t_n]$ and $n \in \{1, \dots, N\}$. In the same way, we define $\boldsymbol{B}_{N,h}$, $\overline{\boldsymbol{B}}_{N,h}$ and $\overline{\boldsymbol{f}}_N$. Furthermore, we introduce the function $\varphi_N \colon [0,T] \times \boldsymbol{L}^2(\Omega) \to \mathbb{R}$ by

$$\text{(4.22)}\qquad \begin{cases} \varphi_N(0, \boldsymbol{v}) \coloneqq \varphi(\theta(0), \boldsymbol{v}) = \displaystyle\int_\Omega j_c(x, \theta(x,0)) |\boldsymbol{v}(x)| \, dx \\ \varphi_N(t, \boldsymbol{v}) \coloneqq \varphi^n(\boldsymbol{v}) = \displaystyle\int_\Omega j_c(x, \theta(x,t_n)) |\boldsymbol{v}(x)| \, dx \quad \forall t \in (t_{n-1}, t_n], \end{cases}$$

for $\boldsymbol{v} \in \boldsymbol{L}^2(\Omega)$ and $n \in \{1, \dots, N\}$. Now, we can rewrite ($\mathrm{VI}_{N,h}$) in the following manner:

$$\text{(4.23)}\qquad \begin{cases} \displaystyle\int_\Omega \epsilon \partial_t \boldsymbol{E}_{N,h}(t) \cdot (\boldsymbol{v}_h - \overline{\boldsymbol{E}}_{N,h}(t)) + \nu \partial_t \boldsymbol{B}_{N,h}(t) \cdot (\boldsymbol{w}_h - \overline{\boldsymbol{B}}_{N,h}(t)) \, dx \\ \qquad + \displaystyle\int_\Omega \nu \, \mathbf{curl}\, \overline{\boldsymbol{E}}_{N,h}(t) \cdot \boldsymbol{w}_h - \nu \overline{\boldsymbol{B}}_{N,h}(t) \cdot \mathbf{curl}\, \boldsymbol{v}_h \, dx \\ \qquad + \varphi_N(t, \boldsymbol{v}_h) - \varphi_N(t, \overline{\boldsymbol{E}}_{N,h}(t)) \geq \displaystyle\int_\Omega \overline{\boldsymbol{f}}_N(t) \cdot (\boldsymbol{v}_h - \overline{\boldsymbol{E}}_{N,h}(t)) \, dx \\ \quad \text{for every } (\boldsymbol{v}_h, \boldsymbol{w}_h) \in \boldsymbol{V}_h \times \boldsymbol{W}_h \text{ and a.e. } t \in (0,T) \\ \quad (\boldsymbol{E}_{N,h}(0), \boldsymbol{B}_{N,h}(0)) = (\boldsymbol{E}_{0h}, \boldsymbol{B}_{0h}). \end{cases}$$

Theorem 4.8. *Let Assumptions* 3.10 *and* 4.1 *hold. Then, there exists a pair*

$$(\boldsymbol{E}, \boldsymbol{B}) \in W^{1,\infty}((0,T), \boldsymbol{L}^2_\epsilon(\Omega) \times \boldsymbol{H}_0(\mathrm{div}{=}0)) \cap L^\infty((0,T), \boldsymbol{H}_0(\mathbf{curl}) \times \boldsymbol{H}_0(\mathrm{div}{=}0))$$

such that for $N = N(h)$ with $N(h) \to \infty$ as $h \to 0$ it holds that

$$\begin{aligned} &\boldsymbol{E}_{N,h} \rightharpoonup^* \boldsymbol{E} \text{ and } \overline{\boldsymbol{E}}_{N,h} \rightharpoonup^* \boldsymbol{E} && \text{weakly-* in } L^\infty((0,T), \boldsymbol{H}_0(\mathbf{curl})), \\ &\boldsymbol{B}_{N,h} \rightharpoonup^* \boldsymbol{B} \text{ and } \overline{\boldsymbol{B}}_{N,h} \rightharpoonup^* \boldsymbol{B} && \text{weakly-* in } L^\infty((0,T), \boldsymbol{H}_0(\mathrm{div}{=}0)), \\ &\partial_t \boldsymbol{E}_{N,h} \rightharpoonup^* \partial_t \boldsymbol{E} && \text{weakly-* in } L^\infty((0,T), \boldsymbol{L}^2_\epsilon(\Omega)), \\ &\partial_t \boldsymbol{B}_{N,h} \rightharpoonup^* \partial_t \boldsymbol{B} && \text{weakly-* in } L^\infty((0,T), \boldsymbol{H}_0(\mathrm{div}{=}0)), \end{aligned}$$

and $(\boldsymbol{E}, \boldsymbol{B})$ is the unique solution to (VI).

Proof. First of all, we emphasize that $N = N(h)$ denotes a family of natural numbers with $N(h) \to \infty$ for $h \to 0$. As shown in Lemma 4.6 and Lemma 4.7, $\{\boldsymbol{E}_{N,h}\}_{h>0}$, $\{\boldsymbol{B}_{N,h}\}_{h>0}$, $\{\overline{\boldsymbol{E}}_{N,h}\}_{h>0}$, $\{\overline{\boldsymbol{B}}_{N,h}\}_{h>0}$, and $\{\partial_t \boldsymbol{E}_{N,h}\}_{h>0}$, $\{\partial_t \boldsymbol{B}_{N,h}\}_{h>0}$ are bounded in their respective spaces. Therefore, we may extract weakly-* converging subsequences, which will not be denoted in a special way:

$$\text{(4.24)}\qquad \begin{cases} \overline{\boldsymbol{E}}_{N,h} \rightharpoonup^* \overline{\boldsymbol{E}} & \text{weakly-* in } L^\infty((0,T), \boldsymbol{H}_0(\mathbf{curl})), \\ \overline{\boldsymbol{B}}_{N,h} \rightharpoonup^* \overline{\boldsymbol{B}} & \text{weakly-* in } L^\infty((0,T), \boldsymbol{H}_0(\mathrm{div}{=}0)), \\ \boldsymbol{E}_{N,h} \rightharpoonup^* \boldsymbol{E} & \text{weakly-* in } L^\infty((0,T), \boldsymbol{H}_0(\mathbf{curl})), \\ \boldsymbol{B}_{N,h} \rightharpoonup^* \boldsymbol{B} & \text{weakly-* in } L^\infty((0,T), \boldsymbol{H}_0(\mathrm{div}{=}0)), \\ \partial_t \boldsymbol{E}_{N,h} \rightharpoonup^* \xi & \text{weakly-* in } L^\infty((0,T), \boldsymbol{L}^2_\epsilon(\Omega)), \\ \partial_t \boldsymbol{B}_{N,h} \rightharpoonup^* \chi & \text{weakly-* in } L^\infty((0,T), \boldsymbol{H}_0(\mathrm{div}{=}0)), \end{cases}$$

for some $\boldsymbol{E}, \boldsymbol{B}, \overline{\boldsymbol{E}}, \overline{\boldsymbol{B}}, \xi, \chi$ as $h \to 0$. First of all, we verify that $\boldsymbol{E} = \overline{\boldsymbol{E}}$ and $\boldsymbol{B} = \overline{\boldsymbol{B}}$. However, this is readily seen by the definition (4.21) and Lemma 4.7 since

$$\begin{aligned} \|\overline{\boldsymbol{E}}_{N,h} - \boldsymbol{E}_{N,h}\|_{L^\infty((0,T),\boldsymbol{L}^2_\epsilon(\Omega))} &\le \tau \max_{n\in\{1,\dots,N\}} \|\delta \boldsymbol{E}_h^n\|_{\boldsymbol{L}^2_\epsilon(\Omega)} \le C\tau, \\ \|\overline{\boldsymbol{B}}_{N,h} - \boldsymbol{B}_{N,h}\|_{L^\infty((0,T),\boldsymbol{L}^2_\nu(\Omega))} &\le \tau \max_{n\in\{1,\dots,N\}} \|\delta \boldsymbol{B}_h^n\|_{\boldsymbol{L}^2_\nu(\Omega)} \le C\tau. \end{aligned} \tag{4.25}$$

Next, derivation in the sense of distributions gives

$$\begin{aligned} \int_0^T (\xi(t), \boldsymbol{v})_{\boldsymbol{L}^2_\epsilon(\Omega)} \phi(t) dt &\underbrace{\leftarrow}_{(4.24)} \int_0^T (\partial_t \boldsymbol{E}_{N,h}(t), \boldsymbol{v})_{\boldsymbol{L}^2_\epsilon(\Omega)} \phi(t) dt \\ &= -\int_0^T (\boldsymbol{E}_{N,h}(t), \boldsymbol{v})_{\boldsymbol{L}^2_\epsilon(\Omega)} \phi'(t) dt \underbrace{\to}_{(4.24)} - \int_0^T (\boldsymbol{E}(t), \boldsymbol{v})_{\boldsymbol{L}^2_\epsilon(\Omega)} \phi'(t) dt \end{aligned}$$

for every $\boldsymbol{v} \in \boldsymbol{L}^2(\Omega)$ and $\phi \in \mathcal{C}_0^\infty(0,T)$, which yields $\xi = \partial_t \boldsymbol{E}$ and so

$$\boldsymbol{E} \in W^{1,\infty}((0,T), \boldsymbol{L}^2_\epsilon(\Omega)) \cap L^\infty((0,T), \boldsymbol{H}_0(\mathbf{curl})).$$

Obviously, the same conclusion can be drawn for $\chi = \partial_t \boldsymbol{B}$, which implies the regularity $\boldsymbol{B} \in W^{1,\infty}((0,T), \boldsymbol{H}_0(\text{div=0}))$. Note that

$$(\boldsymbol{E}, \boldsymbol{B}) \in W^{1,\infty}((0,T), \boldsymbol{L}^2_\epsilon(\Omega) \times \boldsymbol{H}_0(\text{div=0})) \hookrightarrow \mathcal{C}([0,T], \boldsymbol{L}^2_\epsilon(\Omega) \times \boldsymbol{H}_0(\text{div=0}))$$

implies – possibly after a modification on a subset of $[0,T]$ with measure zero – that $(\boldsymbol{E}, \boldsymbol{B}) \in \mathcal{C}([0,T], \boldsymbol{L}^2_\epsilon(\Omega) \times \boldsymbol{H}_0(\text{div=0}))$. Next, we prove the pointwise weak convergence

$$\boldsymbol{E}_{N,h}(t) \rightharpoonup \boldsymbol{E}(t) \text{ weakly in } \boldsymbol{L}^2_\epsilon(\Omega) \text{ and } \boldsymbol{B}_{N,h}(t) \rightharpoonup \boldsymbol{B}(t) \text{ weakly in } \boldsymbol{H}_0(\text{div=0}) \tag{4.26}$$

for every $t \in [0,T]$. For that purpose, we fix $t \in (0,T]$, $\boldsymbol{w} \in \boldsymbol{L}^2(\Omega)$ and $\phi \in \mathcal{C}^1([0,t])$. Then, integration by parts yields

$$\begin{aligned} &\int_0^t (\partial_t \boldsymbol{E}(s), \boldsymbol{w})_{\boldsymbol{L}^2_\epsilon(\Omega)} \phi(s) ds \leftarrow \int_0^t (\partial_t \boldsymbol{E}_{N,h}(s), \boldsymbol{w})_{\boldsymbol{L}^2_\epsilon(\Omega)} \phi(s) ds \\ &= -\int_0^t (\boldsymbol{E}_{N,h}(s), \boldsymbol{w})_{\boldsymbol{L}^2_\epsilon(\Omega)} \phi'(s) ds + (\boldsymbol{E}_{N,h}(t), \boldsymbol{w})_{\boldsymbol{L}^2_\epsilon(\Omega)} \phi(t) - (\boldsymbol{E}_{N,h}(0), \boldsymbol{w})_{\boldsymbol{L}^2_\epsilon(\Omega)} \phi(0). \end{aligned} \tag{4.27}$$

Choosing $\phi(0) = 0$ as well as $\phi(t) \neq 0$ and applying integration by parts again gives

$$\lim_{h\to 0} (\boldsymbol{E}_{N,h}(t), \boldsymbol{w})_{\boldsymbol{L}^2_\epsilon(\Omega)} = (\boldsymbol{E}(t), \boldsymbol{w})_{\boldsymbol{L}^2_\epsilon(\Omega)} \quad \forall \boldsymbol{w} \in \boldsymbol{L}^2(\Omega).$$

Applying the above convergence to (4.27) and choosing $\phi(0) \neq 0$ leads to

$$\lim_{h\to 0} (\boldsymbol{E}_{N,h}(0), \boldsymbol{w})_{\boldsymbol{L}^2_\epsilon(\Omega)} = (\boldsymbol{E}(0), \boldsymbol{w})_{\boldsymbol{L}^2_\epsilon(\Omega)} \quad \forall \boldsymbol{w} \in \boldsymbol{L}^2(\Omega).$$

The same results hold also for $\boldsymbol{B}_{N,h}$, and so we conclude that (4.26) is valid. From Lemma 4.3, (4.21) and (4.26) with $t = 0$, it follows that

$$\boldsymbol{E}(0) = \boldsymbol{E}_0 \text{ and } \boldsymbol{B}(0) = \boldsymbol{B}_0. \tag{4.28}$$

We continue and recall the classical identity:

$$\begin{aligned} \int_0^t (\partial_t \boldsymbol{E}_{N,h}(s), \boldsymbol{E}_{N,h}(s))_{\boldsymbol{L}^2_\epsilon(\Omega)} ds &= \frac{1}{2}\|\boldsymbol{E}_{N,h}(t)\|^2_{\boldsymbol{L}^2_\epsilon(\Omega)} - \frac{1}{2}\|\boldsymbol{E}_{N,h}(0)\|^2_{\boldsymbol{L}^2_\epsilon(\Omega)} \\ &= \frac{1}{2}\|\boldsymbol{E}_{N,h}(t)\|^2_{\boldsymbol{L}^2_\epsilon(\Omega)} - \frac{1}{2}\|\boldsymbol{E}_{0h}\|^2_{\boldsymbol{L}^2_\epsilon(\Omega)}. \end{aligned} \tag{4.29}$$

Combining (4.29) with (4.26) and Lemma 4.3 yields

$$
\begin{aligned}
(4.30)\qquad & \liminf_{h\to 0}\int_0^t (\partial_t \boldsymbol{E}_{N,h}(s), \overline{\boldsymbol{E}}_{N,h}(s))_{\boldsymbol{L}^2_\epsilon(\Omega)} ds \\
&\underbrace{=}_{(4.25)} \liminf_{h\to 0}\int_0^t (\partial_t \boldsymbol{E}_{N,h}(s), \boldsymbol{E}_{N,h}(s))_{\boldsymbol{L}^2_\epsilon(\Omega)} ds \\
&\underbrace{=}_{(4.29)} \liminf_{h\to 0} \frac{1}{2}\|\boldsymbol{E}_{N,h}(t)\|^2_{\boldsymbol{L}^2_\epsilon(\Omega)} - \frac{1}{2}\|\boldsymbol{E}_{0h}\|^2_{\boldsymbol{L}^2_\epsilon(\Omega)} \\
&\geq \frac{1}{2}\|\boldsymbol{E}(t)\|^2_{\boldsymbol{L}^2_\epsilon(\Omega)} - \frac{1}{2}\|\boldsymbol{E}(0)\|^2_{\mathbf{L}^2_\epsilon} = \int_0^t (\partial_t \boldsymbol{E}(s), \boldsymbol{E}(s))_{\boldsymbol{L}^2_\epsilon(\Omega)} ds,
\end{aligned}
$$

where the above inequality holds due to the fact that the squared norm is weakly lower semicontinuous. Analogously, we obtain

$$
(4.31)\qquad \liminf_{h\to 0}\int_0^t (\partial_t \boldsymbol{B}_{N,h}(s), \overline{\boldsymbol{B}}_{N,h}(s))_{\boldsymbol{L}^2_\nu(\Omega)} ds \geq \int_0^t (\partial_t \boldsymbol{B}(s), \boldsymbol{B}(s))_{\boldsymbol{L}^2_\nu(\Omega)} ds.
$$

Next, we prove

$$
(4.32)\qquad \liminf_{h\to 0} \varphi_N(t, \overline{\boldsymbol{E}}_{N,h}(t)) ds \geq \varphi(\theta(t), \boldsymbol{E}(t)) \quad \forall t \in [0,T].
$$

For $t = 0$, Lemma 4.3 and (4.21), (4.22), and (4.28) grant even the strong convergence

$$
\lim_{h\to 0} \varphi_N(0, \overline{\boldsymbol{E}}_{N,h}(0)) = \lim_{h\to 0}\int_\Omega j_c(x, \theta(x,0))|\boldsymbol{E}_{0h}|\, dx = \varphi(\theta(0), \boldsymbol{E}(0)).
$$

Let now $t \in (0,T]$. Then, for every $N \in \mathbb{N}$, there exists a unique $n \in \{1,\dots,N\}$ such that $t \in (t_{n-1}, t_n]$. Hence, the sequence $\tilde{t}_{N,h} \coloneqq t_n$ fulfills $\tilde{t}_{N,h} \to t$ as $h \to 0$. Making use of this sequence, we obtain that

$$
\begin{aligned}
(4.33)\qquad & \liminf_{h\to 0} \varphi_N(t, \overline{\boldsymbol{E}}_{N,h}(t)) \\
&= \liminf_{h\to 0}\left(\varphi(\theta(t), \overline{\boldsymbol{E}}_{N,h}(t)) + \int_\Omega (j_c(x, \theta(x, \tilde{t}_{N,h})) - j_c(x, \theta(x,t)))|\overline{\boldsymbol{E}}_{N,h}(t)|\, dx\right) \\
&\geq \varphi(\theta(t), \boldsymbol{E}(t)) + \liminf_{h\to\infty}\int_\Omega (j_c(x, \theta(x, \tilde{t}_{N,h})) - j_c(x, \theta(x,t)))|\overline{\boldsymbol{E}}_{N,h}(t)|\, dx,
\end{aligned}
$$

where we have employed (4.26) and the fact that $\varphi(\theta(t),\cdot)\colon \boldsymbol{L}^2_\epsilon(\Omega) \to \mathbb{R}$, for every fixed $t \in [0,T]$, is sequentially weakly lower semicontinuous. In order to pass to the limit in the second term in (4.33), we make use of (A3.4) and (A3.5) to deduce after selecting a subsequence that

$$
(4.34)\qquad \lim_{h\to 0} j_c(x, \theta(x, \tilde{t}_{N,h})) - j_c(x, \theta(x,t)) = 0 \quad \text{for a.e. } x \in \Omega,
$$

and so, thanks to (A3.3)–(A3.5) and Lemma 4.6, Lebesgue's dominated convergence theorem yields

$$
(4.35)\qquad \lim_{h\to 0}\int_\Omega |j_c(x, \theta(\tilde{t}_{N,h}, x)) - j_c(x, \theta(t,x))||\overline{\boldsymbol{E}}_{N,h}(t)| dx = 0.
$$

In conclusion, (4.32) is valid.

Now, we show that $(\boldsymbol{E}, \boldsymbol{B})$ is a solution to (VI): Let $(\boldsymbol{v}, \boldsymbol{w}) \in L^2((0,T), \boldsymbol{H}_0(\mathbf{curl}) \times \boldsymbol{L}^2(\Omega))$. It is well-known that the space of simple functions[1] with values in $\boldsymbol{H}_0(\mathbf{curl}) \times \boldsymbol{L}^2(\Omega)$ lies densely in

[1] Let X be a Banach space. A function $f\colon [0,T] \to X$ is called a simple function if $f(t) = \sum_{k=1}^K x_k \chi_{A_k}(t)$ for every $t \in [0,T]$ where $\{A_k\}_{k=1}^K$ are disjoint sets in $[0,T]$ and $\{x_k\}_{k=1}^K \subset X$.

$L^2\big((0,T),\boldsymbol{H}_0(\mathbf{curl})\times\boldsymbol{L}^2(\Omega)$ (see [148, Proposition 1.36]). Combining this fact with the density properties of $\boldsymbol{V}_h$ and $\boldsymbol{W}_h$ (see (2.20) and (2.21)) yields that there exists a family of simple functions $\{(\boldsymbol{v}_h,\boldsymbol{w}_h)\}_{h>0}$ satisfying $(\boldsymbol{v}_h(s),\boldsymbol{w}_h(s))\in\boldsymbol{V}_h\times\boldsymbol{W}_h$ for every $s\in[0,T]$ and every $h>0$ as well as

$$\lim_{h\to0}\|\boldsymbol{v}_h-\boldsymbol{v}\|_{L^2((0,T),\boldsymbol{H}_0(\mathbf{curl}))}=\lim_{h\to0}\|\boldsymbol{w}_h-\boldsymbol{w}\|_{L^2((0,T),\boldsymbol{L}^2(\Omega))}=0. \tag{4.36}$$

Thus, test (4.23) with $(\boldsymbol{v}_h(s),\boldsymbol{w}_h(s))$ for $s\in(0,T)$ and integrate over $[0,T]$. Afterwards, we apply the limit superior to the resulting inequality to deduce with the strong convergence of $\overline{\boldsymbol{f}}_N$ toward $\boldsymbol{f}$ and (4.26) and (4.36) that

$$\begin{aligned}
\int_0^T(\boldsymbol{f}(s),\boldsymbol{v}(s)-\boldsymbol{E}(s))_{\boldsymbol{L}^2(\Omega)}ds&=\lim_{h\to0}\int_0^T(\overline{\boldsymbol{f}}_N(s),\boldsymbol{v}_h(s)-\overline{\boldsymbol{E}}_{N,h}(s))_{\boldsymbol{L}^2(\Omega)}ds\\
\underbrace{\leq}_{(4.23)}\quad&\limsup_{h\to0}\bigg[\int_0^T(\partial_t\boldsymbol{E}_{N,h}(s),\boldsymbol{v}_h(s)-\overline{\boldsymbol{E}}_{N,h}(s))_{\boldsymbol{L}^2_\epsilon(\Omega)}ds\\
&\quad+\int_0^T(\partial_t\boldsymbol{B}_{N,h}(s),\boldsymbol{w}_h(s)-\overline{\boldsymbol{B}}_{N,h}(s))_{\boldsymbol{L}^2_\nu(\Omega)}+(\mathbf{curl}\,\overline{\boldsymbol{E}}_{N,h}(s),\boldsymbol{w}_h(s))_{\boldsymbol{L}^2_\nu(\Omega)}ds\\
&\quad-\int_0^T(\overline{\boldsymbol{B}}_{N,h}(s),\mathbf{curl}\,\boldsymbol{v}_h(s))_{\boldsymbol{L}^2_\nu(\Omega)}ds+\int_0^T\varphi_N(s,\boldsymbol{v}_h(s))-\varphi_N(s,\overline{\boldsymbol{E}}_{N,h}(s))ds\bigg]\\
\underbrace{\leq}_{(4.24),(4.30),(4.31)}&\int_0^T(\partial_t\boldsymbol{E}(s),\boldsymbol{v}(s)-\boldsymbol{E}(s))_{\boldsymbol{L}^2_\epsilon(\Omega)}+(\partial_t\boldsymbol{B}(s),\boldsymbol{w}(s)-\boldsymbol{B}(s))_{\boldsymbol{L}^2_\nu(\Omega)}ds\\
&+\int_0^T(\mathbf{curl}\,\boldsymbol{E}(s),\boldsymbol{w}(s))_{\boldsymbol{L}^2_\nu(\Omega)}-(\boldsymbol{B}(s),\mathbf{curl}\,\boldsymbol{v}(s))_{\boldsymbol{L}^2_\nu(\Omega)}ds\\
&+\int_0^T\varphi(\theta(s),\boldsymbol{v}(s))-\varphi(\theta(s),\boldsymbol{E}(s))ds,
\end{aligned}\tag{4.37}$$

where we have also used (4.32) and Fatou's lemma to obtain convergence of the last time integral. Finally, fix $t\in(0,T)$, $\iota\in(0,T-\iota)$, and $(\tilde{\boldsymbol{v}},\tilde{\boldsymbol{w}})\in\boldsymbol{H}_0(\mathbf{curl})\times\boldsymbol{L}^2(\Omega)$. Hence, choosing

$$(\boldsymbol{v},\boldsymbol{w})(s)=\begin{cases}(\tilde{\boldsymbol{v}},\tilde{\boldsymbol{w}}) & \text{if } s\in(t,t+\iota),\\ (\boldsymbol{E}(s),\boldsymbol{B}(s)) & \text{else,}\end{cases}$$

multiplying (4.37) with $1/\iota$ and letting $\iota\to0$ yields that

$$(\boldsymbol{E},\boldsymbol{B})\in W^{1,\infty}((0,T),\boldsymbol{L}^2_\epsilon(\Omega)\times\boldsymbol{H}_0(\text{div=0}))\cap L^\infty((0,T),\boldsymbol{H}_0(\mathbf{curl})\times\boldsymbol{H}_0(\text{div=0}))$$

satisfies the evolutionary variational inequality (VI).

The uniqueness of the solution to (VI) follows by an energy argument: Let

$$(\tilde{\boldsymbol{E}},\tilde{\boldsymbol{B}})\in W^{1,\infty}((0,T),\boldsymbol{L}^2_\epsilon(\Omega)\times\boldsymbol{L}^2_\nu(\Omega))\cap L^\infty((0,T),\boldsymbol{H}_0(\mathbf{curl})\times\boldsymbol{L}^2_\nu(\Omega))$$

be another solution to (VI). Then, inserting $(\boldsymbol{v},\boldsymbol{w})=(\tilde{\boldsymbol{E}}(t),\tilde{\boldsymbol{B}}(t))$ in (VI) associated with $(\boldsymbol{E},\boldsymbol{B})$ and $(\boldsymbol{v},\boldsymbol{w})=(\boldsymbol{E}(t),\boldsymbol{B}(t))$ in (VI) associated with $(\tilde{\boldsymbol{E}},\tilde{\boldsymbol{B}})$, and then adding the resulting inequalities together, we obtain

$$\int_\Omega\epsilon(\partial_t\boldsymbol{E}(t)-\partial_t\tilde{\boldsymbol{E}}(t))\cdot(\boldsymbol{E}(t)-\tilde{\boldsymbol{E}}(t))+\nu(\partial_t\boldsymbol{B}(t)-\partial_t\tilde{\boldsymbol{B}}(t))\cdot(\boldsymbol{B}(t)-\tilde{\boldsymbol{B}}(t))\,dx\leq0,$$

which implies that the difference $(\boldsymbol{e}(t),\boldsymbol{b}(t))=(\boldsymbol{E}(t)-\tilde{\boldsymbol{E}}(t),\boldsymbol{B}(t)-\tilde{\boldsymbol{B}}(t))$ fulfills

$$\frac12\frac{d}{dt}\|\boldsymbol{e}(t)\|^2_{\boldsymbol{L}^2_\epsilon(\Omega)}+\frac12\frac{d}{dt}\|\boldsymbol{b}(t)\|^2_{\boldsymbol{L}^2_\nu(\Omega)}\leq0.$$

Since $\boldsymbol{e}(0) = \boldsymbol{b}(0) = 0$, the above inequality yields that $\boldsymbol{e}(t) = \boldsymbol{b}(t) = 0$ for all $t \in [0,T]$. Hence, $(\boldsymbol{E}, \boldsymbol{B})$ is the unique solution to (VI). ■

Remark 4.9. A main consequence of Theorem 4.8 is the global well-posedness for (VI). We point out that [182] proved existence and uniqueness results for hyperbolic Maxwell's variational inequalities with a general nonlinearity, based on a *direct* approach, without discretization techniques. However, due to the temperature-dependent critical current density j_c, [182] cannot be applied to deduce the well-posedness of (VI). Here, their approach would require a substantial extension of [182] to the case of time-dependent nonlinearities.

We now in place to prove our main result on the uniform convergence of the solutions of (4.23) towards the solution of (VI).

Theorem 4.10. *Let $N = N(h)$ be a family of natural numbers with $N(h) \to \infty$ for $h \to 0$. Then, under Assumptions* 3.10 *and* 4.1*, the solution $(\boldsymbol{E}_{N,h}, \boldsymbol{B}_{N,h})$ to* (4.23) *converges uniformly to the solution $(\boldsymbol{E}, \boldsymbol{B})$ of* (VI)*, i.e.,*

$$\begin{aligned}
\lim_{h\to 0} \|\boldsymbol{E}_{N,h} - \boldsymbol{E}\|_{\mathcal{C}([0,T],\boldsymbol{L}^2_\epsilon(\Omega))} &= \lim_{h\to 0} \|\boldsymbol{B}_{N,h} - \boldsymbol{B}\|_{\mathcal{C}([0,T],\boldsymbol{L}^2_\nu(\Omega))} = 0,\\
\lim_{h\to 0} \|\overline{\boldsymbol{E}}_{N,h} - \boldsymbol{E}\|_{L^\infty((0,T),\boldsymbol{L}^2_\epsilon(\Omega))} &= \lim_{h\to 0} \|\overline{\boldsymbol{B}}_{N,h} - \boldsymbol{B}\|_{L^\infty((0,T),\boldsymbol{L}^2_\nu(\Omega))} = 0.
\end{aligned}$$

Proof. First of all, we test (VI) with $(\boldsymbol{v}, \boldsymbol{w}) = (\overline{\boldsymbol{E}}_{N,h}(t), \overline{\boldsymbol{B}}_{N,h}(t))$ to obtain

$$\begin{aligned}
&\int_\Omega \epsilon\partial_t \boldsymbol{E}(t)\cdot(\overline{\boldsymbol{E}}_{N,h}(t) - \boldsymbol{E}(t)) + \nu\partial_t\boldsymbol{B}(t)\cdot(\overline{\boldsymbol{B}}_{N,h}(t) - \boldsymbol{B}(t))\,dx\\
&\quad + \int_\Omega \nu\,\mathbf{curl}\,\boldsymbol{E}(t)\cdot\overline{\boldsymbol{B}}_{N,h}(t) - \nu\boldsymbol{B}(t)\cdot\mathbf{curl}\,\overline{\boldsymbol{E}}_{N,h}(t)\,dx\\
&\quad + \varphi(\theta(t),\overline{\boldsymbol{E}}_{N,h}(t)) - \varphi(\theta(t),\boldsymbol{E}(t)) \geq \int_\Omega \boldsymbol{f}(t)\cdot(\overline{\boldsymbol{E}}_{N,h}(t) - \boldsymbol{E}(t))\,dx
\end{aligned} \tag{4.38}$$

for a.e. $t \in (0,T)$. Next, inserting $(\boldsymbol{v}_h, \boldsymbol{w}_h) = (\boldsymbol{\Phi}_h\boldsymbol{E}(t), 0) \in \boldsymbol{V}_h \times \boldsymbol{W}_h$ in (4.23) leads to

$$\begin{aligned}
&\int_\Omega \epsilon\partial_t\boldsymbol{E}_{N,h}(t)\cdot(\boldsymbol{E}(t) - \overline{\boldsymbol{E}}_{N,h}(t)) + \nu\partial_t\boldsymbol{B}_{N,h}(t)\cdot(\boldsymbol{B}(t) - \overline{\boldsymbol{B}}_{N,h}(t))\,dx\\
&\quad + \int_\Omega \epsilon\partial_t\boldsymbol{E}_{N,h}(t)\cdot(\boldsymbol{\Phi}_h\boldsymbol{E}(t) - \boldsymbol{E}(t))\,dx - \int_\Omega \nu\partial_t\boldsymbol{B}_{N,h}(t)\cdot\boldsymbol{B}(t)\,dx\\
&\quad - \int_\Omega \nu\overline{\boldsymbol{B}}_{N,h}(t)\cdot\mathbf{curl}\,\boldsymbol{\Phi}_h\boldsymbol{E}(t)\,dx + \varphi_N(t,\boldsymbol{\Phi}_h\boldsymbol{E}(t)) - \varphi_N(t,\overline{\boldsymbol{E}}_{N,h}(t))\\
&\geq \int_\Omega \overline{\boldsymbol{f}}_N(t)\cdot(\boldsymbol{\Phi}_h\boldsymbol{E}(t) - \overline{\boldsymbol{E}}_{N,h}(t))\,dx
\end{aligned} \tag{4.39}$$

for a.e. $t \in (0,T)$. Now, by using the fact that $\partial_t\boldsymbol{B}_{N,h}(t) = -\,\mathbf{curl}\,\overline{\boldsymbol{E}}_{N,h}(t)$ holds for a.e. $t \in (0,T)$ (see (4.11) and (4.21)), we obtain

$$\int_\Omega \nu(\partial_t\boldsymbol{B}_{N,h}(t) + \mathbf{curl}\,\overline{\boldsymbol{E}}_{N,h}(t))\cdot\boldsymbol{B}(t)\,dx = 0 \quad \text{for a.e. } t \in (0,T). \tag{4.40}$$

Moreover, we know from Theorem 4.4 that $\overline{\boldsymbol{B}}_{N,h}(t) \in \mathbf{curl}\,\boldsymbol{V}_h$, which implies by (2.22) that

$$\int_\Omega \nu\overline{\boldsymbol{B}}_{N,h}(t)\cdot\mathbf{curl}(\boldsymbol{E}(t) - \boldsymbol{\Phi}_h\boldsymbol{E}(t))\,dx = 0 \quad \text{for a.e. } t \in (0,T). \tag{4.41}$$

In view of (4.40)–(4.41), adding (4.38) and (4.39) together and then integrating the resulting inequality over the time interval $[0,\sigma]$ with $\sigma \in (0,T]$ yield that

$$
\begin{aligned}
(4.42)\qquad & \int_0^\sigma \int_\Omega \epsilon(\partial_t \boldsymbol{E}_{N,h}(t) - \partial_t \boldsymbol{E}(t)) \cdot (\overline{\boldsymbol{E}}_{N,h}(t) - \boldsymbol{E}(t))\, dxdt \\
& \quad + \int_0^\sigma \int_\Omega \nu(\partial_t \boldsymbol{B}_{N,h}(t) - \partial_t \boldsymbol{B}(t)) \cdot (\overline{\boldsymbol{B}}_{N,h}(t) - \boldsymbol{B}(t))\, dxdt \\
& \le \int_0^\sigma \Big[\int_\Omega \overline{\boldsymbol{f}}_N(t) \cdot (\boldsymbol{E}(t) - \boldsymbol{\Phi}_h \boldsymbol{E}(t)) + (\boldsymbol{f}(t) - \overline{\boldsymbol{f}}_N(t)) \cdot (\boldsymbol{E}(t) - \overline{\boldsymbol{E}}_{N,h}(t))\, dx \\
& \quad + \int_\Omega \epsilon \partial_t \boldsymbol{E}_{N,h}(t) \cdot (\boldsymbol{\Phi}_h \boldsymbol{E}(t) - \boldsymbol{E}(t))\, dx + \big(\varphi_N(t, \boldsymbol{\Phi}_h \boldsymbol{E}(t)) - \varphi(\theta(t), \boldsymbol{E}(t))\big) \\
& \quad + \big(\varphi(\theta(t), \overline{\boldsymbol{E}}_{N,h}(t)) - \varphi_N(t, \overline{\boldsymbol{E}}_{N,h}(t))\big) \Big] dt =: \sum_{i=1}^5 C_i.
\end{aligned}
$$

We proceed by showing the convergence of C_i, $i \in \{1,\dots,5\}$, towards 0 as $h \to 0$. This obviously exploits the convergence property of $\boldsymbol{\Phi}_h$. Therefore, we use (2.28) and (2.29) to deduce by Lebesgue's dominated convergence theorem that

$$
(4.43)\qquad \lim_{h\to 0} \int_0^\sigma \|\boldsymbol{\Phi}_h \boldsymbol{E}(t) - \boldsymbol{E}(t)\|_{\boldsymbol{L}^2_\epsilon(\Omega)}\, dt = 0 \quad \forall \sigma \in [0,T].
$$

Now, (A3.5), Lemma 4.7 and (4.43) imply for $i \in \{1,3\}$ that $|C_i| \to 0$ as $h \to 0$. Also, the Lipschitz continuity of $\boldsymbol{f}$ (A3.5) together with Theorem 4.8 implies that $|C_2| \to 0$ as $h \to 0$. Next, the convergence for C_4 is shown: We begin with

$$
\begin{aligned}
(4.44)\qquad & \Big| \int_0^\sigma \varphi_N(t, \boldsymbol{\Phi}_h \boldsymbol{E}(t)) - \varphi(\theta(t), \boldsymbol{E}(t)) dt \Big| \\
& \le \int_0^T |\varphi_N(t, \boldsymbol{\Phi}_h \boldsymbol{E}(t)) - \varphi_N(t, \boldsymbol{E}(t))| dt + \int_0^T |\varphi_N(t, \boldsymbol{E}(t)) - \varphi(\theta(t), \boldsymbol{E}(t))| dt.
\end{aligned}
$$

Because of (A3.3) and (A3.5), the first term on the right-hand side of (4.44) satisfies

$$
(4.45)\qquad \int_0^T |\varphi_N(t, \boldsymbol{\Phi}_h \boldsymbol{E}(t)) - \varphi_N(t, \boldsymbol{E}(t))| dt \le C \int_0^T \|\boldsymbol{\Phi}_h \boldsymbol{E}(t) - \boldsymbol{E}(t)\|_{\boldsymbol{L}^2_\epsilon(\Omega)} dt,
$$

with a constant $C > 0$, independent of h. On the other hand, the second term in (4.44) is estimated by using (A3.4) and (A3.5):

$$
\begin{aligned}
(4.46)\qquad & \int_0^T |\varphi_N(t, \boldsymbol{E}(t)) - \varphi(\theta(t), \boldsymbol{E}(t))| dt \\
& \underbrace{=}_{(4.22)} \sum_{n=1}^N \int_{t_{n-1}}^{t_n} \int_\Omega |j_c(x, \theta(t_n, x)) - j_c(x, \theta(t,x))|\, |\boldsymbol{E}(t)|\, dxdt \\
& \le C \sum_{n=1}^N \int_{t_{n-1}}^{t_n} \tau \|\boldsymbol{E}(t)\|_{\boldsymbol{L}^2_\epsilon(\Omega)} dt = C\tau \|\boldsymbol{E}\|_{L^1((0,T),\boldsymbol{L}^2_\epsilon(\Omega))}.
\end{aligned}
$$

Thus, combining (4.44)–(4.46) gives

$$
(4.47)\qquad |C_4| \le C \Big(\int_0^T \|\boldsymbol{\Phi}_h \boldsymbol{E}(t) - \boldsymbol{E}(t)\|_{\boldsymbol{L}^2_\epsilon(\Omega)} dt + \tau \|\boldsymbol{E}\|_{L^1((0,T),\boldsymbol{L}^2_\epsilon(\Omega))} \Big) \overbrace{\to}^{(4.43)} 0 \quad \text{as } h \to 0.
$$

We reuse the arguments from (4.46) in combination with Lemma 4.6 to obtain the convergence $|C_5| \to 0$ as $h \to 0$. Finally, we extract the desired norms on the left hand side of (4.42) as follows:

$$\begin{aligned}(4.48)\qquad \int_0^\sigma \int_\Omega \epsilon(\partial_t \boldsymbol{E}_{N,h}(t) - \partial_t \boldsymbol{E}(t)) \cdot (\overline{\boldsymbol{E}}_{N,h}(t) - \boldsymbol{E}(t))\, dxdt &= \frac{1}{2}\|\boldsymbol{E}_{N,h}(\sigma) - \boldsymbol{E}(\sigma)\|^2_{\boldsymbol{L}^2_\epsilon(\Omega)} \\ -\frac{1}{2}\|\boldsymbol{E}_{0h} - \boldsymbol{E}_0\|^2_{\boldsymbol{L}^2_\epsilon(\Omega)} + \int_0^\sigma \int_\Omega \epsilon(\partial_t \boldsymbol{E}_{N,h}(t) - \partial_t \boldsymbol{E}(t)) \cdot (\overline{\boldsymbol{E}}_{N,h}(t) - \boldsymbol{E}_{N,h}(t))\, dxdt\end{aligned}$$

and

$$\begin{aligned}(4.49)\qquad &\int_0^\sigma \int_\Omega \nu(\partial_t \boldsymbol{B}_{N,h}(t) - \partial_t \boldsymbol{B}(t)) \cdot (\overline{\boldsymbol{B}}_{N,h}(t) - \boldsymbol{B}(t))\, dxdt \\ &= \frac{1}{2}\|\boldsymbol{B}_{N,h}(\sigma) - \boldsymbol{B}(\sigma)\|^2_{\boldsymbol{L}^2_\nu(\Omega)} - \frac{1}{2}\|\boldsymbol{B}_{0h} - \boldsymbol{B}_0\|^2_{\boldsymbol{L}^2_\nu(\Omega)} \\ &\quad + \int_0^\sigma \int_\Omega \nu(\partial_t \boldsymbol{B}_{N,h}(t) - \partial_t \boldsymbol{B}(t)) \cdot (\overline{\boldsymbol{B}}_{N,h}(t) - \boldsymbol{B}_{N,h}(t))\, dxdt.\end{aligned}$$

In view of (4.25) and Lemma 4.7, we have

$$\begin{aligned}(4.50)\qquad &\left| \int_0^\sigma \int_\Omega \epsilon(\partial_t \boldsymbol{E}_{N,h}(t) - \partial_t \boldsymbol{E}(t)) \cdot (\overline{\boldsymbol{E}}_{N,h}(t) - \boldsymbol{E}_{N,h}(t))\, dxdt \right| \\ &\leq \|\partial_t \boldsymbol{E}_{N,h} - \partial_t \boldsymbol{E}\|_{L^1((0,T),\boldsymbol{L}^2_\epsilon(\Omega))} \|\overline{\boldsymbol{E}}_{N,h} - \boldsymbol{E}_{N,h}\|_{L^\infty((0,T),\boldsymbol{L}^2_\epsilon(\Omega))} \\ &\leq C\tau \|\partial_t \boldsymbol{E}_{N,h} - \partial_t \boldsymbol{E}\|_{L^1((0,T),\boldsymbol{L}^2_\epsilon(\Omega))} \leq C\tau(\|\partial_t \boldsymbol{E}\|_{L^1((0,T),\boldsymbol{L}^2_\epsilon(\Omega))} + 1),\end{aligned}$$

and analogously

$$\begin{aligned}(4.51)\qquad &\left| \int_0^\sigma \int_\Omega \nu(\partial_t \boldsymbol{B}_{N,h}(t) - \partial_t \boldsymbol{B}(t)) \cdot (\overline{\boldsymbol{B}}_{N,h}(t) - \boldsymbol{B}_{N,h}(t))\, dxdt \right| \\ &\leq C\tau(\|\partial_t \boldsymbol{B}\|_{L^1((0,T),\boldsymbol{L}^2_\nu(\Omega))} + 1).\end{aligned}$$

From (4.42) and (4.48)–(4.51) combined with the previously proved convergence for C_i for all $i \in \{1, \ldots, 5\}$ and Lemma 4.3, we obtain

$$(4.52)\qquad \lim_{h\to 0} \|\boldsymbol{E}_{N,h}(t) - \boldsymbol{E}(t)\|_{\boldsymbol{L}^2_\epsilon(\Omega)} = \lim_{h\to 0} \|\boldsymbol{B}_{N,h}(t) - \boldsymbol{B}(t)\|_{\boldsymbol{L}^2_\nu(\Omega)} = 0 \quad \forall t \in [0,T].$$

On the other hand, Lemmas 4.6 and 4.7 imply the existence of a positive constant $C > 0$, independent of N and h, such that

$$(4.53)\qquad \|(\boldsymbol{E}_{N,h}, \boldsymbol{B}_{N,h})\|_{W^{1,\infty}((0,T),\boldsymbol{L}^2_\epsilon(\Omega)\times\boldsymbol{L}^2_\nu(\Omega))} \leq C \quad \forall h > 0.$$

Thus, $\{(\boldsymbol{E}_{N,h}, \boldsymbol{B}_{N,h})\}_{h>0} \subset \mathcal{C}([0,T], \boldsymbol{L}^2_\epsilon(\Omega)\times\boldsymbol{L}^2_\nu(\Omega))$ is uniformly bounded. Furthermore, by (4.21) and (4.53), we deduce that

$$(4.54)\qquad \|\boldsymbol{E}_{N,h}(t) - \boldsymbol{E}_{N,h}(\tilde{t})\|_{\boldsymbol{L}^2_\epsilon(\Omega)} + \|\boldsymbol{B}_{N,h}(t) - \boldsymbol{B}_{N,h}(\tilde{t})\|_{\boldsymbol{L}^2_\nu(\Omega)} \leq C|t - \tilde{t}|,$$

where $C > 0$ is independent of N, h and $t, \tilde{t}$. Therefore, by (4.52)–(4.54), the Arzelá-Ascoli theorem for Banach space-valued functions (cf. [111, Theorem 3.1]) is applicable and implies the existence of a subsequence of $\{(\boldsymbol{E}_{N,h}, \boldsymbol{B}_{N,h})\}_{h>0}$ converging uniformly towards $(\boldsymbol{E}, \boldsymbol{B})$. As $(\boldsymbol{E}, \boldsymbol{B})$ is the unique solution of (VI), independent of the choice of the converging subsequence, a standard argument yields that the whole sequence converges uniformly, i.e.,

$$\lim_{h\to 0} \|\boldsymbol{E}_{N,h} - \boldsymbol{E}\|_{\mathcal{C}([0,T],\boldsymbol{L}^2_\epsilon(\Omega))} = 0 \underbrace{\Rightarrow}_{(4.25)} \lim_{h\to 0} \|\overline{\boldsymbol{E}}_{N,h} - \boldsymbol{E}\|_{L^\infty((0,T),\boldsymbol{L}^2_\epsilon(\Omega))} = 0.$$

$$\lim_{h\to 0} \|\boldsymbol{B}_{N,h} - \boldsymbol{B}\|_{\mathcal{C}([0,T],\boldsymbol{L}^2_\nu(\Omega))} = 0 \underbrace{\Rightarrow}_{(4.25)} \lim_{h\to 0} \|\overline{\boldsymbol{B}}_{N,h} - \boldsymbol{B}\|_{L^\infty((0,T),\boldsymbol{L}^2_\nu(\Omega))} = 0.$$

This completes the proof. ∎

4.2 ▪ A Priori Error Analysis

Thanks to Corollary 2.9, we have an error estimate with low regularity fields for $\boldsymbol{\Phi}_h \colon \boldsymbol{H}_0(\mathbf{curl}) \to \boldsymbol{V}_h$ introduced in Proposition 2.7 of the form

$$\|\boldsymbol{y} - \boldsymbol{\Phi}_h \boldsymbol{y}\|_{\boldsymbol{H}(\mathbf{curl})} \leq C h^s \|\boldsymbol{y}\|_{\boldsymbol{H}_0^s(\mathbf{curl})} \quad \forall \boldsymbol{y} \in \boldsymbol{H}_0^s(\mathbf{curl})$$

for all $h > 0$ with $s \in (0, 1]$. In order to apply Corollary 2.9 we have to employ an additional regularity assumption on the initial electric field and the electric field of the solution.

Assumption 4.11 (Additional assumptions on the initial data and the solution).

(A4.8) There exists $s \in (0, 1]$ such that the initial electric field $\boldsymbol{E}_0 \in \boldsymbol{H}_0^s(\mathbf{curl})$ and the solution of (VI) satisfies $\boldsymbol{E} \in L^1((0,T), \boldsymbol{H}_0^s(\mathbf{curl}))$.

Assumption 4.11 yields the following error estimate for the initial value, which follows readily from (4.9) by using (A4.8) and Corollary 2.9.

Lemma 4.12. *Let Assumptions* 3.10*,* 4.1 *and* 4.11 *hold. Then there exists a constant $C > 0$, independent of $h > 0$, such that*

$$\|\boldsymbol{E}_{0h} - \boldsymbol{E}_0\|^2_{\boldsymbol{L}^2_\epsilon(\Omega)} + \|\boldsymbol{B}_{0h} - \boldsymbol{B}_0\|^2_{\boldsymbol{L}^2_\nu(\Omega)} \leq C h^s \quad \forall h > 0. \tag{4.55}$$

Theorem 4.13. *Let Assumptions* 3.10*,* 4.1 *and* 4.11 *hold. Then, there exists a constant $C > 0$, independent of N and h, such that*

$$\begin{aligned} &\|\boldsymbol{E}_{N,h} - \boldsymbol{E}\|^2_{\mathcal{C}([0,T],\boldsymbol{L}^2_\epsilon(\Omega))} + \|\boldsymbol{B}_{N,h} - \boldsymbol{B}\|^2_{\mathcal{C}([0,T],\boldsymbol{L}^2_\nu(\Omega))} \\ &\quad \leq C(h^s + \tau)(\|\boldsymbol{E}\|_{L^1((0,T),\boldsymbol{H}_0^s(\mathbf{curl}))} + \|\partial_t \boldsymbol{E}\|_{L^1((0,T),\boldsymbol{L}^2_\epsilon(\Omega))} + \|\partial_t \boldsymbol{B}\|_{L^1((0,T),\boldsymbol{L}^2_\nu(\Omega))} + 1) \end{aligned}$$

holds for every $h > 0$ and every $N \in \mathbb{N}$.

Proof. The lines of the proof are similar to the proof of Theorem 4.10, but, due to the regularity assumption on $\boldsymbol{E}$ (Assumption 4.11), we may use Corollary 2.9 in place of (2.29). Thus, we consider again (4.42) and give estimates for C_i, $i \in \{1, \ldots, 5\}$, instead of simply proving their convergence towards 0. The stability results in Lemma 4.6 and Lemma 4.7 combined with the regularity of $\boldsymbol{E}$ (see (A4.8)) as well as the error estimates for $\boldsymbol{\Phi}_h$ in Corollary 2.9 lead to

$$|C_i| \leq C h^s \|\boldsymbol{E}\|_{L^1((0,T),\boldsymbol{H}_0^s(\mathbf{curl}))} \quad \forall i \in \{1, 3\}, \tag{4.56}$$

with a constant C, independent of the time variable, N, and h. To estimate C_2, we use the Lipschitz continuity of $\boldsymbol{f}$ (see (A3.5)) and Theorem 4.10:

$$|C_2| \leq C\tau \int_0^\sigma \|\boldsymbol{E}(t) - \overline{\boldsymbol{E}}_{N,h}(t)\|_{\boldsymbol{L}^2_\epsilon(\Omega)} dt \leq C\tau. \tag{4.57}$$

Next, C_4 is estimated by applying Corollary 2.9 to (4.47)

$$|C_4| \leq C(h^s + \tau)\|\boldsymbol{E}\|_{L^1((0,T),\boldsymbol{H}_0^s(\mathbf{curl}))}. \tag{4.58}$$

Last but not least, the arguments from (4.46) in combination with Lemma 4.6 imply $|C_5| \leq C\tau$. The combination of (4.42) and (4.48)-(4.49) with (4.50)-(4.51) as well as the previously proved estimation for C_i, $i \in \{1, \ldots, 5\}$ and Lemma 4.12 finally yields the desired error estimate. ■

Remark 4.14. The results by Ern and Guermond [70, 71] are also valid for higher-order finite elements. Therefore, [70, 71] together with the higher-order FEM for linear Maxwell's equations [124] would serve as an important basis for the extension of our approach to the higher-order case.

4.3 ▪ Computations

We close the theoretical analysis by establishing our numerical algorithm along with some numerical results for particular examples of (VI). When it comes to computing the solution $(\boldsymbol{E}, \boldsymbol{B})$ of (VI), Euler's implicit method provides an iterative algorithm, which also enables us to split the mixed problem into two associated problems as we did in Theorem 4.4. We recall (4.11), which gives an explicit formula for $\boldsymbol{B}_h^n$:

$$\boldsymbol{B}_h^n = \boldsymbol{B}_h^{n-1} - \tau \,\mathbf{curl}\, \boldsymbol{E}_h^n \tag{4.59}$$

provided that $\boldsymbol{E}_h^n$ is already computed. In view of (4.13), $\boldsymbol{E}_h^n$ solves an elliptic $\mathbf{curl}$-$\mathbf{curl}$ variational inequality of the form

$$a(\boldsymbol{E}_h^n, \boldsymbol{v}_h - \boldsymbol{E}_h^n) + \varphi^n(\boldsymbol{v}_h) - \varphi^n(\boldsymbol{E}_h^n) \geq \langle \tilde{\boldsymbol{f}}^n, \boldsymbol{v}_h - \boldsymbol{E}_h^n \rangle \quad \forall \boldsymbol{v}_h \in \boldsymbol{V}_h. \tag{4.60}$$

To solve this variational inequality, we use the semismooth Newton method Algorithm 3.1. Therefore, we have to compute (4.59) and (4.60) in every time step. We propose Algorithm 4.1 to solve ($\mathrm{VI}_{N,\,h}$).

Algorithm 4.1 Solution for ($\mathrm{VI}_{N,\,h}$)

1: Fix $N \in \mathbb{N}$, $h > 0$ and set $\tau = 1/N$
2: Initialize $(\boldsymbol{E}_h^0, \boldsymbol{B}_h^0) = (\boldsymbol{E}_{0h}, \boldsymbol{B}_{0h})$ by applying Algorithm 3.1 to (4.4)
3: **for** $n \in \{1, \dots, N\}$ **do**
4: Compute $\boldsymbol{E}_h^n$ as the solution of (4.60) by applying Algorithm 3.1
5: Compute $\boldsymbol{B}_h^n$ as the solution of (4.59)
6: **end for**

4.4 ▪ Numerical Results

Our computational domain is the cube $\Omega = (-1, 1)^3$ and we apply a circular current $\boldsymbol{f} \colon \Omega \to \mathbb{R}^3$ defined by

$$\boldsymbol{f}(x, y, z) = \begin{cases} 1/R\Big(0,\ -z/(y^2+z^2)^{1/2},\ y/(y^2+z^2)^{1/2}\Big) & \text{for } (x, y, z) \in \Omega_p \\ 0 & \text{for } (x, y, z) \notin \Omega_p \end{cases}$$

to a cylindrical pipe coil $\Omega_p \coloneqq \{(x, y, z) \in \mathbb{R}^3 \,:\, |x| \leq 0.5,\ \sqrt{y^2+z^2} \in [0.3, 0.5]\}$. The constant $R > 0$ denotes the electrical resistance of the pipe (here $R = 1$). All implementations were done with the open-source finite element computational platform FENICS [122], and as a visualization tool PARAVIEW was used. For this study, the uniform tetrahedral mesh was locally refined around the coil. If we do not include a superconductor in this setup, the applied current induces an orthogonal magnetic field, which admits its greatest field strength in the center of the coil. Mathematically speaking, this means $j_c \equiv 0$ and thus, (VI) reduces to the linear Maxwell's equations.

4.4.1 ▪ First Example – Superconductor as Ball

In the first example, we place a type-II superconducting ball Ω_{sc} with radius 0.2 in the center of the pipe, set $j_c = 80\chi_{\Omega_{\mathrm{sc}}}$, $\epsilon = \mu = \nu = 1$, and solve the compatibility system (4.4) for the discrete initial value $(\boldsymbol{E}_{0h}, \boldsymbol{B}_{0h})$. In our computation, the mesh was refined around the superconductor such that we end up with roughly $1.300.000$ cells and $5.600.000$ degrees of freedom (DOFs) for the mixed finite

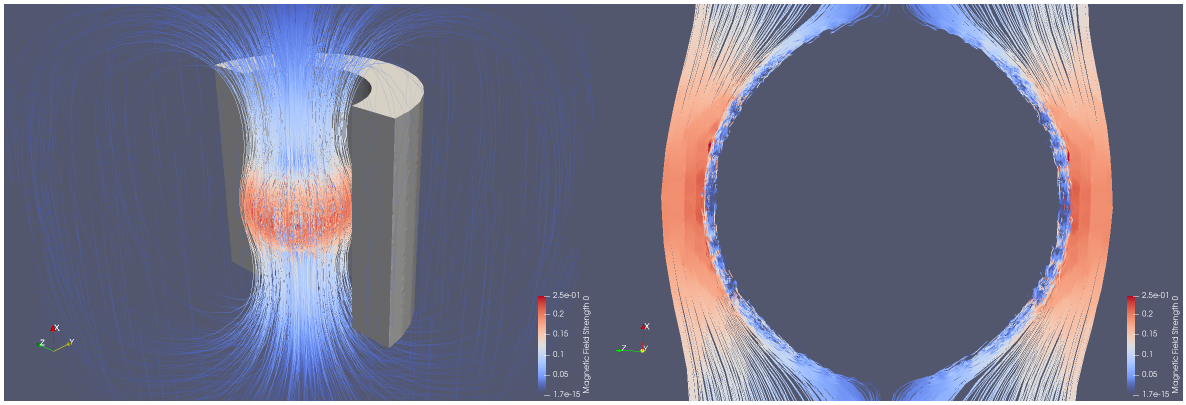

Figure 4.1. *First numerical example. Left: Magnetic field lines and the clipped pipe coil. Right: 2D-slice of the magnetic field along the x-z axis.*

Table 4.1. *Critical current j_c and temperature θ of the superconductor at each the time step.*

n	0	1	2	3	4	5	6
$j_c(\cdot, \theta(t_n))$	$80\chi_{\Omega_{sc}}$	$50\chi_{\Omega_{sc}}$	$35\chi_{\Omega_{sc}}$	$20\chi_{\Omega_{sc}}$	$10\chi_{\Omega_{sc}}$	$5\chi_{\Omega_{sc}}$	$0,5\chi_{\Omega_{sc}}$
$\theta(t_n)$	$60,0K$	$65,0K$	$67,5K$	$70,0K$	$72,5K$	$75,0K$	$80,0K$
t_n	0	$1/6$	$1/3$	$1/2$	$2/3$	$5/6$	1

element space $\boldsymbol{V}_h \times \boldsymbol{W}_h$. The resulting solution $(\boldsymbol{E}_{0h}, \boldsymbol{B}_{0h})$ of (4.4) exhibits the physical phenomenon of the Meissner–Ochsenfeld effect. In Figure 4.1, we see how the magnetic field lines get repelled by the superconductor and since they are squashed between the superconductor and the coil, one observes the highest magnetic field strength in this area. This is in line with the theoretical physics as the shielding currents add up on the outside of the superconductor (cf. section 1.1).

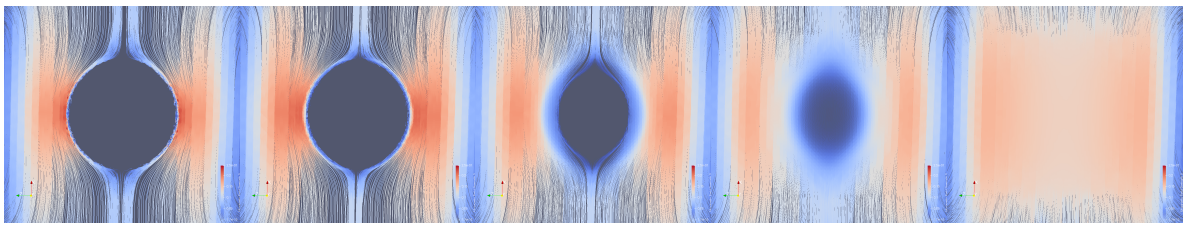

Figure 4.2. *First Example: Evolution of the magnetic field around the superconductor in the time-steps t_n for $n \in \{0, 1, 2, 3, 4\}$.*

Keeping the observations of the stationary example in mind, we continue and compute a time-dependent problem, where the solution of the first example serves as the discrete initial electromagnetic field, since it satisfies the discrete compatibility system (4.4). We consider the temperature dependence in the critical current density j_c for a superconductor with the nominal composition $Y_{1.2}Ba_{0.8}Cu_2O_x$ as it was suggested in [7]. Moreover, we set $T = 1$ as well as $\tau = 1/6$ and use the same amount of DOFs and cells as in the stationary example. We place the cooled down superconductor inside the coil the same way it was done previously, but now the temperature θ increases over time (see Table 4.1), whereas the applied current source $\boldsymbol{f}$ stays constant. The evolution of the magnetic field over time is shown in Figure 4.2. One observes that the magnetic field lines in the squashed area start penetrating the superconductor as the temperature becomes higher and higher. As soon as the temperature θ exceeds the threshold $75K$, the magnetic field completely penetrates the

superconductor and we can no longer observe the Meissner–Ochsenfeld effect.

4.4.2 ▪ Second Example – Superconductor with Hole

In the first example we have seen that a superconductor in the form of a simply connected domain repells magnetic field lines as long as the operating temperature is above the critical threshold. Now, for the second example, we consider a superconductor that is no longer simply connected. For instance, we may choose

$$\Omega_{\mathrm{sc}} \coloneqq \left\{(x,y,z) \in \mathbb{R}^3 \,:\, |x| \leq 0.1,\ \sqrt{y^2+z^2} \in [0.1, 0.2]\right\}.$$

which corresponds to a short pipe coil. By the same local refinement, we obtain roughly $1.000.000$ cells and $4.000.000$ DOFs. In Figure 4.4 we observe that not only the superconductor itself but also the area enclosed by the material is completely shielded from magnetic field penetration. As the temperature of the material rises (see Table 4.1) the Meissner–Ochsenfeld effect weakens until it is completely broken down (see Figure 4.4e). In contrast to the first example, we see in Figure 4.4a that the magnetic field peaks at the outer edges of the superconductor. Therefore, the magnetic field penetration begins at these areas and distributes the condensed field lines more uniformly across the whole outer boundary of the material. Thereafter, the superconductor exhibits a similar behaviour regarding the mixed state as the first example.

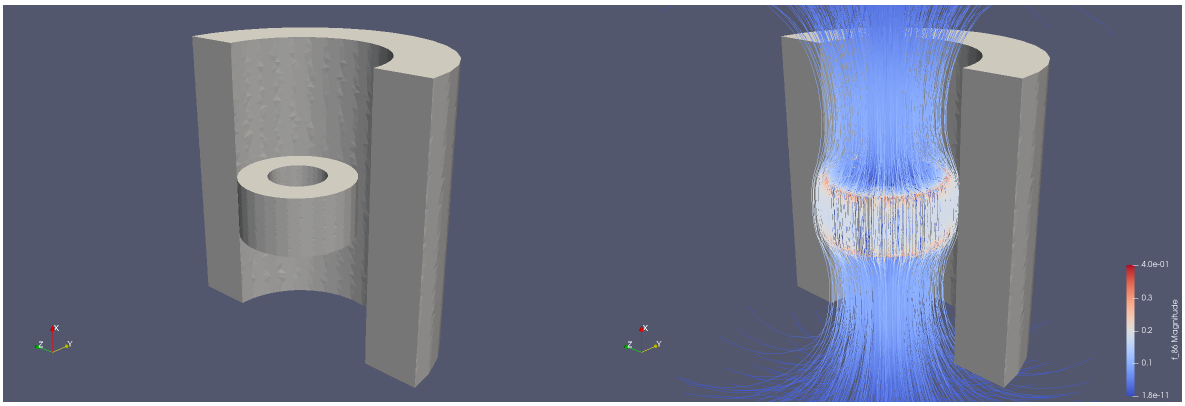

Figure 4.3. *Second Example. Left: Geometry of the superconductor Ω_{sc} and the induction coil. Right: Initial magnetic field and clipped pipe coil.*

As a final remark we would like to emphasize that this shielding effect is far from obvious. Yet a naive point of thinking would in fact indicate the opposite, meaning that the magnetic field simply penetrates through the hole of the material. However, according to physical experiments [110], superconductors shaped as pipe coils still shield its enclosed area even if the open ends are directly facing the field lines. Again, this underlines the accuracy of the model (VI) and its numerical approximation ($\mathrm{VI}_{N,h}$). Let us note that we have reported similar numerical results in [170].

The Next Steps

The Bean critical-state model is a free boundary problem, as it involves unknown superconductive and normal regions, which may change their locations in the course of time depending on the temperature distribution θ and the applied current source $\boldsymbol{f}$. Thus, an adaptive mesh refinement strategy based on rigorous a posteriori error estimators will be useful, not only for increasing the numerical accuracy, but also for capturing the unknown interfaces between the superconductive and normal regions. As

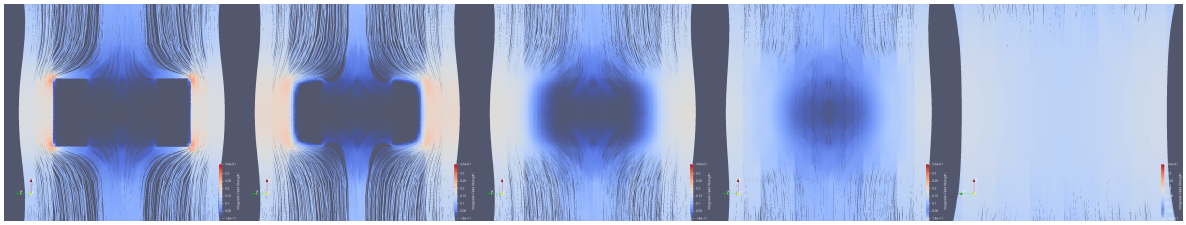

Figure 4.4. *Second example: Evolution of the magnetic field around the superconductor in the time-steps t_n for $n \in \{0, 1, 2, 3, 4\}$.*

for the forthcoming chapter, we will focus on the stationary variational inequalities that are computed in every time step in ($\mathrm{VI}_{N,h}$). The decoupled problem (4.11) and (4.13) offers a promising structure to establish an efficient and reliable adaptive finite element method.

Chapter 5

Adaptive Finite Element Method for Elliptic Maxwell Variational Inequalities

The adaptive finite element method (AFEM) based on a posteriori error estimators is a useful technique to increase the numerical accuracy of solutions to PDE-problems in certain sensitive regions of the concerned domain. For variational inequalities of the first kind or obstacle problems, these regions are typically the (a priori unknown) free boundaries which correspond to the interfaces between the active and inactive areas of the obstacle. AFEM consists of a repeating execution of the loop:

$$\text{SOLVE} \rightarrow \text{ESTIMATE} \rightarrow \text{MARK} \rightarrow \text{REFINE}.$$

At the starting point, common AFEM loops require three input data: a PDE problem, a mesh representing the basic geometry, and a finite element space. In our case, the first component of the loop is handled by Algorithm 3.1. The error estimation procedure collects the local errors between the approximate and exact solution and serves as an indicator to determine which elements should be refined. When it comes to error estimation, there are two different types: A priori (cf. section 4.2) and a posteriori estimators. In the former, constants may still depend on the exact solution. This makes them not suitable for adaptivity. Therefore, we rely on a posteriori error estimators where possible constants are only dependent on the geometry or other known quantities. For a review regarding error estimation induced by the discretization we refer the reader to [83].

Typically, when dealing with obstacle problems, AFEM refines the mesh adaptively where the solution is close to the obstacle, whereas the mesh on the remaining domain stays relatively coarse. This procedure yields a practically important feature to predict and detect the free boundaries without a priori knowledge. For $H^1(\Omega)$-elliptic obstacle problems, earlier results go back to Hoppe and Kornhuber [96,108], and wide studies can be found in this direction (see [28,33,38,134] and the references therein). However, many important physical phenomena, including Bingham fluid, friction, and – as we have seen – high-temperature superconductivity, cannot be modeled by obstacle problems, hence leading to variational inequalities of second kind. Bostan et al. [26] were the first to propose a duality approach to derive reliable a posteriori error estimators for $H^1(\Omega)$-elliptic variational inequalities of second kind. Some years later, Wang and Han [167] adapted the idea by Braess [27] to prove the efficiency of the proposed estimators by considering an auxiliary linear equation taking the associated discrete dual variable into account.

The first contribution toward residual-type a posteriori error estimators for edge element methods in $\boldsymbol{H}(\mathbf{curl})$-elliptic equations went back to Beck et al. [20]. Schöberl [150] established some stability estimates for a Clément-type quasi-interpolation operator, which turned out to be a very useful tool in the a posteriori error analysis of Maxwell's equations. The strong convergence of AFEM algorithms for various Maxwell-type equations with edge elements was analyzed in [31,32,36,39,97,175]. Some of these developments relied on a key strategy with limiting spaces, which was initially adopted by Babuška and Vogelius [10] for a one-dimensional boundary value problem and then extended to several higher-dimensional problems by Morin et al. [128]. We refer the reader to [179, 183] for edge

element methods for optimal control problems.

To the best of the authors' knowledge, a posteriori error analysis and adaptive edge element methods for elliptic **curl**-**curl** variational inequalities are only studied in our recent joint publication [173]. This chapter roughly coincides with [173] and therefore, citations from this work are omitted.

In particular, such a class of problems works with the space $\boldsymbol{H}(\mathbf{curl})$ (instead of H^1) and features various special singularities [44, 52, 53]. These facts, along with the main difficulties arising from the variational inequality character make the numerical analysis (cf. section 3.1), especially the rigorous a posteriori error analysis of the resulting AFEM, rather challenging.

We propose and analyze a posteriori error estimators and an AFEM algorithm for $\boldsymbol{H}(\mathbf{curl})$-elliptic variational inequalities of second kind of the form (4.13). Due to the **curl**-**curl** structure involved, our a posteriori error estimators require a local divergence regularity property of the dual variable. For this reason, unlike all the aforementioned contributions, we make use of a special combination of the Moreau–Yosida regularization (cf. Definition 3.3) and Nédélec's edge elements of first family (2.14). We are able to demonstrate that the proposed error estimators are both reliable and efficient. More important, under a certain condition on the regularization parameter depending on the adaptive mesh, we can even establish the strong convergence of the AFEM algorithm. Let us point out that the Moreau–Yosida regularization is a key feature which is not only crucial to our theoretical analysis but also brings a significant advantage to the numerical implementation of our new AFEM. In fact, it makes our implementation much more realistic and efficient. Our numerical realizations are carried out by Algorithm 3.1 that demands a certain regularity of the dual formulation (see section 3.2). This regularity property is well satisfied by the Moreau–Yosida approximation but in general not by the original variational inequality of second kind (cf. [58]). Our work [173] appears to be the first contribution that makes full use of the Moreau–Yosida regularization with its great flexibility and advantage in the a posteriori error analysis. The regularization strategy is very different from the finite element discretization of the variational inequalities as was done in the previous studies [26, 167] for $H^1(\Omega)$-elliptic variational inequalities of second kind.

We end this section by recalling the $\boldsymbol{H}(\mathbf{curl})$-elliptic variational inequality of second kind of our interest and outlining the main results of this chapter. We are interested in a variational inequality of the form (4.13). However, since (4.13) represents only one time step of ($\mathrm{VI}_{N,h}$), let us rewrite the variational inequality in question to a completely stationary formulation as follows: Find $\boldsymbol{E} \in \boldsymbol{H}_0(\mathbf{curl})$ such that

$$\text{(EVI)} \qquad a(\boldsymbol{E}, \boldsymbol{v}-\boldsymbol{E}) + \psi(\boldsymbol{v}) - \psi(\boldsymbol{E}) \geq \int_\Omega \boldsymbol{f}\cdot(\boldsymbol{v}-\boldsymbol{E})\,dx \quad \forall \boldsymbol{v} \in \boldsymbol{H}_0(\mathbf{curl})\,,$$

where $a\colon \boldsymbol{H}_0(\mathbf{curl}) \times \boldsymbol{H}_0(\mathbf{curl}) \to \mathbb{R}$ is a bilinear form defined by

$$a(\boldsymbol{v},\boldsymbol{w}) = \int_\Omega \epsilon\boldsymbol{v}\cdot\boldsymbol{w}\,dx + \int_\Omega \nu\,\mathbf{curl}\,\boldsymbol{v}\cdot\mathbf{curl}\,\boldsymbol{w}\,dx,$$

and $\psi\colon \boldsymbol{L}^2(\Omega) \to \mathbb{R}$ is a nonlinear and nonsmooth functional of the form

$$\psi(\boldsymbol{v}) = \int_\Omega j_c(x)|\boldsymbol{v}(x)|\,dx. \tag{5.1}$$

Note that (EVI) assumes at least $\boldsymbol{f} \in \boldsymbol{L}^2(\Omega)$ which is priorily not the case for the time-discrete problem ($\mathrm{VI}_{N,h}$) since (4.13) has a right-hand side in $\boldsymbol{H}_0(\mathbf{curl})^*$. Moreover, we have to adjust some technical assumptions from Chapter 4. They are stated in Assumption 5.1. The remainder of this chapter is structured as follows. First, we recall the Moreau–Yosida regularization for the dual formulation of (EVI) (see (5.6); cf. also (3.16)). After showing a crucial regularity property for the dual variable of the regularized problem, we propose the a posteriori error estimator (5.21). Thereafter, its reliability is proven in Theorem 5.6 by considering the linear auxiliary problem (5.8) and

using the Schöberl local regular decomposition (cf. Lemma 5.5). The efficiency of the estimators, stated in Theorem 5.7, follows from a standard argumentation with bubble functions (cf. [1]). With the help of these essential properties, we present the adaptive edge element algorithm for (EVI). The main result is a strong convergence theorem (see Theorem 5.17) of the sequence of adaptive solutions generated by Algorithm 5.1 toward the unique solution of (EVI). Therefore, the limiting space (5.34) as well as the corresponding limiting variational inequality (VI_∞) are the starting points for all that follows. First, the strong convergence toward this limiting problem is established. Hereafter, under a specific condition on the regularization parameter depending on the adaptive mesh (Assumption 5.13), we derive convergence results for the maximal error indicator and the residual corresponding to the sequence of adaptive solutions (Lemmas 5.14 and 5.15). By means of these convergence properties, we are able to prove that the solution to the limiting problem (VI_∞) coincides with the one to (EVI). Hence, strong convergence of Algorithm 5.1 follows as an immediate consequence. We close this chapter by applying our algorithm to the stationary counterparts for the examples in section 4.4.

5.1 ▪ Discretization and A Posteriori Error Analysis

Until now (cf. section 2.2 and Chapter 4) we have marked dependencies on the discretization with the subscript h.[1] This has been reasonable since we have studied the limiting process where h tends toward zero. That is, the diameter of *every* element vanishes in the limit. Now, our approach has changed and we refine the finite element mesh $\mathcal{T}$ adaptively in certain elements – meaning h does not necessarily become small. For now, we mark dependencies of variables on the mesh simply by the subscript $\mathcal{T}$.

With this being said let us present all the necessary assumptions for the material parameters and the given data in (EVI):

Assumption 5.1 (Material parameters and given data).

(A5.1) There are polyhedral Lipschitz subdomains Ω_j in Ω, $j = 1, \dots, M$, such that

$$\Omega_i \cap \Omega_j = \emptyset \quad \text{for } i \neq j \text{ and } \quad \bar{\Omega} = \bigcup_{j=1}^{M} \bar{\Omega}_j.$$

Furthermore, the material parameters ϵ, ν, j_c satisfy

$$\epsilon(x) = c_i^\epsilon \quad \text{and} \quad \nu(x) = c_i^\nu \quad \text{and} \quad j_c(x) = c_i^{j_c} \quad \forall x \in \Omega_i,\ i \in \{1, \dots, M\}$$

for positive constants $c_i^\epsilon, c_i^\nu > 0$ and a nonnegative constant $c_i^{j_c} \geq 0$ for $i \in \{1, \dots, M\}$.

(A5.2) The source $\boldsymbol{f}$ of (EVI) lies in $\boldsymbol{L}^2(\Omega)$ and satisfies the divergence-free condition:

$$(\boldsymbol{f}, \nabla\phi)_{\boldsymbol{L}^2(\Omega)} = 0 \quad \forall \phi \in H_0^1(\Omega).$$

Note that Assumption 5.1 is the counterpart of Assumption 3.10 for the stationary problem (EVI). Due to the new challenges coming from the AFEM approach they are also slightly more restrictive. Under Assumption 5.1 the bilinear form a remains continuous and coercive, i.e., there are positive constants $0 < \underline{\kappa} < \overline{\kappa}$ depending only on ϵ and ν such that

$$|a(\boldsymbol{v}, \boldsymbol{w})| \leq \overline{\kappa} \|\boldsymbol{v}\|_{\boldsymbol{H}(\mathbf{curl})} \|\boldsymbol{w}\|_{\boldsymbol{H}(\mathbf{curl})} \quad \forall \boldsymbol{v}, \boldsymbol{w} \in \boldsymbol{H}_0(\mathbf{curl}), \tag{5.2}$$

$$a(\boldsymbol{v}, \boldsymbol{v}) \geq \underline{\kappa} \|\boldsymbol{v}\|^2_{\boldsymbol{H}(\mathbf{curl})} \quad \forall \boldsymbol{v} \in \boldsymbol{H}_0(\mathbf{curl}). \tag{5.3}$$

[1] The index h stands for the maximal diameter of all elements in the triangulation $\mathcal{T}_h$.

Due to (5.2), (5.3), and its symmetry, the bilinear form a defines a scalar product whose induced norm $\|\cdot\|_a := \sqrt{a(\cdot,\cdot)}$ is equivalent to $\|\cdot\|_{\boldsymbol{H}(\mathbf{curl})}$. Furthermore, the induced norm over an arbitrary measurable set $\omega \subset \Omega$ is denoted by $\|\cdot\|_{a,\omega}$.

We close this section by introducing the discrete approximation to (EVI). Let $\mathcal{T}_0$ be a shape-regular triangulation of $\bar{\Omega}$ such that ϵ, ν, and j_c are constant in every $T \in \mathcal{T}_0$, and let $\mathbb{T}$ be the set of all possible conforming triangulations obtained from $\mathcal{T}_0$ by successive bisection. One key property of the refinement process ensures that all constants depending only on the shape regularity of any $\mathcal{T} \in \mathbb{T}$ are uniformly bounded by a constant depending only on the initial mesh $\mathcal{T}_0$ (cf. [162]). For any $\mathcal{T} \in \mathbb{T}$ we denote the finite element space of Nédélec's first family of edge elements by $\boldsymbol{V}_\mathcal{T}$ (cf. (2.14)). We are now ready to formulate the edge element approximation to (EVI): Find $\boldsymbol{E}_\mathcal{T} \in \boldsymbol{V}_\mathcal{T}$ such that

$$\text{(EVI}_\mathcal{T}\text{)} \qquad a(\boldsymbol{E}_\mathcal{T}, \boldsymbol{v}_\mathcal{T} - \boldsymbol{E}_\mathcal{T}) + \psi(\boldsymbol{v}_\mathcal{T}) - \psi(\boldsymbol{E}_\mathcal{T}) \geq \int_\Omega \boldsymbol{f} \cdot (\boldsymbol{v}_\mathcal{T} - \boldsymbol{E}_\mathcal{T})\, dx \quad \forall \boldsymbol{v}_\mathcal{T} \in \boldsymbol{V}_\mathcal{T}.$$

We emphasize that (EVI) and (EVI$_\mathcal{T}$) are precisely (4.2) and (4.13) for a fixed time step (in the setting of Chapter 4) with an additional regularity assumption for the right-hand side. Clearly, existence and uniqueness of the solutions to (EVI) and (EVI$_\mathcal{T}$) follow by again Theorem 3.1.

5.2 ▪ A Posteriori Error Analysis

As already pointed out in the introduction, our adaptive algorithm is based on efficient and reliable a posteriori error estimators. In order to establish this, we introduce some additional notation: By $\mathcal{F}_\mathcal{T}$, we denote the set of all faces in $\mathcal{T} \in \mathbb{T}$, and $\mathcal{F}_\mathcal{T}(\Omega)$ stands for the set of all interior faces. Let $h_T = \operatorname{diam}(T)$ for $T \in \mathcal{T}$ and $h_F = \operatorname{diam}(F)$ for $F \in \mathcal{F}_\mathcal{T}$. Furthermore, we use D_T (resp. D_F) to denote the union of all elements that have a nonempty intersection with $T \in \mathcal{T}$ (resp. $F \in \mathcal{F}_\mathcal{T}$). Finally, for $T \in \mathcal{T}$, we define the patch set ω_T as the union of all elements sharing a common face with T, and for any face $F \in \mathcal{F}_\mathcal{T}$ shared by two elements $K, \tilde{K} \in \mathcal{T}$, we set $\omega_F = K \cup \tilde{K}$.

According to (3.12) we may equivalently rewrite (EVI) with Lagrange multipliers: Let $\boldsymbol{E} \in \boldsymbol{H}_0(\mathbf{curl})$ be the unique solution to (EVI). Then, there exists a unique $\boldsymbol{\lambda} \in \mathbf{L}^\infty(\Omega)$ such that

$$\begin{cases} a(\boldsymbol{E}, \boldsymbol{v}) + \displaystyle\int_\Omega \boldsymbol{\lambda} \cdot \boldsymbol{v}\, dx = \int_\Omega \boldsymbol{f} \cdot \boldsymbol{v}\, dx \quad \forall \boldsymbol{v} \in \boldsymbol{H}_0(\mathbf{curl}) \\ |\boldsymbol{\lambda}(x)| \leq j_c(x), \quad \boldsymbol{\lambda}(x) \cdot \boldsymbol{E}(x) = j_c(x)|\boldsymbol{E}(x)| \text{ for a.e. } x \in \Omega. \end{cases} \tag{5.4}$$

For (5.4), we denote the active and inactive sets by

$$\mathcal{A} := \{x \in \Omega : |\boldsymbol{E}(x)| > 0\} \quad \text{and} \quad \mathcal{I} = \Omega \backslash \mathcal{A}.$$

Next, we recall the (Moreau–Yosida) regularized version of (EVI$_\mathcal{T}$) introduced in (3.14) for some $\gamma > 0$: Find $\boldsymbol{E}_\mathcal{T}^\gamma \in \boldsymbol{V}_\mathcal{T}$ such that

$$a(\boldsymbol{E}_\mathcal{T}^\gamma, \boldsymbol{v}_\mathcal{T} - \boldsymbol{E}_\mathcal{T}^\gamma) + \psi_\gamma(\boldsymbol{v}_\mathcal{T}) - \psi_\gamma(\boldsymbol{E}_\mathcal{T}^\gamma) \geq \int_\Omega \boldsymbol{f} \cdot (\boldsymbol{v}_\mathcal{T} - \boldsymbol{E}_\mathcal{T}^\gamma)\, dx \quad \forall \boldsymbol{v}_\mathcal{T} \in \boldsymbol{V}_\mathcal{T}, \tag{5.5}$$

where $\psi_\gamma(\boldsymbol{v}) := \int_\Omega j_c \eta_\gamma(\boldsymbol{v})\, dx$ for $\boldsymbol{v} \in \boldsymbol{L}^2(\Omega)$ and η_γ denotes the Moreau–Yosida regularization of $|\cdot|$ (see (3.6)). As in (3.16), (5.5) is equivalent to finding $\boldsymbol{E}_\mathcal{T}^\gamma \in \boldsymbol{V}_\mathcal{T}$ such that

$$\begin{cases} a(\boldsymbol{E}_\mathcal{T}^\gamma, \boldsymbol{v}_\mathcal{T}) + \displaystyle\int_\Omega \boldsymbol{\lambda}_\mathcal{T}^\gamma \cdot \boldsymbol{v}_\mathcal{T}\, dx = \int_\Omega \boldsymbol{f} \cdot \boldsymbol{v}_\mathcal{T}\, dx \quad \forall \boldsymbol{v}_\mathcal{T} \in \boldsymbol{V}_\mathcal{T} \\ \boldsymbol{\lambda}_\mathcal{T}^\gamma(x) = j_c(x) \dfrac{\gamma \boldsymbol{E}_\mathcal{T}^\gamma(x)}{\max\{1, \gamma|\boldsymbol{E}_\mathcal{T}^\gamma(x)|\}} \quad \text{for a.e. } x \in \Omega. \end{cases} \tag{5.6}$$

In this context, the active and inactive sets are given by

$$\mathcal{A}_\gamma \coloneqq \{x \in \Omega \,:\, \gamma|\boldsymbol{E}_{\mathcal{T}}^\gamma(x)| > 1\} \quad \text{and} \quad \mathcal{I}_\gamma \coloneqq \Omega \backslash \mathcal{A}_\gamma. \tag{5.7}$$

Since $\boldsymbol{\lambda}$ and $\boldsymbol{\lambda}_{\mathcal{T}}^\gamma$ are essentially bounded in Ω (see (5.4) and (5.6)), we may interpret them as elements in $\boldsymbol{H}_0(\mathbf{curl})^*$ with the operator norm

$$\|\boldsymbol{\lambda}\|_{*,a} \coloneqq \sup\left\{ \int_\Omega \boldsymbol{\lambda} \cdot \boldsymbol{v}\, dx \;:\; \boldsymbol{v} \in \boldsymbol{H}_0(\mathbf{curl}),\ \|\boldsymbol{v}\|_a = 1 \right\}.$$

As a starting point for a posteriori error analysis, we consider the auxiliary problem of finding $\boldsymbol{z} \in \boldsymbol{H}_0(\mathbf{curl})$ such that

$$a(\boldsymbol{z}, \boldsymbol{v}) + \int_\Omega \boldsymbol{\lambda}_{\mathcal{T}}^\gamma \cdot \boldsymbol{v}\, dx = \int_\Omega \boldsymbol{f} \cdot \boldsymbol{v}\, dx \quad \forall \boldsymbol{v} \in \boldsymbol{H}_0(\mathbf{curl}) \tag{5.8}$$

which admits a unique solution by the Lemma of Lax-Milgram. Let us now establish an error estimate for the primal and dual variables for (EVI) and (5.6) based on the auxiliary solution $\boldsymbol{z}$.

Lemma 5.2. *Under Assumption* 5.1 *and for* $C = \max\{5, 6\|j_c\|_{L^1(\Omega)}\}$*, there holds*

$$\|\boldsymbol{E}_{\mathcal{T}}^\gamma - \boldsymbol{E}\|_a^2 + \|\boldsymbol{\lambda} - \boldsymbol{\lambda}_{\mathcal{T}}^\gamma\|_{*,a}^2 \le C\left(\|\boldsymbol{E}_{\mathcal{T}}^\gamma - \boldsymbol{z}\|_a^2 + \frac{1}{\gamma} \right).$$

Proof. The proof is analogous to the one of Lemma 3.6. We begin by subtracting (5.4) from (5.8) to obtain

$$a(\boldsymbol{z} - \boldsymbol{E}, \boldsymbol{v}) = \int_\Omega (\boldsymbol{\lambda} - \boldsymbol{\lambda}_{\mathcal{T}}^\gamma) \cdot \boldsymbol{v}\, dx \quad \forall \boldsymbol{v} \in \boldsymbol{H}_0(\mathbf{curl}). \tag{5.9}$$

Therefore,

$$a(\boldsymbol{E}_{\mathcal{T}}^\gamma - \boldsymbol{E}, \boldsymbol{v}) = a(\boldsymbol{E}_{\mathcal{T}}^\gamma - \boldsymbol{z}, \boldsymbol{v}) + \int_\Omega (\boldsymbol{\lambda} - \boldsymbol{\lambda}_{\mathcal{T}}^\gamma) \cdot \boldsymbol{v}\, dx \quad \forall \boldsymbol{v} \in \boldsymbol{H}_0(\mathbf{curl}). \tag{5.10}$$

Next, we apply (3.20) in Lemma 3.6 to obtain that

$$\int_\Omega (\boldsymbol{\lambda} - \boldsymbol{\lambda}_{\mathcal{T}}^\gamma) \cdot (\boldsymbol{E}_{\mathcal{T}}^\gamma - \boldsymbol{E})\, dx \le \frac{1}{\gamma} \|j_c\|_{L^1(\Omega)}. \tag{5.11}$$

Thus, inserting $\boldsymbol{v} = \boldsymbol{E}_{\mathcal{T}} - \boldsymbol{E}$ in (5.10), we get from (5.11) that

$$\|\boldsymbol{E}_{\mathcal{T}}^\gamma - \boldsymbol{E}\|_a^2 \le \|\boldsymbol{E}_{\mathcal{T}}^\gamma - \boldsymbol{z}\|_a \|\boldsymbol{E}_{\mathcal{T}}^\gamma - \boldsymbol{E}\|_a + \frac{1}{\gamma} \|j_c\|_{L^1(\Omega)}\,.$$

Further, the application of Young's inequality yields

$$\|\boldsymbol{E}_{\mathcal{T}}^\gamma - \boldsymbol{E}\|_a^2 \le \|\boldsymbol{E}_{\mathcal{T}}^\gamma - \boldsymbol{z}\|_a^2 + \frac{2}{\gamma} \|j_c\|_{L^1(\Omega)}. \tag{5.12}$$

Finally, (5.9), (5.12) and the triangle inequality give us

$$\begin{aligned} \|\boldsymbol{\lambda} - \boldsymbol{\lambda}_{\mathcal{T}}^\gamma\|_{*,a}^2 &\le \|\boldsymbol{z} - \boldsymbol{E}\|_a^2 \le 2\|\boldsymbol{z} - \boldsymbol{E}_{\mathcal{T}}^\gamma\|_a^2 + 2\|\boldsymbol{E}_{\mathcal{T}}^\gamma - \boldsymbol{E}\|_a^2 \\ &\le 4\|\boldsymbol{z} - \boldsymbol{E}_{\mathcal{T}}^\gamma\|_a^2 + \frac{4}{\gamma} \|j_c\|_{L^1(\Omega)}. \end{aligned} \tag{5.13}$$

The desired assertion follows directly from (5.12) and (5.13). ∎

One crucial benefit of the use of the Moreau–Yosida regularization is that the regularized dual variable satisfies a local regularity property.

Lemma 5.3. *Under Assumption* 5.1*, the dual variable from* (5.6) *enjoys the local regularity property* $\boldsymbol{\lambda}_{\mathcal{T}}^{\gamma}|_T \in \boldsymbol{H}(\operatorname{div}, T)$ *for every* $T \in \mathcal{T}$ *and the following stability estimate:*

$$\|\operatorname{div} \boldsymbol{\lambda}_{\mathcal{T}}^{\gamma}|_T\|_{\boldsymbol{L}^2(T)} \leq \frac{\gamma \|j_c\|_{L^\infty(\Omega)}}{\sqrt{2}} \|\operatorname{\mathbf{curl}} \boldsymbol{E}_{\mathcal{T}}^{\gamma}\|_{\boldsymbol{L}^2(T)} \quad \forall T \in \mathcal{T}.$$

Proof. Let $T \in \mathcal{T}$ be an arbitrarily fixed element. As $\boldsymbol{E}_{\mathcal{T}}^{\gamma} \in \boldsymbol{V}_{\mathcal{T}}$, it holds that $\boldsymbol{E}_{\mathcal{T}}^{\gamma}|_T \in \boldsymbol{\mathcal{C}}^\infty(T)$, and thus $\max\{1, \gamma|\boldsymbol{E}_{\mathcal{T}}^{\gamma}|_T|\} \in W^{1,\infty}(T)$ (see [105, Corollary A.6]). For this reason and the fact that $j_c|_T$ is constant, (5.6) implies

$$\boldsymbol{\lambda}_{\mathcal{T}}^{\gamma}|_T \in \boldsymbol{W}^{1,\infty}(T) \tag{5.14}$$

Now, we show that

$$\operatorname{div} \boldsymbol{\lambda}_{\mathcal{T}}^{\gamma}|_T = \begin{cases} -\dfrac{j_c|_T}{|\boldsymbol{E}_{\mathcal{T}}^{\gamma}|_T|^3} (\nabla \boldsymbol{E}_{\mathcal{T}}^{\gamma}|_T \boldsymbol{E}_{\mathcal{T}}^{\gamma}|_T) \cdot \boldsymbol{E}_{\mathcal{T}}^{\gamma}|_T & \text{in } \mathcal{A}_\gamma \cap T, \\ 0 & \text{in } \mathcal{I}_\gamma \cap T, \end{cases} \tag{5.15}$$

where $\nabla \boldsymbol{E}_{\mathcal{T}}^{\gamma}|_T = (\nabla \boldsymbol{E}_{\mathcal{T}}^{\gamma}|_{T,1}\ \nabla \boldsymbol{E}_{\mathcal{T}}^{\gamma}|_{T,2}\ \nabla \boldsymbol{E}_{\mathcal{T}}^{\gamma}|_{T,3})$. Indeed, since j_c is piecewise constant (see (A3.1)) and according to (5.6) and (5.7), we may compute

$$\begin{aligned} \partial_i \boldsymbol{\lambda}_{\mathcal{T}}^{\gamma}|_{T,i} &= j_c|_T \partial_i \left(\frac{\gamma \boldsymbol{E}_{\mathcal{T}}^{\gamma}|_{T,i}}{\max\{1, \gamma|\boldsymbol{E}_{\mathcal{T}}^{\gamma}|_T|\}} \right) \\ &= j_c|_T \left(\frac{\gamma \partial_i \boldsymbol{E}_{\mathcal{T}}^{\gamma}|_{T,i}}{\max\{1, \gamma|\boldsymbol{E}_{\mathcal{T}}^{\gamma}|_T|\}} - \frac{\gamma \boldsymbol{E}_{\mathcal{T}}^{\gamma}|_{T,i}}{\max\{1, \gamma|\boldsymbol{E}_{\mathcal{T}}^{\gamma}|_T|\}^2} \partial_i \big(\max\{1, \gamma|\boldsymbol{E}_{\mathcal{T}}^{\gamma}|_T|\} \big) \right). \end{aligned} \tag{5.16}$$

Additionally, thanks to [105, Corollary A.6], it holds that

$$\partial_i \big(\max\{1, \gamma|\boldsymbol{E}_{\mathcal{T}}^{\gamma}|_T|\} \big) = \begin{cases} \dfrac{\gamma \boldsymbol{E}_{\mathcal{T}}^{\gamma}|_T \cdot \partial_i \boldsymbol{E}_{\mathcal{T}}^{\gamma}|_T}{|\boldsymbol{E}_{\mathcal{T}}^{\gamma}|_T|} & \text{in } \mathcal{A}_\gamma \cap T, \\ 0 & \text{in } \mathcal{I}_\gamma \cap T. \end{cases} \tag{5.17}$$

Thus, in view of (5.16), (5.17), and $\operatorname{div} \boldsymbol{E}_{\mathcal{T}}^{\gamma}|_T \equiv 0$, it follows that

$$\operatorname{div} \boldsymbol{\lambda}_{\mathcal{T}}^{\gamma}|_T \overset{(5.14)}{=} \sum_{i=1}^{3} \partial_i \boldsymbol{\lambda}_{\mathcal{T}}^{\gamma}|_{T,i} = \begin{cases} -\dfrac{j_c|_T}{|\boldsymbol{E}_{\mathcal{T}}^{\gamma}|_T|^3} \displaystyle\sum_{i=1}^{3} \boldsymbol{E}_{\mathcal{T}}^{\gamma}|_{T,i} \big(\partial_i \boldsymbol{E}_{\mathcal{T}}^{\gamma}|_T \cdot \boldsymbol{E}_{\mathcal{T}}^{\gamma}|_T \big) & \text{in } \mathcal{A}_\gamma \cap T, \\ 0 & \text{in } \mathcal{I}_\gamma \cap T, \end{cases}$$

which yields that (5.15) is valid. Note that according to (5.7), (5.15) implies that $\operatorname{div} \boldsymbol{\lambda}_{\mathcal{T}}^{\gamma}|_T = 0$ a.e. in $\{x \in T : \gamma|\boldsymbol{E}_{\mathcal{T}}^{\gamma}|_T(x)| = 1\}$. Next, (5.15) together with the inequality $|\boldsymbol{E}_{\mathcal{T}}^{\gamma}(x)| > \frac{1}{\gamma}$ for a.e. $x \in \mathcal{A}_\gamma$ (see (5.7)) leads to

$$\begin{aligned} \|\operatorname{div} \boldsymbol{\lambda}_{\mathcal{T}}^{\gamma}|_T\|_{\boldsymbol{L}^2(T)}^2 = \|\operatorname{div} \boldsymbol{\lambda}_{\mathcal{T}}^{\gamma}|_T\|_{L^2(T \cap \mathcal{A}_\gamma)}^2 &\leq \|j_c\|_{L^\infty(\Omega)}^2 \int_{T \cap \mathcal{A}_\gamma} \frac{|\nabla \boldsymbol{E}_{\mathcal{T}}^{\gamma}|_T(x)|^2}{|\boldsymbol{E}_{\mathcal{T}}^{\gamma}|_T(x)|^2}\, dx \\ &\leq \gamma^2 \|j_c\|_{L^\infty(\Omega)}^2 \|\nabla \boldsymbol{E}_{\mathcal{T}}^{\gamma}|_T\|_{\boldsymbol{L}^2(T)}^2. \end{aligned} \tag{5.18}$$

But, for every $x \in T$, we know that $\boldsymbol{E}_{\mathcal{T}}^{\gamma}|_T(x) = a_T \times x + b_T$ for some $a_T, b_T \in \mathbb{R}^3$. Thus,

$$\nabla \boldsymbol{E}_{\mathcal{T}}^{\gamma}|_T(x) = \begin{bmatrix} 0 & -a_{T,3} & a_{T,2} \\ a_{T,3} & 0 & -a_{T,1} \\ -a_{T,2} & a_{T,1} & 0 \end{bmatrix} \quad \text{and} \quad \operatorname{\mathbf{curl}} \boldsymbol{E}_{\mathcal{T}}^{\gamma}|_T(x) = 2 \begin{bmatrix} a_{T,1} \\ a_{T,2} \\ a_{T,3} \end{bmatrix}$$

which implies that $\sqrt{2}|\nabla \boldsymbol{E}_{\mathcal{T}}^{\gamma}|_T(x)| = |\operatorname{\mathbf{curl}} \boldsymbol{E}_{\mathcal{T}}^{\gamma}|_T(x)|$ for all $x \in T$. Combining this with (5.18) yields the desired estimate. ∎

Remark 5.4. Lemma 5.3 does not hold true in general for the unregularized dual variable corresponding to ($\mathrm{EVI}_{\mathcal{T}}$) due to the lack of information in the inactive set.

Next, we start to investigate the a posteriori error estimate of the edge element solution $(\boldsymbol{E}_{\mathcal{T}}^{\gamma}, \boldsymbol{\lambda}_{\mathcal{T}}^{\gamma}) \in \boldsymbol{V}_{\mathcal{T}} \times \boldsymbol{L}^{\infty}(\Omega)$ to the discrete system (5.6). To do so, we define for $(\boldsymbol{E}_{\mathcal{T}}^{\gamma}, \boldsymbol{\lambda}_{\mathcal{T}}^{\gamma})$ the element residual $\mathbf{R}_T$ for every $T \in \mathcal{T}$ and the normal and tangential jumps across every face $F \in \mathcal{F}_{\mathcal{T}}$:

$$\mathbf{R}_T \coloneqq \boldsymbol{f}|_T - \epsilon \boldsymbol{E}_{\mathcal{T}}^{\gamma}|_T - \mathbf{curl}\, \nu\, \mathbf{curl}\, \boldsymbol{E}_{\mathcal{T}}^{\gamma}|_T - \boldsymbol{\lambda}_{\mathcal{T}}^{\gamma}|_T, \tag{5.19}$$

$$\mathbf{J}_{F,1} \coloneqq [\nu\, \mathbf{curl}\, \boldsymbol{E}_{\mathcal{T}}^{\gamma} \times \boldsymbol{n}_F] \quad \text{and} \quad J_{F,2} \coloneqq [(\boldsymbol{\lambda}_{\mathcal{T}}^{\gamma} + \epsilon \boldsymbol{E}_{\mathcal{T}}^{\gamma}) \cdot \boldsymbol{n}_F]. \tag{5.20}$$

For any subset $\mathcal{M}$ of elements from $\mathcal{T}$, we define its error estimator

$$\eta_{\mathcal{T}}^2(\boldsymbol{E}_{\mathcal{T}}^{\gamma}, \boldsymbol{\lambda}_{\mathcal{T}}^{\gamma}, \boldsymbol{f}, \mathcal{M}) \coloneqq \sum_{T \in \mathcal{M}} \eta_{\mathcal{T},1}^2(\boldsymbol{E}_{\mathcal{T}}^{\gamma}, \boldsymbol{\lambda}_{\mathcal{T}}^{\gamma}, \boldsymbol{f}, T) + \eta_{\mathcal{T},2}^2(\boldsymbol{E}_{\mathcal{T}}^{\gamma}, \boldsymbol{\lambda}_{\mathcal{T}}^{\gamma}, T), \tag{5.21}$$

where $\eta_{\mathcal{T},1}(\boldsymbol{E}_{\mathcal{T}}^{\gamma}, \boldsymbol{\lambda}_{\mathcal{T}}^{\gamma}, \boldsymbol{f}, T)$ and $\eta_{\mathcal{T},2}(\boldsymbol{E}_{\mathcal{T}}^{\gamma}, \boldsymbol{\lambda}_{\mathcal{T}}^{\gamma}, T)$ are given by

$$\eta_{\mathcal{T},1}^2(\boldsymbol{E}_{\mathcal{T}}^{\gamma}, \boldsymbol{\lambda}_{\mathcal{T}}^{\gamma}, \boldsymbol{f}, T) \coloneqq h_T^2 \|\mathbf{R}_T\|_{\boldsymbol{L}^2(T)}^2 + \sum_{F \in \partial T \cap \Omega} h_F \|\mathbf{J}_{F,1}\|_{\boldsymbol{L}^2(F)}^2,$$

$$\eta_{\mathcal{T},2}^2(\boldsymbol{E}_{\mathcal{T}}^{\gamma}, \boldsymbol{\lambda}_{\mathcal{T}}^{\gamma}, T) \coloneqq h_T^2 \|\operatorname{div} \boldsymbol{\lambda}_{\mathcal{T}}^{\gamma}\|_{\boldsymbol{L}^2(T)}^2 + \sum_{F \in \partial T \cap \Omega} h_F \|J_{F,2}\|_{\boldsymbol{L}^2(F)}^2.$$

We further define an oscillation term associated with the subset $\mathcal{M}$, namely,

$$\mathrm{osc}_{\mathcal{T}}{}^2(\boldsymbol{E}_{\mathcal{T}}^{\gamma}, \boldsymbol{\lambda}_{\mathcal{T}}^{\gamma}, \boldsymbol{f}, \mathcal{M}) \coloneqq \sum_{T \in \mathcal{M}} \mathrm{osc}_{\mathcal{T}}{}^2(\boldsymbol{E}_{\mathcal{T}}^{\gamma}, \boldsymbol{\lambda}_{\mathcal{T}}^{\gamma}, \boldsymbol{f}, T)$$

with

$$\begin{aligned}\mathrm{osc}_{\mathcal{T}}{}^2(\boldsymbol{E}_{\mathcal{T}}^{\gamma}, \boldsymbol{\lambda}_{\mathcal{T}}^{\gamma}, \boldsymbol{f}, T) \coloneqq\, & h_T^2 \|\mathbf{R}_T - \bar{\mathbf{R}}_T\|_{\boldsymbol{L}^2(T)}^2 + h_T^2 \|\overline{\operatorname{div} \boldsymbol{\lambda}_{\mathcal{T}}^{\gamma}}|_T - \operatorname{div} \boldsymbol{\lambda}_{\mathcal{T}}^{\gamma}\|_{\boldsymbol{L}^2(T)}^2 \\ & + \sum_{F \in \partial T \cap \Omega} h_F \|\mathbf{J}_{F,1} - \bar{\mathbf{J}}_{F,1}\|_{\boldsymbol{L}^2(F)}^2 + h_F \|J_{F,2} - \bar{J}_{F,2}\|_{\boldsymbol{L}^2(F)}^2,\end{aligned}$$

where $\bar{\mathbf{R}}_T$, $\overline{\operatorname{div} \boldsymbol{\lambda}_{\mathcal{T}}^{\gamma}}|_T$, $\bar{\mathbf{J}}_{F,1}$, and $\bar{J}_{F,2}$ denote the averages of $\mathbf{R}_T$, $\operatorname{div} \boldsymbol{\lambda}_{\mathcal{T}}^{\gamma}$, $\mathbf{J}_{F,1}$, and $J_{F,2}$ over $T \in \mathcal{T}$ and $\mathcal{F} \in \mathcal{F}_{\mathcal{T}}$, respectively, i.e.,

$$\bar{\mathbf{R}}_T \coloneqq \frac{1}{|T|} \int_T \mathbf{R}_T \, dx, \quad \overline{\operatorname{div} \boldsymbol{\lambda}_{\mathcal{T}}^{\gamma}}|_T \coloneqq \frac{1}{|T|} \int_T \operatorname{div} \boldsymbol{\lambda}_{\mathcal{T}}^{\gamma} \, dx, \quad \bar{\mathbf{J}}_{F,1} \coloneqq \frac{1}{|F|} \int_F \mathbf{J}_{F,1} \, dS,$$

and analogously for $\bar{J}_{F,2}$. In the case of $\mathcal{M} = \mathcal{T}$, we drop $\mathcal{T}$ in the notation and simply write $\eta_{\mathcal{T}}(\boldsymbol{E}_{\mathcal{T}}^{\gamma}, \boldsymbol{\lambda}_{\mathcal{T}}^{\gamma}, \boldsymbol{f}, \mathcal{T})$ as $\eta_{\mathcal{T}}(\boldsymbol{E}_{\mathcal{T}}^{\gamma}, \boldsymbol{\lambda}_{\mathcal{T}}^{\gamma}, \boldsymbol{f})$ as well as $\mathrm{osc}_{\mathcal{T}}(\boldsymbol{E}_{\mathcal{T}}^{\gamma}, \boldsymbol{\lambda}_{\mathcal{T}}^{\gamma}, \boldsymbol{f}, \mathcal{T})$ as $\mathrm{osc}_{\mathcal{T}}(\boldsymbol{E}_{\mathcal{T}}^{\gamma}, \boldsymbol{\lambda}_{\mathcal{T}}^{\gamma}, \boldsymbol{f})$.

Let us now recall a quasi-interpolation operator to relate $\boldsymbol{H}_0(\mathbf{curl})$ to the finite element space $\boldsymbol{V}_{\mathcal{T}}$ (see [150, Theorem 1]):

Lemma 5.5 (Schöberl interpolation operator). *Under Assumption* 5.1*, there exists a quasi-interpolation operator* $\boldsymbol{\Pi}_{\mathcal{T}}^{s} \colon \boldsymbol{H}_0(\mathbf{curl}) \to \boldsymbol{V}_{\mathcal{T}}$ *such that for every* $\boldsymbol{v} \in \boldsymbol{H}_0(\mathbf{curl})$ *there exist* $\boldsymbol{\phi} \in \boldsymbol{H}_0^1(\Omega)$ *and* $\varphi \in H_0^1(\Omega)$ *satisfying*

$$\boldsymbol{v} - \boldsymbol{\Pi}_{\mathcal{T}}^{s} \boldsymbol{v} = \boldsymbol{\phi} + \nabla \varphi$$

with the stability estimates

$$h_T^{-1} \|\boldsymbol{\phi}\|_{\boldsymbol{L}^2(T)} + \|\nabla \boldsymbol{\phi}\|_{\boldsymbol{L}^2(T)} \leq C \|\, \mathbf{curl}\, \boldsymbol{v}\|_{\boldsymbol{L}^2(\tilde{D}_T)},$$

$$h_T^{-1} \|\varphi\|_{\boldsymbol{L}^2(T)} + \|\nabla \varphi\|_{\boldsymbol{L}^2(T)} \leq C \|\boldsymbol{v}\|_{\boldsymbol{L}^2(\tilde{D}_T)},$$

where the constant $C > 0$ *depends only on the shape of the elements in the enlarged element patch* $\tilde{D}_T \coloneqq \{T' \in \mathcal{T} \mid T' \cap D_T \neq \emptyset\}$.

We have now collected all the necessary preparations for the a posteriori error analysis. Let us begin by proving the reliability of (5.21) in the following theorem.

Theorem 5.6. *Under Assumption* 5.1*, there exists a constant $C > 0$ depending only on Ω, the shape-regularity of $\mathcal{T}$, and the material parameters ϵ, ν as well as j_c such that the solutions $(\boldsymbol{E}, \boldsymbol{\lambda})$ and $(\boldsymbol{E}_\mathcal{T}, \boldsymbol{\lambda}_\mathcal{T})$ to* (5.4) *and* (5.6) *satisfy*

$$\|\boldsymbol{E} - \boldsymbol{E}_\mathcal{T}^\gamma\|_a^2 + \|\boldsymbol{\lambda} - \boldsymbol{\lambda}_\mathcal{T}\|_{*,a}^2 \leq C\bigg(\eta_\mathcal{T}^2(\boldsymbol{E}_\mathcal{T}^\gamma, \boldsymbol{\lambda}_\mathcal{T}^\gamma, \boldsymbol{f}) + \frac{1}{\gamma}\bigg).$$

Proof. We define $\boldsymbol{v} \coloneqq \boldsymbol{z} - \boldsymbol{E}_\mathcal{T}^\gamma \in \boldsymbol{H}_0(\mathbf{curl})$ and use Lemma 5.5 to decompose $\boldsymbol{v} - \boldsymbol{\Pi}_\mathcal{T}^s \boldsymbol{v} = \boldsymbol{\phi} + \nabla\varphi$ with $\boldsymbol{\phi} \in \boldsymbol{H}_0^1(\Omega)$ and $\varphi \in H_0^1(\Omega)$. Then, we take (A3.3), (5.6), and (5.8) into account and use integration by parts, the stability estimates in Lemma 5.5, as well as the trace theorem (cf. [166, page 87]) to obtain

$$\begin{aligned}
\|\boldsymbol{v}\|_a^2 &= a(\boldsymbol{v}, \boldsymbol{v}) = a(\boldsymbol{z}, \boldsymbol{v}) - a(\boldsymbol{E}_\mathcal{T}^\gamma, \boldsymbol{v}) = \big(\boldsymbol{f} - \boldsymbol{\lambda}_\mathcal{T}^\gamma, \boldsymbol{v}\big)_{\boldsymbol{L}^2(\Omega)} - a(\boldsymbol{E}_\mathcal{T}^\gamma, \boldsymbol{v}) \\
&= \big(\boldsymbol{f} - \boldsymbol{\lambda}_\mathcal{T}^\gamma, \boldsymbol{v} - \boldsymbol{\Pi}_\mathcal{T}^s \boldsymbol{v}\big)_{\boldsymbol{L}^2(\Omega)} + \big(\boldsymbol{f} - \boldsymbol{\lambda}_\mathcal{T}^\gamma, \boldsymbol{\Pi}_\mathcal{T}^s \boldsymbol{v}\big)_{\boldsymbol{L}^2(\Omega)} - a(\boldsymbol{E}_\mathcal{T}^\gamma, \boldsymbol{v}) \\
&= \big(\boldsymbol{f} - \boldsymbol{\lambda}_\mathcal{T}^\gamma, \boldsymbol{v} - \boldsymbol{\Pi}_\mathcal{T}^s \boldsymbol{v}\big)_{\boldsymbol{L}^2(\Omega)} - a(\boldsymbol{E}_\mathcal{T}^\gamma, \boldsymbol{v} - \boldsymbol{\Pi}_\mathcal{T}^s \boldsymbol{v}) \\
&= \big(\boldsymbol{f} - \boldsymbol{\lambda}_\mathcal{T}^\gamma, \boldsymbol{\phi} + \nabla\varphi\big)_{\boldsymbol{L}^2(\Omega)} - a(\boldsymbol{E}_\mathcal{T}^\gamma, \boldsymbol{\phi} + \nabla\varphi) \\
&= \big(\boldsymbol{f} - \boldsymbol{\lambda}_\mathcal{T}^\gamma, \boldsymbol{\phi}\big)_{\boldsymbol{L}^2(\Omega)} - a(\boldsymbol{E}_\mathcal{T}^\gamma, \boldsymbol{\phi}) - \big(\boldsymbol{\lambda}_\mathcal{T}^\gamma + \epsilon \boldsymbol{E}_\mathcal{T}^\gamma, \nabla\varphi\big)_{\boldsymbol{L}^2(\Omega)} \\
&= \sum_{T \in \mathcal{T}} (\mathbf{R}_T, \boldsymbol{\phi})_{\boldsymbol{L}^2(T)} - \sum_{F \in \mathcal{F}_\mathcal{T}} (\mathbf{J}_{F,1}, \boldsymbol{\phi})_{\boldsymbol{L}^2(F)} - \big(\boldsymbol{\lambda}_\mathcal{T}^\gamma + \epsilon \boldsymbol{E}_\mathcal{T}^\gamma, \nabla\varphi\big)_{\boldsymbol{L}^2(\Omega)} \\
&\leq \sum_{T \in \mathcal{T}} h_T \|\mathbf{R}_T\|_{\boldsymbol{L}^2(T)} h_T^{-1} \|\boldsymbol{\phi}\|_{\boldsymbol{L}^2(T)} + \sum_{F \in \mathcal{F}_\mathcal{T}} h_F^{1/2} \|\mathbf{J}_{F,1}\|_{\boldsymbol{L}^2(F)} h_F^{-1/2} \|\boldsymbol{\phi}\|_{\boldsymbol{L}^2(F)} \\
&\quad - \big(\boldsymbol{\lambda}_\mathcal{T}^\gamma + \epsilon \boldsymbol{E}_\mathcal{T}^\gamma, \nabla\varphi\big)_{\boldsymbol{L}^2(\Omega)} \\
&\leq C \sum_{T \in \mathcal{T}} \eta_{\mathcal{T},1}(\boldsymbol{E}_\mathcal{T}^\gamma, \boldsymbol{\lambda}_\mathcal{T}^\gamma, \boldsymbol{f}, T)\big(h_T^{-1} \|\boldsymbol{\phi}\|_{\boldsymbol{L}^2(T)} + \|\nabla\boldsymbol{\phi}\|_{\boldsymbol{L}^2(T)}\big) \\
&\quad - \big(\boldsymbol{\lambda}_\mathcal{T}^\gamma + \epsilon \boldsymbol{E}_\mathcal{T}^\gamma, \nabla\varphi\big)_{\boldsymbol{L}^2(\Omega)} \\
&\leq C \sum_{T \in \mathcal{T}} \eta_{\mathcal{T},1}(\boldsymbol{E}_\mathcal{T}^\gamma, \boldsymbol{\lambda}_\mathcal{T}^\gamma, \boldsymbol{f}, T) \|\mathbf{curl}\, \boldsymbol{v}\|_{\boldsymbol{L}^2(\tilde{D}_T)} - \big(\boldsymbol{\lambda}_\mathcal{T}^\gamma + \epsilon \boldsymbol{E}_\mathcal{T}^\gamma, \nabla\varphi\big)_{\boldsymbol{L}^2(\Omega)}.
\end{aligned} \tag{5.22}$$

For the last term on the right-hand side of (5.22), we apply integration by parts, using Lemma 5.3 and the fact that $\operatorname{div} \epsilon \boldsymbol{E}_\mathcal{T}^\gamma|_T = 0$ over every $T \in \mathcal{T}$, as well as the trace theorem and the stability estimates from Lemma 5.5 to obtain

$$\begin{aligned}
&- \big(\boldsymbol{\lambda}_\mathcal{T}^\gamma + \epsilon \boldsymbol{E}_\mathcal{T}^\gamma, \nabla\varphi\big)_{\boldsymbol{L}^2(\Omega)} = \sum_{T \in \mathcal{T}} \big(\operatorname{div} \boldsymbol{\lambda}_\mathcal{T}^\gamma, \varphi\big)_{\boldsymbol{L}^2(T)} - \sum_{F \in \mathcal{F}_\mathcal{T}} (J_{F,2}, \varphi)_{\boldsymbol{L}^2(F)} \\
&\leq C \sum_{T \in \mathcal{T}} h_T \|\operatorname{div} \boldsymbol{\lambda}_\mathcal{T}^\gamma\|_{\boldsymbol{L}^2(T)} h_T^{-1} \|\varphi\|_{\boldsymbol{L}^2(T)} + \sum_{F \in \mathcal{F}_\mathcal{T}} h_F^{1/2} \|J_{F,2}\|_{\boldsymbol{L}^2(F)} h_F^{-1/2} \|\varphi\|_{\boldsymbol{L}^2(F)} \\
&\leq C \sum_{T \in \mathcal{T}} \eta_{\mathcal{T},2}(\boldsymbol{E}_\mathcal{T}, \boldsymbol{\lambda}_\mathcal{T}, T)\big(h_T^{-1} \|\varphi\|_{\boldsymbol{L}^2(T)} + \|\nabla\varphi\|_{\boldsymbol{L}^2(T)}\big) \\
&\leq C \sum_{T \in \mathcal{T}} \eta_{\mathcal{T},2}(\boldsymbol{E}_\mathcal{T}, \boldsymbol{\lambda}_\mathcal{T}, T) \|\boldsymbol{v}\|_{\boldsymbol{L}^2(\tilde{D}_T)}.
\end{aligned} \tag{5.23}$$

Finally, by inserting (5.23) into (5.22) and making use of the finite overlapping property of elements

in $\tilde{D}_T$ as well as the equivalence between $\|\cdot\|_a$ and $\|\cdot\|_{\boldsymbol{H}(\mathbf{curl})}$, we deduce that

$$\|\boldsymbol{z}-\boldsymbol{E}_{\mathcal{T}}^{\gamma}\|_a^2 \le C\sum_{T\in\mathcal{T}_k}\eta_{\mathcal{T}}(\boldsymbol{E}_{\mathcal{T}}^{\gamma},\boldsymbol{\lambda}_{\mathcal{T}}^{\gamma},\boldsymbol{f},T)\|\boldsymbol{z}-\boldsymbol{E}_{\mathcal{T}}^{\gamma}\|_{a,\tilde{D}_T} \le C\eta_{\mathcal{T}}(\boldsymbol{E}_{\mathcal{T}}^{\gamma},\boldsymbol{\lambda}_{\mathcal{T}}^{\gamma},\boldsymbol{f})\|\boldsymbol{z}-\boldsymbol{E}_{\mathcal{T}}^{\gamma}\|_a$$

$$\overset{\text{Lemma 5.2}}{\Rightarrow} \quad \|\boldsymbol{E}-\boldsymbol{E}_{\mathcal{T}}^{\gamma}\|_a^2+\|\boldsymbol{\lambda}-\boldsymbol{\lambda}_{\mathcal{T}}\|_{*,a}^2 \le C\left(\eta_{\mathcal{T}}^2(\boldsymbol{E}_{\mathcal{T}}^{\gamma},\boldsymbol{\lambda}_{\mathcal{T}}^{\gamma},\boldsymbol{f})+\frac{1}{\gamma}\right),$$

where the constant $C>0$ depends only on Ω,ϵ,ν,j_c and the shape-regularity of $\mathcal{T}$. ■

The next theorem establishes the efficiency of the a posteriori error estimator.

Theorem 5.7. *Under Assumption* 5.1*, there exists a constant $C>0$ depending only on the shape-regularity of $\mathcal{T}$ and the material parameters such that the solutions $(\boldsymbol{E},\boldsymbol{\lambda})$ and $(\boldsymbol{E}_{\mathcal{T}},\boldsymbol{\lambda}_{\mathcal{T}})$ to* (5.4) *and* (5.6) *fulfill*

$$C\eta_{\mathcal{T}}^2(\boldsymbol{E}_{\mathcal{T}}^{\gamma},\boldsymbol{\lambda}_{\mathcal{T}}^{\gamma},\boldsymbol{f},T) \le \|\boldsymbol{E}-\boldsymbol{E}_{\mathcal{T}}^{\gamma}\|_{a,\omega_T}^2+\|\boldsymbol{\lambda}-\boldsymbol{\lambda}_{\mathcal{T}}^{\gamma}\|_{*,a,\omega_T}^2 + \operatorname{osc}_{\mathcal{T}}{}^2(\boldsymbol{E}_{\mathcal{T}}^{\gamma},\boldsymbol{\lambda}_{\mathcal{T}}^{\gamma},\boldsymbol{f},\omega_T) \quad \forall T\in\mathcal{T}. \tag{5.24}$$

Proof. To prove this result, we use the well-known tetrahedral bubble functions b_T for every given $T\in\mathcal{T}$ and their associated estimates (see [1, page 23]). We choose $\boldsymbol{v}=\boldsymbol{v}_T=\bar{\mathbf{R}}_T b_T\in\mathbf{H}_0^1(T)$ and obtain by means of (5.4) and integration by parts,

$$\begin{aligned}
C\|\bar{\mathbf{R}}_T\|_{\boldsymbol{L}^2(T)}^2 &\le \big(\bar{\mathbf{R}}_T,\boldsymbol{v}_T\big)_{\boldsymbol{L}^2(T)} = \big(\bar{\mathbf{R}}_T-\mathbf{R}_T,\boldsymbol{v}_T\big)_{\boldsymbol{L}^2(T)}+(\mathbf{R}_T,\boldsymbol{v}_T)_{\boldsymbol{L}^2(T)}\\
&= \big(\boldsymbol{f}-\mathbf{curl}\,\nu\,\mathbf{curl}\,\boldsymbol{E}_{\mathcal{T}}^{\gamma}-\epsilon\boldsymbol{E}_{\mathcal{T}}^{\gamma}-\boldsymbol{\lambda}_{\mathcal{T}}^{\gamma},\boldsymbol{v}_T\big)_{\boldsymbol{L}^2(T)}+\big(\bar{\mathbf{R}}_T-\mathbf{R}_T,\boldsymbol{v}_T\big)_{\boldsymbol{L}^2(T)}\\
&= \big(\epsilon(\boldsymbol{E}-\boldsymbol{E}_{\mathcal{T}}^{\gamma}),\boldsymbol{v}_T\big)_{\boldsymbol{L}^2(T)}+\big(\boldsymbol{\lambda}-\boldsymbol{\lambda}_{\mathcal{T}}^{\gamma},\boldsymbol{v}_T\big)_{\boldsymbol{L}^2(T)}\\
&\quad+\big(\nu\,\mathbf{curl}(\boldsymbol{E}-\boldsymbol{E}_{\mathcal{T}}^{\gamma}),\mathbf{curl}\,\boldsymbol{v}_T\big)_{\boldsymbol{L}^2(T)}+\big(\bar{\mathbf{R}}_T-\mathbf{R}_T,\boldsymbol{v}_T\big)_{\boldsymbol{L}^2(T)}\\
&\le C\|\boldsymbol{E}-\boldsymbol{E}_{\mathcal{T}}^{\gamma}\|_{a,T}\|\boldsymbol{v}_T\|_{\mathbf{H}(\mathbf{curl},T)}+\|\boldsymbol{\lambda}-\boldsymbol{\lambda}_{\mathcal{T}}^{\gamma}\|_{*,a,T}\|\boldsymbol{v}_T\|_{\mathbf{H}(\mathbf{curl},T)}\\
&\quad+\|\bar{\mathbf{R}}_T-\mathbf{R}_T\|_{\boldsymbol{L}^2(T)}\|\boldsymbol{v}_T\|_{\boldsymbol{L}^2(T)}.
\end{aligned}$$

Now, the estimates for $\boldsymbol{v}_T$ [1, Theorem 2.2] give us

$$\|\boldsymbol{v}_T\|_{\boldsymbol{L}^2(T)}+h_T\|\mathbf{curl}\,\boldsymbol{v}_T\|_{\boldsymbol{L}^2(T)} \le C\|\bar{\mathbf{R}}_T\|_{\boldsymbol{L}^2(T)} \tag{5.25}$$

which, together with the triangle inequality, implies

$$Ch_T^2\|\mathbf{R}_T\|_{\boldsymbol{L}^2(T)}^2 \le \|\boldsymbol{E}-\boldsymbol{E}_{\mathcal{T}}^{\gamma}\|_{a,T}^2+\|\boldsymbol{\lambda}-\boldsymbol{\lambda}_{\mathcal{T}}^{\gamma}\|_{*,a,T}^2+h_T^2\|\bar{\mathbf{R}}_T-\mathbf{R}_T\|_{\boldsymbol{L}^2(T)}^2. \tag{5.26}$$

Next, we set $v=v_T=\overline{\operatorname{div}\boldsymbol{\lambda}_{\mathcal{T}}^{\gamma}}|_T\,b_T\in H_0^1(T)$ and obtain by (5.4) and the fact $\operatorname{div}\boldsymbol{E}_{\mathcal{T}}^{\gamma}|_T=0$ for every $T\in\mathcal{T}$ that

$$\begin{aligned}
&C\|\overline{\operatorname{div}\boldsymbol{\lambda}_{\mathcal{T}}^{\gamma}}|_T\|_{\boldsymbol{L}^2(T)}^2 \le \Big(\overline{\operatorname{div}\boldsymbol{\lambda}_{\mathcal{T}}^{\gamma}}|_T,v_T\Big)_{\boldsymbol{L}^2(T)}\\
=&\big(\operatorname{div}\boldsymbol{\lambda}_{\mathcal{T}}^{\gamma},v_T\big)_{\boldsymbol{L}^2(T)}+\Big(\overline{\operatorname{div}\boldsymbol{\lambda}_{\mathcal{T}}^{\gamma}}|_T-\operatorname{div}\boldsymbol{\lambda}_{\mathcal{T}}^{\gamma},v_T\Big)_{\boldsymbol{L}^2(T)}\\
=&\big(\boldsymbol{\lambda}_{\mathcal{T}}^{\gamma},\nabla v_T\big)_{\boldsymbol{L}^2(T)}+\Big(\overline{\operatorname{div}\boldsymbol{\lambda}_{\mathcal{T}}^{\gamma}}|_T-\operatorname{div}\boldsymbol{\lambda}_{\mathcal{T}}^{\gamma},v_T\Big)_{\boldsymbol{L}^2(T)}\\
=&\big(\boldsymbol{\lambda}_{\mathcal{T}}^{\gamma}-\boldsymbol{\lambda},\nabla v_T\big)_{\boldsymbol{L}^2(T)}+\big(\epsilon(\boldsymbol{E}_{\mathcal{T}}^{\gamma}-\boldsymbol{E}),\nabla v_T\big)_{\boldsymbol{L}^2(T)}+\Big(\overline{\operatorname{div}\boldsymbol{\lambda}_{\mathcal{T}}^{\gamma}}|_T-\operatorname{div}\boldsymbol{\lambda}_{\mathcal{T}}^{\gamma},v_T\Big)_{\boldsymbol{L}^2(T)}.
\end{aligned}$$

Hence, the estimates for v_T yield

$$Ch_T^2\|\operatorname{div}\boldsymbol{\lambda}_{\mathcal{T}}^{\gamma}\|_{\boldsymbol{L}^2(T)}^2 \le \|\boldsymbol{E}-\boldsymbol{E}_{\mathcal{T}}^{\gamma}\|_{a,T}^2+\|\boldsymbol{\lambda}-\boldsymbol{\lambda}_{\mathcal{T}}^{\gamma}\|_{*,a,T}^2+h_T^2\|\overline{\operatorname{div}\boldsymbol{\lambda}_{\mathcal{T}}^{\gamma}}|_T-\operatorname{div}\boldsymbol{E}_{\mathcal{T}}^{\gamma}\|_{\boldsymbol{L}^2(T)}^2. \tag{5.27}$$

For a face $F \in \mathcal{F}_{\mathcal{T}}$, we use the face bubble function b_F [1] and set $\boldsymbol{v} = \boldsymbol{v}_F = \bar{\mathbf{J}}_{F,1} b_F \in \mathbf{H}_0^1(\omega_F)$. Then similar arguments yield

$$\begin{aligned}
C\|\bar{\mathbf{J}}_{F,1}\|^2_{\boldsymbol{L}^2(F)} &\le \big(\bar{\mathbf{J}}_{F,1}, \boldsymbol{v}_F\big)_{\boldsymbol{L}^2(F)} = (\mathbf{J}_{F,1}, \boldsymbol{v}_F)_{\boldsymbol{L}^2(F)} + \big(\bar{\mathbf{J}}_{F,1} - \mathbf{J}_{F,1}, \boldsymbol{v}_F\big)_{\boldsymbol{L}^2(F)} \\
&= (\mathbf{R}_T, \boldsymbol{v}_F)_{\boldsymbol{L}^2(\omega_F)} - \big(\boldsymbol{f} - \epsilon \boldsymbol{E}^\gamma_{\mathcal{T}} - \boldsymbol{\lambda}^\gamma_{\mathcal{T}}, \boldsymbol{v}_F\big)_{\boldsymbol{L}^2(\omega_F)} + \big(\nu\, \mathbf{curl}\, \boldsymbol{E}^\gamma_{\mathcal{T}}, \mathbf{curl}\, \boldsymbol{v}_F\big)_{\boldsymbol{L}^2(\omega_F)} \\
&\quad + \big(\bar{\mathbf{J}}_{F,1} - \mathbf{J}_{F,1}, \boldsymbol{v}_F\big)_{\boldsymbol{L}^2(F)} \\
&= (\mathbf{R}_T, \boldsymbol{v}_F)_{\boldsymbol{L}^2(\omega_F)} - \big(\epsilon(\boldsymbol{E} - \boldsymbol{E}^\gamma_{\mathcal{T}}), \boldsymbol{v}_F\big)_{\boldsymbol{L}^2(\omega_F)} - \big(\boldsymbol{\lambda} - \boldsymbol{\lambda}^\gamma_{\mathcal{T}}, \boldsymbol{v}_F\big)_{\boldsymbol{L}^2(\omega_F)} \\
&\quad - \big(\nu\, \mathbf{curl}(\boldsymbol{E} - \boldsymbol{E}^\gamma_{\mathcal{T}}), \mathbf{curl}\, \boldsymbol{v}_F\big)_{\boldsymbol{L}^2(\omega_F)} + \big(\bar{\mathbf{J}}_{F,1} - \mathbf{J}_{F,1}, \boldsymbol{v}_F\big)_{\boldsymbol{L}^2(F)}.
\end{aligned}$$

We use the estimates for $\boldsymbol{v}_F$ [1, Theorem 2.4] again, along with (5.26), to obtain

$$\begin{aligned}
Ch_F\|\mathbf{J}_{F,1}\|^2_{\boldsymbol{L}^2(F)} \le \sum_{T\in\omega_F} \Big(&\|\boldsymbol{E} - \boldsymbol{E}^\gamma_{\mathcal{T}}\|^2_{\mathbf{H}(\mathbf{curl},T)} + \|\boldsymbol{\lambda} - \boldsymbol{\lambda}^\gamma_{\mathcal{T}}\|^2_{*,T} \\
&+ h_T^2 \|\bar{\mathbf{R}}_T - \mathbf{R}_T\|^2_{\boldsymbol{L}^2(T)}\Big) + h_F\|\bar{\mathbf{J}}_{F,1} - \mathbf{J}_{F,1}\|^2_{\boldsymbol{L}^2(F)}.
\end{aligned} \tag{5.28}$$

Next, we set $q = q_F = \bar{J}_{F,2} b_F \in H_0^1(\omega_F)$ to derive analogously

$$\begin{aligned}
C\|\bar{J}_{F,2}\|^2_{\boldsymbol{L}^2(F)} &\le \big(\bar{J}_{F,2}, q_F\big)_{\boldsymbol{L}^2(F)} = (J_{F,2}, q_F)_{\boldsymbol{L}^2(F)} + \big(\bar{J}_{F,2} - J_{F,2}, q_F\big)_{\boldsymbol{L}^2(F)} \\
&= \big(\epsilon(\boldsymbol{E} - \boldsymbol{E}^\gamma_{\mathcal{T}}), \nabla q_F\big)_{\boldsymbol{L}^2(\omega_F)} + \big(\boldsymbol{\lambda} - \boldsymbol{\lambda}^\gamma_{\mathcal{T}}, \nabla q_F\big)_{\boldsymbol{L}^2(\omega_F)} + \big(\operatorname{div} \boldsymbol{\lambda}^\gamma_{\mathcal{T}}, q_F\big)_{\boldsymbol{L}^2(\omega_F)} \\
&\quad + \big(\bar{J}_{F,2} - J_{F,2}, q_F\big)_{\boldsymbol{L}^2(F)} \\
&\le C \Bigg(h_F^{-1/2} \sum_{T\in\omega_F} \|\boldsymbol{E} - \boldsymbol{E}^\gamma_{\mathcal{T}}\|_{\boldsymbol{L}^2(T)} + \|\boldsymbol{\lambda} - \boldsymbol{\lambda}^\gamma_{\mathcal{T}}\|_{*,a,T} \\
&\qquad + h_F^{1/2} \sum_{T\in\omega_F} \|\operatorname{div} \boldsymbol{\lambda}^\gamma_{\mathcal{T}}\|_{\boldsymbol{L}^2(T)} + h_F^{1/2}\|\bar{J}_{F,2} - J_{F,2}\|_{\boldsymbol{L}^2(F)} \Bigg) \|\bar{J}_{F,2}\|_{\boldsymbol{L}^2(F)}.
\end{aligned}$$

Hence,

$$\begin{aligned}
Ch_F\|J_{F,2}\|^2_{\boldsymbol{L}^2(F)} \le \sum_{T\in\omega_F} &\|\boldsymbol{E} - \boldsymbol{E}^\gamma_{\mathcal{T}}\|^2_{\boldsymbol{L}^2(T)} + \|\boldsymbol{\lambda} - \boldsymbol{\lambda}^\gamma_{\mathcal{T}}\|^2_{*,a,T} + h_T^2 \|\overline{\operatorname{div} \boldsymbol{\lambda}^\gamma_{\mathcal{T}}}|_T - \operatorname{div} \boldsymbol{\lambda}^\gamma_{\mathcal{T}}\|^2_{\boldsymbol{L}^2(T)} \\
&+ h_F\|\bar{J}_{F,2} - J_{F,2}\|^2_{\boldsymbol{L}^2(F)}.
\end{aligned}$$

This, along with (5.26)–(5.28), leads directly to the efficiency of the estimator (5.24). ■

5.3 ▪ Adaptive Algorithm and its Convergence

This section is devoted to the development of an adaptive mesh refinement algorithm for solving elliptic variational inequalities of the second kind and a rigorous convergence analysis thereof. The algorithm is based on the reliable and efficient a posteriori error estimator (5.21). It consists of the standard *Solve–Estimate–Mark–Refine* loop.

While we were using the subscript $\mathcal{T}$ to indicate the finite element spaces in the previous section, we will now work with triangulations generated by our new adaptive mesh refinement algorithm. So it will be more convenient for us to indicate the dependencies on the triangulations by the number of refinement steps $k \in \mathbb{N}_0$.

Remark 5.8. (i) Besides giving enough regularity to establish the local regularity property for the regularized dual variable (see Lemma 5.3), the Moreau–Yosida regularization enables us to accomplish step 2 of Algorithm 5.1 by using the semismooth Newton method (cf. Algorithm 3.1).

Algorithm 5.1 Adaptive mesh refinement algorithm

1: Set $k = 0$, and choose an initial conforming mesh $\mathcal{T}_0$
2: (SOLVE) Compute the solution $(\boldsymbol{E}_k, \boldsymbol{\lambda}_k)$ of (5.6) for $\mathcal{T} = \mathcal{T}_k, \gamma = \gamma_k$ with Algorithm 3.1
3: (ESTIMATE) Compute the error estimator $\eta_{\mathcal{T}}(\boldsymbol{E}_k, \boldsymbol{\lambda}_k, \boldsymbol{f})$ defined in (5.21)
4: (MARK) Mark a subset $\mathcal{M}_k \subset \mathcal{T}_k$ containing at least the element $\tilde{T} \in \mathcal{T}_k$ with the largest error indicator, i.e.,

$$\eta_k(\boldsymbol{E}_k, \boldsymbol{\lambda}_k, \boldsymbol{f}, \tilde{T}) = \max_{T \in \mathcal{T}_k} \eta_k(\boldsymbol{E}_k, \boldsymbol{\lambda}_k, \boldsymbol{f}, T). \tag{5.29}$$

5: (REFINE) Refine each $T \in \mathcal{M}_k$ by bisection to obtain $\mathcal{T}_{k+1}$
6: Set $k = k + 1$ and go to step 2 unless a stopping criterion is satisfied

(ii) We emphasize that many practical marking strategies satisfy (5.29), including the maximum strategy [9], the equidistribution strategy [68], the modified equidistribution strategy, as well as Dörfler's strategy [63].
(iii) The refinement by bisection is based on the strategy proposed in [140].

In order to guarantee the strong convergence of Algorithm 5.1, we shall choose the sequence of Moreau–Yosida regularization parameters such that

$$\lim_{k \to \infty} \gamma_k = \infty. \tag{5.30}$$

For instance, we may set $\gamma_k = \sqrt{|\mathcal{T}_k|} + \gamma_0$, where $\gamma_0 > 0$ and $|\mathcal{T}_k|$ denotes the number of elements in $\mathcal{T}_k$. As a first result in this section we establish a stability estimate for the a posteriori error estimator.

Lemma 5.9. *Let Assumption* 5.1 *hold and* $\{(\boldsymbol{E}_k, \boldsymbol{\lambda}_k)\}_{k \in \mathbb{N}_0}$ *be the sequence of solutions of* (5.6) *generated by Algorithm* 5.1. *Then, there exists a constant* $C > 0$ *independent of* $k \in \mathbb{N}_0$ *such that for every* $T \in \mathcal{T}_k$,

$$\eta_k(\boldsymbol{E}_k, \boldsymbol{\lambda}_k, \boldsymbol{f}, T) \leq C\big(\|\boldsymbol{E}_k\|_{\boldsymbol{L}^2(\omega_T)} + (1 + \gamma_k h_T)\|\operatorname{\mathbf{curl}} \boldsymbol{E}_k\|_{\boldsymbol{L}^2(\omega_T)} + \|\boldsymbol{\lambda}_k\|_{\boldsymbol{L}^2(\omega_T)} + h_T\|\boldsymbol{f}\|_{\boldsymbol{L}^2(T)}\big).$$

Proof. Using the fact that $\operatorname{\mathbf{curl}} \nu \operatorname{\mathbf{curl}} \boldsymbol{E}_k|_T \equiv 0$ holds for all $T \in \mathcal{T}_k$, we have

$$h_T\|\mathbf{R}_T\|_{\boldsymbol{L}^2(T)} \leq C h_T\big(\|\boldsymbol{f}\|_{\boldsymbol{L}^2(T)} + \|\boldsymbol{E}_k\|_{\boldsymbol{L}^2(T)} + \|\boldsymbol{\lambda}_k\|_{\boldsymbol{L}^2(T)}\big). \tag{5.31}$$

Further, by the trace theorem [166, page 87], we can estimate the tangential and normal jump terms across a face $F \in \mathcal{F}_k(\Omega)$ shared by $T, T' \in \mathcal{T}_k$, respectively, by

$$\begin{aligned} h_F^{1/2}\|\mathbf{J}_{F,1}\|_{\boldsymbol{L}^2(F)} &\leq C h_F^{1/2}\big(\|\operatorname{\mathbf{curl}} \boldsymbol{E}_k|_T\|_{\boldsymbol{L}^2(F)} + \|\operatorname{\mathbf{curl}} \boldsymbol{E}_k|_{T'}\|_{\boldsymbol{L}^2(F)}\big) \\ &\leq C\|\operatorname{\mathbf{curl}} \boldsymbol{E}_k\|_{\boldsymbol{L}^2(\omega_F)}, \end{aligned} \tag{5.32}$$

$$h_F^{1/2}\|J_{F,2}\|_{\boldsymbol{L}^2(F)} \leq C(\|\boldsymbol{E}_k\|_{\boldsymbol{L}^2(\omega_F)} + \|\boldsymbol{\lambda}_k\|_{\boldsymbol{L}^2(\omega_F)}). \tag{5.33}$$

Now the desired estimate follows directly from (5.31)–(5.33) and Lemma 5.3. ∎

To proceed with the convergence analysis, we introduce the following limiting problem: Find $\boldsymbol{E}_\infty \in \boldsymbol{V}_\infty$ such that

$$a(\boldsymbol{E}_\infty, \boldsymbol{v}_\infty - \boldsymbol{E}_\infty) + \psi(\boldsymbol{v}_\infty) - \psi(\boldsymbol{E}_\infty) \geq \int_\Omega \boldsymbol{f} \cdot (\boldsymbol{v}_\infty - \boldsymbol{E}_\infty)\, dx \quad \forall\, \boldsymbol{v}_\infty \in \boldsymbol{V}_\infty, \tag{VI_∞}$$

where $\boldsymbol{V}_\infty$ is a limiting space formed by the discrete spaces $\boldsymbol{V}_k$ generated by Algorithm 5.1, namely,

$$\boldsymbol{V}_\infty := \overline{\bigcup_{k \in \mathbb{N}_0} \boldsymbol{V}_k}^{\|\cdot\|_{\boldsymbol{H}(\operatorname{\mathbf{curl}})}}. \tag{5.34}$$

Since $\boldsymbol{V}_\infty$ is a closed subspace of $\boldsymbol{H}(\mathbf{curl})$, the existence and uniqueness of the solutions to (VI_∞) follows again by Theorem 3.1. The next lemma shows the existence of a corresponding Lagrange multiplier similar to (5.6).

Lemma 5.10. *Under Assumption* 5.1*, there exists a Lagrange multiplier* $\boldsymbol{\lambda}_\infty \in \mathbf{L}^\infty(\Omega)$ *for the solution* $\boldsymbol{E}_\infty \in \boldsymbol{V}_\infty$ *to* (VI_∞) *such that*

$$\begin{cases} a(\boldsymbol{E}_\infty, \boldsymbol{v}_\infty) + \displaystyle\int_\Omega \boldsymbol{\lambda}_\infty \cdot \boldsymbol{v}_\infty \, dx = \int_\Omega \boldsymbol{f} \cdot \boldsymbol{v}_\infty \, dx \quad \forall \boldsymbol{v}_\infty \in \boldsymbol{V}_\infty \\ |\boldsymbol{\lambda}_\infty(x)| \le j_c(x), \quad \boldsymbol{\lambda}_\infty(x) \cdot \boldsymbol{E}_\infty(x) = j_c(x)|\boldsymbol{E}_\infty(x)| \text{ for a.e. } x \in \Omega. \end{cases} \tag{5.35}$$

Proof. For the convenience of the reader, we provide a quick proof for this result. Choosing $\boldsymbol{v}_\infty = 0$ and $\boldsymbol{v}_\infty = 2\boldsymbol{E}_\infty$, respectively, in ($\mathrm{VI}_\infty$) yields

$$a(\boldsymbol{E}_\infty, \boldsymbol{E}_\infty) + \psi(\boldsymbol{E}_\infty) = \int_\Omega \boldsymbol{f} \cdot \boldsymbol{E}_\infty \, dx. \tag{5.36}$$

Applying this identity to (VI_∞) leads to

$$\int_\Omega \boldsymbol{f} \cdot \boldsymbol{v}_\infty \, dx - a(\boldsymbol{E}_\infty, \boldsymbol{v}_\infty) =: l(\boldsymbol{v}_\infty) \le \psi(\boldsymbol{v}_\infty) \underbrace{=}_{(5.1)} \int_\Omega j_c |\boldsymbol{v}_\infty| \, dx \quad \forall \, \boldsymbol{v}_\infty \in \boldsymbol{V}_\infty.$$

As $\boldsymbol{V}_\infty \subset \boldsymbol{L}^2(\Omega)$ is a subspace, $l : \boldsymbol{V}_\infty \to \mathbb{R}$ is a linear functional, and $\psi : \boldsymbol{L}^2(\Omega) \to \mathbb{R}$ is sublinear, the Hahn-Banach theorem implies the existence of a linear extension $F : \boldsymbol{L}^2(\Omega) \to \mathbb{R}$ such that

$$F(\boldsymbol{v}_\infty) = l(\boldsymbol{v}_\infty) \quad \forall \boldsymbol{v}_\infty \in \boldsymbol{V}_\infty \, ; \quad |F(\boldsymbol{v})| \le \psi(\boldsymbol{v}) \quad \forall \boldsymbol{v} \in \boldsymbol{L}^2(\Omega). \tag{5.37}$$

By the boundedness of $\psi : \boldsymbol{L}^2(\Omega) \to \mathbb{R}$, the Riesz representation theorem yields the existence of $\boldsymbol{\lambda}_\infty \in \boldsymbol{L}^2(\Omega)$ satisfying

$$F(\boldsymbol{v}) = (\boldsymbol{\lambda}_\infty, \boldsymbol{v})_{\boldsymbol{L}^2(\Omega)} \quad \forall \boldsymbol{v} \in \boldsymbol{L}^2(\Omega).$$

Thus, the equation in (5.37) is equivalent to

$$a(\boldsymbol{E}_\infty, \boldsymbol{v}_\infty) + \int_\Omega \boldsymbol{\lambda}_\infty \cdot \boldsymbol{v}_\infty \, dx = \int_\Omega \boldsymbol{f} \cdot \boldsymbol{v}_\infty \, dx \quad \forall \boldsymbol{v}_\infty \in \boldsymbol{V}_\infty. \tag{5.38}$$

Assume now that there exists a measurable set $\omega \subset \Omega$ with $|\omega| \neq 0$ such that $|\boldsymbol{\lambda}_\infty(x)| > j_c(x)$ for a.e. $x \in \omega$. By this assumption, the function $\hat{\boldsymbol{v}} := \frac{\boldsymbol{\lambda}_\infty}{|\boldsymbol{\lambda}_\infty|}\chi_\omega$ belongs to $\boldsymbol{L}^2(\Omega)$. Then taking $\boldsymbol{v} = \hat{\boldsymbol{v}}$ in the inequality in (5.37) leads readily to a contradiction

$$\int_\omega j_c \, dx < \int_\omega |\boldsymbol{\lambda}_\infty| \, dx \le \int_\omega j_c \, dx.$$

Thus,

$$|\boldsymbol{\lambda}_\infty(x)| \le j_c(x) \text{ a.e. } x \in \Omega \quad \Rightarrow \quad \boldsymbol{\lambda}_\infty \in \mathbf{L}^\infty(\Omega). \tag{5.39}$$

Finally, inserting $\boldsymbol{v}_\infty = \boldsymbol{E}_\infty$ into (5.38), we deduce from (5.36) that

$$\int_\Omega j_c(x)|\boldsymbol{E}_\infty(x)| - \boldsymbol{\lambda}_\infty(x) \cdot \boldsymbol{E}_\infty(x) \, dx = 0$$
$$\underbrace{\Rightarrow}_{(5.39)} \boldsymbol{\lambda}_\infty(x) \cdot \boldsymbol{E}_\infty(x) = j_c(x)|\boldsymbol{E}_\infty(x)| \text{ for a.e. } x \in \Omega.$$

In conclusion, $(\boldsymbol{E}_\infty, \boldsymbol{\lambda}_\infty) \in \boldsymbol{V}_\infty \times \mathbf{L}^\infty(\Omega)$ satisfies (5.35). ∎

Next, we prove the strong convergence of the edge element sequence $\{\boldsymbol{E}_k\}_{k\in\mathbb{N}_0}$ toward the unique solution of (VI_∞).

Theorem 5.11. *Let Assumption* 5.1 *hold. Moreover, let* $\boldsymbol{E}_\infty \in \boldsymbol{V}_\infty$ *be the unique solution to* (VI_∞) *and* $\{\boldsymbol{E}_k\}_{k\in\mathbb{N}_0}$ *be the sequence generated by Algorithm* 5.1. *Then, the following convergence holds:*

$$\lim_{k\to\infty} \|\boldsymbol{E}_k - \boldsymbol{E}_\infty\|_a = 0.$$

Proof. Let us begin this proof by showing that the sequence $\{\boldsymbol{E}_k\}_{k\in\mathbb{N}_0} \subset \boldsymbol{H}(\mathbf{curl})$ is bounded. Since $\boldsymbol{E}_k$ solves ($\mathrm{EVI}_{\mathcal{T}}$), we obtain

$$a(\boldsymbol{E}_k, \boldsymbol{E}_k) \le (\boldsymbol{f}, \boldsymbol{E}_k - \boldsymbol{v}_k)_{\boldsymbol{L}^2(\Omega)} + a(\boldsymbol{E}_k, \boldsymbol{v}_k) + \psi_{\gamma_k}(\boldsymbol{v}_k) - \psi_{\gamma_k}(\boldsymbol{E}_k) \quad \forall \boldsymbol{v}_k \in \boldsymbol{V}_k. \tag{5.40}$$

Then, setting $\boldsymbol{v}_k = 0$ in (5.40), we derive by Hölder's inequality and Lemma 3.4 that

$$\|\boldsymbol{E}_k\|_a^2 \le C(\|\boldsymbol{E}_k\|_a + 1) \quad \Rightarrow \quad \|\boldsymbol{E}_k\|_a \le C,$$

where the constant $C > 0$ is independent of k. Hence, there exists a $\boldsymbol{w}_\infty \in \boldsymbol{V}_\infty$ and a subsequence of $\{\boldsymbol{E}_k\}_{k\in\mathbb{N}_0}$, still denoted by $\{\boldsymbol{E}_k\}_{k\in\mathbb{N}_0}$, such that

$$\boldsymbol{E}_k \rightharpoonup \boldsymbol{w}_\infty \text{ weakly in } \boldsymbol{H}_0(\mathbf{curl}) \text{ as } k \to \infty. \tag{5.41}$$

By exploiting the weak lower semicontinuity of the squared norm $\|\cdot\|_a^2$, we obtain

$$a(\boldsymbol{w}_\infty, \boldsymbol{w}_\infty) \le \liminf_{k\to\infty} a(\boldsymbol{E}_k, \boldsymbol{E}_k). \tag{5.42}$$

Now, fix $\boldsymbol{v}_\infty \in \boldsymbol{V}_\infty$. Thanks to (5.34), we may find a sequence $\{\boldsymbol{v}_k\}_{k\in\mathbb{N}_0}$ such that $\boldsymbol{v}_k \in \boldsymbol{V}_k$ for every $k \in \mathbb{N}_0$ and $\boldsymbol{v}_k \to \boldsymbol{v}_\infty$ in $\boldsymbol{H}(\mathbf{curl})$ as $k \to \infty$. Thus, (5.5), Lemma 3.4 with (5.30), (5.41), and (5.42) lead to

$$\begin{aligned}
&(\boldsymbol{f}, \boldsymbol{v}_\infty - \boldsymbol{w}_\infty)_{\boldsymbol{L}^2(\Omega)} = \lim_{k\to\infty} (\boldsymbol{f}, \boldsymbol{v}_k - \boldsymbol{E}_k)_{\boldsymbol{L}^2(\Omega)} \\
&\le \limsup_{k\to\infty} \left[a(\boldsymbol{E}_k, \boldsymbol{v}_k - \boldsymbol{E}_k) + \psi_{\gamma_k}(\boldsymbol{v}_k) - \psi_{\gamma_k}(\boldsymbol{E}_k)\right] \\
&\le \limsup_{k\to\infty} a(\boldsymbol{E}_k, \boldsymbol{v}_k) - \liminf_{k\to\infty} a(\boldsymbol{E}_k, \boldsymbol{E}_k) + \limsup_{k\to\infty} \psi_{\gamma_k}(\boldsymbol{v}_k) - \liminf_{k\to\infty} \psi_{\gamma_k}(\boldsymbol{E}_k) \\
&\le a(\boldsymbol{w}_\infty, \boldsymbol{v}_\infty - \boldsymbol{w}_\infty) + \psi(\boldsymbol{v}_\infty) - \psi(\boldsymbol{w}_\infty).
\end{aligned}$$

Since $\boldsymbol{v}_\infty \in \boldsymbol{V}_\infty$ was chosen arbitrarily, the uniqueness of the solution to (VI_∞) implies that $\boldsymbol{w}_\infty = \boldsymbol{E}_\infty$ and $\boldsymbol{E}_k \rightharpoonup \boldsymbol{E}_\infty$ in $\boldsymbol{H}_0(\mathbf{curl})$ as $k \to \infty$.

To further show the strong convergence, we consider $\{\boldsymbol{v}_k\}_{k\in\mathbb{N}_0}$ such that $\boldsymbol{v}_k \in \boldsymbol{V}_k$ for every $k \in \mathbb{N}_0$ and $\boldsymbol{v}_k \to \boldsymbol{E}_\infty$ in $\boldsymbol{H}(\mathbf{curl})$ as $k \to \infty$. The existence of such a sequence follows by the definition of $\boldsymbol{V}_\infty$ in (5.34). Therefore, we deduce by means of (5.40) that

$$\begin{aligned}
0 \le \|\boldsymbol{E}_k - \boldsymbol{E}_\infty\|_a^2 \le a(\boldsymbol{E}_k, \boldsymbol{E}_k) - a(\boldsymbol{E}_k, \boldsymbol{E}_\infty) - a(\boldsymbol{E}_\infty, \boldsymbol{E}_k - \boldsymbol{E}_\infty) \le (\boldsymbol{f}, \boldsymbol{E}_k - \boldsymbol{v}_k)_{\boldsymbol{L}^2(\Omega)} \\
+ a(\boldsymbol{E}_k, \boldsymbol{v}_k) + \psi_{\gamma_k}(\boldsymbol{v}_k) - \psi_{\gamma_k}(\boldsymbol{E}_k) - a(\boldsymbol{E}_k, \boldsymbol{E}_\infty) - a(\boldsymbol{E}_\infty, \boldsymbol{E}_k - \boldsymbol{E}_\infty).
\end{aligned}$$

Ultimately, by passing to the $\limsup$ in the previous estimate, the strong convergence of the sequence $\{\boldsymbol{E}_k\}_{k\in\mathbb{N}_0}$ follows readily from Lemma 3.4 and (5.41). ∎

From Theorem 5.11, we can easily see the convergence of Algorithm 5.1 if we are able to prove that $\boldsymbol{E}_\infty$ is also the unique solution to (EVI). To do so, let us first split each $\mathcal{T}_k$ as follows:

$$\mathcal{T}_k^+ := \bigcap_{l\ge k} \mathcal{T}_l, \quad \mathcal{T}_k^0 := \mathcal{T}_k \backslash \mathcal{T}_k^+, \quad \Omega_k^+ := \bigcup_{T\in\mathcal{T}_k^+} D_T, \quad \Omega_k^0 := \bigcup_{T\in\mathcal{T}_k^0} D_T.$$

In (other) words, $\mathcal{T}_k^+$ consists of all elements that are not refined after the k-th iteration, whereas elements in $\mathcal{T}_k^0$ are refined at least once after the k-th iteration. Obviously, $\mathcal{T}_l^+ \subset \mathcal{T}_k^+$ for $l < k$, and we have $\mathcal{M}_k \subset \mathcal{T}_k^0$ for the set of the marked elements from Algorithm 5.1. Furthermore, we define a mesh-size function $h_k \colon \bar{\Omega} \to \mathbb{R}_+$ by $h_k(x) = h_T$ for x in the interior of an element $T \in \mathcal{T}_k$ and $h_k(x) = h_F$ for x in the relative interior of a face $F \in \mathcal{F}_k$. This mesh-size function has a property that is crucial for our further analysis (see [128, Corollary 4.1] and [152, Corollary 3.3]).

Lemma 5.12. *Let χ_k^0 be the characteristic function of Ω_k^0. Then, it holds that*

$$\lim_{k\to\infty} \|h_k \chi_k^0\|_{L^\infty(\Omega)} = 0.$$

In order to prove that the maximal error indicator in each loop of Algorithm 5.1 converges to zero, we need an additional assumption for the sequence of regularization parameters $\{\gamma_k\}_{k\in\mathbb{N}_0}$.

Assumption 5.13. There is a constant $C > 0$ independent of $k \in \mathbb{N}_0$ such that the sequence of Moreau–Yosida regularization parameters $\{\gamma_k\}_{k\in\mathbb{N}_0}$ satisfies

$$\gamma_k h_{\tilde{T}_k} \le C \quad \forall k \in \mathbb{N}_0, \tag{5.43}$$

where $\tilde{T}_k$ denotes the element with the largest error estimator in the k-th refinement step of Algorithm 5.1.

Lemma 5.14. *Let Assumptions* 5.1 *and* 5.13 *hold, and let $\{(\mathcal{T}_k, \mathcal{M}_k, \boldsymbol{E}_k, \boldsymbol{\lambda}_k)\}_{k\in\mathbb{N}_0}$ be the sequence generated by Algorithm* 5.1*. Then, it holds that*

$$\lim_{k\to\infty} \max_{T\in\mathcal{M}_k} \eta_k(\boldsymbol{E}_k, \boldsymbol{\lambda}_k, \boldsymbol{f}, T) = 0.$$

Proof. For convenience, we denote the element with the largest error indicator in $\mathcal{M}_k$ by $\tilde{T}_k$. Since $\tilde{T}_k \in \Omega_k^0$, the local quasi-uniformity and Lemma 5.12 imply

$$|\omega_{\tilde{T}_k}| \le C|\tilde{T}_k| \le C\|h_k\chi_k^0\|_{L^\infty(\Omega)}^3 \to 0 \quad \text{as } k \to \infty. \tag{5.44}$$

By using Lemma 5.9 and (5.6), (5.43), and (5.44), we obtain

$$\begin{aligned}
&\eta_k(\boldsymbol{E}_k, \boldsymbol{\lambda}_k, \boldsymbol{f}, j_c, \tilde{T}_k)\\
&\le C\Big(\|\boldsymbol{E}_k\|_{\boldsymbol{L}^2(\omega_{\tilde{T}_k})} + (1+\gamma_k h_{\tilde{T}_k})\|\operatorname{\mathbf{curl}} \boldsymbol{E}_k\|_{\boldsymbol{L}^2(\omega_{\tilde{T}_k})} + \|\boldsymbol{\lambda}_k\|_{\boldsymbol{L}^2(\omega_{\tilde{T}_k})} + h_{\tilde{T}_k}\|\boldsymbol{f}\|_{\boldsymbol{L}^2(\tilde{T}_k)}\Big)\\
&\le C\Big(\|\operatorname{\mathbf{curl}}(\boldsymbol{E}_k - \boldsymbol{E}_\infty)\|_{\boldsymbol{L}^2(\Omega)} + \|\boldsymbol{E}_k - \boldsymbol{E}_\infty\|_{\boldsymbol{L}^2(\Omega)} + \|\operatorname{\mathbf{curl}} \boldsymbol{E}_\infty\|_{\boldsymbol{L}^2(\omega_{\tilde{T}_k})}\\
&\qquad + \|\boldsymbol{E}_\infty\|_{\boldsymbol{L}^2(\omega_{\tilde{T}_k})} + h_{\tilde{T}_k}^{3/2}\|j_c\|_{L^\infty(\Omega)} + h_{\tilde{T}_k}\|\boldsymbol{f}\|_{\boldsymbol{L}^2(\tilde{T}_k)}\Big).
\end{aligned}$$

Now, Theorem 5.11 readily implies the convergence of the first two terms, and (5.44) yields the convergence of the remaining terms, leading to the desired result. ∎

To proceed our analysis, we introduce the residual with respect to $\boldsymbol{E}_k \in \boldsymbol{V}_k$:

$$\langle \boldsymbol{\mathcal{R}}(\boldsymbol{E}_k), \boldsymbol{v}\rangle := a(\boldsymbol{E}_k, \boldsymbol{v}) + (\boldsymbol{\lambda}_k, \boldsymbol{v})_{\boldsymbol{L}^2(\Omega)} - (\boldsymbol{f}, \boldsymbol{v})_{\boldsymbol{L}^2(\Omega)} \quad \forall \boldsymbol{v} \in \boldsymbol{H}_0(\operatorname{\mathbf{curl}}), \tag{5.45}$$

which satisfies the Galerkin-orthogonality (as $\boldsymbol{E}_k$ solves (5.6))

$$\langle \boldsymbol{\mathcal{R}}(\boldsymbol{E}_k), \boldsymbol{v}_k\rangle = 0 \quad \forall \boldsymbol{v}_k \in \boldsymbol{V}_k, k \in \mathbb{N}_0. \tag{5.46}$$

Lemma 5.15. *Under Assumptions* 5.1 *and* 5.13*, the following convergence holds for the residual defined in* (5.45) *for the sequence $\{\boldsymbol{E}_k\}_{k\in\mathbb{N}_0}$ generated by Algorithm* 5.1*:*

$$\lim_{k\to\infty} \langle \boldsymbol{\mathcal{R}}(\boldsymbol{E}_k), \boldsymbol{v}\rangle = 0 \quad \forall \boldsymbol{v} \in \boldsymbol{H}_0(\operatorname{\mathbf{curl}}).$$

Proof. Let $\boldsymbol{v} \in \boldsymbol{C}_0^\infty(\Omega)$ and set $\boldsymbol{w} \coloneqq \boldsymbol{v} - \boldsymbol{\Pi}_k \boldsymbol{v}$, where $\boldsymbol{\Pi}_k \colon \boldsymbol{H}_0(\mathbf{curl}) \to \boldsymbol{V}_k$ denotes the $\mathbf{curl}$-conforming Nédélec interpolant [127]. By virtue of Lemma 5.5, there exist $\boldsymbol{\phi} \in H_0^1(\Omega)$ and $\varphi \in H_0^1(\Omega)$ such that

$$\boldsymbol{w} - \boldsymbol{\Pi}_k^s \boldsymbol{w} = \boldsymbol{\phi} + \nabla \varphi.$$

Hence, the Galerkin orthogonality (5.46) yields

$$\begin{aligned} \langle \boldsymbol{\mathcal{R}}(\boldsymbol{E}_k), \boldsymbol{v} \rangle &= \langle \boldsymbol{\mathcal{R}}(\boldsymbol{E}_k), \boldsymbol{v} - \boldsymbol{\Pi}_k \boldsymbol{v} \rangle = \langle \boldsymbol{\mathcal{R}}(\boldsymbol{E}_k), \boldsymbol{w} - \boldsymbol{\Pi}_k^s \boldsymbol{w} \rangle \\ &= \langle \boldsymbol{\mathcal{R}}(\boldsymbol{E}_k), \boldsymbol{\phi} \rangle + \langle \boldsymbol{\mathcal{R}}(\boldsymbol{E}_k), \nabla \varphi \rangle. \end{aligned} \tag{5.47}$$

We will begin by estimating the first term on the right-hand side of (5.47). It follows by integration by parts, the trace theorem [166, page 87], and the stability estimate for $\boldsymbol{\phi}$ (cf. Lemma 5.5) that

$$\begin{aligned} \langle \boldsymbol{\mathcal{R}}(\boldsymbol{E}_k), \boldsymbol{\phi} \rangle &= - \sum_{T \in \mathcal{T}_k} (\mathbf{R}_T, \boldsymbol{\phi})_{\boldsymbol{L}^2(T)} + \sum_{F \in \mathcal{F}_k(\Omega)} (\mathbf{J}_{F,1}, \boldsymbol{\phi})_{\boldsymbol{L}^2(F)} \\ &\leq \sum_{T \in \mathcal{T}_k} h_T \|\mathbf{R}_T\|_{\boldsymbol{L}^2(T)} h_T^{-1} \|\boldsymbol{\phi}\|_{\boldsymbol{L}^2(T)} + \sum_{F \in \mathcal{F}_k(\Omega)} h_F^{1/2} \|\mathbf{J}_{F,1}\|_{\boldsymbol{L}^2(F)} h_F^{-1/2} \|\boldsymbol{\phi}\|_{\boldsymbol{L}^2(F)} \\ &\leq C \sum_{T \in \mathcal{T}_k} \eta_{k,1}(\boldsymbol{E}_k, \boldsymbol{\lambda}_k, \boldsymbol{f}, T) (h_T^{-1} \|\boldsymbol{\phi}\|_{\boldsymbol{L}^2(T)} + \|\nabla \boldsymbol{\phi}\|_{\boldsymbol{L}^2(T)}) \\ &\leq C \sum_{T \in \mathcal{T}_k} \eta_{k,1}(\boldsymbol{E}_k, \boldsymbol{\lambda}_k, \boldsymbol{f}, T) \| \mathbf{curl}(\boldsymbol{v} - \boldsymbol{\Pi}_k \boldsymbol{v}) \|_{\boldsymbol{L}^2(\tilde{D}_T)}. \end{aligned}$$

To estimate the second term on the right-hand side of (5.47), we use similar arguments and the fact that $\operatorname{div} \epsilon \boldsymbol{E}_k|_T = 0$ in every $T \in \mathcal{T}_k$, the regularity of $\boldsymbol{\lambda}_k|_T \in \boldsymbol{H}(\operatorname{div}, T)$ from Lemma 5.3, as well as Lemma 5.5 to derive

$$\begin{aligned} \langle \boldsymbol{\mathcal{R}}(\boldsymbol{E}_k), \nabla \varphi \rangle &= (\epsilon \boldsymbol{E}_k + \boldsymbol{\lambda}_k, \nabla \varphi)_{\boldsymbol{L}^2(\Omega)} = - \sum_{T \in \mathcal{T}_k} (\operatorname{div} \boldsymbol{\lambda}_k, \varphi)_{\boldsymbol{L}^2(T)} + \sum_{F \in \mathcal{F}_k(\Omega)} (J_{F,2}, \varphi)_{\boldsymbol{L}^2(F)} \\ &\leq C \sum_{T \in \mathcal{T}_k} h_T \| \operatorname{div} \boldsymbol{\lambda}_k \|_{\boldsymbol{L}^2(T)} h_T^{-1} \|\varphi\|_{\boldsymbol{L}^2(T)} + \sum_{F \in \mathcal{F}_k} h_F^{1/2} \|J_{F,2}\|_{\boldsymbol{L}^2(F)} h_F^{-1/2} \|\varphi\|_{\boldsymbol{L}^2(F)} \\ &\leq C \sum_{T \in \mathcal{T}_k} \eta_{k,2}(\boldsymbol{E}_k, \boldsymbol{\lambda}_k, T) (h_T^{-1} \|\varphi\|_{\boldsymbol{L}^2(T)} + \|\nabla \varphi\|_{\boldsymbol{L}^2(T)}) \\ &\leq C \sum_{T \in \mathcal{T}_k} \eta_{k,2}(\boldsymbol{E}_k, \boldsymbol{\lambda}_k, T) \|\boldsymbol{v} - \boldsymbol{\Pi}_k \boldsymbol{v}\|_{\boldsymbol{L}^2(\tilde{D}_T)}. \end{aligned}$$

Thus, combining the above estimates with (5.47) yields

$$|\langle \boldsymbol{\mathcal{R}}(\boldsymbol{E}_k), \boldsymbol{v} \rangle| \leq C \sum_{T \in \mathcal{T}_k} \eta_k(\boldsymbol{E}_k, \boldsymbol{\lambda}_k, \boldsymbol{f}, T) \|\boldsymbol{v} - \boldsymbol{\Pi}_k \boldsymbol{v}\|_{\mathbf{H}(\mathbf{curl}, \tilde{D}_T)}. \tag{5.48}$$

Since the right-hand side of (5.48) depends on the enlarged element patch $\tilde{D}_T$, we introduce a buffer layer of elements between T_l and T_k for $k, l \in \mathbb{N}$ with $k > l$ by

$$\mathcal{T}_{k,l}^b \coloneqq \{ T \in \mathcal{T}_k \backslash \mathcal{T}_l^+ \ : \ T \cap T' \neq \emptyset \quad \forall T' \in \mathcal{T}_l^+ \}.$$

The uniform shape regularity of $\{\mathcal{T}_k\}_{k \in \mathbb{N}}$ and the fact that $\mathcal{T}_l^+ \subset \mathcal{T}_k^+ \subset \mathcal{T}_k$ yield

$$|\mathcal{T}_{k,l}^b| \leq C_l |\mathcal{T}_l^+| \tag{5.49}$$

with a constant $C_l > 0$ depending only on $\mathcal{T}_0$ and $\tilde{D}_T \subset \Omega_l^0$ for any $T \in \mathcal{T}_k \backslash (\mathcal{T}_l^+ \cup \mathcal{T}_{k,l}^b)$ (cf. [175]). We note that in this context, $|\mathcal{M}|$ denotes the number of elements contained in $\mathcal{M} \subset \mathcal{T}_k$. With these preparations, we can split $\mathcal{T}_k$ into $\mathcal{T}_l^+ \cup \mathcal{T}_{k,l}^b$ and $\mathcal{T}_k \backslash (\mathcal{T}_l^+ \cup \mathcal{T}_{k,l}^b)$ and derive by (5.48) that

$$|\langle \boldsymbol{\mathcal{R}}(\boldsymbol{E}_k), \boldsymbol{v}\rangle| \leq C\Big(\eta_k(\boldsymbol{E}_k, \boldsymbol{\lambda}_k, \boldsymbol{f}, \mathcal{T}_k \backslash (\mathcal{T}_l^+ \cup \mathcal{T}_{k,l}^b))\|\boldsymbol{v} - \boldsymbol{\Pi}_k \boldsymbol{v}\|_{\mathbf{H}(\mathbf{curl}, \Omega_l^0)} + \eta_k(\boldsymbol{E}_k, \boldsymbol{\lambda}_k, \boldsymbol{f}, \mathcal{T}_l^+ \cup \mathcal{T}_{k,l}^b)\|\boldsymbol{v} - \boldsymbol{\Pi}_k \boldsymbol{v}\|_{\boldsymbol{H}(\mathbf{curl})}\Big). \tag{5.50}$$

The stability estimate in Lemma 5.9 and Theorem 5.11 together with the error estimate for $\boldsymbol{\Pi}_k$ (see [127, Theorem 5.41]) yield

$$\eta_k(\boldsymbol{E}_k, \boldsymbol{\lambda}_k, \boldsymbol{f}, \mathcal{T}_k \backslash (\mathcal{T}_l^+ \cup \mathcal{T}_{k,l}^b))\|\boldsymbol{v} - \boldsymbol{\Pi}_k \boldsymbol{v}\|_{\mathbf{H}(\mathbf{curl}, \Omega_l^0)} \leq C\|h_l \chi_l^0\|_{L^\infty(\Omega)} \|\boldsymbol{v}\|_{\mathbf{H}^2(\Omega)}. \tag{5.51}$$

As before, Lemma 5.12 ensures that (5.51) becomes small for a (fixed) sufficiently large $l \in \mathbb{N}$. Moreover, by using (5.29) and (5.49), we obtain

$$\begin{aligned} \eta_k(\boldsymbol{E}_k, \boldsymbol{\lambda}_k, \boldsymbol{f}, \mathcal{T}_l^+ \cup \mathcal{T}_{k,l}^b) &\leq \sqrt{|\mathcal{T}_l^+| + |\mathcal{T}_{k,l}^b|} \max_{T \in \mathcal{T}_l^+ \cup \mathcal{T}_{k,l}^b} \eta_k(\boldsymbol{E}_k, \boldsymbol{\lambda}_k, \boldsymbol{f}, T) \\ &\leq \sqrt{(C_l + 1)|\mathcal{T}_l^+|} \max_{T \in \mathcal{M}_k} \eta_k(\boldsymbol{E}_k, \boldsymbol{\lambda}_k, \boldsymbol{f}, T). \end{aligned} \tag{5.52}$$

In view of Lemma 5.14, this gets smaller and smaller for increasing $k > k_0$ with a sufficiently large $k_0 \in \mathbb{N}$. Hence, we can combine (5.50)–(5.52) to obtain

$$\lim_{k \to \infty} \langle \boldsymbol{\mathcal{R}}(\boldsymbol{E}_k), \boldsymbol{v}\rangle = 0 \quad \forall \boldsymbol{v} \in \boldsymbol{C}_0^\infty(\Omega),$$

which completes the proof by exploiting the density of $\boldsymbol{C}_0^\infty(\Omega)$ in $\boldsymbol{H}_0(\mathbf{curl})$. ■

With the help of Lemma 5.15, we are able to prove that the limiting problem (VI_∞) is in fact equivalent to (EVI).

Theorem 5.16. *Under Assumptions* 5.1 *and* 5.13*, the solution* $\boldsymbol{E}_\infty \in \boldsymbol{H}_0(\mathbf{curl})$ *of* (VI_∞) *solves* (EVI)*, i.e.,*

$$a(\boldsymbol{E}_\infty, \boldsymbol{v} - \boldsymbol{E}_\infty) + \psi(\boldsymbol{v}) - \psi(\boldsymbol{E}_\infty) \geq \int_\Omega \boldsymbol{f} \cdot (\boldsymbol{v} - \boldsymbol{E}_\infty)\, dx \quad \forall \boldsymbol{v} \in \boldsymbol{H}_0(\mathbf{curl}).$$

Proof. Let $\boldsymbol{v} \in \boldsymbol{H}_0(\mathbf{curl})$. By virtue of (5.45), it holds for every $k \in \mathbb{N}$ that

$$a(\boldsymbol{E}_k, \boldsymbol{v} - \boldsymbol{E}_\infty) = \langle \boldsymbol{\mathcal{R}}(\boldsymbol{E}_k), \boldsymbol{v} - \boldsymbol{E}_\infty\rangle + (\boldsymbol{f}, \boldsymbol{v} - \boldsymbol{E}_\infty)_{\boldsymbol{L}^2(\Omega)} - (\boldsymbol{\lambda}_k, \boldsymbol{v} - \boldsymbol{E}_\infty)_{\boldsymbol{L}^2(\Omega)},$$

from which we can derive

$$\begin{aligned} &a(\boldsymbol{E}_\infty, \boldsymbol{v} - \boldsymbol{E}_\infty) + \psi(\boldsymbol{v}) - \psi(\boldsymbol{E}_\infty) \\ &= \liminf_{k \to \infty} \big[a(\boldsymbol{E}_\infty - \boldsymbol{E}_k, \boldsymbol{v} - \boldsymbol{E}_\infty) + \psi(\boldsymbol{v}) - \psi(\boldsymbol{E}_\infty) + a(\boldsymbol{E}_k, \boldsymbol{v} - \boldsymbol{E}_\infty)\big] \\ &= \liminf_{k \to \infty} \big[a(\boldsymbol{E}_\infty - \boldsymbol{E}_k, \boldsymbol{v} - \boldsymbol{E}_\infty) + \langle \boldsymbol{\mathcal{R}}(\boldsymbol{E}_k), \boldsymbol{v} - \boldsymbol{E}_\infty\rangle \\ &\qquad + \psi(\boldsymbol{v}) - \psi(\boldsymbol{E}_\infty) - (\boldsymbol{\lambda}_k, \boldsymbol{v} - \boldsymbol{E}_\infty)_{\boldsymbol{L}^2(\Omega)}\big] + (\boldsymbol{f}, \boldsymbol{v} - \boldsymbol{E}_\infty)_{\boldsymbol{L}^2(\Omega)} \\ &\geq \liminf_{k \to \infty} \big[a(\boldsymbol{E}_\infty - \boldsymbol{E}_k, \boldsymbol{v} - \boldsymbol{E}_\infty) + \langle \boldsymbol{\mathcal{R}}(\boldsymbol{E}_k), \boldsymbol{v} - \boldsymbol{E}_\infty\rangle\big] \\ &\qquad + \liminf_{k \to \infty} \big[\psi(\boldsymbol{v}) - \psi(\boldsymbol{E}_\infty) - (\boldsymbol{\lambda}_k, \boldsymbol{v} - \boldsymbol{E}_\infty)_{\boldsymbol{L}^2(\Omega)}\big] + (\boldsymbol{f}, \boldsymbol{v} - \boldsymbol{E}_\infty)_{\boldsymbol{L}^2(\Omega)}. \end{aligned} \tag{5.53}$$

Using Theorem 5.11 and Lemma 5.15, we get the convergence of the first limit on the right-hand side of (5.53):

$$
\begin{aligned}
&|a(\boldsymbol{E}_\infty - \boldsymbol{E}_k, \boldsymbol{v} - \boldsymbol{E}_\infty) + \langle \boldsymbol{\mathcal{R}}(\boldsymbol{E}_k), \boldsymbol{v} - \boldsymbol{E}_\infty \rangle| \\
&\leq \|\boldsymbol{E}_\infty - \boldsymbol{E}_k\|_a \|\boldsymbol{v} - \boldsymbol{E}_\infty\|_a + |\langle \boldsymbol{\mathcal{R}}(\boldsymbol{E}_k), \boldsymbol{v} - \boldsymbol{E}_\infty \rangle| \to 0 \text{ as } k \to \infty.
\end{aligned} \tag{5.54}
$$

In order to estimate the remaining terms on the right-hand side of (5.53), we subtract (5.6) from (5.35) to obtain with $\boldsymbol{v}_\infty = \boldsymbol{v}_k = \boldsymbol{E}_k$ that

$$
a(\boldsymbol{E}_\infty - \boldsymbol{E}_k, \boldsymbol{E}_k) = \int_\Omega (\boldsymbol{\lambda}_k - \boldsymbol{\lambda}_\infty) \cdot \boldsymbol{E}_k \, dx \quad \forall k \in \mathbb{N}. \tag{5.55}
$$

Then, all these remaining terms can be estimated (with $|\boldsymbol{\lambda}_k| \leq j_c$ a.e. in Ω) as follows:

$$
\begin{aligned}
&\liminf_{k\to\infty} \left[\psi(\boldsymbol{v}) - \psi(\boldsymbol{E}_\infty) - (\boldsymbol{\lambda}_k, \boldsymbol{v})_{\boldsymbol{L}^2(\Omega)} + (\boldsymbol{\lambda}_k, \boldsymbol{E}_\infty)_{\boldsymbol{L}^2(\Omega)}\right] \\
&\geq \liminf_{k\to\infty} (\boldsymbol{\lambda}_k, \boldsymbol{E}_\infty)_{\boldsymbol{L}^2(\Omega)} - \psi(\boldsymbol{E}_\infty) \underbrace{=}_{(5.35)} \liminf_{k\to\infty} (\boldsymbol{\lambda}_k - \boldsymbol{\lambda}_\infty, \boldsymbol{E}_\infty)_{\boldsymbol{L}^2(\Omega)} \\
&= \liminf_{k\to\infty} \left[(\boldsymbol{\lambda}_k - \boldsymbol{\lambda}_\infty, \boldsymbol{E}_\infty - \boldsymbol{E}_k)_{\boldsymbol{L}^2(\Omega)} + (\boldsymbol{\lambda}_k - \boldsymbol{\lambda}_\infty, \boldsymbol{E}_k)_{\boldsymbol{L}^2(\Omega)}\right] \\
&\overbrace{=}^{(5.55)} \liminf_{k\to\infty} \left[(\boldsymbol{\lambda}_k - \boldsymbol{\lambda}_\infty, \boldsymbol{E}_\infty - \boldsymbol{E}_k)_{\boldsymbol{L}^2(\Omega)} + a(\boldsymbol{E}_\infty - \boldsymbol{E}_k, \boldsymbol{E}_k)\right] = 0.
\end{aligned} \tag{5.56}
$$

Finally, inserting (5.54) and (5.56) into (5.53) concludes that $\boldsymbol{E}_\infty \in \boldsymbol{H}_0(\mathbf{curl})$ is the unique solution to (EVI). ■

Theorems 5.11 and 5.16 lead to our main convergence result for Algorithm 5.1:

Theorem 5.17. *Let Assumptions* 5.1 *and* 5.13 *hold. Furthermore, let* $\{\boldsymbol{E}_k\}_{k\in\mathbb{N}_0}$ *be the sequence generated by Algorithm* 5.1*, and* $\boldsymbol{E} \in \boldsymbol{H}_0(\mathbf{curl})$ *denote the solution to* (EVI)*. Then,*

$$
\lim_{k\to\infty} \|\boldsymbol{E}_k - \boldsymbol{E}\|_{\boldsymbol{H}(\mathbf{curl})} = 0 \quad \textit{and} \quad \lim_{k\to\infty} \|\boldsymbol{\lambda}_k - \boldsymbol{\lambda}_\infty\|_{\boldsymbol{V}_k^*} = 0, \tag{5.57}
$$

where the dual norm is defined by

$$
\|\boldsymbol{\lambda}_k - \boldsymbol{\lambda}\|_{\boldsymbol{V}_k^*} \coloneqq \sup\left\{ \frac{(\boldsymbol{\lambda}_k - \boldsymbol{\lambda}, \boldsymbol{v})_{\boldsymbol{L}^2(\Omega)}}{\|\boldsymbol{v}\|_{\boldsymbol{H}(\mathbf{curl})}} : \boldsymbol{v} \in \boldsymbol{V}_k \setminus \{0\} \right\} \quad \forall k \in \mathbb{N}_0.
$$

Proof. The first convergence in (5.57) follows by combining Theorems 5.11 and 5.16. Furthermore, in view of (5.4) and (5.6), we have that

$$
\sup_{\boldsymbol{v}\in\boldsymbol{V}_k\setminus\{0\}} \frac{(\boldsymbol{\lambda}_k - \boldsymbol{\lambda}, \boldsymbol{v})_{\boldsymbol{L}^2(\Omega)}}{\|\boldsymbol{v}\|_{\boldsymbol{H}(\mathbf{curl})}} = \sup_{\boldsymbol{v}\in\boldsymbol{V}_k\setminus\{0\}} \frac{a(\boldsymbol{E} - \boldsymbol{E}_k, \boldsymbol{v})}{\|\boldsymbol{v}\|_{\boldsymbol{H}(\mathbf{curl})}} \leq 2\max\{\overline{\epsilon}, \overline{\nu}\} \|\boldsymbol{E} - \boldsymbol{E}_k\|_{\boldsymbol{H}(\mathbf{curl})},
$$

which implies the second convergence in (5.57) and concludes the proof. ■

5.4 ▪ Numerical Results

As pointed out earlier, we apply Algorithm 5.1 to a variational inequality of the form (4.2). Such a variational inequality is motivated by the physical phenomenon of type-II superconductivity and follows by considering, e.g., a semi-discretization in time of (VI). We may consider the mixed variational inequality for the initial electromagnetic field of (VI) (cf. Assumption 4.1) since it satisfies

Assumption 5.1. It reads as follows:

$$\begin{cases} \displaystyle\int_\Omega \epsilon \boldsymbol{E}\cdot(\boldsymbol{v}-\boldsymbol{E}) + \nu \boldsymbol{B}\cdot(\boldsymbol{w}-\boldsymbol{B})\,dx \\ \quad \displaystyle + \int_\Omega \nu\,\mathbf{curl}\,\boldsymbol{E}\cdot\boldsymbol{w} - \nu\boldsymbol{B}\cdot\mathbf{curl}\,\boldsymbol{v}\,dx \\ \quad \displaystyle + \int_{\Omega_{\mathrm{sc}}} j_c|\boldsymbol{v}|\;dx - \int_{\Omega_{\mathrm{sc}}} j_c|\boldsymbol{E}|\;dx \geq \int_\Omega \boldsymbol{f}\cdot(\boldsymbol{v}-\boldsymbol{E})\,dx \\ \quad \text{for all } (\boldsymbol{v},\boldsymbol{w}) \in \boldsymbol{H}_0(\mathbf{curl}) \times \boldsymbol{L}^2(\Omega), \end{cases} \tag{5.58}$$

Now, with the decoupling method from (4.1) and (4.2) we obtain (EVI) from (5.58) to compute the electric field $\boldsymbol{E}$ and get the magnetic induction from $\boldsymbol{B} = -\,\mathbf{curl}\,\boldsymbol{E}$. This also corresponds to the computation of the solution to one time step in ($\mathrm{VI}_{N,h}$) under an additional regularity assumption on the right-hand side, meaning that we require $\boldsymbol{f} \in \boldsymbol{L}^2(\Omega)$ with the divergence-free condition (A5.2) instead of $\boldsymbol{f} \in \boldsymbol{H}_0(\mathbf{curl})$.

Let us now specify the numerical setup. We choose the specification of section 4.4. The computational hold-all domain is $\Omega = (-1,1)^3$ and the right-hand side $\boldsymbol{f} \in \boldsymbol{L}^2(\Omega)$ satisfies the divergence-free condition (A3.3) as a circular current applied to a pipe coil $\Omega_p \subset \Omega$ with inner radius $r_p = 0.3$ and height $h_{\Omega_p} = 0.5$, e.g.,

$$\boldsymbol{f}(x,y,z) = \begin{cases} 1/R\Big(0,\ -z/(y^2+z^2)^{1/2},\ y/(y^2+z^2)^{1/2}\Big) & \text{for } (x,y,z) \in \Omega_p, \\ 0 & \text{for } (x,y,z) \notin \Omega_p, \end{cases}$$

where the constant $R > 0$ denotes the electrical resistance of the pipe coil Ω_p. It is set to $R = 10^3$ in our experiments. The physical parameters ϵ and ν both taken to be 1. All implementations were realized with the open-source finite element computational software FENICS [122] and we used PARAVIEW to visualize the numerical outcome. All the figures presented in this section are 2d slices of the original 3d plots. We initialize Algorithm 5.1 with a coarse uniform mesh $\mathcal{T}_0$ consisting of 384 cells and set

$$\gamma_k(\mathcal{T}_k) = \sqrt{|\mathcal{T}_k|} + \gamma_0, \quad \gamma_0 = 7 \cdot 10^4,$$

which apparently satisfies (5.30) due to the requirement (5.29) in the marking step of Algorithm 5.1. Let us note that the very complicated structure of (EVI) makes it practically impossible to find an analytical solution. Thus, based on our knowledge from section 4.4, we tested Algorithm 5.1 in a setup where we would expect a certain behaviour. For this purpose, we selected the critical current density $j_c(x) = 0.1\chi_{\Omega_{\mathrm{sc}}}(x)$, where we know the interface between the superconducting and the normal region a priori – due to the comparatively high critical current density, there is no penetration of the superconductor at all. Hence, the interface corresponds to the surface of the superconductor Ω_{sc}. We will specify two different geometries for Ω_{sc} below.

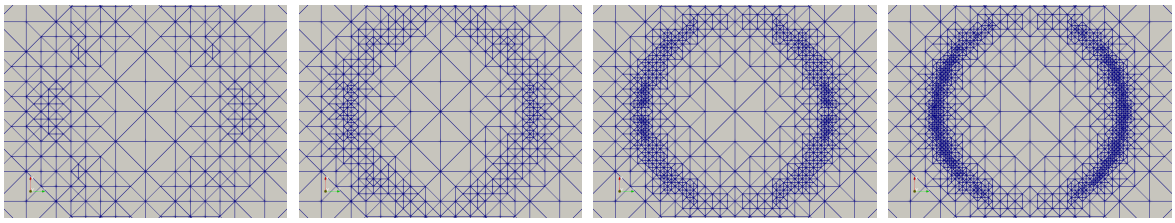

Figure 5.1. *Evolution of the adaptive mesh (2d-slice) for the first example (high j_c) in steps $k = 6, 7, 8, 9$.*

5.4.1 ▪ First Example – Superconductor as Ball

As a first example, we choose Ω_{sc} as a ball around the origin with radius $r_{sc} = 0.2$. In Figure 5.1 the evolution of the adaptive mesh is shown, and the corresponding magnetic field lines are displayed in Figure 5.3a. Our expectations are confirmed since we can observe that Algorithm 5.1 adaptively refines the mesh around the surface of the superconductor and that there is no magnetic field penetration through Ω_{sc}. At the final iteration, the mesh has roughly $1.400.000$ cells and the corresponding Nédélec finite element space has around $1.600.000$ degrees of freedom. Keeping these observations in mind, we choose a significantly smaller critical current density $j_c(x) = 0.001\chi_{\Omega_{\text{sc}}}(x)$ as the second example. The remaining parameters in the setup remain the same. In this case, we do not have any (a priori) knowledge of the approximate position and shape of the mentioned interface. Therefore, this example is much more challenging, and the adaptivity is necessary to extract the interface. Again, Algorithm 5.1 adaptively refines the mesh, but now it exhibits a wider interface than the experiment for high j_c, which indicates that the superconductor is partially penetrated by the magnetic field lines (see Figure 5.2b). This is also confirmed by the magnetic field shown in Figure 5.3b. In Figures 5.4a and 5.4b we present the meshes at the final iteration from a total perspective.

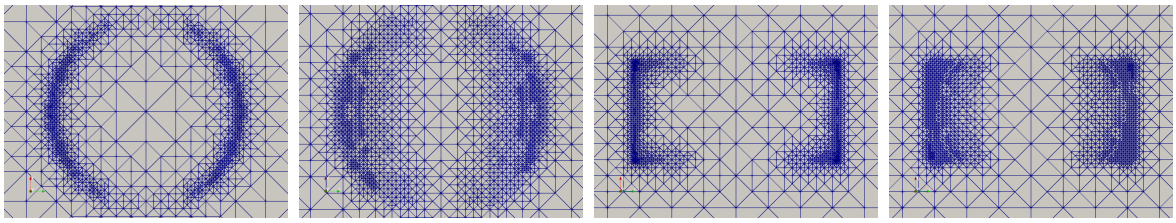

Figure 5.2. *Close-up to the mesh (2d-slice) at the final iteration for all examples.*

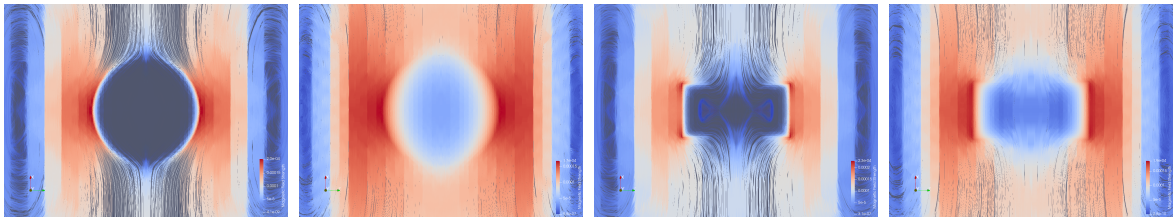

Figure 5.3. *2d-slices of the magnetic field lines.*

5.4.2 ▪ Second Example – Superconductor with Hole

Let us now consider a short pipe coil as the domain of the superconductor. We have already seen in the second example of section 4.4 that even a domain with a hole exhibits the Meissner–Ochsenfeld effect shielding its inside from magnetic field penetration. Therefore, we specify

$$\Omega_{\text{sc}} \coloneqq \left\{(x, y, z) \in \mathbb{R}^3 \,:\, |x| \leq 0.1,\ \sqrt{y^2 + z^2} \in [0.1, 0.2]\right\}.$$

For the same reason as before, we will first consider a rather high critical current density $j_c(x) = 0.1\chi_{\Omega_{\text{sc}}}(x)$. In Figure 5.2c, it becomes evident that our algorithm refines the mesh only around the outer boundary of Ω_{sc}. The corresponding magnetic field lines are displayed in Figure 5.3c. Due to the structure of the superconductor with its sharp edges, the magnetic field strength peaks around the right angles. If we consider the lower critical current density $j_c(x) = 0.001\chi_{\Omega_{\text{sc}}}$, we observe that the

Table 5.1. *Experimental rates of convergence for the first example (left) and the second example (right).*

k	4	5	8
ERC_k	0.1445	0.1558	0.1832

k	3	5	8
ERC_k	0.3288	0.3698	0.3663

mesh refinement tends to be slightly circular (cf. Figure 5.2d). This underlines the accuracy of our AFEM as the superconductor gets penetrated first in the areas where the magnetic field peaks.

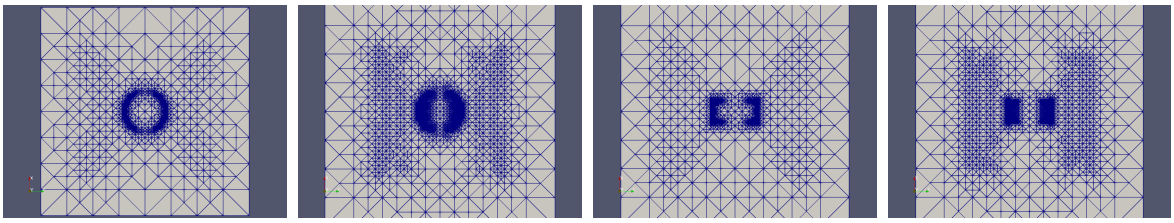

Figure 5.4. *2d-slices of the final meshes in total.*

Moreover, to verify Assumption 5.13 numerically, we computed the factor $\gamma_k h_{\tilde{T}_k}$ in every step of Algorithm 5.1 (see Tables 5.2 and 5.3). Our numerical results confirmed Assumption 5.13 for the above choice of γ_k. Indeed, it holds that

$$\gamma_k h_{\tilde{T}_k} \leq \gamma_1 h_{\tilde{T}_1}$$

for all iterations k.

Last but not least, we compare the final meshes in Figure 5.4 and observe that in all examples the coil Ω_p is also refined. We justify this behaviour with the fact that there is also a strong change of the magnetic field strength around Ω_p (see also Figure 5.3).

5.4.3 ▪ Convergence Rate Tests

We close this chapter by reporting the numerical convergence order of Algorithm 5.1 for our numerical example. Since we do not know the exact solution, we consider a reference solution $\boldsymbol{E}_{ref}$ at a very fine adaptive mesh and test the convergence behaviour of the adaptive solutions $\boldsymbol{E}_k$ toward the reference one. More precisely, this can be quantitatively clarified by evaluating the experimental rate of convergence (ERC) using two consecutive adaptive solutions and #DoFs:

$$\mathrm{ERC}_k = \left| \frac{\log(\|\boldsymbol{E}_k - \boldsymbol{E}_{ref}\|_{\boldsymbol{H}(\mathbf{curl})}) - \log(\|\boldsymbol{E}_{k-1} - \boldsymbol{E}_{ref}\|_{\boldsymbol{H}(\mathbf{curl})})}{\log(\#\mathrm{DoFs}_k) - \log(\#\mathrm{DoFs}_{k-1})} \right|.$$

For our two examples, we computed the experimental rate of convergence at different levels k and conclude a convergence order of around 0.15 for the first example and 0.35 for the second one (see Table 5.1). The very sharp phase transition in the first example implies that the corresponding solution is discontinuous around Ω_{sc} (see Figure 5.3a). On the other hand, for the second example, this transition is significantly smoother (see Figure 5.3b). This fact may explain the difference in the convergence rates.

Table 5.2. *The DOFs and a numerical verification of Assumption* 5.13 *(first example, high j_c).*

k	3	4	5	6	7	8	9	10
$\gamma_k h_{\tilde{T}_k}$	3.032e+4	1.751e+4	8.756e+3	1.238e+4	4.383e+3	3.104e+3	1.230e+3	9.587e+2
#DoFs	2728	3692	7651	21096	67793	225494	850688	1675270

Table 5.3. *The DOFs and a numerical verification of Assumption* 5.13 *(first example, medium j_c).*

k	2	3	4	5	6	7	8	9
$\gamma_k h_{\tilde{T}_k}$	6.063e+4	3.032e+4	1.516e+4	7.586e+3	3.036e+4	1.520e+4	1.907e+3	1.276e+3
#DoFs	1016	3374	7313	21074	65748	273020	1191217	1933071

Table 5.4. *The DOFs and a numerical verification of Assumption* 5.13 *(second example, high j_c).*

k	1	2	3	4	5	6	7
$\gamma_k h_{\tilde{T}_k}$	1.238e+4	6.195e+3	6.199e+3	3.102e+3	1.554e+3	9.561e+2	4.775e+2
#DoFs	7010	10745	23077	51679	153919	504836	1944478

Table 5.5. *The DOFs and a numerical verification of Assumption* 5.13 *(second example, medium j_c).*

k	1	2	3	4	5	6
$\gamma_k h_{\tilde{T}_k}$	8.759e+4	6.196e+3	3.039e+4	1.554e+3	1.531e+4	6.323e+3
#DoFs	7010	14285	46472	157997	621138	2789474

Part III

Optimization

Chapter 6

Shape Optimization for Maxwell Variational Inequalities

In our previous numerical experiments (sections 4.4 and 5.4) we have seen that not only simply connected superconducting shapes repell magnetic field lines. For instance, a superconducting pipe coil does not allow penetration through the hole if the operating temperature is sufficiently low (see Figure 4.4). Therefore, efficiently designed superconducting shields are a practical way to protect certain areas from magnetic fields. In particular, to improve and optimize their efficiency and reliability, advanced shape optimization (design) methods are highly desirable.

Basically, there are only two possible ways for a magnetic field to penetrate an area shielded by a superconductor – through the material itself and through opened parts such as holes or gaps. The former depends solely on the properties of the material, the operating temperature, and the magnetic field strength, whereas the latter is also highly affected by the geometry. In the case of an HTS coil for instance, physical experiments [110] show that the enclosed area is still shielded even if the opened ends are directly facing the field lines. On the other hand, if the diameter gets too large, field lines start penetrating the inside. Thus, the following question arises: how should we design superconducting shields in order to save material and still keep the electromagnetic field penetration at a minimum?

This chapter focuses on the sensitivity analysis and numerical investigation for a shape optimization problem in HTS based on Bean's critical-state law (cf. (B1) to (B3)). Our task is to find an admissible superconductor shape which minimizes a tracking-type objective functional under a given target on the electric field over a specific domain of interest. For the governing PDE-model, we consider the elliptic (time-discrete) counterpart to Bean's law governed by Maxwell's equations (cf. (VI)), given by the elliptic $\mathbf{curl}$-$\mathbf{curl}$ variational inequality of the second kind (4.2). Before we set up the minimization problem and discuss our methodology in detail, let us briefly introduce the basic concepts and difficulties in the optimization of shapes.

6.1 ▪ Basic Concepts of Shape Optimization

The aim of shape optimization is solving minimization (or maximization) problems where the admissible set does no longer contain parameters or functions but geometries or shapes. That is, we try to find and characterize a solution $\omega_\star$ of the problem

$$\min_{\omega \in \mathcal{O}} J(\omega),$$

where $\mathcal{O}$ is a class of subsets of $\mathbb{R}^N$ and $J\colon \mathcal{O} \to \mathbb{R}$. Elements in $\mathcal{O}$ are called *admissible shapes* and J is referred to as a *shape functional*. If the optimization problem is constrained by an additional equation, we call this equation the *state equation*.

Concerning the optimal control of partial differential equations, lots of techniques and results are

available to prove the existence of minimizers, obtain optimality conditions, and establish numerical algorithms. Here, we refer to the monograph by Tröltzsch [163] and the references therein. These tools are usually build upon the underlying vector space structure of the admissible set. In shape optimization, this structure is lost.

However, in order to adapt the standard method to prove the existence of a minimizer – namely a limiting analysis with minimizing sequences[1]–, we need to define a suitable topology on the set of admissible shapes $\mathcal{O}$. A first idea would be to link Lebesgue measurable sets to their corresponding characteristic function and define a convergence based on their L^1-norm (cf. [85, Definition 2.2.3]).

Definition 6.1. Let $\{\omega_n\}_{n\in\mathbb{N}}$ and ω be measurable sets contained in a (fixed) set $C \subset \mathbb{R}^N$ with finite Lebesgue measure. We say that ω_n converges to ω in *the sense of characteristic functions* if

$$\lim_{n\to\infty} \|\chi_{\omega_n} - \chi_\omega\|_{L^1(C)} = 0.$$

Although convergence in the sense of characteristic functions has some serious restrictions,[2] we may use it for our analysis. Another well-known topology for sets is determined by the Hausdorff-convergence. Here, we may only consider open sets that are uniformly contained in a fixed (possibly large) compact set $C \subset \mathbb{R}^N$. For two compact sets $K_1, K_2 \subset C$, we set

$$\begin{aligned} \forall x \in C:\ d(x, K_1) &\coloneqq \inf_{y\in K_1} |x - y|, \\ d(K_1, K_2) &\coloneqq \sup_{x\in K_1} d(x, K_2), \\ d^H(K_1, K_2) &\coloneqq \max\{d(K_1, K_2), d(K_2, K_1)\}. \end{aligned}$$

The latter is called the *Hausdorff-distance* for compact sets. Now, we define a convergence for open sets via d^H (see [85, Definition 2.2.8]).

Definition 6.2. Let $\{\omega_n\}_{n\in\mathbb{N}}$ and ω be open sets contained in a (fixed) compact set $C \subset \mathbb{R}^N$. We say that ω_n converges to ω in *the sense of Hausdorff* if

$$\lim_{n\to\infty} d^H\big(C \setminus \omega_n, C \setminus \omega\big) = 0.$$

For both concepts (Definitions 6.1 and 6.2) we will simply denote

$$\omega_n \to \omega \quad \text{as } n \to \infty.$$

In order to use an adapted *direct method of calculus*, we need a compactness result for our topologies which enables us to extract converging subsequences. Let $\Omega \subset \mathbb{R}^N$ be a bounded Lipschitz domain and $B \subset \Omega$. In terms of the application, Ω can be seen as the hold-all domain and B is a bounding box for the superconductor – we want to minimize the electromagnetic field penetration through B by an efficient design. We focus on the following class of open sets

$$\mathcal{O} = \{\omega \subset B\ :\ \omega \text{ is open, Lipschitz, with uniform Lipschitz constant } L\}$$

The following compactness result for the set of domains $\mathcal{O}$ is pivotal to our upcoming analysis (see [85, Theorem 2.4.10]).

[1] This is also known as the *direct method of calculus* and widely used to prove the existence of minimizers of convex functionals (cf. [163]).

[2] The characteristic functions do not distinguish between open sets and its modifications with measure zero. However, these changes may have an impact on the solution to certain PDE (cf. [85, p. 27]).

Theorem 6.3. *Let $B \subset \mathbb{R}^N$ be an open bounded Lipschitz domain and $\{\omega_n\}_{n\in\mathbb{N}} \subset \mathcal{O}$. Then, there exist $\omega \in \mathcal{O}$ and a subsequence $\{\omega_{n_k}\}_{k\in\mathbb{N}}$ which converges to ω in the sense of Hausdorff and in the sense of characteristic functions. Moreover, $\overline{\omega}_{n_k}$ and $\partial\omega_{n_k}$ converge in the sense of Hausdorff toward $\overline{\omega}$ and $\partial\omega$, respectively.*

In Theorem 6.7 we present a short proof for our HTS design problem to illustrate the direct method in shape calculus.

Now that we have the tools at hand to prove the existence of a minimizing shape, the natural next task is the characterization of first-order optimality conditions. For a convex optimization problem in a Banach space X the following equivalence is well-known (see [163, Lemma 2.20 and Lemma 2.21])

$$\overline{u} \in X \text{ solves } \min_{u\in X} f(u) \quad \Leftrightarrow \quad f'(\overline{u}) = 0 \text{ in } X^*,$$

where f' is the Gâteaux-derivative of the cost-functional $f\colon X \to \mathbb{R}$. Therefore, it is necessary to define a notion of a *gradient* for shape-functionals. This would also open a way to establish descent methods of gradient type to compute a minimizer numerically. Similar to the Gâteaux-derivative, a shape derivative relies on a limiting process with a small perturbation ω_t of a domain $\omega \in \mathcal{O}$. We thus have to define such a perturbation of ω. An intuitive possibility is choosing a regular vector field $\boldsymbol{\theta}\colon \Omega \to \Omega$ and consider $\omega_t = \boldsymbol{T}_t(\omega)$, where $\boldsymbol{T}_t = I + t\boldsymbol{\theta}$. However, there is a more general approach known as the *velocity method*. Therefore, let $\boldsymbol{T}_t : \Omega \to \Omega$ be the flow of a vector field $\boldsymbol{\theta} \in \boldsymbol{\mathcal{C}}_c^{0,1}(\Omega, \mathbb{R}^3)$ with compact support in B. That is by definition that $\boldsymbol{T}_t(\boldsymbol{\theta})(X) = x(t, X)$ solves the ordinary differential equation

$$\frac{\mathrm{d}}{\mathrm{d}t}x(t, X) = \boldsymbol{\theta}(x(t, X)) \quad \text{for } t \in [0, \tau], \quad x(0, X) = X \in \Omega, \tag{6.1}$$

for some given $\tau > 0$. It is well-known (see [155, p. 50]) that (6.1) admits a unique solution if $\tau > 0$ is sufficiently small. Moreover, $\boldsymbol{T}_t$ is a diffeomorphism[3] (see [155, Theorem 2.16]) and, since $\boldsymbol{\theta}$ has compact support in B, $\boldsymbol{T}_t(B) = B$ and $\boldsymbol{T}_t(X) = X$ for every $X \in \Omega\backslash B$. For $\omega \in \mathcal{O}$, we introduce the parameterized family of domains $\omega_t := \boldsymbol{T}_t(\omega)$, for all $t \in [0, \tau]$. Let us now define the concept of shape derivative – the basis for the sensitivity analysis of shape functionals (cf. [59, 85, 155]).

Definition 6.4 (Shape derivative). Let $K : \mathcal{O} \to \mathbb{R}$ be a shape functional. The Eulerian semiderivative of K at $\omega \in \mathcal{O}$ in direction $\boldsymbol{\theta} \in \boldsymbol{\mathcal{C}}_c^{0,1}(\Omega, \mathbb{R}^3)$ is defined as the limit, if it exists,

$$dK(\omega)(\boldsymbol{\theta}) := \lim_{t\searrow 0} \frac{K(\omega_t) - K(\omega)}{t},$$

where $\omega_t = \boldsymbol{T}_t(\omega)$. Moreover, K is said to be *shape differentiable* at ω if it has a Eulerian semiderivative at ω for all $\boldsymbol{\theta} \in \boldsymbol{\mathcal{C}}_c^{0,1}(\Omega, \mathbb{R}^3)$ and the mapping

$$dK(\omega) : \boldsymbol{\mathcal{C}}_c^{0,1}(\Omega, \mathbb{R}^3) \to \mathbb{R}, \quad \boldsymbol{\theta} \mapsto dK(\omega)(\boldsymbol{\theta})$$

is linear and continuous. In this case $dK(\omega)(\boldsymbol{\theta})$ is called the *shape derivative of* K at ω.

Although it might be delicate to compute a shape derivative for a PDE-constrained problem, some methods have been developed over the past decades. Obviously, we cannot expect that the solution to a general PDE obtains a derivative in the classical sense. Therefore, *Lagrangian methods* are commonly used in shape optimization as they have the advantage of providing the shape derivative without the need to compute the material derivative of the state[4]. A widely-used approach goes back

[3] A map $f\colon U \to V$ for open $U, V \subset \mathbb{R}^N$ is called a *diffeomorphism* if f is bijective, continuously differentiable, and its inverse function is also continuously differentiable.

[4] The material derivative refers to the sensitivity of the state with respect to a perturbation of the domain. That is, if u_t is the solution to the state equation posed on $\omega_t = \boldsymbol{T}_t(\omega)$, the material derivative is given as $\frac{d}{dt}u_t(\boldsymbol{T}_t(x)|_{t=0}$ (cf. [155, Definition 2.71]). Hence, it requires a careful analysis if the *control-to-state* operator is not differentiable.

to Céa [34]. However, it is only formal since it assumes that the shape derivative of the PDE and the adjoint equation exist (cf. [138]). The *minimax method* by Correa and Seeger [51] which was adapted to shape functionals by Delfour and Zolesio [59] is rigorously proven under a non-trivial saddle-point assumption. Applications of this result can be found for instance in [2,92]. We note that there are also several variational methods available (cf. [100, 104]).

We will rely on the *averaged adjoint method* (see Theorem 6.10) – a recent generalization of the Lagrangian method by [59] introduced in [114, 160]. The huge advantage is that no saddle-point assumption is required. Therefore, it is also suitable for nonlinear problems. Moreover, compared to the previous approaches, the averaged adjoint method is fairly general due to minimal required conditions. We state the precise theorem with all requirements in the remainder (Theorem 6.10).

6.2 ▪ Shape Optimization for Bean's Law

We are interested in minimizing the electromagnetic field penetration through the domain B located somewhere in the hold-all domain Ω with minimal use of material. Hence, we propose the following tracking-type functional to model the optimal HTS design problem:

$$\text{(P)} \qquad \min_{\omega\in\mathcal{O}} J(\omega) := \frac{1}{2}\int_B \kappa|\boldsymbol{E}(\omega)-\boldsymbol{E}_d|^2\,dx + \int_\omega dx,$$

for some given target $\boldsymbol{E}_d : B \to \mathbb{R}^3$ and weight coefficient $\kappa : B \to (0,\infty)$. For every admissible superconductor shape $\omega \in \mathcal{O}$, let $\boldsymbol{E} = \boldsymbol{E}(\omega) \in \boldsymbol{H}_0(\mathbf{curl})$ denote the associated electric field given as the solution of (4.2). For convenience of the reader, we recall the variational inequality in question again

$$\text{(EVI}_\omega\text{)} \qquad a(\boldsymbol{E},\boldsymbol{v}-\boldsymbol{E})+\varphi_\omega(\boldsymbol{v})-\varphi_\omega(\boldsymbol{E}) \geq \int_\Omega \boldsymbol{f}\cdot(\boldsymbol{v}-\boldsymbol{E})\,dx \quad \forall \boldsymbol{v}\in\boldsymbol{H}_0(\mathbf{curl}),$$

with the elliptic $\mathbf{curl}$-$\mathbf{curl}$ bilinear form $a\colon \boldsymbol{H}_0(\mathbf{curl})\times\boldsymbol{H}_0(\mathbf{curl})\to\mathbb{R}$ defined by

$$a(\boldsymbol{v},\boldsymbol{w}) := \int_\Omega \varepsilon\boldsymbol{v}\cdot\boldsymbol{w}\,dx + \int_\Omega \nu\,\mathbf{curl}\,\boldsymbol{v}\cdot\mathbf{curl}\,\boldsymbol{w}\,dx,$$

and the nonsmooth L^1-type functional $\varphi_\omega\colon \boldsymbol{L}^1(\Omega)\to\mathbb{R}$, $\boldsymbol{v}\mapsto j_c\int_\omega|\boldsymbol{v}(x)|\,dx$. For the physical meaning of the data we refer to section 1.2. The precise mathematical assumptions for all data involved in (P) are specified in Assumption 6.5. It is necessary to employ stronger regularity assumptions on the material parameters and the given data. More precisely, we need classical differentiability properties in order to compute the shape derivative of J in (P) (see Definition 6.4).

Let us now present all the standing assumptions throughout this chapter.

Assumption 6.5 (Material parameters and given data).

(A6.1) The subset $B\subset\Omega$ is an open bounded Lipschitz domain, $\boldsymbol{E}_d\in\boldsymbol{\mathcal{C}}^1(B)$, and $\kappa\in\mathcal{C}^1(B)$.

(A6.2) We assume $j_c\in\mathbb{R}^+$, and the material parameters $\epsilon,\nu\colon\Omega\to\mathbb{R}^{3\times3}$ are assumed to be $L^\infty(\Omega,\mathbb{R}^{3\times3})\cap\mathcal{C}^1(B,\mathbb{R}^{3\times3})$, symmetric and uniformly positive definite, i.e., there exist $\underline{\nu},\underline{\epsilon}>0$ such that

$$\text{(6.2)} \qquad \xi^{\mathsf{T}}\nu(x)\xi\geq\underline{\nu}|\xi|^2 \text{ and } \xi^{\mathsf{T}}\epsilon(x)\xi\geq\underline{\epsilon}|\xi|^2 \quad \text{for a.e. } x\in\Omega \text{ and all } \xi\in\mathbb{R}^3.$$

(A6.3) The right-hand side satisfies $\boldsymbol{f}\in\boldsymbol{L}^2(\Omega)\cap\boldsymbol{\mathcal{C}}^1(B)$.

Remark 6.6.

(i) As pointed out earlier, in the context of superconducting shields, one looks for an optimal superconductor shape ω that minimizes both the electromagnetic field penetration and the volume of the material. This can be realized by solving (P) with $\boldsymbol{E}_d\equiv 0$ which obviously satisfies (A6.1).

(ii) The material assumption (A6.2) holds true for instance in the case of homogeneous HTS material. In this case, ϵ, ν are constant in B.

(iii) A choice for the $\boldsymbol{f}$ satisfying (A6.3) is given by an induction coil away from the superconducting region B. In this case, $\boldsymbol{f} \equiv 0$ in B.

For every fixed $\omega \subset \mathcal{O}$, the existence of a unique solution $\boldsymbol{E} \in \boldsymbol{H}_0(\mathbf{curl})$ of (EVI$_\omega$) is covered by Theorem 3.1 since (A6.2) implies that the bilinear form $a : \boldsymbol{H}_0(\mathbf{curl}) \times \boldsymbol{H}_0(\mathbf{curl}) \to \mathbb{R}$ is coercive and continuous. Additionally, we recall that there exists a unique Lagrange multiplier $\boldsymbol{\lambda} \in \boldsymbol{L}^\infty(\omega)$ such that (see (3.12))

$$\begin{cases} a(\boldsymbol{E}, \boldsymbol{v}) + \displaystyle\int_\omega \boldsymbol{\lambda} \cdot \boldsymbol{v}\, dx = \int_\Omega \boldsymbol{f} \cdot \boldsymbol{v}\, dx \quad \forall \boldsymbol{v} \in \boldsymbol{H}_0(\mathbf{curl}), \\ |\boldsymbol{\lambda}(x)| \le j_c, \quad \boldsymbol{\lambda}(x) \cdot \boldsymbol{E}(x) = j_c |\boldsymbol{E}(x)| \text{ for a.e. } x \in \omega. \end{cases} \tag{6.3}$$

Let us now verify the existence of a minimizer of (P) by using the compactness result Theorem 6.3 and a direct method.

Theorem 6.7. *Under Assumption* 6.5*, the shape optimization problem* (P) *has an optimal solution* $\omega_\star \in \mathcal{O}$.

Proof. Let $\{\omega_n\}_{n\in\mathbb{N}} \in \mathcal{O}$ be a minimizing sequence for (P). According to Theorem 6.3, we may extract a converging subsequence of $\{\omega_n\}_{n\in\mathbb{N}}$, which will not be denoted in special way, such that

$$\omega_n \to \omega_\star \quad \text{as } n \to \infty \tag{6.4}$$

for some $\omega_\star \in \mathcal{O}$. Our aim is to show that $\omega_\star$ is a solution of (P). By $\boldsymbol{E}$ and $\boldsymbol{E}_n$ we denote the solutions of (EVI$_\omega$) with $\omega = \omega_\star$ and $\omega = \omega_n$ respectively. Inserting $\boldsymbol{v} = \boldsymbol{E}_n$ into (EVI$_\omega$) for $\boldsymbol{E}$ and adding it to (EVI$_\omega$) for $\boldsymbol{E}_n$ tested with $\boldsymbol{v} = \boldsymbol{E}$ lead to

$$\begin{aligned} \int_\Omega \varepsilon(\boldsymbol{E}_n - \boldsymbol{E}) \cdot (\boldsymbol{E}_n - \boldsymbol{E})\, dx + \int_\Omega \nu\, \mathbf{curl}(\boldsymbol{E}_n - \boldsymbol{E}) \cdot \mathbf{curl}(\boldsymbol{E}_n - \boldsymbol{E})\, dx \\ \le j_c \int_\Omega (\chi_{\omega_\star} - \chi_{\omega_n})(|\boldsymbol{E}_n| - |\boldsymbol{E}|)\, dx \end{aligned}$$

which yields by (A6.2) that

$$\begin{aligned} \min\{\underline{\nu}, \underline{\epsilon}\} \|\boldsymbol{E}_n - \boldsymbol{E}\|^2_{\boldsymbol{H}(\mathbf{curl})} \le j_c \|\chi_{\omega_\star} - \chi_{\omega_n}\|_{L^2(\Omega)} \|\boldsymbol{E}_n - \boldsymbol{E}\|_{\boldsymbol{L}^2(\Omega)} \\ \Rightarrow \|\boldsymbol{E}_n - \boldsymbol{E}\|_{\boldsymbol{H}(\mathbf{curl})} \le C \|\chi_{\omega_\star} - \chi_{\omega_n}\|_{L^2(\Omega)}, \end{aligned} \tag{6.5}$$

where $C > 0$ depends only on ν, ϵ and j_c. Thus, (6.5) implies, using the fact that ω_n converges to $\omega_\star$ in the sense of characteristic functions, that $\boldsymbol{E}_n \to \boldsymbol{E}$ in $\boldsymbol{H}_0(\mathbf{curl})$ as $n \to \infty$. By combining the strong convergence of $\{\boldsymbol{E}_n\}_{n\in\mathbb{N}}$ with (6.4) we deduce

$$J(\omega_n) = \frac{1}{2} \int_\Omega \kappa |\boldsymbol{E}_n - \boldsymbol{E}_d|^2\, dx + \int_{\omega_n} dx \to \frac{1}{2} \int_\Omega \kappa |\boldsymbol{E} - \boldsymbol{E}_d|^2\, dx + \int_{\omega_\star} dx = J(\omega_\star). \tag{6.6}$$

Note that the convergence of the second addend is an immediate consequence of the convergence $\chi_{\omega_n} \to \chi_{\omega_\star}$ in $L^2(\Omega)$. Finally, since ω_n is a minimizing sequence for (P), we obtain

$$J(\omega_\star) = \min_{\omega \in \mathcal{O}} J(\omega),$$

which shows that $\omega_\star$ is an optimal solution of (P). ∎

To the best of author's knowledge, there are no theoretical and numerical study of the shape optimization subject to $\boldsymbol{H}(\mathbf{curl})$-elliptic VI of the second kind besides the article [115]. Both the involved $\boldsymbol{H}(\mathbf{curl})$-structure and the nonsmooth variational inequality character make the corresponding analysis truly challenging. We refer to [164, 165, 178, 179] for the optimal control of static Maxwell equations. Quite recently, the optimal control of hyperbolic Maxwell variational inequalities arising in HTS was investigated in [181]. While (P) admits an optimal solution (Theorem 6.7), the differentiability of the dual variable mapping associated with (EVI_ω) cannot be guaranteed. This property is however indispensable for our shape sensitivity analysis. Therefore, we propose to approximate (P) by replacing (EVI_ω) through its penalized dual formulation (6.7), for which the corresponding dual variable mapping is Gâteaux-differentiable (Lemma 6.8). This allows us to prove our main theoretical result (Theorem 6.13) on the distributed shape derivative of the cost functional through rigorous shape calculus on the basis of the averaged adjoint method. Importantly, the established shape derivative is uniformly stable with respect to the penalization parameter (Theorem 6.14), and strong convergence of the penalized approach can be guaranteed (Theorem 6.16). In addition, the Newton method is applicable to the penalized dual formulation (6.7). Thus, efficient numerical optimal shapes can be realized by means of a level set algorithm along with the developed shape derivative and a symmetrization strategy. All these theoretical and numerical evidences indicate the favourable performance of our approach to deal with shape optimization problems subject to a VI of the second kind.

Theoretical results on optimal design problems were obtained in [14, 60, 61, 74, 84, 121, 132, 155], but there are few early references for VI-constrained numerical shape optimization (see [76, 106, 130, 154]). Recent publications include [91] regarding a solution algorithm in the infinite dimensional setting for shape optimization problems governed by VIs of the first kind and [75] concerning a shape optimization method based on a regularized variant of VI of the first kind.

6.3 ▪ Penalized Shape Optimization Approach

As pointed out earlier, our shape sensitivity analysis requires the differentiability of the dual variable mapping $\boldsymbol{E} \mapsto \boldsymbol{\lambda}$ in $\boldsymbol{L}^2(\Omega)$, which cannot be guaranteed in general. To cope with this regularity issue, we approximate (P) by

$$\min_{\omega\in\mathcal{O}} J_\gamma(\omega) := \frac{1}{2}\int_B \kappa|\boldsymbol{E}^\gamma(\omega) - \boldsymbol{E}_d|^2\,dx + \int_\omega dx, \tag{P_γ}$$

where $\boldsymbol{E}^\gamma := \boldsymbol{E}^\gamma(\omega) \in \boldsymbol{H}_0(\mathbf{curl})$ is specified by the penalized dual formulation of (6.3):

$$\begin{cases} a(\boldsymbol{E}^\gamma, \boldsymbol{v}) + \displaystyle\int_\omega \boldsymbol{\lambda}^\gamma \cdot \boldsymbol{v}\,dx = \int_\Omega \boldsymbol{f}\cdot\boldsymbol{v}\,dx \quad \forall \boldsymbol{v} \in \boldsymbol{H}_0(\mathbf{curl}) \\ \boldsymbol{\lambda}^\gamma(x) = \dfrac{j_c\gamma \boldsymbol{E}^\gamma(x)}{\max_\gamma\{1, \gamma|\boldsymbol{E}^\gamma(x)|\}} \text{ for a.e. } x \in \omega. \end{cases} \tag{6.7}$$

In this context, $\max_\gamma\colon \mathbb{R}\to\mathbb{R}$ denotes the Moreau–Yosida type regularization (cf. [55]) of the $\max$-function given by

$$\max_\gamma\{1, x\} := \begin{cases} x & \text{if } x - 1 \geq \dfrac{1}{2\gamma}, \\ 1 + \dfrac{\gamma}{2}\left(x - 1 + \dfrac{1}{2\gamma}\right)^2 & \text{if } |x-1| \leq \dfrac{1}{2\gamma}, \\ 1 & \text{if } x - 1 \leq -\dfrac{1}{2\gamma}. \end{cases} \tag{6.8}$$

Let us emphasize that (6.7) follows by employing (6.8) to the Moreau–Yosida regularized version of (3.16) of (EVI_ω). The additional penalization is necessary as the dual variable mapping for (3.16) is *not* Gâteaux-differentiable.

The following lemma summarizes the Gâteaux-differentiability result for the dual variable mapping associated with (6.7):

Lemma 6.8 (Theorem 4.1 in [55]). *Let $\gamma > 0$ and Assumption 6.5 hold. Then,*

$$\boldsymbol{\Lambda}_\gamma \colon \boldsymbol{L}^2(\Omega) \to \boldsymbol{L}^2(\Omega), \quad \boldsymbol{\Lambda}_\gamma(\boldsymbol{e}) \coloneqq \frac{j_c \gamma \boldsymbol{e}}{\max_\gamma\{1, \gamma|\boldsymbol{e}|\}} \tag{6.9}$$

is Gâteaux-differentiable with the Gâteaux-derivative

$$\begin{aligned} \boldsymbol{\Lambda}'_\gamma(\boldsymbol{e})\boldsymbol{w} = {} & \frac{j_c \gamma \boldsymbol{w}}{\max_\gamma\{1, \gamma|\boldsymbol{e}|\}} \\ & - \gamma\left(\chi_{\mathcal{A}_\gamma(\boldsymbol{e})} + \gamma\left(\gamma|\boldsymbol{e}| - 1 + \frac{1}{2\gamma}\right)\chi_{\mathcal{S}_\gamma(\boldsymbol{e})}\right)\frac{(\boldsymbol{e}\cdot\boldsymbol{w})\boldsymbol{\Lambda}_\gamma(\boldsymbol{e})}{\max_\gamma\{1, \gamma|\boldsymbol{e}|\}|\boldsymbol{e}|} \quad \forall \boldsymbol{e}, \boldsymbol{w} \in \boldsymbol{L}^2(\Omega), \end{aligned} \tag{6.10}$$

where $\chi_{\mathcal{A}_\gamma(\boldsymbol{e})}$ and $\chi_{\mathcal{S}_\gamma(\boldsymbol{e})}$ stand for the characteristic functions of the disjoint sets

$$\mathcal{A}_\gamma(\boldsymbol{e}) = \{x \in \Omega \,:\, \gamma|\boldsymbol{e}(x)| \geq 1 + 1/2\gamma\} \quad \textit{and} \quad \mathcal{S}_\gamma(\boldsymbol{e}) = \{x \in \Omega \,:\, |\gamma|\boldsymbol{e}(x)| - 1| < 1/2\gamma\},$$

respectively. Furthermore, $\boldsymbol{\Lambda}_\gamma$ is Lipschitz continuous and monotone, i.e.,

$$(\boldsymbol{\Lambda}_\gamma(\boldsymbol{w}_1) - \boldsymbol{\Lambda}_\gamma(\boldsymbol{w}_2), \boldsymbol{w}_1 - \boldsymbol{w}_2)_{\boldsymbol{L}^2(\Omega)} \geq 0 \quad \forall \boldsymbol{w}_1, \boldsymbol{w}_2 \in \boldsymbol{L}^2(\Omega). \tag{6.11}$$

In addition to Lemma 6.8, it is easy to see that the following estimate holds by definition of $\mathcal{S}_\gamma(\boldsymbol{e})$ for every $\boldsymbol{e} \in \boldsymbol{L}^2(\Omega)$:

$$\gamma\left(\gamma|\boldsymbol{e}| - 1 + \frac{1}{2\gamma}\right) \leq 1 \quad \text{a.e. in } \mathcal{S}_\gamma(\boldsymbol{e}). \tag{6.12}$$

For convenience we define the matrix-valued function $\boldsymbol{\psi}^\gamma : \boldsymbol{L}^2(\Omega) \to L^2(\Omega, \mathbb{R}^{3\times 3})$ by

$$\boldsymbol{\psi}^\gamma(\boldsymbol{e}) \coloneqq \frac{j_c \gamma \boldsymbol{I}_3}{\max_\gamma\{1, \gamma|\boldsymbol{e}|\}} - \gamma\left(\chi_{\mathcal{A}_\gamma(\boldsymbol{e})} + \gamma\left(\gamma|\boldsymbol{e}| - 1 + \frac{1}{2\gamma}\right)\chi_{\mathcal{S}_\gamma(\boldsymbol{e})}\right)\frac{\boldsymbol{e}\otimes\boldsymbol{\Lambda}_\gamma(\boldsymbol{e})}{\max_\gamma\{1, \gamma|\boldsymbol{e}|\}|\boldsymbol{e}|}, \tag{6.13}$$

where $\boldsymbol{I}_3$ denotes the identity mapping in $\mathbb{R}^3$. By multiplying (6.10) with $\boldsymbol{v} \in \boldsymbol{L}^2(\Omega)$ and using $(\boldsymbol{e}\cdot\boldsymbol{w})(\boldsymbol{\Lambda}_\gamma(\boldsymbol{e})\cdot\boldsymbol{v}) = \big(\boldsymbol{e}\otimes\boldsymbol{\Lambda}_\gamma(\boldsymbol{e})\big)\boldsymbol{v}\cdot\boldsymbol{w}$, for all $\boldsymbol{e}, \boldsymbol{v}, \boldsymbol{w} \in \mathbb{R}^3$, we obtain

$$\boldsymbol{\Lambda}'_\gamma(\boldsymbol{e})\boldsymbol{w}\cdot\boldsymbol{v} = \boldsymbol{\psi}^\gamma(\boldsymbol{e})\boldsymbol{v}\cdot\boldsymbol{w} \quad \forall \boldsymbol{e}, \boldsymbol{w}, \boldsymbol{v} \in \boldsymbol{L}^2(\Omega). \tag{6.14}$$

With Lemma 6.8 at hand, the well-posedness of (6.7) follows by the theory of monotone operators [148, p. 40]. Moreover, (6.8) implies for every $\boldsymbol{e} \in \boldsymbol{L}^2(\Omega)$ that

$$\max_\gamma\{1, \gamma|\boldsymbol{e}|\} \geq \gamma|\boldsymbol{e}| \text{ a.e. in } \Omega. \tag{6.15}$$

Applying this estimate to (6.9) yields that

$$\|\boldsymbol{\Lambda}_\gamma(\boldsymbol{e})\|_{\boldsymbol{L}^\infty(\Omega)} \leq j_c \quad \forall \boldsymbol{e} \in \boldsymbol{L}^2(\Omega). \tag{6.16}$$

Obviously, (6.8) yields for every $\boldsymbol{e} \in \boldsymbol{L}^2(\Omega)$ that $\max_\gamma\{1, \gamma|\boldsymbol{e}|\} \geq 1$ almost everywhere in Ω. Hence, we obtain the following estimate for all $\boldsymbol{e}, \boldsymbol{v}, \boldsymbol{w} \in \boldsymbol{L}^2(\Omega)$

$$\begin{aligned} \int_\Omega |\boldsymbol{\psi}^\gamma(\boldsymbol{e})\boldsymbol{v}\cdot\boldsymbol{w}|\,dx & \overbrace{\leq}^{(6.12)} \int_\Omega \frac{j_c\gamma|\boldsymbol{v}\cdot\boldsymbol{w}|}{\max_\gamma\{1,\gamma|\boldsymbol{e}|\}}\,dx + \gamma\int_\Omega \frac{\big|\big(\boldsymbol{e}\otimes\boldsymbol{\Lambda}_\gamma(\boldsymbol{e})\big)\boldsymbol{v}\cdot\boldsymbol{w}\big|}{\max_\gamma\{1,\gamma|\boldsymbol{e}|\}|\boldsymbol{e}|}\,dx \\ & \overbrace{\leq}^{(6.16)} 2j_c\gamma\|\boldsymbol{v}\|_{\boldsymbol{L}^2(\Omega)}\|\boldsymbol{w}\|_{\boldsymbol{L}^2(\Omega)}. \end{aligned} \tag{6.17}$$

The next result states the existence of an optimal solution to (P_γ).

Theorem 6.9. *Under Assumption* 6.5, (P_γ) *admits an optimal shape* $\omega_\star^\gamma \in \mathcal{O}$ *for every* $\gamma > 0$.

Proof. Let $\{\omega_n^\gamma\}_{n\in\mathbb{N}} \subset \mathcal{O}$ be a minimizing sequence for (P_γ) with the corresponding states $\boldsymbol{E}_n^\gamma \in \boldsymbol{H}_0(\mathbf{curl})$ solving (6.7) for $\omega = \omega_n^\gamma$ and $\boldsymbol{\lambda}_n^\gamma := \boldsymbol{\Lambda}(\boldsymbol{E}_n^\gamma)$. Thanks to Theorem 6.3, there exists a subsequence of $\{\omega_n^\gamma\}_{n\in\mathbb{N}}$ (with a slight abuse of notation we use the same index for the subsequence) and $\omega_\star^\gamma \subset \mathcal{O}$ such that $\omega_n^\gamma \to \omega_\star^\gamma$ as $n \to \infty$ in the sense of characteristic functions.

We denote the solution to (6.7) for $\omega = \omega_\star^\gamma$ by $\boldsymbol{E}_\star^\gamma \in \boldsymbol{H}_0(\mathbf{curl})$ and $\boldsymbol{\lambda}_\star^\gamma := \boldsymbol{\Lambda}_\gamma(\boldsymbol{E}_\star^\gamma)$. Now, subtracting (6.7) for $\boldsymbol{E}_n^\gamma$ from (6.7) for $\boldsymbol{E}_\star^\gamma$ and testing the resulting equation with $\boldsymbol{v} = \boldsymbol{E}_\star^\gamma - \boldsymbol{E}_n^\gamma$ yields

$$
\begin{aligned}
a(\boldsymbol{E}_\star^\gamma - \boldsymbol{E}_n^\gamma, \boldsymbol{E}_\star^\gamma - \boldsymbol{E}_n^\gamma) \;&=\; \int_\Omega (\chi_{\omega_\star^\gamma}\boldsymbol{\lambda}_\star^\gamma - \chi_{\omega_n^\gamma}\boldsymbol{\lambda}_n^\gamma)\cdot(\boldsymbol{E}_n^\gamma - \boldsymbol{E}_\star^\gamma)\,dx \\
&= \int_\Omega (\chi_{\omega_\star^\gamma} - \chi_{\omega_n^\gamma})\boldsymbol{\lambda}_n^\gamma\cdot(\boldsymbol{E}_n^\gamma - \boldsymbol{E}_\star^\gamma)\,dx - \underbrace{\int_\Omega \chi_{\omega_\star^\gamma}(\boldsymbol{\lambda}_\star^\gamma - \boldsymbol{\lambda}_n^\gamma)\cdot(\boldsymbol{E}_\star^\gamma - \boldsymbol{E}_n^\gamma)\,dx}_{=(\boldsymbol{\Lambda}_\gamma(\chi_{\omega_\star^\gamma}\boldsymbol{E}_n^\gamma)-\boldsymbol{\Lambda}_\gamma(\chi_{\omega_\star^\gamma}\boldsymbol{E}_\star^\gamma),\chi_{\omega_\star^\gamma}\boldsymbol{E}_n^\gamma-\chi_{\omega_\star^\gamma}\boldsymbol{E}_\star^\gamma)_{\boldsymbol{L}^2(\Omega)}} \\
&\underbrace{\leq}_{(6.11)} \int_\Omega (\chi_{\omega_\star^\gamma} - \chi_{\omega_n^\gamma})\boldsymbol{\lambda}_n^\gamma\cdot(\boldsymbol{E}_n^\gamma - \boldsymbol{E}_\star^\gamma)\,dx.
\end{aligned}
\tag{6.18}
$$

Thus, (6.18) and (A6.2) of Assumption 6.5 yield

$$
\begin{aligned}
\min\{\underline{\nu},\underline{\epsilon}\}\|\boldsymbol{E}_\star^\gamma - \boldsymbol{E}_n^\gamma\|_{\boldsymbol{H}(\mathbf{curl})}^2 &\leq \|\chi_{\omega_\star^\gamma} - \chi_{\omega_n^\gamma}\|_{L^2(\Omega)}\|\boldsymbol{\lambda}_n^\gamma\|_{\boldsymbol{L}^\infty(\Omega)}\|\boldsymbol{E}_\star^\gamma - \boldsymbol{E}_n^\gamma\|_{\boldsymbol{H}(\mathbf{curl})} \\
&\overset{(6.15)}{\Rightarrow} \quad \|\boldsymbol{E}_\star^\gamma - \boldsymbol{E}_n^\gamma\|_{\boldsymbol{H}(\mathbf{curl})} \leq \frac{j_c}{\min\{\underline{\nu},\underline{\epsilon}\}}\|\chi_{\omega_\star^\gamma} - \chi_{\omega_n^\gamma}\|_{L^2(\Omega)}.
\end{aligned}
\tag{6.19}
$$

This implies $\boldsymbol{E}_n^\gamma \to \boldsymbol{E}_\star^\gamma$ in $\boldsymbol{H}_0(\mathbf{curl})$ since ω_n^γ converges to $\omega_\star^\gamma$ in the sense of characteristic functions as $n \to \infty$. Hence, we obtain

$$
J_\gamma(\omega_n^\gamma) = \frac{1}{2}\int_B \kappa|\boldsymbol{E}_n^\gamma - \boldsymbol{E}_d|^2\,dx + \int_{\omega_n^\gamma} dx \to \frac{1}{2}\int_B \kappa|\boldsymbol{E}_\star^\gamma - \boldsymbol{E}_d|^2\,dx + \int_{\omega_\star^\gamma} dx = J_\gamma(\omega_\star^\gamma).
$$

Finally, the assertion follows since ω_n^γ is a minimizing sequence for (P_γ). ∎

6.4 ▪ Shape Sensitivity Analysis

This section is devoted to the sensitivity analysis of the shape functional $J_\gamma(\omega)$ in (P_γ) for $\gamma > 0$ fixed. We compute the shape derivative using the averaged adjoint method (see [114, 160]).

6.4.1 ▪ Averaged Adjoint Method

We begin by introducing the Lagrangian $\mathcal{L} : \mathcal{O} \times \boldsymbol{H}_0(\mathbf{curl}) \times \boldsymbol{H}_0(\mathbf{curl}) \to \mathbb{R}$ associated with (P_γ) as follows:

$$
\mathcal{L}(\omega, \boldsymbol{e}, \boldsymbol{v}) := \frac{1}{2}\int_B \kappa|\boldsymbol{e} - \boldsymbol{E}_d|^2\,dx + \int_\omega dx + a(\boldsymbol{e}, \boldsymbol{v}) + \int_\omega \boldsymbol{\Lambda}_\gamma(\boldsymbol{e})\cdot\boldsymbol{v}\,dx - \int_\Omega \boldsymbol{f}\cdot\boldsymbol{v}\,dx,
\tag{6.20}
$$

where $\boldsymbol{\Lambda}_\gamma$ is the penalized dual variable mapping given in (6.9). In view of (6.20), we have for $\omega \in \mathcal{O}$ and $t \in [0, \tau]$ that

$$
J_\gamma(\omega_t) = \mathcal{L}(\omega_t, \boldsymbol{E}_t^\gamma, \boldsymbol{v}) \quad \forall \boldsymbol{v} \in \boldsymbol{H}_0(\mathbf{curl}).
\tag{6.21}
$$

Moreover, as $\mathcal{L}$ is linear in $\boldsymbol{v}$, the problem of finding $\boldsymbol{e} \in \boldsymbol{H}_0(\mathbf{curl})$ such that

$$\partial_{\boldsymbol{v}}\mathcal{L}(\omega_t, \boldsymbol{e}, \boldsymbol{v}; \hat{\boldsymbol{v}}) = a(\boldsymbol{e}, \hat{\boldsymbol{v}}) + \int_{\omega_t} \boldsymbol{\Lambda}_\gamma(\boldsymbol{e}) \cdot \hat{\boldsymbol{v}}\, dx - \int_\Omega \boldsymbol{f} \cdot \hat{\boldsymbol{v}}\, dx = 0 \quad \forall \hat{\boldsymbol{v}} \in \boldsymbol{H}_0(\mathbf{curl})$$

is equivalent to the penalized dual formulation (6.7) with $\omega = \omega_t$ and admits the same unique solution $\boldsymbol{E}_t^\gamma \in \boldsymbol{H}_0(\mathbf{curl})$. In order to pull back the integrals over ω_t to the reference domain ω, one uses the change of variables $x \mapsto \boldsymbol{T}_t(x)$. Furthermore, to avoid the appearance of the composed functions $\boldsymbol{e} \circ \boldsymbol{T}_t$ and $\boldsymbol{v} \circ \boldsymbol{T}_t$ due to this change of variables, we reparameterize the Lagrangian using the following covariant transformation, which is known to be a bijection for $\boldsymbol{H}_0(\mathbf{curl})$ (cf. (2.9))

$$\Psi_t \colon \boldsymbol{H}_0(\mathbf{curl}) \to \boldsymbol{H}_0(\mathbf{curl}), \qquad \Psi_t(\boldsymbol{e}) \coloneqq (D\boldsymbol{T}_t^{-\mathsf{T}}\boldsymbol{e}) \circ \boldsymbol{T}_t^{-1}. \tag{6.22}$$

Here $D\boldsymbol{T}_t \colon \mathbb{R}^3 \to \mathbb{R}^{3\times 3}$ stands for the Jacobian matrix function of $\boldsymbol{T}_t$ and we denote $D\boldsymbol{T}_t^{-\mathsf{T}} \coloneqq \big(D\boldsymbol{T}_t^{-1}\big)^{\mathsf{T}}$. It satisfies the important identity (see Remark 2.5, cf. [101, Lemma 11])

$$\big(\mathbf{curl}\, \Psi_t(\boldsymbol{e})\big) \circ \boldsymbol{T}_t = \xi(t)^{-1} D\boldsymbol{T}_t\, \mathbf{curl}\, \boldsymbol{e}, \tag{6.23}$$

with $\xi(t) \coloneqq \det D\boldsymbol{T}_t$. In this paper we always assume $\tau > 0$ small enough such that $\xi(t) > 0$ for every $t \in [0, \tau]$. That is, the transformation $\boldsymbol{T}_t$ preserves orientation. In view of the above discussion, we introduce the *shape-Lagrangian* $G : [0,\tau] \times \boldsymbol{H}_0(\mathbf{curl}) \times \boldsymbol{H}_0(\mathbf{curl}) \to \mathbb{R}$ as

$$\begin{aligned} G(t, \boldsymbol{e}, \boldsymbol{v}) \coloneqq \mathcal{L}(\omega_t, \Psi_t(\boldsymbol{e}), \Psi_t(\boldsymbol{v})) = \frac{1}{2}\int_B \kappa |\Psi_t(\boldsymbol{e}) - \boldsymbol{E}_d|^2\, dx + \int_{\omega_t} dx \\ + a(\Psi_t(\boldsymbol{e}), \Psi_t(\boldsymbol{v})) + \int_{\omega_t} \boldsymbol{\Lambda}_\gamma(\Psi_t(\boldsymbol{e})) \cdot \Psi_t(\boldsymbol{v})\, dx - \int_\Omega \boldsymbol{f} \cdot \Psi_t(\boldsymbol{v})\, dx. \end{aligned} \tag{6.24}$$

The change of variables $x \mapsto \boldsymbol{T}_t(x)$ inside the integrals (6.22) and (6.23) yields

$$\begin{aligned} G(t, \boldsymbol{e}, \boldsymbol{v}) =& \frac{1}{2}\int_B \kappa \circ \boldsymbol{T}_t |D\boldsymbol{T}_t^{-\mathsf{T}}\boldsymbol{e} - \boldsymbol{E}_d \circ \boldsymbol{T}_t|^2 \xi(t)\, dx + \int_\omega \xi(t)\, dx + \int_\Omega \mathbb{M}_1(t)\, \mathbf{curl}\, \boldsymbol{e} \cdot \mathbf{curl}\, \boldsymbol{v} \\ &+ \mathbb{M}_2(t)\boldsymbol{e} \cdot \boldsymbol{v}\, dx + \int_\omega \mathbb{M}_3(t, \boldsymbol{e}) \cdot \boldsymbol{v}\, dx - \int_\Omega (\boldsymbol{f} \circ \boldsymbol{T}_t) \cdot (D\boldsymbol{T}_t^{-\mathsf{T}}\boldsymbol{v})\xi(t)\, dx, \end{aligned} \tag{6.25}$$

with the notations

$$\begin{aligned} \mathbb{M}_1(t) &\coloneqq \xi(t)^{-1} D\boldsymbol{T}_t^{\mathsf{T}} (\nu \circ \boldsymbol{T}_t) D\boldsymbol{T}_t, \\ \mathbb{M}_2(t) &\coloneqq \xi(t) D\boldsymbol{T}_t^{-1} (\varepsilon \circ \boldsymbol{T}_t) D\boldsymbol{T}_t^{-\mathsf{T}}, \\ \mathbb{M}_3(t, \boldsymbol{e}) &\coloneqq \xi(t) D\boldsymbol{T}_t^{-1} \boldsymbol{\Lambda}_\gamma(D\boldsymbol{T}_t^{-\mathsf{T}}\boldsymbol{e}). \end{aligned}$$

Note that the problem of finding $\boldsymbol{e}_t \in \boldsymbol{H}_0(\mathbf{curl})$ such that $\partial_{\boldsymbol{v}} G(t, \boldsymbol{e}_t, 0; \hat{\boldsymbol{v}}) = 0$ for all $\hat{\boldsymbol{v}} \in \boldsymbol{H}_0(\mathbf{curl})$ is equivalent to (6.7) with $\omega = \omega_t$ after applying the change of variables $x \mapsto \boldsymbol{T}_t(x)$. Hence, it has the same unique solution $\boldsymbol{E}_t^\gamma \in \boldsymbol{H}_0(\mathbf{curl})$.

Next, the shape derivative of J_γ is obtained as the partial derivative with respect to t of the shape-Lagrangian G given by (6.25). For the convenience of the reader, we recall the main result of the averaged adjoint method, adapted to our case. A proof can be found in [114, Theorem 2.1] (cf. [160]).

Theorem 6.10 (Averaged adjoint method). *Let $\gamma > 0$. Moreover, we assume that there exists $\tau \in (0, 1]$ such that for every $(t, \boldsymbol{v}) \in [0, \tau] \times \boldsymbol{H}_0(\mathbf{curl})$*

(H1) *the mapping $[0, 1] \ni s \mapsto G(t, s\boldsymbol{E}_t^\gamma + (1-s)\boldsymbol{E}_0^\gamma, \boldsymbol{v})$ is absolutely continuous;*

(H2) *the mapping $[0, 1] \ni s \mapsto \partial_{\boldsymbol{e}} G(t, s\boldsymbol{E}_t^\gamma + (1-s)\boldsymbol{E}_0^\gamma, \boldsymbol{v}; \hat{\boldsymbol{e}})$ belongs to $L^1(0, 1)$ for every $\hat{\boldsymbol{e}} \in \boldsymbol{H}_0(\mathbf{curl})$;*

(H3) *there exists a unique* $\boldsymbol{P}_t^\gamma \in \boldsymbol{H}_0(\mathbf{curl})$ *that solves the averaged adjoint equation*

$$\int_0^1 \partial_{\boldsymbol{e}} G(t, s\boldsymbol{E}_t^\gamma + (1-s)\boldsymbol{E}_0^\gamma, \boldsymbol{P}_t^\gamma; \hat{\boldsymbol{e}})\, ds = 0 \quad \forall \hat{\boldsymbol{e}} \in \boldsymbol{H}_0(\mathbf{curl}); \tag{6.26}$$

(H4) *the family* $\{\boldsymbol{P}_t^\gamma\}_{t\in[0,\tau]}$ *satisfies*

$$\lim_{t\searrow 0} \frac{G(t, \boldsymbol{E}_0^\gamma, \boldsymbol{P}_t^\gamma) - G(0, \boldsymbol{E}_0^\gamma, \boldsymbol{P}_t^\gamma)}{t} = \partial_t G(0, \boldsymbol{E}_0^\gamma, \boldsymbol{P}_0^\gamma). \tag{6.27}$$

Then, J_γ *is shape-differentiable in the sense of Definition* 6.4 *and it holds that*

$$dJ_\gamma(\omega)(\boldsymbol{\theta}) = \frac{d}{dt} J_\gamma(\omega_t)|_{t=0} = \partial_t G(0, \boldsymbol{E}_0^\gamma, \boldsymbol{P}_0^\gamma),$$

where $\boldsymbol{P}_0^\gamma$ *is the so-called adjoint state solution of* (6.26) *with* $t = 0$.

We verify that (H1)–(H4) are satisfied so that we may apply Theorem 6.10.

Lemma 6.11. *Let Assumption* 6.5 *be satisfied. Then,* (H1) *and* (H2) *hold for every* $(t, \boldsymbol{v}) \in [0,1] \times \boldsymbol{H}_0(\mathbf{curl})$.

Proof. First of all, (H1) is a direct consequence of (6.25) and Lemma 6.8. Before we proceed to prove (H2), let us introduce the notation $\mathcal{E}(s) := s\boldsymbol{E}_t^\gamma + (1-s)\boldsymbol{E}_0^\gamma$. Now, fix $\tau \in (0,1]$ and $(t, \boldsymbol{v}) \in [0,\tau] \times \boldsymbol{H}_0(\mathbf{curl})$. Thanks to the Gâteaux-differentiability of $\boldsymbol{\Lambda}_\gamma$ (Lemma 6.8) and using (6.25), we may compute

$$\begin{aligned} \partial_{\boldsymbol{e}} G(t, \mathcal{E}(s), \boldsymbol{v}; \hat{\boldsymbol{e}}) &= \int_B \kappa \circ \boldsymbol{T}_t \big(D\boldsymbol{T}_t^{-\mathsf{T}} \hat{\boldsymbol{e}} \cdot (D\boldsymbol{T}_t^{-\mathsf{T}} \mathcal{E}(s) - \boldsymbol{E}_d \circ \boldsymbol{T}_t) \big) \xi(t)\, dx \\ &\quad + \int_\Omega \mathbb{M}_1(t)\, \mathbf{curl}\, \hat{\boldsymbol{e}} \cdot \mathbf{curl}\, \boldsymbol{v} + \mathbb{M}_2(t) \hat{\boldsymbol{e}} \cdot \boldsymbol{v}\, dx + \int_\omega \partial_{\boldsymbol{e}} \mathbb{M}_3\big(t, \mathcal{E}(s)\big) \hat{\boldsymbol{e}} \cdot \boldsymbol{v}\, dx \end{aligned} \tag{6.28}$$

for every $\hat{\boldsymbol{e}} \in \boldsymbol{H}_0(\mathbf{curl})$, where

$$\begin{aligned} \int_\omega \partial_{\boldsymbol{e}} \mathbb{M}_3\big(t, \mathcal{E}(s)\big) \hat{\boldsymbol{e}} \cdot \boldsymbol{v}\, dx &= \int_\omega \xi(t) D\boldsymbol{T}_t^{-1} \boldsymbol{\Lambda}_\gamma' \big(D\boldsymbol{T}_t^{-\mathsf{T}} \mathcal{E}(s) \big) (D\boldsymbol{T}_t^{-\mathsf{T}} \hat{\boldsymbol{e}}) \cdot \boldsymbol{v}\, dx \\ &\overset{(6.13)\&(6.14)}{=} \int_\omega \xi(t) D\boldsymbol{T}_t^{-2} \boldsymbol{\psi}^\gamma \big(D\boldsymbol{T}_t^{-\mathsf{T}} \mathcal{E}(s) \big) \boldsymbol{v} \cdot \hat{\boldsymbol{e}}\, dx, \end{aligned} \tag{6.29}$$

Moreover, the following asymptotic expansions hold (see [155, Lemma 2.31]):

$$\begin{aligned} \xi(t) &= 1 + t \operatorname{div}(\boldsymbol{\theta}) + o(t), \\ D\boldsymbol{T}_t &= \boldsymbol{I}_3 + tD\boldsymbol{\theta} + o(t), \\ D\boldsymbol{T}_t^{-1} &= \boldsymbol{I}_3 - tD\boldsymbol{\theta} + o(t) \end{aligned} \tag{6.30}$$

such that $o(t)/t \to 0$ as $t \to 0$ with respect to $\|\cdot\|_{\mathcal{C}(\Omega)}$ and $\|\cdot\|_{\mathcal{C}(\Omega,\mathbb{R}^{3\times 3})}$, respectively. Hence, (6.30) implies that there exists a constant $C > 0$ only dependent on $\boldsymbol{\theta}$ such that

$$\|\xi(t)\|_{L^\infty(\Omega)} + \|D\boldsymbol{T}_t\|_{L^\infty(\Omega,\mathbb{R}^{3\times 3})} + \|D\boldsymbol{T}_t^{-1}\|_{L^\infty(\Omega,\mathbb{R}^{3\times 3})} \leq 1 + C\tau. \tag{6.31}$$

Applying (6.31) in (6.29) leads to

$$\begin{aligned} \left| \int_\omega \partial_{\boldsymbol{e}} \mathbb{M}_3(t, \mathcal{E}(s)) \hat{\boldsymbol{e}} \cdot \boldsymbol{v}\, dx \right| &\leq (1 + C\tau)^3 \int_\omega \left| \boldsymbol{\psi}^\gamma \big(D\boldsymbol{T}_t^{-\mathsf{T}} \mathcal{E}(s) \big) \boldsymbol{v} \cdot \hat{\boldsymbol{e}} \right| dx \\ &\overset{(6.17)}{\leq} 2 j_c \gamma (1 + C\tau)^3 \|\hat{\boldsymbol{e}}\|_{\boldsymbol{L}^2(\Omega)} \|\boldsymbol{v}\|_{\boldsymbol{L}^2(\Omega)} \quad \forall s \in (0,1). \end{aligned} \tag{6.32}$$

Thus, the mapping $s \mapsto \int_\omega \partial_{\boldsymbol{e}} \mathbb{M}_3(t, \mathcal{E}(s))\hat{\boldsymbol{e}} \cdot \boldsymbol{v}\, dx$ belongs to $L^\infty(0,1) \subset L^1(0,1)$. In a similar way, since $t \in [0,\tau]$ and $\gamma > 0$ are fixed, (6.31) and (A6.1) of Assumption 6.5 yield

$$
\begin{aligned}
(6.33) \qquad & \int_B \big|\kappa \circ \boldsymbol{T}_t\big(D\boldsymbol{T}_t^{-\mathsf{T}}\hat{\boldsymbol{e}} \cdot D\boldsymbol{T}_t^{-\mathsf{T}}\mathcal{E}(s)\big)\xi(t)\big|\, dx \\
&\qquad \le (1+C\tau)^3 \|\kappa\|_{\mathcal{C}(\Omega)} \|\hat{\boldsymbol{e}}\|_{\boldsymbol{L}^2(\Omega)} \|\mathcal{E}(s)\|_{\boldsymbol{L}^2(\Omega)} \\
&\qquad \le (1+C\tau)^3 \|\kappa\|_{\mathcal{C}(\Omega)} \|\hat{\boldsymbol{e}}\|_{\boldsymbol{L}^2(\Omega)} \big(\|\boldsymbol{E}_0^\gamma\|_{\boldsymbol{L}^2(\Omega)} + s\|\boldsymbol{E}_t^\gamma - \boldsymbol{E}_0^\gamma\|_{\boldsymbol{L}^2(\Omega)}\big) \\
&\qquad \le (1+s)(1+C\tau)^3 \|\kappa\|_{\mathcal{C}(\Omega)} \|\hat{\boldsymbol{e}}\|_{\boldsymbol{L}^2(\Omega)} \big(\|\boldsymbol{E}_t^\gamma - \boldsymbol{E}_0^\gamma\|_{\boldsymbol{L}^2(\Omega)} + \|\boldsymbol{E}_0^\gamma\|_{\boldsymbol{L}^2(\Omega)}\big).
\end{aligned}
$$

As the remaining terms in (6.28) are independent of s, (6.32) and (6.33) imply that the mapping $s \mapsto \partial_{\boldsymbol{e}} G(t, \mathcal{E}(s), \boldsymbol{v}; \hat{\boldsymbol{e}})$ belongs to $L^1(0,1)$ for all $\hat{\boldsymbol{e}} \in \boldsymbol{H}_0(\mathbf{curl})$ and $(t, \boldsymbol{v}) \in [0,\tau] \times \boldsymbol{H}_0(\mathbf{curl})$. Thus, the proof is complete. ∎

Lemma 6.12. *Let Assumption* 6.5 *hold. Then, there exists* $\tau \in (0,1]$ *such that* (H3) *is satisfied for every* $t \in [0,\tau]$. *Moreover,* (H4) *holds as well.*

Proof. Fix some arbitrary $\tau > 0$ and denote $\mathcal{E}(s) := s\boldsymbol{E}_t^\gamma + (1-s)\boldsymbol{E}_0^\gamma$ for $s \in (0,1)$. Let $\tau \in (0,1]$ be arbitrarily fixed. In the following, if necessary, we shall reduce $\tau \in (0,1]$ step by step to prove our result. Let $t \in [0,\tau]$ and $\hat{\boldsymbol{e}} \in \boldsymbol{H}_0(\mathbf{curl})$. Thanks to Lemma 6.11, the left-hand side of (6.26) is well-defined, and our goal is to prove the existence of a unique $\boldsymbol{P}_t^\gamma \in \boldsymbol{H}_0(\mathbf{curl})$ satisfying (6.26). In view of (6.28), we note that (6.26) can be written as

$$
(6.34) \qquad B_t(\boldsymbol{P}_t^\gamma, \hat{\boldsymbol{e}}) = F_t(\hat{\boldsymbol{e}}) \quad \forall \hat{\boldsymbol{e}} \in \boldsymbol{H}_0(\mathbf{curl})
$$

with $B_t \colon \boldsymbol{H}_0(\mathbf{curl}) \times \boldsymbol{H}_0(\mathbf{curl}) \to \mathbb{R}$ and $F_t \colon \boldsymbol{H}_0(\mathbf{curl}) \to \mathbb{R}$ defined by

$$
\begin{aligned}
B_t(\boldsymbol{v}, \hat{\boldsymbol{e}}) &:= \int_\Omega \mathbb{M}_1(t)\mathbf{curl}\,\hat{\boldsymbol{e}} \cdot \mathbf{curl}\,\boldsymbol{v} + \mathbb{M}_2(t)\hat{\boldsymbol{e}} \cdot \boldsymbol{v}\, dx + \int_0^1 \int_\omega \partial_{\boldsymbol{e}} \mathbb{M}_3(t, \mathcal{E}(s))\hat{\boldsymbol{e}} \cdot \boldsymbol{v}\, dx\, ds, \\
F_t(\hat{\boldsymbol{e}}) &:= -\int_0^1 \int_B \kappa \circ \boldsymbol{T}_t\Big(D\boldsymbol{T}_t^{-\mathsf{T}}\hat{\boldsymbol{e}} \cdot \Big(D\boldsymbol{T}_t^{-\mathsf{T}}\mathcal{E}(s) - \boldsymbol{E}_d \circ \boldsymbol{T}_t\Big)\Big)\xi(t)\, dx\, ds.
\end{aligned}
$$

Thanks to (A6.2) and (6.31) and (6.32), B_t is a bounded bilinear form. In order to apply the Lax–Milgram lemma, we have to prove the coercivity of B_t. The asymptotic expansions (6.30) show that $\mathbb{M}_1(t)$ and $\mathbb{M}_2(t)$ are small perturbations of ν and ϵ, respectively. Thus, if necessary, we may reduce the number $\tau \in (0,1]$ such that, in view of (6.2), $\mathbb{M}_1(t)$ and $\mathbb{M}_2(t)$ are uniformly positive definite for all $t \in [0,\tau]$ with:

$$
(6.35) \qquad \int_\Omega \mathbb{M}_1(t)\,\mathbf{curl}\,\boldsymbol{v} \cdot \mathbf{curl}\,\boldsymbol{v} + \mathbb{M}_2(t)\boldsymbol{v} \cdot \boldsymbol{v}\, dx \ge C_1 \|\boldsymbol{v}\|^2_{\boldsymbol{H}(\mathbf{curl})} \quad \forall \boldsymbol{v} \in \boldsymbol{H}_0(\mathbf{curl}),
$$

for some constant $C_1 > 0$ depending only on $\boldsymbol{\theta}, \epsilon$ and ν. In order to keep the notation short, let us define $\mathcal{K}(s) := D\boldsymbol{T}_t^{-\mathsf{T}}\mathcal{E}(s) \in \boldsymbol{H}_0(\mathbf{curl})$ as well as the sets $\mathcal{A}_\gamma(s) := \mathcal{A}_\gamma(\mathcal{K}(s)) \subset \Omega$ and $\mathcal{S}_\gamma(s) := \mathcal{S}_\gamma(\mathcal{K}(s)) \subset \Omega$ for $s \in (0,1)$ (cf. Lemma 6.8). We estimate the third term in B_t which, in view of (6.13) and (6.29), corresponds to

$$
\begin{aligned}
(6.36) \qquad \int_0^1 \int_\omega \partial_e \mathbb{M}_3(t, \mathcal{E}(s))\boldsymbol{v} \cdot \boldsymbol{v}\, dx\, ds &= \int_0^1 \int_\omega \xi(t) D\boldsymbol{T}_t^{-2} \Bigg[\frac{j_c\gamma \boldsymbol{I}_3}{\max_\gamma\{1, \gamma|\mathcal{K}(s)|\}} \\
&\quad -\gamma\Bigg(\chi_{\mathcal{A}_\gamma(s)} + \gamma\Bigg(\gamma|\mathcal{K}(s)| - 1 + \frac{1}{2\gamma}\Bigg)\chi_{\mathcal{S}_\gamma(s)}\Bigg)\frac{\mathcal{K}(s) \otimes \boldsymbol{\Lambda}_\gamma(\mathcal{K}(s))}{\max_\gamma\{1, \gamma|\mathcal{K}(s)|\}|\mathcal{K}(s)|}\Bigg]\boldsymbol{v} \cdot \boldsymbol{v}\, dx\, ds.
\end{aligned}
$$

Therefore, we fix $s \in (0,1)$ and estimate the three summands in (6.36) separately. We begin with the first term and note that (6.30) implies, possibly after reducing $\tau > 0$, the existence of a constant

$C > 0$, depending only on $\boldsymbol{\theta}$, such that $\xi(t) \geq 1 - C\tau > 0$, and $D\boldsymbol{T}_t^{-2}\boldsymbol{\eta} \cdot \boldsymbol{\eta} \geq (1 - C\tau)^2 |\boldsymbol{\eta}|^2$ for all $\boldsymbol{\eta} \in \mathbb{R}^3$ and almost everywhere in Ω. Hence,

$$\int_\omega j_c \gamma \xi(t) \frac{D\boldsymbol{T}_t^{-2}\boldsymbol{v} \cdot \boldsymbol{v}}{\max_\gamma\{1, \gamma|\mathcal{K}(s)|\}}\, dx \geq (1 - C\tau)^3 \int_\omega \frac{j_c \gamma |\boldsymbol{v}|^2}{\max_\gamma\{1, \gamma|\mathcal{K}(s)|\}}\, dx. \tag{6.37}$$

Now, we proceed to estimate the integrals over the disjoint sets $\omega \cap \mathcal{A}_\gamma(s)$ and $\omega \cap \mathcal{S}_\gamma(s)$ appearing in the last two summands in (6.36). We obtain

$$\begin{aligned} &\left| \int_{\omega \cap \mathcal{A}_\gamma(s)} \gamma \xi(t) D\boldsymbol{T}_t^{-2} \frac{\mathcal{K}(s) \otimes \boldsymbol{\Lambda}_\gamma(\mathcal{K}(s))\boldsymbol{v} \cdot \boldsymbol{v}}{\max_\gamma\{1, \gamma|\mathcal{K}(s)|\}|\mathcal{K}(s)|}\, dx \right| \\ &\overbrace{\leq}^{(6.9)\&(6.16)} \|\xi(t)\|_{L^\infty(\Omega)} \|D\boldsymbol{T}_t^{-1}\|^2_{L^\infty(\Omega, \mathbb{R}^{3\times 3})} \int_{\omega \cap \mathcal{A}_\gamma(s)} \frac{j_c \gamma |\boldsymbol{v}|^2}{\max_\gamma\{1, \gamma|\mathcal{K}(s)|\}}\, dx \\ &\overbrace{\leq}^{(6.31)} (1 + C\tau)^3 \int_{\omega \cap \mathcal{A}_\gamma(s)} \frac{j_c \gamma |\boldsymbol{v}|^2}{\max_\gamma\{1, \gamma|\mathcal{K}(s)|\}}\, dx. \end{aligned} \tag{6.38}$$

For the last summand, we use the same arguments and also (6.12) to deduce

$$\begin{aligned} &\left| \int_{\omega \cap \mathcal{S}_\gamma(s)} \gamma^2 \left(\gamma|\mathcal{K}(s)| - 1 + \frac{1}{2\gamma}\right) \xi(t) D\boldsymbol{T}_t^{-2} \frac{\mathcal{K}(s) \otimes \boldsymbol{\Lambda}_\gamma(\mathcal{K}(s))\boldsymbol{v} \cdot \boldsymbol{v}}{\max_\gamma\{1, \gamma|\mathcal{K}(s)|\}\, |\mathcal{K}(s)|}\, dx \right| \\ &\qquad \leq (1 + C\tau)^3 \int_{\omega \cap \mathcal{S}_\gamma(s)} \frac{j_c \gamma |\boldsymbol{v}|^2}{\max_\gamma\{1, \gamma|\mathcal{K}(s)|\}}\, dx. \end{aligned} \tag{6.39}$$

Note that the constant $C > 0$ in (6.37)–(6.39) is the same in the three inequalities. Thus, we sum up (6.38) and (6.39) and subtract the result from (6.37) to obtain

$$\begin{aligned} \int_\omega \partial_e \mathbb{M}_3(t, \mathcal{E}(s))\boldsymbol{v} \cdot \boldsymbol{v}\, dx \geq \big(1 + 3(C\tau)^2\big) &\int_{\omega \setminus (\mathcal{A}_\gamma(s) \cup \mathcal{S}_\gamma(s))} \frac{j_c \gamma |\boldsymbol{v}|^2}{\max_\gamma\{1, \gamma|\mathcal{K}(s)|\}}\, dx \\ &- (6C\tau + 2(C\tau)^3) \int_\omega \frac{j_c \gamma |\boldsymbol{v}|^2}{\max_\gamma\{1, \gamma|\mathcal{K}(s)|\}}\, dx. \end{aligned}$$

As the first term is nonnegative and $\max_\gamma\{1, \gamma|\mathcal{K}(s)|\} \geq 1$, we conclude for (6.36)

$$\int_0^1 \int_\omega \partial_e \mathbb{M}_3(t, \mathcal{E}(s))\boldsymbol{v} \cdot \boldsymbol{v}\, dx\, ds \geq -(6C\tau + 2(C\tau)^3) j_c \gamma \|\boldsymbol{v}\|^2_{\boldsymbol{L}^2(\omega)}. \tag{6.40}$$

The coercivity of B_t follows, as (6.35) in combination with (6.40) implies

$$B_t(\boldsymbol{v}, \boldsymbol{v}) \geq \underbrace{(C_1 - 6C\tau - 2(C\tau)^3)}_{=:C_2} \|\boldsymbol{v}\|^2_{\boldsymbol{H}(\mathbf{curl})} \quad \forall \boldsymbol{v} \in \boldsymbol{H}_0(\mathbf{curl}). \tag{6.41}$$

If necessary, we further reduce $\tau \in (0, 1]$ such that $C_2 > 0$ holds true. In turn, for all $t \in [0, \tau]$, B_t is coercive with the coercivity constant $C_2 > 0$, independent of t. Ultimately, the Lax–Milgram lemma yields the existence of a unique solution $\boldsymbol{P}_t^\gamma \in \boldsymbol{H}_0(\mathbf{curl})$ of the averaged adjoint equation (6.26). Thus, (H3) holds.

We finish this proof by verifying (H4). To this aim, let $\{t_k\}_{k\in\mathbb{N}} \subset (0, \tau]$ be a null sequence. First of all, the sequence $\{\boldsymbol{E}_{t_k}^\gamma\}_{k\in\mathbb{N}} \subset \boldsymbol{H}_0(\mathbf{curl})$ of solutions to the perturbed state equations (6.7) with $\omega = \omega_{t_k}$ is bounded. This follows readily by inserting $\boldsymbol{v} = \boldsymbol{E}_{t_k}^\gamma$ into (6.7) which yields

$$\begin{aligned} &\min(\underline{\nu}, \underline{\epsilon})\|\boldsymbol{E}_{t_k}^\gamma\|^2_{\boldsymbol{H}(\mathbf{curl})} \leq a(\boldsymbol{E}_{t_k}^\gamma, \boldsymbol{E}_{t_k}^\gamma) \leq (\|\boldsymbol{f}\|_{\boldsymbol{L}^2(\Omega)} + j_c)\|\boldsymbol{E}_{t_k}^\gamma\|_{\boldsymbol{H}(\mathbf{curl})} \\ &\qquad \Rightarrow \quad \|\boldsymbol{E}_{t_k}^\gamma\|_{\boldsymbol{H}(\mathbf{curl})} \leq \min(\underline{\nu}, \underline{\epsilon})^{-1}(\|\boldsymbol{f}\|_{\boldsymbol{L}^2(\Omega)} + j_c) \quad \forall k \in \mathbb{N}. \end{aligned} \tag{6.42}$$

Hereafter, we deduce a similar estimate for $\{\boldsymbol{P}_{t_k}^\gamma\}_{k\in\mathbb{N}}$ by testing (6.34) with $\hat{\boldsymbol{e}} = \boldsymbol{P}_{t_k}^\gamma$ and using (6.41) along with (6.31):

$$
\begin{aligned}
(6.43)\quad C_2\|\boldsymbol{P}_{t_k}^\gamma\|^2_{\boldsymbol{H}_0(\mathbf{curl})} &\le B_t(\boldsymbol{P}_{t_k}^\gamma, \boldsymbol{P}_{t_k}^\gamma) = F_t(\boldsymbol{P}_{t_k}^\gamma)\\
&\le \|\kappa\|_{\mathcal{C}(\Omega)}(1+C\tau)^3(\|\boldsymbol{E}_{t_k}^\gamma\|_{\boldsymbol{L}^2(\Omega)} + \|\boldsymbol{E}_0^\gamma\|_{\boldsymbol{L}^2(\Omega)} + \|\boldsymbol{E}_d\|_{\boldsymbol{L}^2(\Omega)})\|\boldsymbol{P}_{t_k}^\gamma\|_{\boldsymbol{L}^2(\Omega)} \quad \forall k\in\mathbb{N}.
\end{aligned}
$$

Since the constant C_2 and C are independent of $k\in\mathbb{N}$, the above estimate implies the boundedness of $\{\boldsymbol{P}_{t_k}^\gamma\}_{k\in\mathbb{N}} \subset \boldsymbol{H}_0(\mathbf{curl})$. Hence, there exists a subsequence $\{t_{k_j}\}_{j\in\mathbb{N}} \subset \{t_k\}_{k\in\mathbb{N}}$ converging weakly in $\boldsymbol{H}_0(\mathbf{curl})$ to some $\boldsymbol{P}^\star \in \boldsymbol{H}_0(\mathbf{curl})$. By (6.30) and as the solution of (6.34) is unique, passing to the limit $t = t_{k_j} \to 0$ in (6.34) yields $\boldsymbol{P}^\star = \boldsymbol{P}_0^\gamma$. Since $\boldsymbol{P}_0^\gamma$ is independent of the choice of the subsequence $\{t_{k_j}\}_{j\in\mathbb{N}}$, a standard argument implies the weak convergence of the whole sequence:

$$
(6.44)\qquad \boldsymbol{P}_{t_k}^\gamma \rightharpoonup \boldsymbol{P}^\star \quad \text{weakly in } \boldsymbol{H}_0(\mathbf{curl}) \quad \text{as } k\to\infty.
$$

Let us now consider the differential quotient

$$
\begin{aligned}
(6.45)\quad \frac{G(t_k,\boldsymbol{E}_0^\gamma,\boldsymbol{P}_{t_k}^\gamma) - G(0,\boldsymbol{E}_0^\gamma,\boldsymbol{P}_{t_k}^\gamma)}{t_k} &= \int_B \frac{\mathbb{M}_0(t_k)-\mathbb{M}_0(0)}{t_k}\,dx + \int_\omega \frac{\xi(t_k)-\xi(0)}{t_k}\,dx\\
&+ \int_\Omega \frac{\mathbb{M}_1(t_k)-\mathbb{M}_1(0)}{t_k}\,\mathbf{curl}\,\boldsymbol{E}_0^\gamma\cdot\mathbf{curl}\,\boldsymbol{P}_{t_k}^\gamma + \frac{\mathbb{M}_2(t_k)-\mathbb{M}_2(0)}{t_k}\boldsymbol{E}_0^\gamma\cdot\boldsymbol{P}_{t_k}^\gamma\,dx\\
&+ \int_\omega \frac{\mathbb{M}_3(t_k,\boldsymbol{E}_0^\gamma)-\mathbb{M}_3(0,\boldsymbol{E}_0^\gamma)}{t_k}\cdot\boldsymbol{P}_{t_k}^\gamma\,dx - \int_\Omega \frac{\mathbb{M}_4(t_k)-\mathbb{M}_4(0)}{t_k}\cdot\boldsymbol{P}_{t_k}^\gamma\,dx,
\end{aligned}
$$

with $\mathbb{M}_0(t_k) := \frac{1}{2}\kappa\circ\boldsymbol{T}_{t_k}|D\boldsymbol{T}_{t_k}^{-\mathsf{T}}\boldsymbol{E}_0^\gamma - \boldsymbol{E}_d\circ\boldsymbol{T}_{t_k}|^2\xi(t_k)$ and $\mathbb{M}_4(t_k) := \xi(t_k)D\boldsymbol{T}_{t_k}^{-1}(\boldsymbol{f}\circ\boldsymbol{T}_{t_k})$. First, (6.30) yields the strong convergence

$$
(6.46)\qquad \lim_{k\to\infty}\frac{\xi(t_k)-\xi(0)}{t_k} = \operatorname{div}\boldsymbol{\theta} \quad \text{in } \mathcal{C}(\Omega).
$$

Moreover, thanks to Assumption 6.5, (6.30) and $\operatorname{supp}\boldsymbol{\theta}\subset\subset B$, we obtain the strong convergence of $\big(\mathbb{M}_i(t_k)-\mathbb{M}_i(0)\big)/t_k$, $i=0,1,2,4$, as $k\to\infty$ in $L^\infty(\Omega)$:

$$
\begin{aligned}
(6.47)\quad \lim_{k\to\infty}\frac{\mathbb{M}_0(t_k)-\mathbb{M}_0(0)}{t_k} &= \frac{1}{2}(\widetilde{\nabla\kappa}\cdot\boldsymbol{\theta} + \kappa\operatorname{div}\boldsymbol{\theta})|\boldsymbol{E}_0^\gamma-\boldsymbol{E}_d|^2\\
&\quad - \kappa(\boldsymbol{E}_0^\gamma-\boldsymbol{E}_d)\cdot(D\boldsymbol{\theta}^{\mathsf{T}}\boldsymbol{E}_0^\gamma - \widetilde{D\boldsymbol{E}_d}\boldsymbol{\theta})\\
(6.48)\quad \lim_{k\to\infty}\frac{\mathbb{M}_1(t_k)-\mathbb{M}_1(0)}{t_k} &= -(\operatorname{div}\boldsymbol{\theta})\nu + D\boldsymbol{\theta}^{\mathsf{T}}\nu + \nu D\boldsymbol{\theta} + \widetilde{D\nu}\boldsymbol{\theta},\\
(6.49)\quad \lim_{k\to\infty}\frac{\mathbb{M}_2(t_k)-\mathbb{M}_2(0)}{t_k} &= (\operatorname{div}\boldsymbol{\theta})\varepsilon - D\boldsymbol{\theta}\varepsilon - \varepsilon D\boldsymbol{\theta}^{\mathsf{T}} + \widetilde{D\varepsilon}\boldsymbol{\theta},\\
(6.50)\quad \lim_{k\to\infty}\frac{\mathbb{M}_4(t_k)-\mathbb{M}_4(0)}{t_k} &= (\operatorname{div}\boldsymbol{\theta})\boldsymbol{f} - D\boldsymbol{\theta}\boldsymbol{f} + \widetilde{D\boldsymbol{f}}\boldsymbol{\theta}.
\end{aligned}
$$

Note that $\widetilde{\nabla\kappa}$ denotes the zero extension of $\nabla\kappa_{|B} \in \boldsymbol{\mathcal{C}}(B)$ to Ω. The same notation is used for $\widetilde{D\boldsymbol{E}_d}, \widetilde{D\varepsilon}, \widetilde{D\nu}, \widetilde{D\boldsymbol{f}}$. Similarly, by the Gâteaux-differentiability of $\boldsymbol{\Lambda}_\gamma$ (see Lemma 6.8), (6.14) and (6.44), we deduce that

$$
\begin{aligned}
(6.51)\quad \lim_{k\to\infty}\frac{\mathbb{M}_3(t_k)-\mathbb{M}_3(0)}{t_k}\cdot\boldsymbol{P}_{t_k}^\gamma &= \big((\operatorname{div}\boldsymbol{\theta})\boldsymbol{\Lambda}_\gamma(\boldsymbol{E}_0^\gamma) - D\boldsymbol{\theta}\boldsymbol{\Lambda}_\gamma(\boldsymbol{E}_0^\gamma)\big)\cdot\boldsymbol{P}_0^\gamma\\
&\quad - \boldsymbol{\psi}^\gamma(\boldsymbol{E}_0^\gamma)\boldsymbol{P}_0^\gamma\cdot(D\boldsymbol{\theta}^{\mathsf{T}}\boldsymbol{E}_0^\gamma).
\end{aligned}
$$

From (6.46)–(6.51) along with the weak convergence (6.44) and $\operatorname{supp}\boldsymbol{\theta} \subset\subset B$, it follows that

$$
\begin{aligned}
(6.52)\qquad & \lim_{k\to\infty} \frac{G(t_k, \boldsymbol{E}_0^\gamma, \boldsymbol{P}_{t_k}^\gamma) - G(0, \boldsymbol{E}_0^\gamma, \boldsymbol{P}_{t_k}^\gamma)}{t_k} \\
&= \int_B \frac{1}{2}(\nabla\kappa\cdot\boldsymbol{\theta} + \kappa \operatorname{div}\boldsymbol{\theta})|\boldsymbol{E}_0^\gamma - \boldsymbol{E}_d|^2 - \kappa(\boldsymbol{E}_0^\gamma - \boldsymbol{E}_d)\cdot(D\boldsymbol{\theta}^\mathsf{T}\boldsymbol{E}_0^\gamma + D\boldsymbol{E}_d\boldsymbol{\theta})\,dx \\
&\quad + \int_\omega \operatorname{div}\boldsymbol{\theta}\,dx + \int_B \big(-(\operatorname{div}\boldsymbol{\theta})\nu + D\boldsymbol{\theta}^\mathsf{T}\nu + \nu D\boldsymbol{\theta} + D\nu\boldsymbol{\theta}\big)\operatorname{\mathbf{curl}}\boldsymbol{E}_0^\gamma\cdot\operatorname{\mathbf{curl}}\boldsymbol{P}_0^\gamma\,dx \\
&\quad + \int_B \big((\operatorname{div}\boldsymbol{\theta})\varepsilon - D\boldsymbol{\theta}\varepsilon - \varepsilon D\boldsymbol{\theta}^\mathsf{T} + D\varepsilon\boldsymbol{\theta}\big)\boldsymbol{E}_0^\gamma\cdot\boldsymbol{P}_0^\gamma\,dx \\
&\quad + \int_\omega (\operatorname{div}\boldsymbol{\theta})\boldsymbol{\Lambda}_\gamma(\boldsymbol{E}_0^\gamma)\cdot\boldsymbol{P}_0^\gamma - D\boldsymbol{\theta}\boldsymbol{\Lambda}_\gamma(\boldsymbol{E}_0^\gamma)\cdot\boldsymbol{P}_0^\gamma - \boldsymbol{\psi}^\gamma(\boldsymbol{E}_0^\gamma)\boldsymbol{P}_0^\gamma\cdot(D\boldsymbol{\theta}^\mathsf{T}\boldsymbol{E}_0^\gamma)\,dx \\
&\quad - \int_B (D\boldsymbol{f}\boldsymbol{\theta} + (\operatorname{div}\boldsymbol{\theta})\boldsymbol{f})\cdot\boldsymbol{P}_0^\gamma - \boldsymbol{f}\cdot D\boldsymbol{\theta}^\mathsf{T}\boldsymbol{P}_0^\gamma\,dx \\
&= \lim_{k\to\infty} \frac{G(t_k, \boldsymbol{E}_0^\gamma, \boldsymbol{P}_0^\gamma) - G(0, \boldsymbol{E}_0^\gamma, \boldsymbol{P}_0^\gamma)}{t_k} = \partial_t G(0, \boldsymbol{E}_0^\gamma, \boldsymbol{P}_0^\gamma).
\end{aligned}
$$

Thus, (H4) is valid. ∎

It is easy to see that, in the case $t = 0$, the solution $\boldsymbol{P}_0^\gamma \in \boldsymbol{H}_0(\mathbf{curl})$ of (6.26) also satisfies the equation

$$
(6.53)\qquad \partial_{\boldsymbol{e}}\mathcal{L}(\omega, \boldsymbol{E}_0^\gamma, \boldsymbol{P}_0^\gamma; \hat{\boldsymbol{e}}) = 0 \quad \forall \hat{\boldsymbol{e}} \in \boldsymbol{H}_0(\mathbf{curl}).
$$

By definition of the Lagrangian (6.20) and by (6.29) we conclude that (6.53) is equivalent to

$$
(6.54)\qquad a(\hat{\boldsymbol{e}}, \boldsymbol{P}_0^\gamma) + \int_\omega \boldsymbol{\psi}^\gamma(\boldsymbol{E}_0^\gamma)\boldsymbol{P}_0^\gamma\cdot\hat{\boldsymbol{e}}\,dx = -\int_B \kappa(\boldsymbol{E}_0^\gamma - \boldsymbol{E}_d)\cdot\hat{\boldsymbol{e}}\,dx, \quad \forall \hat{\boldsymbol{e}} \in \boldsymbol{H}_0(\mathbf{curl}).
$$

We refer to (6.54) as the *adjoint equation* and we write for simplicity $(\boldsymbol{E}^\gamma, \boldsymbol{P}^\gamma) = (\boldsymbol{E}_0^\gamma, \boldsymbol{P}_0^\gamma)$. We now have all the elements at hand to prove the shape differentiability of J_γ and write the distributed expression of the shape derivative of J_γ.

Theorem 6.13. *Let Assumption* 6.5 *be satisfied, $\gamma > 0$, $\omega \in \mathcal{O}$ and $\boldsymbol{\theta} \in \boldsymbol{\mathcal{C}}_c^{0,1}(\Omega)$ with a compact support in B. Furthermore, $\boldsymbol{E}^\gamma \in \boldsymbol{H}_0(\mathbf{curl})$ and $\boldsymbol{P}^\gamma \in \boldsymbol{H}_0(\mathbf{curl})$ denote the solutions to* (6.7) *and* (6.54)*, respectively. Then, the functional J_γ in* (P_γ) *is shape differentiable with*

$$
(6.55)\qquad dJ_\gamma(\omega)(\boldsymbol{\theta}) = \partial_t G(0, \boldsymbol{E}^\gamma, \boldsymbol{P}^\gamma) = \int_B S_1^\gamma : D\boldsymbol{\theta} + \boldsymbol{S}_0^\gamma\cdot\boldsymbol{\theta}\,dx,
$$

where $S_1^\gamma \in L^1(B, \mathbb{R}^{3\times3})$ and $\boldsymbol{S}_0^\gamma \in \boldsymbol{L}^1(B)$ are given by

$$
\begin{aligned}
S_1^\gamma &= \Big[\frac{\kappa}{2}|\boldsymbol{E}^\gamma - \boldsymbol{E}_d|^2 + \chi_\omega - \nu\operatorname{\mathbf{curl}}\boldsymbol{E}^\gamma\cdot\operatorname{\mathbf{curl}}\boldsymbol{P}^\gamma + \varepsilon\boldsymbol{E}^\gamma\cdot\boldsymbol{P}^\gamma + \chi_\omega\boldsymbol{\Lambda}_\gamma(\boldsymbol{E}^\gamma)\cdot\boldsymbol{P}^\gamma \\
&\qquad - \boldsymbol{f}\cdot\boldsymbol{P}^\gamma\Big]\boldsymbol{I}_3 - \kappa\boldsymbol{E}^\gamma\otimes(\boldsymbol{E}^\gamma - \boldsymbol{E}_d) + \nu\operatorname{\mathbf{curl}}\boldsymbol{E}^\gamma\otimes\operatorname{\mathbf{curl}}\boldsymbol{P}^\gamma \\
&\quad + \nu^\mathsf{T}\operatorname{\mathbf{curl}}\boldsymbol{P}^\gamma\otimes\operatorname{\mathbf{curl}}\boldsymbol{E}^\gamma - \boldsymbol{P}^\gamma\otimes\varepsilon\boldsymbol{E}^\gamma - \boldsymbol{E}^\gamma\otimes\varepsilon^\mathsf{T}\boldsymbol{P}^\gamma + \boldsymbol{P}^\gamma\otimes\boldsymbol{f} \\
&\quad - \chi_\omega\boldsymbol{\Lambda}_\gamma(\boldsymbol{E}^\gamma)\otimes\boldsymbol{P}^\gamma - \boldsymbol{E}^\gamma\otimes\boldsymbol{\psi}^\gamma(\boldsymbol{E}^\gamma)\boldsymbol{P}^\gamma, \\
\boldsymbol{S}_0^\gamma &= \frac{\nabla\kappa}{2}|\boldsymbol{E}^\gamma - \boldsymbol{E}_d|^2 - \kappa D\boldsymbol{E}_d^\mathsf{T}(\boldsymbol{E}^\gamma - \boldsymbol{E}_d) + (D\nu^\mathsf{T}\operatorname{\mathbf{curl}}\boldsymbol{E}^\gamma)\operatorname{\mathbf{curl}}\boldsymbol{P}^\gamma \\
&\quad + (D\epsilon^\mathsf{T}\boldsymbol{E}^\gamma)\boldsymbol{P}^\gamma - D\boldsymbol{f}^\mathsf{T}\boldsymbol{P}^\gamma.
\end{aligned}
$$

Proof. Thanks to Lemmas 6.11 and 6.12, we may apply the averaged adjoint method (see Theorem 6.10). This yields that J_γ is shape-differentiable in the sense of Definition 6.4 and the shape derivative satisfies

$$dJ_\gamma(\omega)(\boldsymbol{\theta}) = \frac{d}{dt} J_\gamma(\omega_t)|_{t=0} = \partial_t G(0, \boldsymbol{E}^\gamma, \boldsymbol{P}^\gamma), \tag{6.56}$$

where $\partial_t G(0, \boldsymbol{E}^\gamma, \boldsymbol{P}^\gamma)$ is given by (6.52). We note that $D\epsilon, D\nu \colon \Omega \to \mathbb{R}^{3\times3\times3}$ are third-order tensors, and their transpose $D\epsilon^\mathsf{T}$, $D\nu^\mathsf{T}$ satisfy (see [143, Proposition 3.1])

$$(D\epsilon\boldsymbol{\theta})\boldsymbol{E}^\gamma \cdot \boldsymbol{P}^\gamma = (D\epsilon^\mathsf{T}\boldsymbol{E}^\gamma)\boldsymbol{P}^\gamma \cdot \boldsymbol{\theta}$$

as well as

$$(D\nu\boldsymbol{\theta})\,\mathbf{curl}\,\boldsymbol{E}^\gamma \cdot \mathbf{curl}\,\boldsymbol{P}^\gamma = (D\nu^\mathsf{T}\,\mathbf{curl}\,\boldsymbol{E}^\gamma)\,\mathbf{curl}\,\boldsymbol{P}^\gamma \cdot \boldsymbol{\theta}.$$

Furthermore, for vectors $\boldsymbol{x}, \boldsymbol{y} \in \mathbb{R}^3$ we have the relations $D\boldsymbol{\theta} : (\boldsymbol{x} \otimes \boldsymbol{y}) = \boldsymbol{x} \cdot D\boldsymbol{\theta}\boldsymbol{y} = D\boldsymbol{\theta}^\mathsf{T}\boldsymbol{x} \cdot \boldsymbol{y}$. Applying these to (6.52) and combining it with (6.56), the tensor expression (6.55) for the shape derivative follows. Finally, the fact that $S_1^\gamma \in L^1(B, \mathbb{R}^{3\times3})$ and $\boldsymbol{S}_0^\gamma \in \boldsymbol{L}^1(B)$ is a straightforward consequence of the regularity of $\boldsymbol{E}^\gamma, \boldsymbol{P}^\gamma$ and of the other functions involved in the expressions of $\boldsymbol{S}_0^\gamma$ and S_1^γ. This completes the proof. ∎

6.5 ▪ Stability and Convergence Analysis

In this section we analyze the stability of the shape derivative (6.55) with respect to the penalization parameter $\gamma > 0$. Furthermore, the strong convergence of (P_γ) towards (P) as $\gamma \to \infty$ is studied. The latter also implies the existence of an optimal shape for (P) (see Theorem 6.7).

6.5.1 ▪ Stability Analysis of the Shape Derivative

Theorem 6.14. *Let $\omega \in \mathcal{O}$ and Assumption* 6.5 *hold. Then, the following stability estimate holds for the shape derivative of J_γ:*

$$|dJ_\gamma(\omega)(\boldsymbol{\theta})| \le C\|\boldsymbol{\theta}\|_{\boldsymbol{\mathcal{C}}^{0,1}(B)} \quad \forall \boldsymbol{\theta} \in \boldsymbol{\mathcal{C}}_c^{0,1}(\Omega),\ \operatorname{supp}\boldsymbol{\theta} \subset\subset B, \tag{6.57}$$

with a constant $C = C(j_c, \kappa, \epsilon, \nu, \boldsymbol{f}, \boldsymbol{E}_d, B, \omega)$ independent of γ.

Proof. First of all, the distributed shape derivative from (6.55) yields the estimate

$$|dJ_\gamma(\omega)(\boldsymbol{\theta})| \le \big(\|S_1^\gamma\|_{L^1(B,\mathbb{R}^{3\times3})} + \|\boldsymbol{S}_0^\gamma\|_{\boldsymbol{L}^1(B)}\big)\|\boldsymbol{\theta}\|_{\boldsymbol{\mathcal{C}}^{0,1}(B)}. \tag{6.58}$$

In order to derive upper bounds for $\|S_1^\gamma\|_{L^1(B,\mathbb{R}^{3\times3})}$ and $\|\boldsymbol{S}_0^\gamma\|_{\boldsymbol{L}^1(B)}$, we begin by proving that the families $\{\boldsymbol{E}^\gamma\}_{\gamma>0}$ and $\{\boldsymbol{P}^\gamma\}_{\gamma>0}$ are uniformly bounded in $\boldsymbol{H}_0(\mathbf{curl})$. In view of (6.42), we have

$$\|\boldsymbol{E}^\gamma\|_{\boldsymbol{H}(\mathbf{curl})} \le \min(\underline{\nu}, \underline{\epsilon})^{-1}(\|\boldsymbol{f}\|_{\boldsymbol{L}^2(\Omega)} + j_c) =: C_{\boldsymbol{E}}. \tag{6.59}$$

Moreover, we set $t, s = 0$ in (6.29), which yields

$$\int_\omega \partial_{\boldsymbol{e}}\mathbb{M}_3(0, \mathcal{E}(0))(\boldsymbol{P}^\gamma) \cdot \boldsymbol{P}^\gamma\, dx = \int_\omega \boldsymbol{\psi}^\gamma(\boldsymbol{E}^\gamma)\boldsymbol{P}^\gamma \cdot \boldsymbol{P}^\gamma\, dx \ge 0. \tag{6.60}$$

In fact, the nonnegativity of (6.60) follows by similar calculations as (6.36)–(6.40) in the special case $t, s, \tau = 0$. As $\boldsymbol{P}^\gamma$ is the unique solution to (6.54), inserting $\hat{\boldsymbol{e}} = \boldsymbol{P}^\gamma$ implies with (A6.2)

$$\begin{aligned}\min(\underline{\epsilon}, \underline{\nu})\|\boldsymbol{P}^\gamma\|^2_{\boldsymbol{H}(\mathbf{curl})} &\leq a(\boldsymbol{P}^\gamma, \boldsymbol{P}^\gamma)\\ &= -\int_B \kappa(\boldsymbol{E}^\gamma - \boldsymbol{E}_d)\cdot \boldsymbol{P}^\gamma\,dx - \int_\omega \boldsymbol{\psi}^\gamma(\boldsymbol{E}^\gamma)\boldsymbol{P}^\gamma\cdot\boldsymbol{P}^\gamma\,dx.\end{aligned}$$

Hence, we obtain a uniform bound for $\boldsymbol{P}^\gamma$ by means of (6.59) and (6.60), i.e.,

$$\|\boldsymbol{P}^\gamma\|_{\boldsymbol{H}(\mathbf{curl})} \leq \|\kappa\|_{\mathcal{C}(\Omega)} \min(\underline{\epsilon}, \underline{\nu})^{-1}\big(C_{\boldsymbol{E}} + \|\boldsymbol{E}_d\|_{\boldsymbol{L}^2(B)}\big) =: C_{\boldsymbol{P}}. \tag{6.61}$$

With (6.59) and (6.61) we may now estimate both terms in (6.58) separately. Therefore, let us introduce the notation (see Theorem 6.13)

$$S_1^\gamma := \sum_{i=1}^{14} \Theta_i, \tag{6.62}$$

where $\Theta_i \in L^1(B, \mathbb{R}^{3\times 3})$ for every $i \in \{1, \dots, 14\}$. Now, Assumption 6.5, (6.59), and (6.61) together with Hölder's and Young's inequalities yield

$$\begin{aligned}&\sum_{i=1}^{6} \|\Theta_i\|_{L^1(B,\mathbb{R}^{3\times3})}\\ \leq\ & \int_B \frac{|\kappa|}{2}|\boldsymbol{E}^\gamma - \boldsymbol{E}_d|^2 + \chi_\omega\,dx + \int_B |\nu\,\mathbf{curl}\,\boldsymbol{E}^\gamma\cdot\mathbf{curl}\,\boldsymbol{P}^\gamma| + |\epsilon\boldsymbol{E}^\gamma\cdot\boldsymbol{P}^\gamma|\,dx\\ &+ \int_\omega |\boldsymbol{\Lambda}_\gamma(\boldsymbol{E}^\gamma)\cdot\boldsymbol{P}^\gamma|\,dx + \int_B |\boldsymbol{f}\cdot\boldsymbol{P}^\gamma|\,dx\\ \overbrace{\leq}^{(6.59)\&(6.61)}\ & \|\kappa\|_{\mathcal{C}(B)}\big(C_{\boldsymbol{E}}^2 + \|\boldsymbol{E}_d\|^2_{\boldsymbol{L}^2(B)}\big) + |\omega| + \big(\|\nu\|_{\mathcal{C}(B,\mathbb{R}^{3\times3})} + \|\epsilon\|_{\mathcal{C}(B,\mathbb{R}^{3\times3})}\big)C_{\boldsymbol{E}}C_{\boldsymbol{P}}\\ &+ (j_c\sqrt{|\omega|} + \|\boldsymbol{f}\|_{\boldsymbol{L}^2(B)})C_{\boldsymbol{P}}\end{aligned} \tag{6.63}$$

For the remaining terms, we use again Assumption 6.5, (6.59), and (6.61) as well as the identity $|\boldsymbol{x}\otimes\boldsymbol{y}| = |\boldsymbol{x}|\cdot|\boldsymbol{y}|$ for all $\boldsymbol{x}, \boldsymbol{y} \in \mathbb{R}^3$ to infer

$$\begin{aligned}\sum_{i=7}^{13} \|\Theta_i\|_{L^1(B,\mathbb{R}^{3\times3})} &\leq \frac{1}{2}\|\kappa\|_{\mathcal{C}(B)}\big(3C_{\boldsymbol{E}}^2 + \|\boldsymbol{E}_d\|^2_{\boldsymbol{L}^2(B)}\big)\\ &\quad + 2(\|\nu\|_{\mathcal{C}(B,\mathbb{R}^{3\times3})} + \|\epsilon\|_{\mathcal{C}(B,\mathbb{R}^{3\times3})})C_{\boldsymbol{E}}C_{\boldsymbol{P}} + (\|\boldsymbol{f}\|_{\boldsymbol{L}^2(B)} + j_c\sqrt{|\omega|})C_{\boldsymbol{P}},\end{aligned} \tag{6.64}$$

where we have also used Young's inequality to obtain the first term in (6.64). Moreover, we may estimate the last summand of S_1^γ as follows

$$\begin{aligned}\|\Theta_{14}\|_{L^1(\Omega,\mathbb{R}^{3\times3})} = \|\boldsymbol{E}^\gamma\otimes\boldsymbol{\psi}^\gamma(\boldsymbol{E}^\gamma)\boldsymbol{P}^\gamma\|_{L^1(\Omega,\mathbb{R}^{3\times3})} &\leq \int_\omega |\boldsymbol{\psi}^\gamma(\boldsymbol{E}^\gamma)\boldsymbol{P}^\gamma|\cdot|\boldsymbol{E}^\gamma|\,dx\\ \overbrace{\leq}^{(6.12)\&(6.13)}\ & \int_\omega \left(\frac{j_c\gamma|\boldsymbol{P}^\gamma|}{\max_\gamma\{1,\gamma|\boldsymbol{E}^\gamma|\}} + \frac{\gamma|\boldsymbol{E}^\gamma\otimes\boldsymbol{\Lambda}_\gamma(\boldsymbol{E}^\gamma)|\cdot|\boldsymbol{P}^\gamma|}{\max_\gamma\{1,\gamma|\boldsymbol{E}^\gamma|\}|\boldsymbol{E}^\gamma|}\right)|\boldsymbol{E}^\gamma|\,dx\\ \overbrace{\leq}^{(6.15)}\ & \int_\omega 2j_c|\boldsymbol{P}^\gamma|\,dx \leq 2j_c\sqrt{|\omega|}C_{\boldsymbol{P}}.\end{aligned} \tag{6.65}$$

Gathering (6.63)–(6.65) we deduce the final estimate for S_1^γ

$$\begin{aligned}(6.66)\quad \|S_1^\gamma\|_{L^1(B,\mathbb{R}^{3\times 3})} &\leq \frac{1}{2}\|\kappa\|_{\mathcal{C}(B)}\big(5C_{\boldsymbol{E}}^2 + 3\|\boldsymbol{E}_d\|^2_{\boldsymbol{L}^2(B)}\big) + |\omega| \\ &\quad + 3\big(\|\nu\|_{\mathcal{C}(B,\mathbb{R}^{3\times 3})} + \|\epsilon\|_{\mathcal{C}(B,\mathbb{R}^{3\times 3})}\big)C_{\boldsymbol{E}}C_{\boldsymbol{P}} + \big(2\|\boldsymbol{f}\|_{\boldsymbol{L}^2(B)} + 4j_c\sqrt{|\omega|}\big)C_{\boldsymbol{P}}.\end{aligned}$$

Again, (6.59) and (6.61) with Hölder's and Young's inequalities imply

$$\begin{aligned}\|\boldsymbol{S}_0^\gamma\|_{\boldsymbol{L}^1(B)} &\leq \int_B \frac{1}{2}|\nabla\kappa|\cdot|\boldsymbol{E}^\gamma - \boldsymbol{E}_d|^2 + |\kappa D\boldsymbol{E}_d^{\mathsf{T}}(\boldsymbol{E}^\gamma - \boldsymbol{E}_d)|\,dx \\ &\quad + \int_B |D\nu^{\mathsf{T}}\,\mathbf{curl}\,\boldsymbol{E}^\gamma|\cdot|\,\mathbf{curl}\,\boldsymbol{P}^\gamma| + |D\epsilon^{\mathsf{T}}\boldsymbol{E}^\gamma|\cdot|\boldsymbol{P}^\gamma| + |D\boldsymbol{f}^{\mathsf{T}}\boldsymbol{P}^\gamma|\,dx \\ &\leq \frac{1}{2}\|\kappa\|_{\mathcal{C}^1(B)}\big(3C_{\boldsymbol{E}}^2 + 5\|\boldsymbol{E}_d\|^2_{\boldsymbol{H}^1(B)}\big) \\ &\quad + \big(\|\nu\|_{\mathcal{C}^1(B,\mathbb{R}^{3\times 3})} + \|\epsilon\|_{\mathcal{C}^1(B,\mathbb{R}^{3\times 3})}\big)C_{\boldsymbol{P}}C_{\boldsymbol{E}} + \|\boldsymbol{f}\|_{\boldsymbol{H}^1(B)}C_{\boldsymbol{P}}. \qquad (6.67)\end{aligned}$$

Finally, we combine (6.58), (6.66), and (6.67) to conclude

$$\begin{aligned}|dJ_\gamma(\omega)(\boldsymbol{\theta})| \leq \Big[&4\|\kappa\|_{\mathcal{C}^1(B)}\big(C_{\boldsymbol{E}}^2 + \|\boldsymbol{E}_d\|^2_{\boldsymbol{H}^1(B)}\big) + 4\big(\|\nu\|_{\mathcal{C}^1(B,\mathbb{R}^{3\times 3})} + \|\epsilon\|_{\mathcal{C}^1(B,\mathbb{R}^{3\times 3})}\big)C_{\boldsymbol{E}}C_{\boldsymbol{P}} \\ &+ |\omega| + \big(3\|\boldsymbol{f}\|_{\boldsymbol{H}^1(B)} + 4j_c\sqrt{|\omega|}\big)C_{\boldsymbol{P}}\Big]\|\boldsymbol{\theta}\|_{\boldsymbol{\mathcal{C}}^{0,1}(B)}\end{aligned}$$

Hence, the proof is finished. ■

6.5.2 ▪ Convergence of the Regularized Shape Optimization Problem

Our aim is to prove the strong convergence of (P_γ) towards (P). For this purpose, we recall a helpful result which states the strong convergence of the solution to (6.7) for a fixed $\omega \in \mathcal{O}$. A proof can be found in [55, Corollary 4.3]:

Lemma 6.15. *Let Assumption* 6.5 *be satisfied and $\omega \in \mathcal{O}$. Moreover, for every $\gamma > 0$, let $(\boldsymbol{E}^\gamma, \boldsymbol{\lambda}^\gamma) \in \boldsymbol{H}_0(\mathbf{curl}) \times \boldsymbol{L}^\infty(\omega)$ denote the solution to* (6.7)*. Then,*

$$(6.68)\qquad (\boldsymbol{E}^\gamma, \boldsymbol{\lambda}^\gamma) \to (\boldsymbol{E}, \boldsymbol{\lambda}) \quad \textit{strongly in } \boldsymbol{H}_0(\mathbf{curl}) \times \boldsymbol{H}_0(\mathbf{curl})^* \textit{ as } \gamma \to \infty,$$

where $(\boldsymbol{E}, \boldsymbol{\lambda}) \in \boldsymbol{H}_0(\mathbf{curl}) \times \boldsymbol{L}^\infty(\omega)$ is the unique solution to (6.3)*.*

Let us point out that in (6.68) we extended the Lagrange multipliers $\boldsymbol{\lambda}^\gamma, \boldsymbol{\lambda}$ by zero as functions in $\boldsymbol{L}^2(\Omega)$, i.e., we set $\boldsymbol{\lambda}^\gamma(x) = 0$ and $\boldsymbol{\lambda}(x) = 0$ for all $x \in \Omega\backslash\omega$. This zero extension shall also be used in the following theorem.

Theorem 6.16. *Let Assumption* 6.5 *hold and $\{\gamma_n\}_{n\in\mathbb{N}} \subset \mathbb{R}^+$ be such that $\gamma_n \to \infty$ as $n \to \infty$. Then, there exists a subsequence of $\{\gamma_n\}_{n\in\mathbb{N}}$, still denoted by $\{\gamma_n\}_{n\in\mathbb{N}}$, such that the sequence of solutions $\{\omega^{\gamma_n}\}_{n\in\mathbb{N}}$ of* (P_γ) *with $\gamma = \gamma_n$ converges towards an optimal solution $\omega_\star \subset \mathcal{O}$ of* (P) *in the sense of Hausdorff and in the sense of characteristic functions.*

Moreover, $\{(\boldsymbol{E}^{\gamma_n}(\omega^{\gamma_n}), \boldsymbol{\lambda}^{\gamma_n}(\omega^{\gamma_n}))\}_{n\in\mathbb{N}}$ and $(\boldsymbol{E}(\omega_\star), \boldsymbol{\lambda}(\omega_\star))$ as the solutions of (6.7) *for $\omega = \omega^{\gamma_n}$ and* (6.3) *for $\omega = \omega_\star$, respectively, satisfy*

$$(6.69)\qquad \lim_{\gamma\to\infty} \|\boldsymbol{E}^{\gamma_n}(\omega^{\gamma_n}) - \boldsymbol{E}(\omega_\star)\|_{\boldsymbol{H}(\mathbf{curl})} = 0,$$

$$(6.70)\qquad \lim_{\gamma\to\infty} \|\boldsymbol{\lambda}^{\gamma_n}(\omega^{\gamma_n}) - \boldsymbol{\lambda}(\omega_\star)\|_{\boldsymbol{H}_0(\mathbf{curl})^*} = 0,$$

where $\boldsymbol{\lambda}^{\gamma_n}(\omega^{\gamma_n})$ (resp. $\boldsymbol{\lambda}(\omega_\star)$) is extended by zero in $\Omega \setminus \omega^{\gamma_n}$ (resp. in $\Omega \setminus \omega_\star$).

Proof. Thanks to Theorem 6.3 and $\gamma_n \to \infty$, there exists $\omega_\star \in \mathcal{O}$ such that, possibly for a subsequence,

$$\omega^{\gamma_n} \to \omega_\star \quad \text{as } n \to \infty \tag{6.71}$$

in the sense of Hausdorff and in the sense of characteristic functions. Furthermore, we have the estimate

$$\begin{aligned}\|\boldsymbol{E}^{\gamma_n}(\omega^{\gamma_n}) - \boldsymbol{E}(\omega_\star)\|_{\boldsymbol{H}(\mathbf{curl})} \leq \|\boldsymbol{E}^{\gamma_n}(\omega^{\gamma_n}) - \boldsymbol{E}^{\gamma_n}(\omega_\star)\|_{\boldsymbol{H}(\mathbf{curl})} \\ + \|\boldsymbol{E}^{\gamma_n}(\omega_\star) - \boldsymbol{E}(\omega_\star)\|_{\boldsymbol{H}(\mathbf{curl})}.\end{aligned} \tag{6.72}$$

Now, by virtue of Lemma 6.15, the second term on the right-hand side of (6.72) converges to 0 as $n \to \infty$. For the first term we observe (for every $n \in \mathbb{N}$) that the arguments used to derive (6.19) are applicable. Thus, we subtract (6.7) for $\boldsymbol{E}^{\gamma_n}(\omega^{\gamma_n})$ and (6.7) for $\boldsymbol{E}^{\gamma_n}(\omega_\star)$ and test the resulting equation with $\boldsymbol{v} = \boldsymbol{E}^{\gamma_n}(\omega_\star) - \boldsymbol{E}^{\gamma_n}(\omega^{\gamma_n})$. Hereafter, analogously to (6.18), calculations involving (6.11) yield

$$\|\boldsymbol{E}^{\gamma_n}(\omega^{\gamma_n}) - \boldsymbol{E}^{\gamma_n}(\omega_\star)\|_{\boldsymbol{H}(\mathbf{curl})} \leq \frac{j_c}{\min\{\underline{\nu}, \underline{\epsilon}\}} \|\chi_{\omega_\star} - \chi_{\omega^{\gamma_n}}\|_{L^2(\Omega)} \quad \forall n \in \mathbb{N}. \tag{6.73}$$

Combining Lemma 6.15 and (6.71)–(6.73) together leads to (6.69).

Furthermore, subtracting (6.3) for $\omega = \omega_\star$ and (6.7) for $\omega = \omega^{\gamma_n}$ implies

$$\begin{aligned}\sup_{\boldsymbol{v} \in \boldsymbol{H}_0(\mathbf{curl})} \frac{(\boldsymbol{\lambda}^{\gamma_n}(\omega^{\gamma_n}) - \boldsymbol{\lambda}(\omega_\star), \boldsymbol{v})_{\boldsymbol{L}^2(\Omega)}}{\|\boldsymbol{v}\|_{\boldsymbol{H}(\mathbf{curl})}} &= \sup_{\boldsymbol{v} \in \boldsymbol{H}_0(\mathbf{curl})} \frac{a(\boldsymbol{E}(\omega_\star) - \boldsymbol{E}^{\gamma_n}(\omega^{\gamma_n}), \boldsymbol{v})}{\|\boldsymbol{v}\|_{\boldsymbol{H}(\mathbf{curl})}} \\ \overbrace{\leq}^{(A6.2)} \max\{\|\epsilon\|_{L^\infty(\Omega,\mathbb{R}^{3\times3})}, \|\nu\|_{L^\infty(\Omega,\mathbb{R}^{3\times3})}\} &\|\boldsymbol{E}(\omega_\star) - \boldsymbol{E}^{\gamma_n}(\omega^{\gamma_n})\|_{\boldsymbol{H}(\mathbf{curl})}.\end{aligned} \tag{6.74}$$

Thus, (6.70) follows from (6.69). It remains to verify that $\omega_\star \in \mathcal{O}$ is in fact a minimizer of (P). First of all, we note that, since ω^{γ_n} is a solution of (P_γ) for $\gamma = \gamma_n$, the following estimate holds

$$J_{\gamma_n}(\omega^{\gamma_n}) = \min_{\omega \in \mathcal{O}} J_{\gamma_n}(\omega) \leq J_{\gamma_n}(\omega) \quad \forall \omega \in \mathcal{O}. \tag{6.75}$$

Finally, gathering all the previous results, we obtain for every $\omega \in \mathcal{O}$ that

$$\begin{aligned} J(\omega_\star) = &\quad \frac{1}{2}\int_B \kappa|\boldsymbol{E}(\omega_\star) - \boldsymbol{E}_d|^2 dx + \int_{\omega_\star} dx \\ \overbrace{=}^{(6.69)\&(6.71)} &\lim_{n\to\infty} \frac{1}{2}\int_B \kappa|\boldsymbol{E}^{\gamma_n}(\omega^{\gamma_n}) - \boldsymbol{E}_d|^2 dx + \int_{\omega^{\gamma_n}} dx = \lim_{n\to\infty} J_{\gamma_n}(\omega^{\gamma_n}) \\ \overbrace{\leq}^{(6.75)} &\lim_{n\to\infty} J_{\gamma_n}(\omega) = \lim_{n\to\infty} \frac{1}{2}\int_B \kappa|\boldsymbol{E}^{\gamma_n}(\omega) - \boldsymbol{E}_d|^2 dx + \int_{\omega} dx \\ \overbrace{=}^{(6.68)} &\frac{1}{2}\int_B \kappa|\boldsymbol{E}(\omega) - \boldsymbol{E}_d|^2 dx + \int_{\omega} dx = J(\omega). \end{aligned}$$

This shows $J(\omega_\star) \leq J(\omega)$ for every $\omega \in \mathcal{O}$ which yields the assertion. ∎

Remark 6.17. As we have obtained the optimal shape $\omega_\star \in \mathcal{O}$ in (6.71) as the limit of the optimal shapes for (P_γ), Theorem 6.7 follows immediately from Theorem 6.16.

6.6 ▪ Computations

After the theoretical analysis, we dedicate this section to the derivation of a numerical algorithm based on a variant of the level set method, where the distributed shape derivative (Theorem 6.13) is used to obtain a computable descent direction (see [114]). Let us briefly describe our method before we present numerical results of the algorithm. We refer to [113] for a detailed description of this algorithm including its implementation in a 2D framework.

6.6.1 ▪ Level Set Algorithm

The original level set method was introduced in [137] and gives a framework to compute evolving interfaces based on an implicit representation. Basically, the method describes the boundary of an evolving shape $\omega_t \subset B$ as the set of roots of a continuous function $\psi(\cdot, t)\colon B \to \mathbb{R}^3$. Thus, we use the level-set representation

$$\omega_t = \{x \in B \,:\, \psi(x,t) < 0\},$$

where $\psi\colon B \times \mathbb{R}_+ \to \mathbb{R}$ is a suitable Lipschitz continuous function. In fact, it holds that

$$\partial\omega_t = \{x \in B \,:\, \psi(x,t) = 0\}$$

if $\nabla\psi(x,t) \neq 0$ for all (x,t) with $\psi(x,t) = 0$. Due to our application of the velocity method (see (6.1)), each point x on the boundary of ω satisfies $\frac{d}{dt}x(t) = \boldsymbol{\theta}(x(t))$. Hence, differentiating $\psi(x(t),t) = 0$ with respect to t yields the *Hamilton–Jacobi-equation*

$$\partial_t\psi(x,t) + \boldsymbol{\theta}(x)\cdot\nabla\psi(x,t) = 0 \quad \forall (x,t) \in B \times \mathbb{R}_+.$$

Here, we have extended the equation to $B \times \mathbb{R}_+$. For a comprehensive introduction of the level set method and the Hamiltion–Jacobi-equations, we refer to the monograph by Fedkiw and Osher [136]. Now, we find a descent direction $\boldsymbol{\theta}$ by the means of our shape derivative (Theorem 6.13) by solving the linear problem

$$\mathcal{B}(\boldsymbol{\theta}, \boldsymbol{\xi}) = -dJ_\gamma(\omega)(\boldsymbol{\xi}) \quad \forall \boldsymbol{\xi} \in \boldsymbol{X}(B), \tag{6.76}$$

where $\mathcal{B}\colon \boldsymbol{X} \times \boldsymbol{X} \to \mathbb{R}$ is a suitable continuous and coercive bilinear form with a Sobolev space $\boldsymbol{X}$. In our computations we choose $\boldsymbol{X} = \boldsymbol{H}_0^1(B)$ and $\mathcal{B}$ as an elliptic ∇-∇ bilinear form. In fact, the solution $\boldsymbol{\theta}$ is a descent direction since $dJ_\gamma(\omega_t)(\boldsymbol{\theta}) = -\mathcal{B}(\boldsymbol{\theta},\boldsymbol{\theta}) < 0$ if $\boldsymbol{\theta} \neq 0$. Therefore, we conclude Algorithm 6.1.

6.6.2 ▪ Numerical Tests

We consider the proposed approach (P_γ) with $\gamma = 7 \cdot 10^4$ and apply Algorithm 6.1. The forward problems (6.7) are computed using the Newton method with a finite element discretization based on the first family of Nédélec's edge elements (2.14) at roughly 2.000.000 DoFs. Thanks to the Gâteaux-differentiability of the dual variable mapping, we are no longer restricted to the semismooth Newton method. We apply Algorithm 6.1 to two problems stemming from high-temperature superconductivity.

We choose $\Omega = [-2,3]^3$ and $B = [0,1]^3$. For simplicity, we take the material parameters $\epsilon = \nu = I_3$ (cf. (A6.2)), where I_3 denotes the identity matrix. Moreover, $\boldsymbol{f}\colon \Omega \to \mathbb{R}^3$ is a circular current

$$\boldsymbol{f}(x,y,z) = \begin{cases} \dfrac{R}{\sqrt{(y-0.5)^2 + (z-0.5)^2}}(0,\ -z+0.5,\ y-0.5) & \text{for } (x,y,z) \in \Omega_p, \\ 0 & \text{for } (x,y,z) \notin \Omega_p, \end{cases}$$

Algorithm 6.1 Level set algorithm to solve (P_γ)

1: Set $k = 0$ and choose an initial level-set function ϕ_0 and $\omega_0 = \{x \in B \,|\, \phi_0(x) < 0\}$
2: Solve state equation (6.7) and adjoint equation (6.27) for $t = 0$ with $\omega = \omega_k$
3: Compute descent direction $\boldsymbol{\theta}_k$ by solving (6.76) with $\omega = \omega_k$, i.e.,

$$\mathcal{B}(\boldsymbol{\theta}, \boldsymbol{\xi}) = -dJ_\gamma(\omega_k)(\boldsymbol{\xi})$$

4: Solve Hamilton-Jacobi equations

$$\partial_t \phi(x,t) + \boldsymbol{\theta}_k(x) \nabla \phi(x,t) = 0 \quad \text{in } B \times \mathbb{R}^+, \qquad \phi(x,0) = \phi_k(x)$$

5: Update $\phi_{k+1}(x) = \phi(x, \Delta t_k)$ and $\omega_{k+1} = \{x \in B \,|\, \phi_{k+1}(x) < 0\}$
6: Set $k = k + 1$ and go to step 2 unless some stopping criterion is satisfied.

applied to a pipe coil $\Omega_p \subset \Omega$ which is defined by

$$\Omega_p := \Big\{(x,y,z) \in \Omega \,:\, |z - 0.5| \leq 0.5,\ \sqrt{(x-0.5)^2 + (y-0.5)^2} \in [1.2, 1.6]\Big\}.$$

The constant $R > 0$ denotes the electrical resistance of Ω_p (here: $R = 10^{-3}$). As $\Omega_p \cap B = \emptyset$, we have $\boldsymbol{f} \equiv 0$ in B and (A6.3) is satisfied. Without a superconductor in the system, this current would induce an orthogonal magnetic field which admits its highest field strength inside the coil.

We use the distributed expression (6.55) of the shape derivative to obtain a descent direction $\boldsymbol{\Theta}$. More precisely, let $\boldsymbol{V}_h \subset \boldsymbol{H}^1(B) \cap \boldsymbol{C}^{0,1}(\overline{B})$ be the space of piecewise linear and continuous finite elements on B. Given the positive definite bilinear form $\mathcal{B} : \boldsymbol{\Theta}_h \times \boldsymbol{\Theta}_h \to \mathbb{R}$ with

$$\mathcal{B}(\boldsymbol{\theta}, \boldsymbol{\xi}) = \int_B \alpha_1 D\boldsymbol{\theta} : D\boldsymbol{\xi} + \alpha_2 \boldsymbol{\theta} \cdot \boldsymbol{\xi}\, dx + \alpha_3 \int_{\partial B} (\boldsymbol{\theta} \cdot \boldsymbol{n})(\boldsymbol{\xi} \cdot \boldsymbol{n})\, ds, \tag{6.77}$$

where $\alpha_1 = 0.5$, $\alpha_2 = 0.5$ and $\alpha_3 = 1.0$, the problem is to find $\boldsymbol{\theta} \in \boldsymbol{\Theta}_h$ such that

$$\mathcal{B}(\boldsymbol{\theta}, \boldsymbol{\xi}) = -dJ_\gamma(\omega)(\boldsymbol{\xi}) \text{ for all } \boldsymbol{\xi} \in \boldsymbol{V}_h. \tag{6.78}$$

Moreover, the geometry was optimized in the class of shapes with two symmetries with respect to the planes $x = 0.5$ and $y = 0.5$. This is achieved by symmetrizing $\boldsymbol{\Theta}$ with respect to these axis, and it can be shown that the symmetrized vector field is still a descent direction according to the symmetrization technique proposed in subsection 6.6.6.

All codes are implemented in PYTHON with the open-source finite-element computational software FENICS [122]. We used PARAVIEW to visualize the 3D plots.

6.6.3 ▪ First Example

We set $\boldsymbol{E}_d \equiv 0$ in compliance with (A6.1) to find the optimal shape of a superconductor that minimizes both the electromagnetic field penetration and the volume of material. This example is motivated by the HTS application in the superconducting shielding (cf. [110]). We take $\kappa \equiv 8 \cdot 10^7$, which is a reasonable choice considering that the electric field strength is roughly $|\boldsymbol{E}| \approx 10^{-3}$ due to the weak applied current strength $|\boldsymbol{f}|$. The initial shape consists of material attached to the boundary of B (see Figure 6.1a). In Figures 6.1b to 6.1d we see some snapshots of the evolving shape generated by our algorithm. The algorithm generates two connected components on the top and the bottom of the (lateral) boundary. It is interesting to observe that the magnetic field ($\mathbf{curl}\, \boldsymbol{E}$) hits the boundary of the bounding box B from above and, despite the small amount of material used, the field lines do not

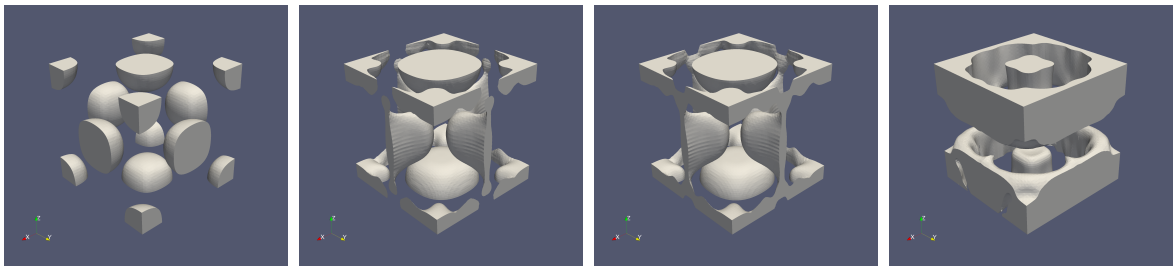

Figure 6.1. *Shapes generated by the algorithm at iterations* $0, 42, 45, 143$.

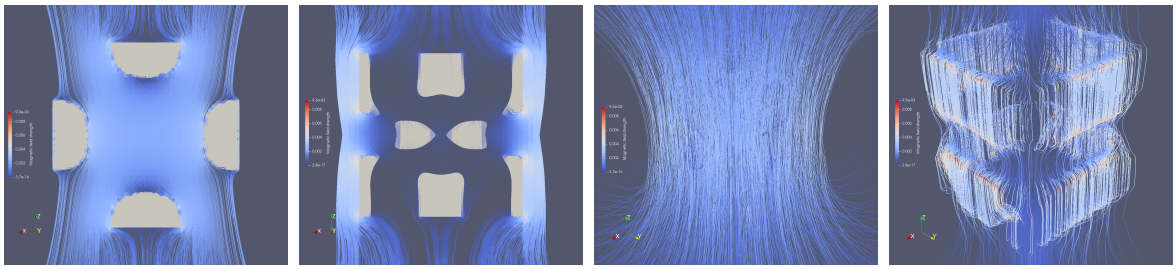

Figure 6.2. *Different views on the magnetic field at the initial and the final iteration. a.)–b.): 2D slice in the center. c.)–d.): Total shot from the same view as Figure* 6.1.

penetrate through the inside of the area enclosed by the superconductor (see Figures 6.2b and 6.2d). Moreover, in Figure 6.2 we can compare the magnetic field penetration for the initial and the final shape from different camera perspectives. The interior of the initial shape is barely protected from penetration, whereas the final shape redirects the magnetic field lines such that they are condensed on the outside of B.

In the final iteration the functional value is around 0.444 at a volume of roughly 0.278 which is only 27.8% of the volume of B. The E-field fraction in the cost functional amounts approximately to 0.166. This means that there is only a weak magnetic field left in small areas of B. The penetration is mostly between the connected components on the lateral surface of the conducting material. The development of the functional value as well as the volume fraction is documented in Figure 6.3a and the minimal value is reached after practically 125 iterations. Thereafter, it remains almost constant.

We also observe a slight increase of the cost functional at iterations 43 and 44, due to a topological change in the design. Indeed, at iteration 42 the components on the lateral sides of the cube are disconnected (see Figure 6.1b), and then merge at iteration 45 (see Figure 6.1c). This increase of the cost functional due to a topological change is a well-known issue with the level set method; see [112] for a recent study on this issue. However, in this example the increase in the functional value is negligible and immediately compensated by a sharp decrease.

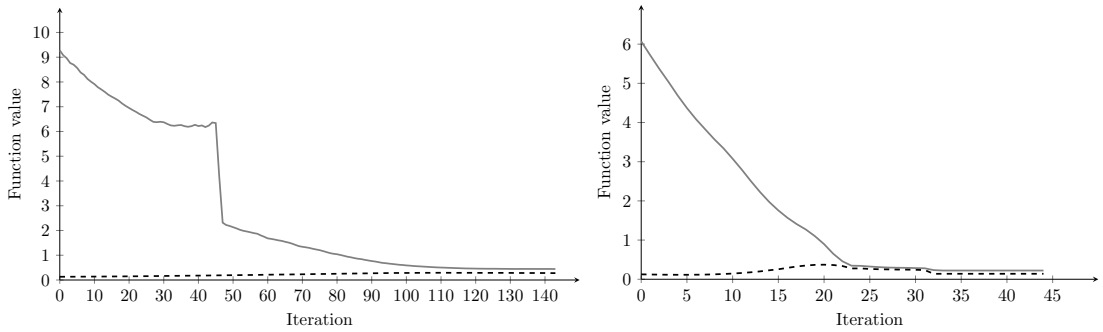

Figure 6.3. *Function value (solid) and volume (dashed): 1. Example (left), 2. Example (right).*

6.6.4 ▪ Second Example

In our second example, we place a superconducting ball ω_b with radius $r_b = 0.5$ inside B (see Figure 6.4a) and compute $\boldsymbol{E}_d$ as the corresponding solution of (6.7). The resulting magnetic field is displayed in Figures 6.5a and 6.5c. We initialized the algorithm with the same parameters and the same initial shape as in the first example (see Figure 6.1a). In the end, we obtain two bell-shaped components connected by small transitions on the boundary. In Figures 6.4b to 6.4d we see this shape from different camera positions. It corresponds to a functional value of 0.223, where the electric field costs get as low as 0.071 at a volume fraction of 0.153. As the original superconductor was a ball with radius 0.5, our algorithm computed an optimal shape with around 70% less material. The development of the functional value and the volume is documented in Figure 6.3b. Moreover, the descent in this example is smoother and notably faster than the first example. We explain this by the fact that the second choice of $\boldsymbol{E}_d$ gives more structure than simply $\boldsymbol{E}_d \equiv 0$. Thus, the algorithm has less possibilities to design the superconductor and converges faster.

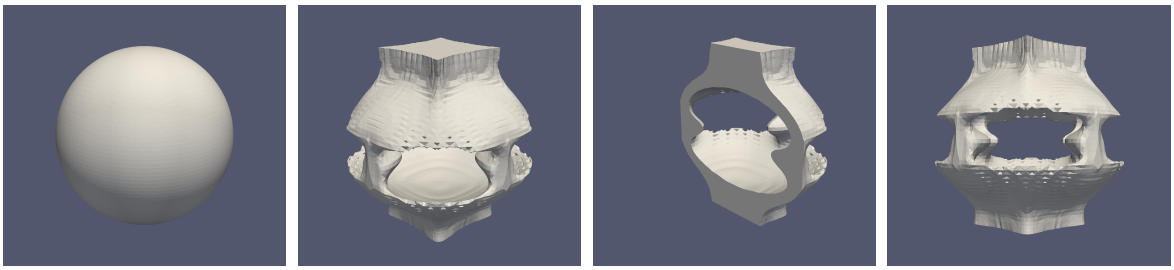

Figure 6.4. *The original superconductor and the final shape generated by the algorithm in the second example. The third figure is the final shape clipped along the plane* $x = 0.5$.

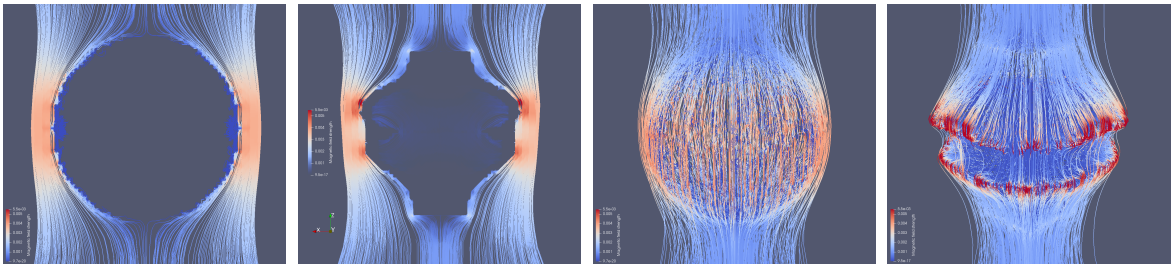

Figure 6.5. *Different views on the magnetic field of the original and the final superconductor. Left: 2D slice in the center. Right: Total shot from the same view as Figures* 6.4a *and* 6.4b.

6.6.5 ▪ Convergence Tests with Respect to gamma

Let us now report on a numerical test to verify our theoretical convergence result (Theorem 6.16). Since no analytical solution is available for the limit case (P), we compare the numerical results of our algorithm with two different regularization parameters $\hat{\gamma} = 7 \cdot 10^4$ and $\tilde{\gamma} = 7 \cdot 10^5$. For these choices, we terminated our algorithm after 143 iterations and computed the norm distance between the two numerical solutions:

$$\|\chi_{\omega^{\hat{\gamma}}} - \chi_{\omega^{\tilde{\gamma}}}\|_{L^1(\Omega)} \approx 2.88 \cdot 10^{-3} \quad \text{and} \quad \|\boldsymbol{E}^{\hat{\gamma}} - \boldsymbol{E}^{\tilde{\gamma}}\|_{\boldsymbol{H}(\mathbf{curl})} \approx 1.39 \cdot 10^{-4}.$$

This relatively small value indicates the convergence for $\gamma \to \infty$ (Theorem 6.16). In particular, we observe that, for sufficiently large penalization parameter γ, a remarkable change in γ would only lead to a small change in the computed optimal shape.

6.6.6 ▪ Shape Optimization with Symmetric Design

In many applications, it is desirable to obtain an optimal design which has certain prescribed symmetries. These can be, for instance, the consequence of symmetries of the geometry and the data that imply symmetries in the continuous solution. However, in practice, the numerically optimized design may deviate substantially from these symmetries, usually due to a non-symmetric discretization. This can be mitigated by refining the discretization which may not always be an affordable option, especially for 3D problems. Thus, imposing the symmetry as a constraint for the discretized problem can be a valuable alternative.

In this section we describe a method to obtain a descent direction for our minimization algorithm for (P_γ) while imposing a symmetry constraint. Therefore, we assume $B \subset \mathbb{R}^3$ (cf. (A6.1)) to be additionally symmetric with respect to some plane $Q \subset \mathbb{R}^3$. Without loss of generality, we may assume that $Q = \{x \in \mathbb{R}^3 \,|\, x_3 = 0\}$. Thanks to Theorem 6.13, the shape derivative of $J_\gamma(\omega)$ exists for every $\omega \in \mathcal{O}$ and admits the following tensor expression (see (6.55))

$$dJ_\gamma(\omega)(\boldsymbol{\theta}) = \int_B S_1 : D\boldsymbol{\theta} + \boldsymbol{S}_0 \cdot \boldsymbol{\theta}\, dx \quad \forall \boldsymbol{\theta} \in \boldsymbol{\mathcal{C}}_c^{0,1}(\Omega) \text{ with } \operatorname{supp}\boldsymbol{\theta} \subset\subset B.$$

Now, a descent direction for J_γ can be found by computing a solution $\widehat{\boldsymbol{\theta}} \in \boldsymbol{V}_h$ of

$$\mathcal{B}(\widehat{\boldsymbol{\theta}}, \boldsymbol{\zeta}) = -dJ_\gamma(\omega)(\boldsymbol{\zeta}) = -\int_B S_1 : D\boldsymbol{\zeta} + \boldsymbol{S}_0 \cdot \boldsymbol{\zeta}\, dx, \quad \forall \boldsymbol{\zeta} \in \boldsymbol{V}_h,$$

where $\mathcal{B}$ is a positive definite bilinear form on $\boldsymbol{V}_h \times \boldsymbol{V}_h$ (see (6.78)). The descent direction $\widehat{\boldsymbol{\theta}} \neq 0$ is not necessarily symmetric with respect to Q. Our aim now is to construct a symmetric descent direction out of $\widehat{\boldsymbol{\theta}}$. Therefore, we denote the reflection with respect to the plane Q by $\boldsymbol{R}_Q : \mathbb{R}^3 \to \mathbb{R}^3$ which is given by $(x_1, x_2, x_3)^\mathsf{T} \mapsto (x_1, x_2, -x_3)^\mathsf{T}$. We choose an appropriate triangulation of B such that the corresponding $\mathbb{P}_1$-finite element space $\boldsymbol{V}_h$ satisfies

$$\boldsymbol{\zeta} \in \boldsymbol{V}_h \quad \Rightarrow \quad \boldsymbol{\zeta} \circ \boldsymbol{R}_Q \in \boldsymbol{V}_h. \tag{6.79}$$

Clearly, a vector field $\boldsymbol{\theta} = (\theta_1, \theta_2, \theta_3)^\mathsf{T} : \mathbb{R}^3 \to \mathbb{R}^3$ is symmetric with respect to Q if and only if

$$\boldsymbol{\theta} \circ \boldsymbol{R}_Q(x) = (\theta_1(x), \theta_2(x), -\theta_3(x))^\mathsf{T} = D\boldsymbol{R}_Q\boldsymbol{\theta}(x) \quad \forall x \in \mathbb{R}^3. \tag{6.80}$$

We define the vector field

$$\boldsymbol{\theta} := \widehat{\boldsymbol{\theta}} + D\boldsymbol{R}_Q\widehat{\boldsymbol{\theta}} \circ \boldsymbol{R}_Q$$

which is indeed symmetric with respect to Q. Due to $\boldsymbol{R}_Q^{-1} = \boldsymbol{R}_Q$ and $D\boldsymbol{R}_Q^{-1} = D\boldsymbol{R}_Q$, we readily obtain that (6.80) holds for $\boldsymbol{\theta}$ by calculating

$$\boldsymbol{\theta} \circ \boldsymbol{R}_Q = \widehat{\boldsymbol{\theta}} \circ \boldsymbol{R}_Q + D\boldsymbol{R}_Q\widehat{\boldsymbol{\theta}} = D\boldsymbol{R}_Q\boldsymbol{\theta}.$$

Next, we will prove that $\boldsymbol{\theta}$ also provides a descent direction. In fact, the bilinear form $\mathcal{B}$ that was used for our numerical experiments (6.77) consists of three summands. However, as the arguments are virtually the same for all of them, we will only focus on the first one, i.e.,

$$\widetilde{\mathcal{B}} : \boldsymbol{V}_h \times \boldsymbol{V}_h \to \mathbb{R}, \quad (\boldsymbol{\eta}, \boldsymbol{\zeta}) \mapsto \int_B D\boldsymbol{\eta} : D\boldsymbol{\zeta}\, dx.$$

Since $\widehat{\boldsymbol{\theta}} \in \boldsymbol{V}_h$, we have due to (6.79) that $\boldsymbol{\theta} \in \boldsymbol{V}_h$, and therefore

$$\begin{aligned}\widetilde{\mathcal{B}}(\widehat{\boldsymbol{\theta}}, \boldsymbol{\theta}) &= \int_B D\widehat{\boldsymbol{\theta}} : D(\widehat{\boldsymbol{\theta}} + D\boldsymbol{R}_Q \widehat{\boldsymbol{\theta}} \circ \boldsymbol{R}_Q)\, dx \\ &= \int_B D\widehat{\boldsymbol{\theta}} : [D\widehat{\boldsymbol{\theta}} + D\boldsymbol{R}_Q D(\widehat{\boldsymbol{\theta}} \circ \boldsymbol{R}_Q)]\, dx \\ &= \int_B D\widehat{\boldsymbol{\theta}} : [D\widehat{\boldsymbol{\theta}} + D\boldsymbol{R}_Q (D\widehat{\boldsymbol{\theta}} \circ \boldsymbol{R}_Q) D\boldsymbol{R}_Q]\, dx.\end{aligned} \tag{6.81}$$

In order to exploit the symmetry properties of B, we introduce half-sets $B^+ = B \cap \{x_3 > 0\}$ and $B^- = B \cap \{x_3 < 0\}$. Thus, we may split the integral in (6.81) and apply the change of variables $x \mapsto \boldsymbol{R}_Q(x)$ in the integral over B^-. Therefore, using the fact that $D\boldsymbol{R}_Q = D\boldsymbol{R}_Q^{-1} = D\boldsymbol{R}_Q^{\mathsf{T}}$ we finally obtain

$$\begin{aligned}\widetilde{\mathcal{B}}(\widehat{\boldsymbol{\theta}}, \boldsymbol{\theta}) &= \int_{B^+} D\widehat{\boldsymbol{\theta}} : [D\widehat{\boldsymbol{\theta}} + D\boldsymbol{R}_Q (D\widehat{\boldsymbol{\theta}} \circ \boldsymbol{R}_Q) D\boldsymbol{R}_Q]\, dx \\ &\quad + \int_{B^+} D\widehat{\boldsymbol{\theta}} \circ \boldsymbol{R}_Q : [D\widehat{\boldsymbol{\theta}} \circ \boldsymbol{R}_Q + D\boldsymbol{R}_Q D\widehat{\boldsymbol{\theta}} D\boldsymbol{R}_Q]\, dx \\ &= \int_{B^+} D\widehat{\boldsymbol{\theta}} : [D\widehat{\boldsymbol{\theta}} + D\boldsymbol{R}_Q (D\widehat{\boldsymbol{\theta}} \circ \boldsymbol{R}_Q) D\boldsymbol{R}_Q]\, dx \\ &\quad + \int_{B^+} D\boldsymbol{R}_Q (D\widehat{\boldsymbol{\theta}} \circ \boldsymbol{R}_Q) D\boldsymbol{R}_Q : [D\boldsymbol{R}_Q (D\widehat{\boldsymbol{\theta}} \circ \boldsymbol{R}_Q) D\boldsymbol{R}_Q + D\widehat{\boldsymbol{\theta}}]\, dx \\ &= \int_{B^+} |D\widehat{\boldsymbol{\theta}} + D\boldsymbol{R}_Q (D\widehat{\boldsymbol{\theta}} \circ \boldsymbol{R}_Q) D\boldsymbol{R}_Q|^2\, dx > 0.\end{aligned}$$

Similar calculations yield $dJ_\gamma(\omega)(\boldsymbol{\theta}) = -\mathcal{B}(\widehat{\boldsymbol{\theta}}, \boldsymbol{\theta}) < 0$. Thus, $\boldsymbol{\theta}$ is a descent direction for J_γ that satisfies the symmetry property (6.80). Using $\boldsymbol{\theta}$ instead of $\widehat{\boldsymbol{\theta}}$ in our numerical algorithm yields an optimized design that is symmetric with respect to Q.

Finally, observe that if two symmetries with respect to two orthogonal planes Q_1 and Q_2 are desired, applying the symmetrization process described above first with respect to Q_1 and then with respect to Q_2 will yield the desired symmetries for $\boldsymbol{\theta}$.

Conclusion and Outlook

This thesis was driven by the lack of results concerning the mathematical modeling of the phenomena in the high-temperature superconductivity based on Bean's critical state law (B1) to (B3). In combination with the full Maxwell equations, we have obtained a hyperbolic mixed nonsmooth system (1.9) where the nonlinearity was explicitly depending on the time-variable as the critical current density j_c is highly affected by the operating temperature. An important basis for our investigation was the weak formulation in form of a variational inequality of the second kind (VI). We have mentioned in the introduction that j_c is also influenced by the magnetic field strength in the system (cf. Figure 1.2) which we have neglected throughout our studies. However, this should be incorporated in a more realistic model. Thus, we shall consider $j_c\colon \Omega \times \mathbb{R} \times \mathbb{R} \to \mathbb{R}$ defining the nonlinear nonsmooth function φ by

$$\varphi(\theta(t), \boldsymbol{H}(t), \boldsymbol{v}) \coloneqq \int_{\Omega_{\mathrm{sc}}} j_c\big(x, \theta(x,t), |\boldsymbol{H}(x,t)|\big)|\boldsymbol{v}(x)|\,dx.$$

In terms of (VI), this leads to a hyperbolic *quasi-variational* inequality of the second kind, meaning that the solution variable $\boldsymbol{H}$ occurs in the nonlinearity. For this new structure, the decoupling approach based on the implicit Euler method (cf. (4.1) and (4.2)) is not adequate since there is no equivalent of Theorem 3.1 applicable for quasi-variational inequalities. Moreover, the only known approaches to compute numerical solutions are limited to rather inefficient fixed point methods (cf. [35, 133, 135]). The only work studying the sensitivity analysis of quasi-variational inequalities is the recent paper by Alphonse et al. [4]. Quasi-variational inequalities in superconductivity were already studied by Barret and Prigozhin [15], Rodrigues and Santos [147], as well as Kunze and Rodrigues [109]. For the sake of completeness, we also refer to the classical monographs by Baiocchi et al. [11] and Mosco [129].

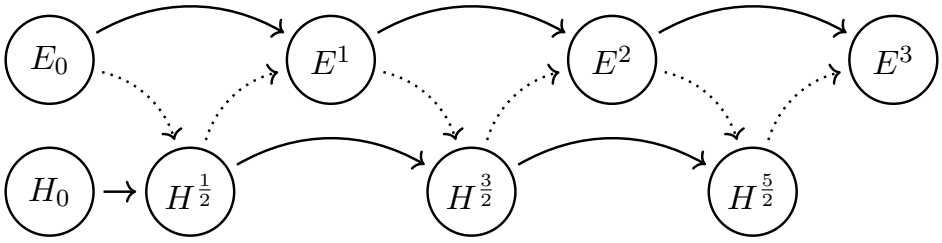

Figure 6.6. *Sketch of leapfrog discretization scheme.*

Our approach differs from all the previously mentioned as we propose a promising discretization strategy based on the *leapfrog scheme*. In our leapfrog-type iteration, the unknown fields $\boldsymbol{E}$ and $\boldsymbol{H}$ are computed at *different* times. We sketch the most basic idea of this discretization in Figure 6.6. Originally, the leapfrog scheme is derived from a (centered) finite difference method and the first contribution toward its application to the Maxwell equations goes back to Yee [177] (cf. [161]). We also refer to the more recent works [24, 25, 118, 146]. However, the leapfrog scheme is mostly used in the engineering community (cf. [77, 78, 86, 107]) but, in our case, we expect that a rigorous mathematical analysis yields fruitful results.

Therefore, we propose our new fully discrete approximation of (VI) with the QVI-character incorporating both, the temperature and the magnetic field dependence of the critical current density, as follows:

$$
(\mathrm{QVI}_{N,\,h}) \qquad \begin{cases} \text{For every } n \in \{1,\dots,N\} \text{ find } (\boldsymbol{E}_h^n, \boldsymbol{H}_h^{n+\frac{1}{2}}) \in \boldsymbol{W}_h \times \boldsymbol{V}_h \text{ such that} \\ \displaystyle\int_\Omega \epsilon \delta \boldsymbol{E}_h^n \cdot \big(\boldsymbol{v}_h - \overline{\boldsymbol{E}}_h^n\big) - \mathbf{curl}\, \boldsymbol{H}_h^{n-\frac{1}{2}} \cdot \big(\boldsymbol{v}_h - \overline{\boldsymbol{E}}_h^n\big)\, dx + \varphi^{n-\frac{1}{2}}(\boldsymbol{v}_h) \\ \qquad - \varphi^{n-\frac{1}{2}}(\overline{\boldsymbol{E}}_h^n) \geq \displaystyle\int_\Omega \boldsymbol{f}^{n-\frac{1}{2}} \cdot \big(\boldsymbol{v}_h - \overline{\boldsymbol{E}}_h^n\big)\, dx \quad \forall \boldsymbol{v}_h \in \boldsymbol{W}_h, \\ \displaystyle\int_\Omega \mu \delta \boldsymbol{H}_h^{n+\frac{1}{2}} \cdot \boldsymbol{w}_h\, dx + \int_\Omega \boldsymbol{E}_h^n \cdot \mathbf{curl}\, \boldsymbol{w}_h\, dx = 0 \quad \forall \boldsymbol{w}_h \in \boldsymbol{V}_h, \end{cases}
$$

where $\boldsymbol{E}_{0h}$ and $\boldsymbol{H}_h^{\frac{1}{2}}$ are assumed to be computed a priorily. We use the notation

$$
\delta \boldsymbol{E}_h^n \coloneqq \frac{\boldsymbol{E}_h^n - \boldsymbol{E}_h^{n-1}}{\tau} \quad \text{and} \quad \delta \boldsymbol{H}_h^{n+\frac{1}{2}} \coloneqq \frac{\boldsymbol{H}_h^{n+\frac{1}{2}} - \boldsymbol{H}_h^{n-\frac{1}{2}}}{\tau}
$$

as well as

$$
\overline{\boldsymbol{E}}_h^n \coloneqq \frac{\boldsymbol{E}_h^n + \boldsymbol{E}_h^{n-1}}{2}.
$$

Moreover, $\varphi^{n-\frac{1}{2}} \colon \boldsymbol{L}^2(\Omega) \to \mathbb{R}$, $n \in \mathbb{N}$, is given by

$$
\varphi^{n-\frac{1}{2}}(\boldsymbol{v}) \coloneqq \varphi\big(\theta(t_{n-\frac{1}{2}}), \boldsymbol{H}_h^{n-\frac{1}{2}}, \boldsymbol{v}\big) \quad \forall \boldsymbol{v} \in \boldsymbol{L}^2(\Omega).
$$

Under suitable assumptions on the initial data $(\boldsymbol{E}_0, \boldsymbol{H}_0)$ and a CFL-condition $\tau \leq Ch$, formulating $(\mathrm{QVI}_{N,\,h})$ has the following advantages:

a.) A careful stability and convergence analysis in the spirit of Lemmas 4.6 and 4.7 and Theorem 4.8 provides a promising framework to obtain the well-posedness of the quasi-variational inequality in the function space.

b.) We should be able to obtain significantly more efficient computations than $(\mathrm{VI}_{N,\,h})$ as the variational inequality in each time-step of $(\mathrm{QVI}_{N,\,h})$ features a simple $\boldsymbol{L}^2(\Omega)$-structure. Thus, we avoid the usage of the (iterative) semismooth Newton method for the $\mathbf{curl}$-$\mathbf{curl}$ variational inequality (4.2).

c.) It is not necessary to employ the Moreau–Yosida regularization since variational inequalities with an $\boldsymbol{L}^2(\Omega)$-structure obtain analytic solutions based on a projection formula.

Besides this research on quasi-variational inequalities, we have also neglected the physical aspect of *energy loss* in HTS. Throughout our studies, the partial electromagnetic field penetration of a superconductor was ubiquitous. While in its mixed state, this motion of magnetic flux leads to instantaneous heating in the material which might be fatal for the superconducting state. The resulting heating power dissipation $\rho \colon \Omega_{\mathrm{sc}} \times [0,T] \to \mathbb{R}_+$ is given by

$$
\rho(x,t) = \boldsymbol{J}(x,t) \cdot \boldsymbol{E}(x,t) \overset{\text{(B3)}}{=} j_c(x, \theta(x,t)) |\boldsymbol{E}(x,t)|. \tag{6.82}
$$

In (6.82), the critical current density is itself depending on the operating temperature θ. Therefore, it would be interesting to consider a *two-way coupling* where the operating temperature is determined by a nonsmooth heat equation incorporating (6.82). As a result we obtain a completely coupled nonsmooth multi-physics system. The methods developed in this thesis could serve as an important basis for the study of this novel system.

List of Figures

List of Tables

Bibliography

[1] M. Ainsworth and J. T. Oden. A posteriori error estimation in finite element analysis. *Comput. Methods Appl. Mech. Engrg.*, 142(1):1–88, 1997.

[2] G. Allaire, F. Jouve, and A.-M. Toader. Structural optimization using sensitivity analysis and a level-set method. *J. Comput. Phys.*, 194(1):363–393, 2004.

[3] A. Alonso and A. Valli. An optimal domain decomposition preconditioner for low-frequency time-harmonic Maxwell equations. *Math. Comp.*, 68(226):607–631, 1999.

[4] A. Alphonse, M. Hintermüller, and C. N. Rautenberg. Directional differentiability for elliptic quasi-variational inequalities of obstacle type. *Calc. Var. Partial Differential Equations*, 58(1):Paper No. 39, 47, 2019.

[5] C. Amrouche, C. Bernardi, M. Dauge, and V. Girault. Vector potentials in three-dimensional non-smooth domains. *Math. Methods Appl. Sci.*, 21(9):823–864, 1998.

[6] S. S. Antman. The influence of elasticity on analysis: modern developments. *Bull. Amer. Math. Soc. (N.S.)*, 9(3):267–291, 1983.

[7] J. Aponte, H. C. Abache, A. Sa-Neto, and M. Octavio. Temperature dependence of the critical current in high-T_c superconductors. *Phys. Rev. B: Condens. Matter*, 39:4, 1989.

[8] D. N. Arnold, R. S. Falk, and R. Winther. Finite element exterior calculus, homological techniques, and applications. *Acta Numerica*, 15:1–155, 2006.

[9] I. Babuška and W. Rheinboldt. Error estimates for adaptive finite element computations. *SIAM J. Numer. Anal.*, 15(4):736–754, 1978.

[10] I. Babuška and M. Vogelius. Feedback and adaptive finite element solution of one-dimensional boundary value problems. *Numer. Math.*, 44(1):75–102, 1984.

[11] C. Baiocchi, A. Capelo, and L. Jayakar. *Variational and Quasivariational Inequalities: Applications to Free Boundary Problems*. A Wiley-Interscience publication. Wiley, 1984.

[12] V. Barbu. *Optimal control of variational inequalities*. Research notes in mathematics. Pitman Advanced Pub. Program, 1984.

[13] V. Barbu. *Analysis and Control of Nonlinear Infinite Dimensional Systems*. Mathematics in Science and Engineering 190. Academic Press, 1993.

[14] V. Barbu and A. Friedman. Optimal design of domains with free-boundary problems. *SIAM J. Control Optim.*, 29(3):623–637, 1991.

[15] J. W. Barrett and L. Prigozhin. A quasi-variational inequality problem in superconductivity. *Math. Models Methods Appl. Sci.*, 20(5):679–706, 2010.

[16] J. W. Barrett and L. Prigozhin. Sandpiles and superconductors: nonconforming linear finite element approximations for mixed formulations of quasi-variational inequalities. *IMA J. Numer. Anal.*, 35(1):1–38, 2015.

[17] H. H. Bauschke and P. L. Combettes. *Convex analysis and monotone operator theory in Hilbert spaces*. CMS Books in Mathematics. Springer-Verlag New York, 1 edition, 2011.

[18] C. P. Bean. Magnetization of hard superconductors. *Phys. Rev. Lett.*, 8:250–253, 1962.

[19] C. P. Bean. Magnetization of high-field superconductors. *Rev. Mod. Phys.*, 36:31–39, 1964.

[20] R. Beck, R. Hiptmair, R. H. W. Hoppe, and B. Wohlmuth. Residual based a posteriori error estimators for eddy current computation. *ESAIM: M2AN*, 34(1):159–182, 2000.

[21] J. G. Bednorz and K. A. Müller. Possible high T_c superconductivity in the Ba-La-Cu-O system. *Z. Physik B - Condensed Matter*, 64:189–193, 1986.

[22] D. Boffi, F. Brezzi, and M. Fortin. *Mixed Finite Element Methods and Applications*. Springer Series in Computational Mathematics 44. Springer-Verlag Berlin Heidelberg, 1 edition, 2013.

[23] D. Boffi and L. Gastaldi. Interpolation estimates for edge finite elements and application to band gap computation. *Applied Numerical Mathematics*, 56(10):1283–1292, 2006. Selected Papers from the First Chilean Workshop on Numerical Analysis of Partial Differential Equations.

[24] A. Bossavit. Discretization of electromagnetic problems: The "Generalized Finite Differences" approach. In *Numerical Methods in Electromagnetics*, volume 13 of *Handbook of Numerical Analysis*, pages 105–197. Elsevier, 2005.

[25] A. Bossavit and L. Kettunen. Yee-like schemes on a tetrahedral mesh, with diagonal lumping. *Int. J. Numer. Model. El.*, 12(1-2):129–142, 1999.

[26] V. Bostan, W. Han, and B. D. Reddy. A posteriori error estimation and adaptive solution of elliptic variational inequalities of the second kind. *Appl. Numer. Math.*, 52(1):13–38, 2005.

[27] D. Braess. A posteriori error estimators for obstacle problems—another look. *Numer. Math.*, 101(3):415–421, 2005.

[28] D. Braess, C. Carstensen, and R. H. W. Hoppe. Convergence analysis of a conforming adaptive finite element method for an obstacle problem. *Numer. Math.*, 107(3):455–471, 2007.

[29] H. Brézis. Problèmes unilatéraux. *J. Math. Pures Appl. (9)*, 51:1–168, 1972.

[30] F. E. Browder. Nonlinear monotone operators and convex sets in Banach spaces. *Bull. Amer. Math. Soc.*, 71:780–785, 1965.

[31] Z. Cai and S. Cao. A recovery-based a posteriori error estimator for H(curl) interface problems. *Comput. Methods Appl. Mech. Engrg.*, 296:169–195, 2015.

[32] Z. Cai, S. Cao, and R. Falgout. Robust a posteriori error estimation for finite element approximation to H(curl) problem. *Comput. Methods Appl. Mech. Engrg.*, 309:182–201, 2016.

[33] C. Carstensen and J. Hu. An optimal adaptive finite element method for an obstacle problem. *Comput. Methods Appl. Math.*, 15(3):259–277, 2015.

[34] J. Céa. Conception optimale ou identification de formes: calcul rapide de la dérivée directionnelle de la fonction coût. *RAIRO Modél. Math. Anal. Numér.*, 20(3):371–402, 1986.

[35] D. Chan and J. S. Pang. The generalized quasi-variational inequality problem. *Mathematics of Operations Research*, 7(2):211–222, 1982.

[36] J. Chen, Y. Xu, and J. Zou. Convergence analysis of an adaptive edge element method for Maxwell's equations. *Appl. Numer. Math.*, 59(12):2950–2969, 2009.

[37] X. Chen, Z. Nashed, and L. Qi. Smoothing methods and semismooth methods for nondifferentiable operator equations. *SIAM J, Numer. Anal.*, 38(4):1200–1216, 2000.

[38] Z. Chen and R. H. Nochetto. Residual type a posteriori error estimates for elliptic obstacle problems. *Numer. Math.*, 84(4):527–548, 2000.

[39] Z. Chen, L. Wang, and W. Zheng. An adaptive multilevel method for time-harmonic Maxwell equations with singularities. *SIAM J. Sci. Comput.*, 29:118–138, 2007.

[40] X.-L. Cheng and W. Han. Inexact Uzawa algorithms for variational inequalities of the second kind. *Comput, Method. Appl. M.*, 192(11):1451–1462, 2003.

[41] S. H. Christiansen. Stability of Hodge decompositions in finite element spaces of differential forms in arbitrary dimension. *Numer. Math.*, 107:87–106, 2007.

[42] S. H. Christiansen and R. Winther. Smoothed projections in finite element exterior calculus. *Math. Comp.*, 77(262):813–829, 2008.

[43] P. Ciarlet, Jr. Analysis of the Scott-Zhang interpolation in the fractional order Sobolev spaces. *J. Numer. Math.*, 21(3):173–180, 2013.

[44] P. Ciarlet, Jr. On the approximation of electromagnetic fields by edge finite elements. Part 1: Sharp interpolation results for low-regularity fields. *Computers Math. Appl.*, 71:85–104, 2016.

[45] P. Ciarlet, Jr., H. Wu, and J. Zou. Edge element methods for Maxwell's equations with strong

convergence for Gauss' laws. *SIAM J. Numer. Anal.*, 52(2):779–807, 2014.

[46] P. Ciarlet, Jr. and J. Zou. Fully discrete finite element approaches for time-dependent Maxwell's equations. *Numer. Math.*, 82(2):193–219, 1999.

[47] P. G. Ciarlet. *The Finite Element Method for Elliptic Problems*, volume 4 of *Studies in mathematics and its applications*. North-Holland, 1978.

[48] D. S. Clark. Short proof of a discrete gronwall inequality. 16(3):279–281, 1987.

[49] F. H. Clarke. *Optimization and Nonsmooth Analysis*. Society for Industrial and Applied Mathematics, 1990.

[50] C. Clason. Nonsmooth analysis and optimization, 2017.

[51] R. Correa and A. Seeger. Directional derivative of a minimax function. *Nonlinear Anal.*, 9(1):13–22, 1985.

[52] M. Costabel and M. Dauge. Singularities of electromagnetic fields in polyhedral domains. *Arch. Ration. Mech. Anal.*, 151(3):221–276, 2000.

[53] M. Costabel, M. Dauge, and S. Nicaise. Singularities of Maxwell interface problems. *ESAIM: M2AN*, 33(3):627–649, 1999.

[54] B. Cox and A. Cohen. *Human Universe*. William Collins, 2014.

[55] J. C. De Los Reyes. Optimal control of a class of variational inequalities of the second kind. *SIAM J. Control Optim.*, 49(4):1629–1658, 2011.

[56] J. C. De Los Reyes and S. González Andrade. Path following methods for steady laminar Bingham flow in cylindrical pipes. *ESAIM: M2AN*, 43(1):81–117, 2009.

[57] J. C. De los Reyes and S. González Andrade. Numerical simulation of two-dimensional Bingham fluid flow by semismooth Newton methods. *J. Comput. Appl. Math*, 235(1):11–32, 2010.

[58] J. C. De Los Reyes and M. Hintermüller. A duality based semismooth Newton framework for solving variational inequalities of the second kind. *IFB*, 13:437–462, 2011.

[59] M. Delfour and J. Zolésio. *Shapes and Geometries*. Society for Industrial and Applied Mathematics, 2 edition, 2011.

[60] Z. Denkowski and S. Migórski. Optimal shape design for elliptic hemivariational inequalities in nonlinear elasticity. In *Variational calculus, optimal control and applications*, volume 124 of *Internat. Ser. Numer. Math.*, pages 31–40. Birkhäuser, Basel, 1998.

[61] Z. Denkowski and S. Migórski. Optimal shape design problems for a class of systems described by hemivariational inequalities. *J. Global Optim.*, 12(1):37–59, 1998.

[62] G. Deutscher and K. A. Müller. Origin of superconductive glassy state and extrinsic critical currents in high-T_c oxides. *Phys. Rev. Lett.*, 59:15, 1987.

[63] W. Dörfler. A convergent adaptive algorithm for Poisson's equation. *SIAM J. Numer. Anal.*, 33(3):1106–1124, 1996.

[64] G. Duvaut and J.-L. Lions. *Les inéquations en mécanique et en physique*. Dunod, Paris, 1972. Travaux et Recherches Mathématiques, No. 21.

[65] C. M. Elliott and Y. Kashima. A finite-element analysis of critical-state models for type-II superconductivity in 3D. *IMA J. Numer. Anal.*, 27(2):293–331, 2007.

[66] C. M. Elliott, D. Kay, and V. Styles. A finite element approximation of a variational inequality formulation of Bean's model for superconductivity. *SIAM J. Numer. Anal.*, 42(3):1324–1341, 2004.

[67] C. M. Elliott, D. Kay, and V. Styles. Finite element analysis of a current density-electric field formulation of Bean's model for superconductivity. *IMA J. Numer. Anal.*, 25(1):182–204, 2005.

[68] K. Eriksson and C. Johnson. Adaptive finite element methods for parabolic problems i: A linear model problem. *SIAM J. Numer. Anal.*, 28(1):43–77, 1991.

[69] A. Ern and J.-L. Guermond. Mollification in strongly Lipschitz domains with application to continuous and discrete de Rham complexes. *Comput. Methods Appl. Math.*, 16(1):51–75, 2016.

[70] A. Ern and J.-L. Guermond. Finite element quasi-interpolation and best approximation. *ESAIM:*

M2AN, 51(4):1367–1385, 2017.

[71] A. Ern and J.-L. Guermond. Analysis of the edge finite element approximation of the Maxwell equations with low regularity solutions. *Comput. Math. Appl.*, 75(3):918 – 932, 2018.

[72] G. Fichera. Problemi elastostatici con vincoli unilaterali: Il problema di Signorini con ambigue condizioni al contorno. *Atti Accad. Naz. Lincei Mem. Cl. Sci. Fis. Mat. Natur. Sez. Ia (8)*, 7:91–140, 1963/64.

[73] K. Fossheim and A. Sudboe. *Superconductivity: Physics and Applications*. John Wiley and Sons, 1 edition, 2004.

[74] G. Frémiot, W. Horn, A. Laurain, M. Rao, and J. Sokołowski. On the analysis of boundary value problems in nonsmooth domains. *Dissertationes Math.*, 462:149, 2009.

[75] B. Führ, V. Schulz, and K. Welker. Shape optimization for interface identification with obstacle problems. *Vietnam J. Math.*, 46(4):967–985, 2018.

[76] P. Fulmański, A. Laurain, J.-F. Scheid, and J. Sokołowski. A level set method in shape and topology optimization for variational inequalities. *Int. J. Appl. Math. Comput. Sci.*, 17(3):413–430, 2007.

[77] A. Gansen, M. El Hachemi, S. Belouettar, O. Hassan, and K. Morgan. An effective 3d leapfrog scheme for electromagnetic modelling of arbitrary shaped dielectric objects using unstructured meshes. *Comput. Mech.*, 56:1023–1037, 2015.

[78] A. Gansen, M. El Hachemi, S. Belouettar, O. Hassan, and K. Morgan. A 3d unstructured mesh FDTD scheme for em modelling. *Arch. Computat. Methods Eng.*, 2020.

[79] V. L. Ginzburg and L. D. Landau. *On the Theory of Superconductivity*, pages 113–137. Springer Berlin Heidelberg, Berlin, Heidelberg, 2009.

[80] V. Girault and P.-A. Raviart. *Finite Element Methods for Navier-Stokes Equations: Theory and Algorithms (Springer Series in Computational Mathematics)*. Springer-Verlag, 1986.

[81] R. Glowinski. *Numerical Methods for Nonlinear Variational Problems*. Scientific Computation. Springer Berlin Heidelberg, 1984.

[82] R. Glowinski, J. L. Lions, and R. Trémolières. *Numerical Analysis of Variational Inequalities*. Studies in Mathematics and its Applications. Elsevier Science, 1981.

[83] T. Grätsch and K.-J. Bathe. Review: A posteriori error estimation techniques in practical finite element analysis. *Comput. Struct.*, 83(4-5):235–265, 2005.

[84] C. Heinemann and K. Sturm. Shape optimization for a class of semilinear variational inequalities with applications to damage models. *SIAM J. Math. Anal.*, 48(5):3579–3617, 2016.

[85] A. Henrot and M. Pierre. *Shape variation and optimization*, volume 28 of *EMS Tracts in Mathematics*. European Mathematical Society (EMS), Zürich, 2018.

[86] F. Hermeline, S. Layouni, and P. Omnes. A finite volume method for the approximation of Maxwell's equations in two space dimensions on arbitrary meshes. *J. Comput. Phys.*, 227(22):9365–9388, 2008.

[87] F. Herzog, T. Kutz, M. Stemmle, and T. Kugel. Cooling unit for the ampacity project – one year successful operation. *Cryogenics*, 80:204–209, 2016.

[88] M. Hintermüller, K. Ito, and K. Kunisch. The primal-dual active set strategy as a semismooth Newton method. *SIAM J. Optim.*, 13(3):865–888, 2002.

[89] M. Hintermüller and K. Kunisch. Path-following methods for a class of constrained minimization problems in function space. *SIAM J. Optim.*, 17(1):159–187, 2006.

[90] M. Hintermüller and K. Kunisch. PDE-constrained optimization subject to pointwise constraints on the control, the state, and its derivative. *SIAM J. Optim.*, 20(3):1133–1156, 2010.

[91] M. Hintermüller and A. Laurain. Optimal shape design subject to elliptic variational inequalities. *SIAM Journal on Control and Optimization*, 49(3):1015–1047, 2011.

[92] M. Hintermüller, A. Laurain, and I. Yousept. Shape sensitivities for an inverse problem in magnetic induction tomography based on the eddy current model. *Inverse Problems*, 31(6):065006, 25, 2015.

[93] R. Hiptmair. Finite elements in computational electromagnetism. *Acta Numerica*, 11(1):237–339, 2002.

[94] I. Hlaváček, J. Haslinger, J. Nečas, and J. Lovíšek. *Solution of Variational Inequalities in Mechanics*. Applied Mathematical Sciences 66. Springer-Verlag New York, 1 edition, 1988.

[95] R. H. W. Hoppe. Multigrid algorithms for variational inequalities. *SIAM J. Numer. Anal.*, 24(5):1046–1065, 1987.

[96] R. H. W. Hoppe and R. Kornhuber. Adaptive multilevel methods for obstacle problems. *SIAM J. Numer. Anal.*, 31(2):301–323, 1994.

[97] R. H. W. Hoppe and J. Schöberl. Convergence of adaptive edge element methods for the 3D eddy currents equations. *J. Comput. Math.*, 27(5):657–676, 2009.

[98] K. Ito and K. Kunisch. Semi-smooth Newton methods for variational inequalities of the first kind. 37(1):41–62, 2003.

[99] K. Ito and K. Kunisch. *Lagrange Multiplier Approach to Variational Problems and Applications*. Society for Industrial and Applied Mathematics, 2008.

[100] K. Ito, K. Kunisch, and G. H. Peichl. Variational approach to shape derivatives. *ESAIM Control Optim. Calc. Var.*, 14(3):517–539, 2008.

[101] F. Jochmann. The semistatic limit for Maxwell's equations in an exterior domain. *Comm. Partial Differential Equations*, 23(11-12):2035–2076, 1998.

[102] F. Jochmann. On a first-order hyperbolic system including Bean's model for superconductors with displacement current. *J. Differential Equations*, 246(6):2151–2191, 2009.

[103] H. Kamerlingh Onnes. Leiden comm. 120b, 122b, 124c. Technical report, 1911.

[104] H. Kasumba and K. Kunisch. On shape sensitivity analysis of the cost functional without shape sensitivity of the state variable. *Control Cybernet.*, 40(4):989–1017, 2011.

[105] D. Kinderlehrer and G. Stampacchia. *An Introduction to Variational Inequalities and Their Applications*. Society for Industrial and Applied Mathematics, 2000.

[106] M. Kočvara and J. V. Outrata. Shape optimization of elastoplastic bodies governed by variational inequalities. In *Boundary control and variation (Sophia Antipolis, 1992)*, volume 163 of *Lecture Notes in Pure and Appl. Math.*, pages 261–271. Dekker, New York, 1994.

[107] H. Kono, M. Fujino, M. Yokoyama, K. Yonezawa, Y. Takahashi, C. Isokawa, and A. Tatematsu. Applying FDTD simulation to lightning surge route analysis in microwave relay stations. *J. Int. Counc. Electr. Eng.*, 1(1):60–66, 2011.

[108] R. Kornhuber. A posteriori error estimates for elliptic variational inequalities. *Comput. Math. Appl.*, 31(8):49–60, 1996.

[109] M. Kunze and J. F. Rodrigues. An elliptic quasi-variational inequality with gradient constraints and some of its applications. *Math. Methods Appl. Sci.*, 23(10):897–908, 2000.

[110] J. Kvitkovic, D. Davis, M. Zhang, and S. Pamidi. Magnetic shielding characteristics of second generation high temperature superconductors at variable temperatures obtained by cryogenic helium gas circulation. *IEEE Trans. Appl. Supercond.*, 25(3), 2015.

[111] S. Lang. *Real and Functional Analysis*. Springer-Verlag New York, 3 edition, 1993.

[112] A. Laurain. Analyzing smooth and singular domain perturbations in level set methods. *SIAM J. Math. Anal.*, 50(4):4327–4370, 2018.

[113] A. Laurain. A level set-based structural optimization code using FEniCS. *Struct. Multidiscip. Optim.*, 58(3):1311–1334, Sep 2018.

[114] A. Laurain and K. Sturm. Distributed shape derivative via averaged adjoint method and applications. *ESAIM Math. Model. Numer. Anal.*, 50(4):1241–1267, 2016.

[115] A. Laurain, M. Winckler, and I. Yousept. Shape optimization for superconductors governed by H(curl)-elliptic variational inequalities. *SIAM J. Control Optim.*, submitted, 2019.

[116] J. Li. Error analysis of fully discrete mixed finite element schemes for 3-D Maxwell's equations in dispersive media. *Comput. Methods Appl. Mech. Engrg.*, 196(33-34):3081–3094, 2007.

[117] J. Li and Y. Huang. *Time-domain finite element methods for Maxwell's equations in metamate-*

rials, volume 43 of *Springer Series in Computational Mathematics*. Springer, 2013.

[118] J. Li and S. Shields. Superconvergence analysis of Yee scheme for metamaterial Maxwell's equations on non-uniform rectangular meshes. *Numer. Math.*, 134(4):741–781, 2016.

[119] J.-L. Lions. *Quelques méthodes de résolution des problèmes aux limites non linéaires*. Dunod; Gauthier-Villars, Paris, 1969.

[120] J. L. Lions and G. Stampacchia. Variational inequalities. *Comm. Pure Appl. Math.*, 20(3):493–519, 1967.

[121] W. B. Liu and J. E. Rubio. Optimal shape design for systems governed by variational inequalities. I. Existence theory for the elliptic case. *JOTA*, 69(2):351–371, 1991.

[122] A. Logg, K.-A. Mardal, G. N. Wells, et al. *Automated Solution of Differential Equations by the Finite Element Method*, volume 84 of *Lecture Notes in Computational Science and Engineering*. Springer, 2012.

[123] F. London and H. London. The electromagnetic equations of the supraconductor. *Proc. R. Soc. A*, 149(866):71–88, 1935.

[124] Ch. G. Makridakis and P. Monk. Time-discrete finite element schemes for Maxwell's equations. *RAIRO Modél. Math. Anal. Numér.*, 29(2):171–197, 1995.

[125] W. Meissner and R. Ochsenfeld. Ein neuer Effekt bei Eintritt der Supraleitfähigkeit. *Naturwissenschaften*, 21:787–788, 1933.

[126] R. Mifflin. Semismooth and semiconvex functions in constrained optimization. *SIAM J. Control Optim.*, 15(6):959–972, 1977.

[127] P. Monk. *Finite Element Methods for Maxwell's Equations*. Numerical Analysis and Scientific Computation. Clarendon Press, 2003.

[128] P. Morin, K. G. Siebert, and A. Veeser. A basic convergence result for conforming adaptive finite elements. *Math. Models Methods Appl. Sci.*, 18(05):707–737, 2008.

[129] U. Mosco. Implicit variational problems and quasi variational inequalities. In *Nonlinear operators and the calculus of variations*, pages 83–156. Springer, 1976.

[130] A. Myśliński. Domain optimization for unilateral problems by an embedding domain method. In *Shape optimization and optimal design (Cambridge, 1999)*, volume 216 of *Lecture Notes in Pure and Appl. Math.*, pages 355–370. Dekker, New York, 2001.

[131] J.-C. Nédélec. Mixed finite elements in $\mathbb{R}^3$. *Numer. Math.*, 35(3):315–341, 1980.

[132] P. Neittaanmäki, J. Sokołowski, and J. P. Zolesio. Optimization of the domain in elliptic variational inequalities. *Appl. Math. Optim.*, 18(1):85–98, 1988.

[133] Y. Nesterov and L. Scrimali. Solving strongly monotone variational and quasi-variational inequalities. *Discrete Contin. Dyn. Syst.*, 31(1078-0947-2011-4-1383):1383, 2011.

[134] R. H. Nochetto, K. G. Siebert, and A. Veeser. Pointwise a posteriori error control for elliptic obstacle problems. *Numer. Math.*, 95(1):163–195, 2003.

[135] M. A. Noor. An iterative scheme for a class of quasi variational inequalities. *J. Math. Anal. Appl.*, 110(2):463–468, 1985.

[136] S. Osher and A. Fedkiw. *Level Set Methods and Dynamic Implicit Surfaces*. Applied Mathematical Sciences 153. Springer-Verlag New York, 1 edition, 2003.

[137] S. Osher and J. A. Sethian. Fronts propagating with curvature-dependent speed: Algorithms based on Hamilton-Jacobi formulations. *J. Comput. Phys.*, 79(1):12–49, 1988.

[138] O. Pantz. Sensibilité de l'équation de la chaleur aux sauts de conductivité. *C. R. Math. Acad. Sci. Paris*, 341(5):333–337, 2005.

[139] E. A. Pashitskii, V. I. Vakaryuk, S. M. Ryabchenko, and Yu. V. Fedotov. Temperature dependence of the critical current in high-T_c superconductors with low-angle boundaries between crystalline blocks. *Low Temp. Phys.*, 27(2):96–102, 2001.

[140] A. Plaza and G. F. Carey. Local refinement of simplicial grids based on the skeleton. *Appl. Numer. Math.*, 32(2):195–218, 2000.

[141] L. Prigozhin. On the Bean critical-state model in superconductivity. *European J. Appl. Math.*,

7(3):237–247, 1996.

[142] L. Prigozhin. Solution of thin film magnetization problems in type-II superconductivity. *J. Comput. Phys.*, 144(1):180–193, 1998.

[143] L. Qi. Transposes, L-eigenvalues and invariants of third order tensors, 2017.

[144] L. Qi and J. Sun. A nonsmooth version of Newton's method. *Math. Program.*, 58:353–367, 01 1993.

[145] A. Quarteroni and A. Valli. *Numerical approximation of partial differential equations*. Springer Series in Computational Mathematics 23. Springer-Verlag Berlin Heidelberg, 1 edition, 1994.

[146] Räbinä, J., Kettunen, L., Mönkölä, S., and Rossi, T. Generalized wave propagation problems and discrete exterior calculus. *ESAIM: M2AN*, 52(3):1195–1218, 2018.

[147] J. F. Rodrigues and L. Santos. A parabolic quasi-variational inequality arising in a superconductivity model. *Ann. Scuola Norm. Sup. Pisa Cl. Sci. (4)*, 29(1):153–169, 2000.

[148] T. Roubícek. *Nonlinear Partial Differential Equations with Applications*. International Series of Numerical Mathematics. Springer Basel, 2013.

[149] J. Schöberl. Commuting quasi-interpolation operators for mixed finite elements, 2001.

[150] J. Schöberl. A posteriori error estimates for Maxwell equations. *Math. Comp.*, 77:633–649, 2007.

[151] L. R. Scott and S. Zhang. Finite element interpolation of nonsmooth functions satisfying boundary conditions. *Math. Comput.*, 54(190):483–493, 1990.

[152] K. G. Siebert. A convergence proof for adaptive finite elements without lower bound. *IMA J. Numer. Anal.*, 31(3):947–970, 2011.

[153] A. Signorini. Questioni di elasticità non linearizzata e semilinearizzata. *Rend. Mat. e Appl. (5)*, 18:95–139, 1959.

[154] J. Sokołowski and A. Żochowski. Modelling of topological derivatives for contact problems. *Numer. Math.*, 102(1):145–179, 2005.

[155] J. Sokołowski and J.-P. Zolésio. *Introduction to shape optimization*, volume 16 of *Springer Series in Computational Mathematics*. Springer-Verlag, Berlin, 1992.

[156] G. Stampacchia. Formes bilinéaires coercitives sur les ensembles convexes. *C. R. Acad. Sci. Paris*, 258:4413–4416, 1964.

[157] M. Stemmle, F. Merschel, M. Noe, and A. Hobl. Ampacity – installation of advanced superconducting 10 kV system in city center replaces conventional 110 kV cables. In *2013 IEEE International Conference on Applied Superconductivity and Electromagnetic Devices*, pages 323–326, 2013.

[158] M. Stemmle, F. Merschel, M. Noe, and A. Hobl. Ampacity project–update on world's first superconducting cable and fault current limiter installation in a German city center. In *23rd International Conference on Electricity Distribution, Lyon, Paper 0678*, 2015.

[159] G. Strang. *Introduction to Linear Algebra*. Wellesley-Cambridge Press, 2009.

[160] K. Sturm. Minimax Lagrangian approach to the differentiability of nonlinear PDE constrained shape functions without saddle point assumption. *SIAM J. Control Optim.*, 53(4):2017–2039, 2015.

[161] A. Taflove. Application of the finite-difference time-domain method to sinusoidal steady-state electromagnetic-penetration problems. *IEEE Trans. Electromagn. Compat.*, EMC-22(3):191–202, 1980.

[162] C. T. Traxler. An algorithm for adaptive mesh refinement in n dimensions. *Computing*, 59(2):115–137, 1997.

[163] F. Tröltzsch. *Optimale Steuerung partieller Differentialgleichungen*. Vieweg+Teubner, 2009.

[164] F. Tröltzsch and A. Valli. Optimal control of low-frequency electromagnetic fields in multiply connected conductors. *Optimization*, 65(9):1651–1673, 2016.

[165] F. Tröltzsch and I. Yousept. PDE-constrained optimization of time-dependent 3D electromagnetic induction heating by alternating voltages. *ESAIM Math. Model. Numer. Anal.*, 46(4):709–

729, 2012.

[166] R. Verfürth. *A Posteriori Error Estimation Techniques for Finite Element Methods*. OUP Oxford, 2013.

[167] F. Wang and W. Han. Another view for a posteriori error estimates for variational inequalities of the second kind. *Appl. Numer. Math.*, 72:225–233, 2013.

[168] C. Weber and P. Werner. A local compactness theorem for Maxwell's equations. *Math. Methods Appl. Sci.*, 2(1):12–25, 1980.

[169] N. Weck. Maxwell's boundary value problem on Riemannian manifolds with nonsmooth boundaries. *J. Math. Anal. Appl.*, 46(2):410–437, 1974.

[170] M. Winckler and I. Yousept. Fully discrete solution for Bean's critical-state model in type-II superconductivity. *PAMM*, 18(1):e201800173, 2018.

[171] M. Winckler and I. Yousept. Fully discrete scheme for Bean's critical-state model with temperature effects in superconductivity. *SIAM J. Numer. Anal.*, 57(6):2685–2706, 2019.

[172] M. Winckler and I. Yousept. Hyperbolic Maxwell variational inequalities in type-II superconductivity. In M. Hintermüller et. al., *SPP1962 Special Issue*. Birkhäuser, 2019. (accepted).

[173] M. Winckler, I. Yousept, and J. Zou. Adaptive edge element approximation for H(curl) elliptic variational inequalities of second kind. *SIAM J. Numer. Anal.*, 58(3):1941–1964, 2020.

[174] M. K. Wu, J. R. Ashburn, C. J. Torng, et al. Superconductivity at 93K in a new mixed-phase Y-Ba-Cu-O compound system at ambient pressure. *Phys. Rev. Lett.*, 58:908–910, 1987.

[175] Y. Xu and J. Zou. A convergent adaptive edge element method for an optimal control problem in magnetostatics. *ESAIM: M2AN*, 51(2):615–640, 2017.

[176] L. Xue and X.-L. Cheng. Convergence rate to elliptic variational inequalities of the second kind by relaxation method. *Appl. Math. Lett.*, 17(4):417–422, 2004.

[177] K. Yee. Numerical solution of initial boundary value problems involving Maxwell's equations in isotropic media. *IEEE T. Antenn. Propag.*, 14(3):302–307, 1966.

[178] I. Yousept. Optimal control of Maxwell's equations with regularized state constraints. *Comput. Optim. Appl.*, 52(2):559–581, 2012.

[179] I. Yousept. Optimal Control of Quasilinear $\boldsymbol{H}(\mathbf{curl})$-Elliptic Partial Differential Equations in Magnetostatic Field Problems. *SIAM J. Control Optim.*, 51(5):3624–3651, 2013.

[180] I. Yousept. Hyperbolic Maxwell variational inequalities for Bean's critical-state model in type-II superconductivity. *SIAM J. Numer. Anal.*, 55(5):2444–2464, 2017.

[181] I. Yousept. Optimal control of non-smooth hyperbolic evolution Maxwell equations in type-II superconductivity. *SIAM J. Control Optim.*, 55(4):2305–2332, 2017.

[182] I. Yousept. Hyperbolic Maxwell variational inequalities of the second kind. *ESAIM: COCV*, 26:34, 2020.

[183] I. Yousept and J. Zou. Edge element method for optimal control of stationary Maxwell system with Gauss law. *SIAM J. Numer. Anal.*, 55(6):2787–2810, 2017.